



Shengqiang Guo  
Kurt-Schumacher-Straße 32  
D - 67663 Kaiserslautern

# Contributions to increase the power efficiency of OFDM communications

deutscher Titel:

## Beiträge zum Erhöhen der Leistungseffizienz der OFDM-Übertragung

Beim Fachbereich Elektrotechnik und Informationstechnik  
der Technischen Universität Kaiserslautern  
zur Verleihung des akademischen Grades  
Doktor-Ingenieur (Dr.-Ing.)  
eingereichte Dissertation

von

Shengqiang Guo, M. Eng.  
D 386

Tag der Einreichung: 22.11.2010  
Tag der mündlichen Prüfung: 04.02.2011

Dekan des Fachbereichs  
Elektrotechnik und  
Informationstechnik: Prof. Dr. G. Föhler

Vorsitzender der  
Prüfungskommission: Prof. Dr.-Ing. Norbert Wehn

1. Berichterstatter: Prof. Dr.-Ing. habil. Dr.-Ing. E.h. P.W. Baier  
2. Berichterstatter: Prof. Dr. techn. J. A. Nossek



# Vorwort

Die vorliegende Arbeit entstand in der Zeit von August 2008 bis November 2010 im Rahmen meiner Tätigkeit als Promotionsstipendiat am Lehrstuhl für Funkkommunikation und Navigation der Technischen Universität Kaiserslautern. Ich möchte all jenen danken, die mich bei der Entstehung dieser Arbeit unterstützt haben.

Mein besonderer Dank gilt Herrn Prof. Dr.-Ing. habil. Dr.-Ing. E. h. P. W. Baier für die Anregung, die Betreuung und die Förderung meiner Arbeit. Durch seine stete Diskussionsbereitschaft sowie durch zahlreiche Ratschläge und Hinweise hat er wesentlich zum Gelingen dieser Arbeit beigetragen.

Herrn Prof. Dr. techn. J. A. Nossek von der TU München danke ich für die Übernahme des Korreferats sowie für eine Reihe konstruktiver Hinweise, die ich in der vorliegenden Endfassung der Dissertation berücksichtigt habe. Weiterhin danke ich dem Vorsitzenden der Promotionskommission, Herrn Prof. Dr.-Ing. Norbert Wehn.

Dank sage ich auch Herrn Dipl.-Ing. (FH) R. Stemler für seine stete Hilfe beim Lösen von Problemen mit der PC-Software sowie Herrn X. Dong, der mit seiner Diplomarbeit und als wissenschaftliche Hilfskraft unter meiner Anleitung Beiträge zu dieser Arbeit geleistet hat. Ein besonderer Dank ergeht auch an Frau S. Ilgner für ihre administrative Unterstützung bei der Kommunikation mit der Universitätsverwaltung und der Ausländerbehörde.

Der Technischen Universität Kaiserslautern danke ich für die Möglichkeit, die leistungsfähigen Rechner des Regionalen Hochschulrechenzentrums Kaiserslautern (RHRK) für meine Forschungsarbeiten zu benutzen. Den Mitarbeitern des RHRK gilt mein Dank für die Beratung in Software- und Hardwarefragen.

Nicht zuletzt möchte ich mich bei meiner Familie und meinen Freunden bedanken, die mir immer ein großer Rückhalt waren. Ganz besonders herzlich danke ich meinen Eltern. Sie haben mir das Studium ermöglicht und mir immer ihre uneingeschränkte Unterstützung zukommen lassen. Ihnen widme ich diese Arbeit.

Kaiserslautern, im Februar 2011

Shengqiang Guo

---

# Contents

<b>1</b>	<b>Introduction</b>	<b>1</b>
1.1	Orthogonal Frequency Division Multiplexing (OFDM) . . . . .	1
1.2	Requirement of power efficient radio communication systems . . . . .	1
1.3	Goals of the thesis . . . . .	2
1.4	Structure of the thesis . . . . .	4
<b>2</b>	<b>Generic OFDM transmission model</b>	<b>6</b>
2.1	System structure . . . . .	6
2.2	Information vector and transmit vector . . . . .	6
2.3	Radio channel . . . . .	11
2.3.1	Delay discrete channel model and channel impulse response (CIR) vector . . . . .	11
2.3.2	Rayleigh fading . . . . .	13
2.3.3	Channel transfer function (CTF) vector and CTF matrix . . . . .	15
2.4	Noise . . . . .	17
2.5	Disturbed receive vector, data detection and demapping . . . . .	17
2.6	Bit error probabilities . . . . .	19
2.7	Continuous time representation of OFDM symbols in the equivalent low pass domain . . . . .	20
<b>3</b>	<b>Combating frequency selectivity of radio channels by partial data spreading</b>	<b>22</b>
3.1	Preliminary remarks . . . . .	22
3.1.1	Impact of Rayleigh fading . . . . .	22
3.1.2	Frequency diversity by data spreading . . . . .	22
3.2	Concept of partial data spreading (PDS) . . . . .	27
3.3	Transmission model . . . . .	27
3.4	Interleaver and deinterleaver . . . . .	29
3.5	Data detection . . . . .	30
3.5.1	Introduction of partial vectors in the receiver, and partial detection	30
3.5.2	ML detection . . . . .	34
3.5.3	MMSE detection . . . . .	35
3.5.4	ZF detection . . . . .	44
3.5.5	Matched Filter (MF) bound . . . . .	46
3.5.6	Unspread transmission . . . . .	47

3.6	Quantitative evaluations . . . . .	47
3.6.1	Preliminary remarks . . . . .	47
3.6.2	Performance comparison of the schemes ML, MMSE and ZF detection . . . . .	48
3.6.3	Detailed investigation of MMSE and ZF detection . . . . .	48
3.6.3.1	SNIR and SNR . . . . .	48
3.6.3.2	Bit error probability $P_b$ . . . . .	49
3.6.3.3	Plausibility explanation of the maximum reasonable spreading factor . . . . .	56
3.6.4	Error statistics . . . . .	60
3.7	PDS versus conventional diversity . . . . .	61
3.8	Generalization to other partial spreading matrices . . . . .	62
3.9	Computational complexity . . . . .	63
<b>4</b>	<b>Combination of PDS with FEC encoding</b>	<b>65</b>
4.1	Preliminary remarks . . . . .	65
4.2	System model . . . . .	65
4.3	Case study . . . . .	69
4.3.1	System characteristics and parameters . . . . .	69
4.3.2	Mathematical description . . . . .	71
4.3.3	Simulation results . . . . .	77
<b>5</b>	<b>PAPR reduction by combining Partial Data Spreading with Selective Data Mapping (SDM)</b>	<b>81</b>
5.1	Preliminary remarks . . . . .	81
5.2	PAPR reduction by PDS . . . . .	86
5.3	Combination of PDS with SDM . . . . .	89
5.3.1	System model . . . . .	89
5.3.2	Simulation results . . . . .	89
5.3.3	Plausible explanations of the simulation results . . . . .	98
<b>6</b>	<b>Enhancing the power efficiency of transmit amplifiers by Optimum Clipping</b>	<b>103</b>
6.1	Some fundamentals of transmit power amplifiers . . . . .	103
6.2	A scheme for clipping and scaling OFDM symbols . . . . .	104
6.3	Performance . . . . .	109
6.3.1	Bit error probability . . . . .	109
6.3.2	Required DC power . . . . .	112

---

<b>7</b>	<b>Joint optimization of pilot based channel estimation and data detection</b>	<b>114</b>
7.1	Introduction . . . . .	114
7.2	Pilot based channel estimation . . . . .	115
7.3	Data detection . . . . .	117
7.4	Approximate closed form expressions for the symbol error probabilities . .	119
7.4.1	Approximation rationale . . . . .	119
7.4.2	QPSK . . . . .	120
7.4.3	16QAM . . . . .	121
7.5	Optimum power partitioning . . . . .	122
7.5.1	QPSK . . . . .	122
7.5.2	16QAM . . . . .	123
7.6	Verification by simulations . . . . .	125
7.7	Results . . . . .	125
7.8	Derivation of integrals $I_{\square}(k_m)$ and $I_{\square}(k_m)$ . . . . .	127
<b>8</b>	<b>Multipoint-to-point transmission</b>	<b>128</b>
8.1	Introduction . . . . .	128
8.2	PAPR . . . . .	128
<b>9</b>	<b>Some open questions and proposals for further research</b>	<b>131</b>
<b>10</b>	<b>Summary</b>	<b>133</b>
10.1	English . . . . .	133
10.2	Deutsch . . . . .	135
<b>A</b>	<b>Acronyms and symbols</b>	<b>137</b>
A.1	Acronyms . . . . .	137
A.2	Symbols . . . . .	138
	<b>References</b>	<b>145</b>

# Chapter 1

## Introduction

### 1.1 Orthogonal Frequency Division Multiplexing (OFDM)

Since Marconi first demonstrated wireless information transmission in 1895, until the 1990ies the foremost technique of radio communications has been single carrier (SC) transmission. In SC systems the information to be transmitted is modulated onto a single RF carrier. Historically, the modulation in SC systems was analog, whereas in today's radio systems digital modulation prevails. An alternative to SC transmission is multi-carrier (MC) transmission, which appeared in literature probably for the first time in 1946 [Bri46]. In MC systems [FK03, FK04], which are particularly suited for digital modulation, the available transmission bandwidth is subdivided among a number  $N_F$  of subcarriers, and each of these subcarriers conveys only a part of the total information to be transmitted. The subcarriers can be made orthogonal by suitably choosing their frequency spacing and the duration they provide for the data elements. Then, the MC system turns into the channel access scheme Orthogonal Frequency Division Multiplexing (OFDM). In [vNP00] this scheme is comprehensively treated, and the main advantages of OFDM transmission over SC transmission are set forth, namely simple implementation and high flexibility. From [DPSB08] it becomes clear that OFDM is the favorite channel access scheme for the evolution of today's and for the design of future cellular mobile radio systems. Already today OFDM enjoys wide acceptance in the worlds of Wireless Local Area Networks (WLAN) [vNP00, HT01] and satellite communications [WJ08, HYW<sup>+</sup>09].

### 1.2 Requirement of power efficient radio communication systems

The proliferation of radio communication systems is still progressing in fast pace, and because such systems increasingly penetrate our world, the involved power consumption no longer can be considered a negligible quantity. It is true that the yearly power consumption of a typical German mobile radio operator, which, according to a private communication, amounts to ca. 500 GWh, constitutes only about 0.0013% of the total yearly consumption of primary energy in Germany, which is about  $4 \cdot 10^3$  TWh [Sta08]. Nevertheless, if it comes to absolute energy values, it would be worthwhile to strive for energy reductions even in the domain of "small" energies needed for radio communications. In doing so, two main



aspects play a role. First, the transmit power required to achieve a certain transmission quality should be as small as possible in order to reduce the interference to other radio links and the electromagnetic pollution of the environment. Second, the ratio  $\eta$  of the required transmit power and the primary, that is the DC power consumed by the transmit amplifier, should be as large as possible.  $\eta$  is termed power efficiency [Cri02], and a high  $\eta$  is desirable with respect to a long battery lifetime in mobile applications, to low cost amplifier designs, and, of course, quite generally, to energy conservation. In the last decade a bundle of approaches to reduce the required transmit power came up. These approaches include, on the physical layer, refined modulation and FEC coding schemes, precoding, interference mitigating techniques, and multi-antenna systems [DPSB08], and on the higher layers for instance the schemes of multi-hops [HF05] and busy burst detection [OHA07]. Concerning the power efficiency  $\eta$  of the transmit amplifiers, promising approaches resort to the application of nonlinear schemes [Chi35, Cox74] in combination with measures to reduce the Peak-to-Average-Power Ratio (PAPR) of the signals to be amplified.

An essential feature of real world OFDM symbols is their extension by a Cyclic Prefix (CP) which enables cost efficient processing in the receiver by FFT [vNP00, BN10]. The CP requires additional transmit energy and has an impact on the power spectral density and the PAPR of the OFDM signals. The author is well aware of these facts. However, in this thesis the CP is not considered with a view to keep the presentation of the proposed schemes and the evaluation of the system performance simple. Nevertheless, said schemes would easily lend themselves also to cases where the CP is included.

### 1.3 Goals of the thesis

The problem of power reductions in OFDM transmission has many faces and facets. A few ones of those will be addressed in this thesis, namely

- combating the detrimental impact of the frequency selective fading of the radio channels by data spreading with a view to reduce the transmit power required for a certain transmission quality,
- reduction of the PAPR by Selective Data Mapping (SDM) in order to enhance the power efficiency  $\eta$  of the transmit amplifiers, and
- joint optimization of pilot based channel estimation and data detection in order to maximize transmission quality for a given transmit power.

In order to achieve a desired performance, OFDM transmission over frequency selective fading radio channels requires a substantially larger transmit power than OFDM transmission over non-fading channels [Pro00]. Conventionally, each of the  $N_F$  OFDM subcarriers

of an OFDM symbol conveys as its complex amplitude a single data element. For the case of frequency selective fading it was proposed to mitigate the impact of fading by spreading each of said  $N_F$  data elements over all  $N_F$  OFDM subcarriers [BEL03, WZZ10]. However, we will see that this known approach to frequency diversity, which we term Full Data Spreading (FDS), would render optimum, that is Maximum Likelihood (ML) data detection [Wha71] prohibitively expensive. In the case of larger subcarrier numbers  $N_F$ , even FDS with suboptimum linear detection applying the Zero Forcing (ZF) or Minimum Mean Square Error (MMSE) rationales [Wha71] would still be excessively expensive. As a way out of this dilemma and in order to affordably seize the advantage of frequency diversity by data spreading, we propose and evaluate in this thesis the scheme Partial Data Spreading (PDS). In the case of unspread transmission, as mentioned above each of the  $N_F$  subcarriers of an OFDM symbol carries as its complex amplitude in a one-to-one relation one data element. In the case of PDS, we subdivide the  $N_F$  data elements into

$$Z = N_F/N \tag{1.1}$$

subsets of size  $N$  each. Then, we spread the  $N$  data elements of each of these subsets over a subset of  $N$  of the  $N_F$  OFDM subcarriers; therefore, we term  $N$  spreading factor. It will be shown that by properly choosing  $N$ , depending on the designer's requirements, PDS allows a balanced compromise of performance and complexity. By signaling the chosen  $N$ , the transmitter can inform the receiver on-line, if PDS is utilized. Therefore, the optional inclusion of PDS in existing and forthcoming OFDM transmission standards would entail not more than a minor extension.

It should be mentioned that our scheme PDS has certain similarity with schemes proposed in [ARDK07].

Concerning our goal of PAPR reduction, we set out from a scheme published in 1996 [BFH96, MS96]. In this scheme, the data vector constituted by the  $N_F$  data elements to be transmitted by an OFDM symbol is subjected in the transmitter to a selection of different linear transformations characterized by diagonal mapping matrices; each such transformation yields another mapped data vector. Then, for transmission, the one of these mapped data vectors is selected which yields the smallest PAPR of the transmit signal. For this scheme the term Selective Data Mapping (SDM) was coined [BFH96]. In the receiver, the mapping performed in the transmitter has to be undone based on the knowledge about which mapping matrix has been selected. This knowledge has to be forwarded from the transmitter to the receiver by signaling. In the thesis, we propose and analyze different approaches to fruitfully combining the schemes SDM and PDS. The PAPR reduction by SDM leads to OFDM symbols, the PAPR of which still depends on the data content so that the power amplifier cannot be designed and optimized for a fixed

maximum signal amplitude. We solve this problem by introducing, in addition to SDM, a specific scheme of clipping and amplitude scaling, which we term Optimum Clipping (OC).

In the receivers of OFDM transmission systems, the knowledge of the channel transfer function (CTF) for the different subcarrier frequencies is required for demodulation. This knowledge has to be made available to the receiver by sacrificing a certain portion of the  $N_F$  OFDM subcarriers for pilot transmission, which then are utilized for channel estimation [vNP00, OA07]. Due to the mobility of radio stations, the radio channels exhibit, as an undesired effect, fading which means that the CTF is time variant. In the thesis we are interested in OFDM transmission over radio channels which fade so fast that channel estimation has to be performed for each OFDM symbol anew. We investigate how in this case the available total transmit power should be subdivided into partial powers for the data carrying subcarriers and for the pilots in order to optimize transmission quality. The obtained results allow the minimization of the total transmit power required for a certain transmission quality.

This thesis basically focuses on point-to-point OFDM transmission systems. However, the above mentioned subdivision of the data elements into  $N$  subsets typical of PDS can be used to transform the point-to-point transmission into a multipoint-to-point transmission, which we for instance encounter in the uplinks of mobile radio systems. This possible extension of PDS is briefly touched in the thesis.

## 1.4 Structure of the thesis

The structure of the thesis complies with the goals formulated in Section 1.3. As the basis of the investigations to be performed in the later chapters, we introduce in Chapter 2 a generic OFDM transmission system model; in this chapter the used data formats and the considered radio channels are characterized. Chapter 3 is dedicated to combating the frequency selectivity of radio channels by PDS for the case of uncoded transmission. In Chapter 4 we extend the investigations of Chapter 3 by including the aspect of FEC encoding. The topic of Chapter 5 is the combination of PDS with SDM with a view to reduce the PAPR. In Chapter 6, we develop the above mentioned scheme OC, and we illustrate its beneficial application in combination with non-linear transmit power amplifiers (PA). Chapter 7 deals with the joint optimization of pilot based channel estimation and data detection. In Chapter 8 we extend OFDM with PDS to multipoint-to-point transmission systems, and in Chapter 9 we mention some open questions and give recommendations for further research. Finally, Chapter 10 summarizes the thesis.

Throughout the thesis we adopt the usual assumption [vNP00] that the number  $N_F$

---

of OFDM subcarriers is a power of two. Further, also the quantities  $Z$  and  $N$  in (1.1) are assumed to be powers of two. Vectors are represented by bold face lower case letters, and matrices by bold face upper case letters. Complex quantities are marked by underlining. The superscript  $*$  designates complex conjugation. In the case of vectors and matrices, the superscript  $T$  indicates transposition and the superscript  $H$  complex conjugate transposition. The symbol  $\odot$  designates the componentwise product (Schur product), and the symbol  $\otimes$  the direct product (Kronecker product) of vectors and matrices. With  $\text{diag}(\cdot)$  we designate a diagonal matrix the diagonal components of which are the components of a vector in parentheses, with  $\text{dg}(\cdot)$  a diagonal matrix the diagonal of which is the diagonal of a matrix in parentheses, and with  $\overline{\text{dg}}(\cdot)$  a matrix obtained by nulling the diagonal elements of a matrix in parentheses. The function  $\text{floor}(\cdot)$  maps a real number to the next smallest integer.

# Chapter 2

## Generic OFDM transmission model

### 2.1 System structure

Essential for the practical operation of OFDM transmission are the Inverse Fast Fourier Transformation (IFFT) on the transmit side and the Fast Fourier Transformation (FFT) on the receive side. Further, in order to enable the application of the FFT on the receive side, in the case of multipath radio channels the transmitted OFDM symbols have to be extended by a cyclic prefix. These issues are treated in detail in [vNP00] and shall not be deepened here. With regard to the investigations to be performed in this thesis, both the Fourier operations and the insertion of the cyclic prefix can be skipped, and then the OFDM system boils down to the generic structure shown in Fig. 2.1. This structure is a time discrete equivalent low-pass model of the OFDM transmission system in the frequency domain. Concerning the relations between bandpass and low-pass transformation, we refer to [SJ67]. The model of Fig. 2.1 consists of the six blocks mapper, radio channel, noise adder, phase equalizer, detector, and demapper. In Fig. 2.1 we indicate which of these blocks constitute the transmitter (Tx), the noisy radio channel (Nrc), and the receiver (Rx). Later, depending on the investigations to be performed, the model of Fig. 2.1 has to be extended by additional blocks and/or modified. In order to guarantee orthogonality of the OFDM subcarriers, the system bandwidth  $B$ , the duration  $T$  of the OFDM symbols and number  $N_F$  of subcarriers have to fulfill the relation [vNP00]

$$BT = N_F. \quad (2.1)$$

### 2.2 Information vector and transmit vector

The information to be transmitted by each OFDM symbol is constituted by the binary vector

$$\mathbf{u} = (u_1 \cdots u_{m_u} \cdots u_{N_u})^T, \quad u_{m_u} \in \{0, 1\}, \quad (2.2)$$

of  $N_u$  information bits. We term this vector information vector.  $\mathbf{u}$  of (2.2) can assume

$$Q_u = 2^{N_u} \quad (2.3)$$

different realizations  $\mathbf{u}^{\{q_u\}}$ ,  $q_u = 1 \cdots Q_u$ . To each of these realizations, a value of the superscript  $q_u$  should be assigned. Many solutions to this task exist. In our solution, we

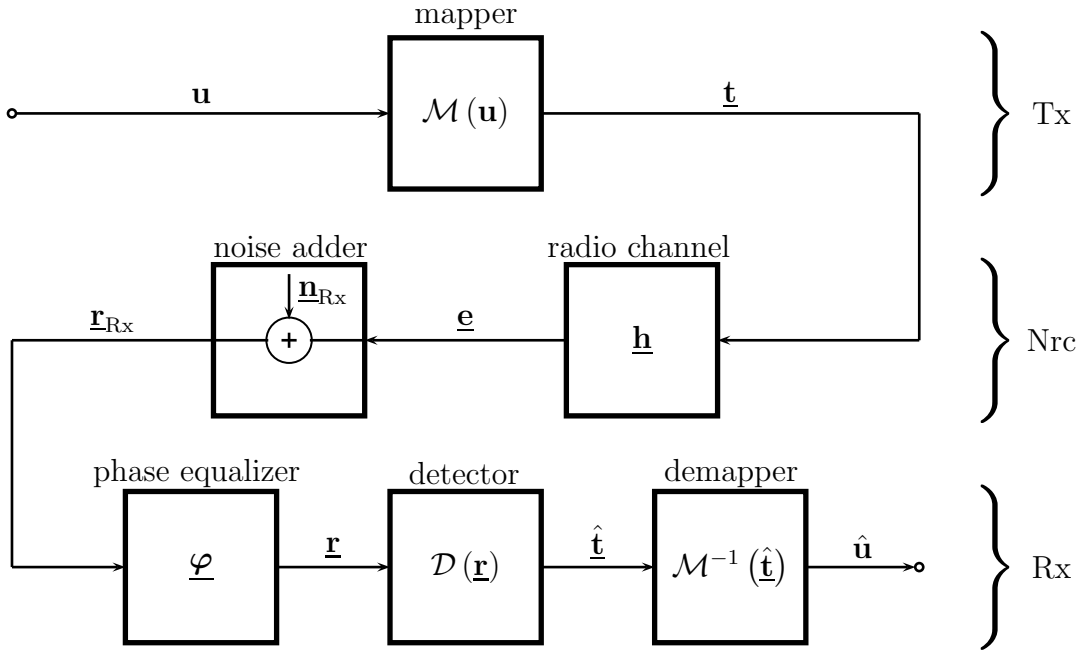


Fig. 2.1. Frequency domain low pass model of OFDM transmission

assign to a realization of  $\mathbf{u}$  given by the values of its  $N_u$  components  $u_{n_u}$  the superscript

$$q_u = 1 + \sum_{n_u=1}^{N_u} 2^{n_u-1} \cdot u_{n_u}. \quad (2.4)$$

In the model of Fig. 2.1  $\mathbf{u}$  is fed into the mapper, which, with the mapping operator  $\mathcal{M}(\cdot)$ , maps  $\mathbf{u}$  on the complex discrete valued transmit vector

$$\mathbf{t} = (t_1 \cdots t_{n_F} \cdots t_{N_F})^T = \mathcal{M}(\mathbf{u}) \quad (2.5)$$

of dimension  $N_F$  equal to the number of OFDM subcarriers. The component  $t_{n_F}$  of  $\mathbf{t}$  represents the complex amplitude of the transmitted OFDM subcarrier number  $n_F$ .

$\mathbf{t}$  of (2.5) can be expressed as

$$\mathbf{t} = \mathbf{x} + j\mathbf{y} \quad (2.6)$$

by a real part transmit vector

$$\mathbf{x} = (x_1 \cdots x_{n_F} \cdots x_{N_F})^T \quad (2.7)$$

and an imaginary part transmit vector

$$\mathbf{y} = (y_1 \cdots y_{n_F} \cdots y_{N_F})^T. \quad (2.8)$$

These two vectors are assumed to be independent of each other.

The  $N_F$  components  $x_{n_F}$  of  $\mathbf{x}$  and  $y_{n_F}$  of  $\mathbf{y}$  are both taken from the discrete valued set

$$\mathbb{V} = \{v_1 \cdots v_m \cdots v_M\} \quad (2.9)$$

of size  $M$ , which we assume to be a power of two.  $\mathbb{V}$  determines the used modulation alphabet. When the transmission system is operated, we assume that the components  $x_{n_F}$  and  $y_{n_F}$  take all  $M$  values  $v_m$  of  $\mathbb{V}$  with equal probability  $1/M$  so that the mean square magnitude of these components is

$$\sigma_t = \sqrt{\frac{1}{M} \sum_{m=1}^M v_m^2}. \quad (2.10)$$

With the number  $N_F$  of subcarriers and  $M$  of (2.9), each of the two vectors  $\mathbf{x}$  and  $\mathbf{y}$  can take on

$$Q = M^{N_F} \quad (2.11)$$

different realizations  $\mathbf{x}^{\{q_x\}}$ ,  $q_x = 1 \cdots Q$ , and  $\mathbf{y}^{\{q_y\}}$ ,  $q_y = 1 \cdots Q$ . Then, the number of possible different realizations of  $\underline{\mathbf{t}}$  of (2.6) becomes

$$\tilde{Q} = Q^2 = M^{2N_F}. \quad (2.12)$$

We assume that this number exactly equals the number  $Q_u$  of (2.3) of the occurring realizations  $\mathbf{u}^{\{q_u\}}$ ,  $q_u = 1 \cdots Q_u$ , of the information vector  $\mathbf{u}$  of (2.2), that is

$$\begin{aligned} \tilde{Q} = Q^2 = M^{2N_F} &= Q_u = 2^{N_u}, \\ 2N_F \log_2 M &= N_u. \end{aligned} \quad (2.13)$$

Then, for each realization  $\mathbf{u}^{\{q_u\}}$  of  $\mathbf{u}$  a realization

$$\underline{\mathbf{t}}^{\{\tilde{q}\}} = \mathbf{x}^{\{q_x\}} + j\mathbf{y}^{\{q_y\}} \quad (2.14)$$

of  $\underline{\mathbf{t}}$  exists, and the assignment described by the mapping operator  $\mathcal{M}(\cdot)$  of (2.5) is a unique one-to-one relation. Concerning the relation of the values of the superscripts  $q_u$  of  $\mathbf{u}^{\{q_u\}}$  and  $\tilde{q}$  of  $\underline{\mathbf{t}}^{\{\tilde{q}\}}$ , we simply choose

$$\tilde{q} = q_u. \quad (2.15)$$

For the assignment of the superscripts  $q_x$  and  $q_y$  to the superscript  $\tilde{q}$  in (2.14) many options exist. From these, we choose the version

$$\tilde{q} = \tilde{q}(q_x, q_y) = q_x + (q_y - 1) \cdot 2^{N_u/2}. \quad (2.16)$$

The quantities  $\tilde{q}$ ,  $q_x$  and  $q_y$  in the single equation (2.16) are positive integers. Therefore, for a given value  $\tilde{q}$  we can solve this equation for the two superscripts  $q_x$  and  $q_y$  and obtain

$$\begin{aligned} q_x &= \tilde{q} - \text{floor}(\tilde{q} / (2^{N_u/2} + 2^{-N_u/2})) \cdot 2^{N_u/2}, \\ q_y &= 1 + \text{floor}(\tilde{q} / (2^{N_u/2} + 2^{-N_u/2})). \end{aligned} \quad (2.17)$$

As just explained, the mapping operator  $\mathcal{M}(\cdot)$  has to assign to each realizations  $\mathbf{u}^{\{q_u\}}$ ,  $q_u = 1 \cdots Q_u$ , of  $\mathbf{u}$  of (2.2) a transmit vector  $\mathbf{t}^{\{\tilde{q}\}}$  of (2.14) with its real and imaginary part vectors  $\mathbf{x}^{\{q_x\}}$  and  $\mathbf{y}^{\{q_y\}}$ , respectively. For a given modulation alphabet various options exist to perform this assignment. In this thesis we consider the two modulation schemes QPSK and 16QAM, and we now explain which mapping options we choose for these.

In the case of QPSK we have

$$M = 2, \quad (2.18)$$

and from (2.13) follows

$$2N_F = N_u. \quad (2.19)$$

For (2.9) we choose

$$\mathbb{V} = \{-0.5, 0.5\}. \quad (2.20)$$

Then, (2.10) yields

$$\sigma_t = 1/2. \quad (2.21)$$

For the mapping operator  $\mathcal{M}(\cdot)$  of (2.5) we write

$$\begin{aligned} \mathcal{M}(\mathbf{u}) &= \mathbf{t} = \mathbf{x} + \mathbf{j}\mathbf{y} : \\ x_{n_F} &= 0.5 \cdot (-1)^{u_{n_F} + 1}, \\ y_{n_F} &= 0.5 \cdot (-1)^{u_{n_F} + N_F + 1}, \\ n_F &= 1 \cdots N_F. \end{aligned} \quad (2.22)$$

In Table 2.1 we visualize (2.22) by listing the component values  $x_1$  and  $y_1$  of  $\mathbf{x}$  and  $\mathbf{y}$ , respectively, versus the component values  $u_1$  and  $u_{1+N_F}$  of  $\mathbf{u}$ .

In the case of 16QAM we have

$$M = 4, \quad (2.23)$$

and from (2.13) follows

$$4N_F = N_u. \quad (2.24)$$



$u_1$	$u_{1+N_F}$	$x_1$	$y_1$
0	0	-0.5	-0.5
0	1	-0.5	0.5
1	0	0.5	-0.5
1	1	0.5	0.5

Table 2.1. Visualization of the mapping operator  $\mathcal{M}(\cdot)$  of (2.22) for QPSK

$u_1$	$u_2$	$u_{1+N_F}$	$u_{2+N_F}$	$x_1$	$y_1$
0	0	0	0	-1.5	-1.5
0	0	0	1	-1.5	-0.5
0	0	1	0	-1.5	1.5
0	0	1	1	-1.5	0.5
0	1	0	0	-0.5	-1.5
0	1	0	1	-0.5	-0.5
0	1	1	0	-0.5	1.5
0	1	1	1	-0.5	0.5
1	0	0	0	1.5	-1.5
1	0	0	1	1.5	-0.5
1	0	1	0	1.5	1.5
1	0	1	1	1.5	0.5
1	1	0	0	0.5	-1.5
1	1	0	1	0.5	-0.5
1	1	1	0	0.5	1.5
1	1	1	1	0.5	0.5

Table 2.2. Visualization of the mapping operator  $\mathcal{M}(\cdot)$  of (2.27) for 16QAM

For (2.9) we choose

$$\mathbb{V} = \{-1.5, -0.5, 0.5, 1.5\}. \quad (2.25)$$

Then, (2.10) yields

$$\sigma_t = \sqrt{5}/2. \quad (2.26)$$

For the mapping operator  $\mathcal{M}(\cdot)$  of (2.5) we write

$$\begin{aligned} \mathcal{M}(\mathbf{u}) &= \underline{\mathbf{t}} = \mathbf{x} + j\mathbf{y} : \\ x_{n_F} &= 0.5 \cdot (-1)^{u_{2n_F-1}+1} \cdot \mathfrak{z}^{(u_{2n_F}+1) \bmod 2}, \\ y_{n_F} &= 0.5 \cdot (-1)^{u_{N_F+2n_F-1}+1} \cdot \mathfrak{z}^{(u_{N_F+2n_F}+1) \bmod 2}, \\ n_F &= 1 \cdots N_F. \end{aligned} \quad (2.27)$$

The mapping operator  $\mathcal{M}(\cdot)$  of (2.27) performs Gray coding [Pro00]. In Table 2.2 we visualize (2.27) by listing the component values  $x_1$  and  $y_1$  of  $\mathbf{x}$  and  $\mathbf{y}$ , respectively, versus

the component values  $u_1, u_2, u_{1+N_F}$  and  $u_{2+N_F}$  of  $\mathbf{u}$ .

Inspection of (2.22) and (2.27) reveals that the components  $x_{n_F}$  of the real part vector  $\mathbf{x}$  are determined by the first  $N_u/2$  components of  $\mathbf{u}$ , whereas the components  $y_{n_F}$  of the imaginary part vector  $\mathbf{y}$  are determined by the second  $N_u/2$  components of  $\mathbf{u}$  of (2.2). By (2.22) or (2.27), respectively, to each realization  $\mathbf{u}^{\{q_u\}}$  of  $\mathbf{u}$ , a realization  $\underline{\mathbf{t}}^{\{\tilde{q}\}}$  of  $\underline{\mathbf{t}}$ , a realization  $\mathbf{x}^{\{q_x\}}$  of  $\mathbf{x}$ , and a realization  $\mathbf{y}^{\{q_y\}}$  of  $\mathbf{y}$  is assigned. Due to (2.4), (2.15) and (2.17), this assignment also includes the superscripts  $q_u, \tilde{q}, q_x$  and  $q_y$ .

## 2.3 Radio channel

### 2.3.1 Delay discrete channel model and channel impulse response (CIR) vector

In general, mobile radio channels are multipath channels. Having this physical situation in mind, the obvious channel models would be delay domain models [Pät02]. Therefore, we start channel modelling in the delay domain. Our channel models pertain to the equivalent low pass domain.

With the system bandwidth  $B$  introduced in Section 2.1 we assume both at the transmitter output and the receiver input ideal filters with the transfer function

$$\underline{G}(f) = \text{rect}\left(\frac{f - B/2}{B}\right). \quad (2.28)$$

The impulse response corresponding to this transfer function is of the type  $\sin x/x$ . Therefore, an infinitely long sequence of input Dirac impulses may lead to a non-convergent signal at the filter output [Fun79]. However, in the present thesis this convergence problem does not occur because each OFDM symbol can be represented by a finite number of such impulses.

Due to Nyquist's sampling theorem [Pro00], the channel impulse response (CIR)  $\underline{\mathbf{h}}(\tau)$  of the radio channel seen through these filters can be fully characterized by samples taken, with

$$\Delta\tau = \frac{1}{B}, \quad (2.29)$$

at the delay instants

$$\tau_w = (w - 1) \Delta\tau, \quad w = 1, 2, \dots, \quad (2.30)$$

where we do not extend on the issue of causality. We express  $\underline{\mathbf{h}}(\tau)$  as a function of the delay  $\tau$ , which is not the real time  $t$ . For the samples of  $\underline{\mathbf{h}}(\tau)$  we introduce the symbols

$$\underline{\mathbf{h}}_w = \underline{\mathbf{h}}(\tau_w). \quad (2.31)$$

These samples constitute a delay discrete model of the radio channel. (2.30) yields  $\tau_1$  equal zero, which means that we assume a vanishing basic delay [Pät02] of the delay discrete radio channel.

The physical structure of the radio channel is made up of reflecting and scattering objects in the propagation environment [Pät02]. The larger the delay  $\tau_w$  of (2.30), the farther the corresponding objects from the transmitter and receiver, and the weaker the contribution  $\underline{h}_w$  of the reflectors. Therefore, we can assume that for  $w$  larger than a maximum value  $W$  typical of the propagation environment, the samples  $\underline{h}_w$  can be set identically zero:

$$\underline{h}_w \equiv 0 \text{ for } w > W. \quad (2.32)$$

We designate the  $W$  not identically vanishing samples  $\underline{h}_w$  as relevant samples. With these, we can express the CIR as

$$\underline{h}(\tau) = \sum_{w=1}^W \underline{h}_w \frac{\sin\left(\frac{\pi}{\Delta\tau}(\tau - (w-1)\Delta\tau)\right)}{\frac{\pi}{\Delta\tau}(\tau - (w-1)\Delta\tau)}. \quad (2.33)$$

In principle, the extension of  $\underline{h}(\tau)$  of (2.33) along the  $\tau$ -axis is infinite. However, with

$$T_s = W\Delta\tau = \frac{W}{B} \quad (2.34)$$

the magnitude of  $\underline{h}(\tau)$  rapidly decreases for

$$\tau < 0 \text{ and } \tau > T_s, \quad (2.35)$$

and, therefore, we take  $T_s$  of (2.34) as the duration of  $\underline{h}(\tau)$  of (2.33).

As a further issue, an OFDM transmission system should be designed in such a way that the duration  $T_s$  of (2.34), which is equal to the required duration of the cyclic prefix mentioned earlier, should not exceed the OFDM symbol duration  $T$  [vNP00]. Then, with (2.1) and (2.34)

$$T_s = \frac{W}{B} \leq T = \frac{N_F}{B} \quad (2.36)$$

and

$$W \leq N_F \quad (2.37)$$

should hold. Throughout this thesis, we assume that (2.37) is valid.

With the  $W$  relevant CIR samples  $\underline{h}_w$  we now form the vector

$$\underline{\mathbf{h}} = \left( \underline{\mathbf{h}}_1 \cdots \underline{\mathbf{h}}_w \cdots \underline{\mathbf{h}}_W \overbrace{0 \cdots 0}^{N_F - W} \right)^T, \quad W/N_F \leq 1, \quad (2.38)$$

of dimension  $N_F$  constituted by  $W$  leading, not identically vanishing elements  $\underline{\mathbf{h}}_w$  of (2.31) followed by  $N_F - W$  zeros. We term  $\underline{\mathbf{h}}$  CIR vector.

### 2.3.2 Rayleigh fading

Due to the movements of the transmitter and/or the receiver in the propagation environment, the CIR vector  $\underline{\mathbf{h}}$  of (2.38) is time variant. As already mentioned earlier, this time variance is termed fading. Fading is constituted by the concurrence of the two different effects of slow and fast fading [vNP00]. The physical reasons behind slow fading are the emergence of new and/or the disappearance of existing shadowing objects; the well-trying countermeasure against slow fading is power control. Fast fading comes about by the constructive and/or destructive superposition of signals arriving at the receiver over different paths. In the present thesis we only deal with fast fading.

At each instant of time  $t$ , the components  $\underline{\mathbf{h}}_w$  of  $\underline{\mathbf{h}}$  take certain values, and these values constitute a realization or a snapshot of  $\underline{\mathbf{h}}$  for said time instant. In this thesis we set out from the usual assumption that within the duration  $T$  of the OFDM symbols the CIR vector  $\underline{\mathbf{h}}$  can be considered constant, because otherwise the conventional OFDM transmission scheme would fail [vNP00]. However,  $\underline{\mathbf{h}}$  may vary from OFDM symbol to OFDM symbol. A measure of the speed of this time variance is the coherence time  $T_{\text{coh}}$  of the radio channel [Pät02]. Throughout this thesis we do not consider signal processing schemes extending beyond the duration  $T$  of the individual OFDM symbols. Therefore, our investigations rely on the fact that fading is present, however, they do not depend on the value of  $T_{\text{coh}}$ . When determining average performance measures as for instance mean bit error probabilities by simulations, we consider sufficiently many independent snapshots of the CIR vector  $\underline{\mathbf{h}}$  obeying the appropriate statistics.

In this thesis we resort to the frequently made assumption that the  $W$  elements  $\underline{\mathbf{h}}_w$  of  $\underline{\mathbf{h}}$  of (2.38) are independent bivariate Gaussian quantities, even though we are aware that this assumption simplifies the physics of real world radio channels. The magnitudes of the quantities  $\underline{\mathbf{h}}_w$  are Rayleigh distributed. As just explained, fading shall not become manifest within the individual OFDM symbol. Such radio channels can be designated as fading delay discrete Deterministic Gaussian Uncorrelated Scattering (DGUS) channels [Pät02].

With the variances

$$2\sigma_{\mathbf{h},w}^2 = \mathbb{E} \left\{ \underline{\mathbf{h}}_w^* \underline{\mathbf{h}}_w \right\} = \mathbb{E} \left\{ \text{Re}^2 \left( \underline{\mathbf{h}}_w \right) \right\} + \mathbb{E} \left\{ \text{Im}^2 \left( \underline{\mathbf{h}}_w \right) \right\} \quad (2.39)$$

we obtain in the case of Rayleigh fading the bivariate Gaussian probability density functions (PDF)

$$p_{\underline{\mathbf{h}}_w} \left( \underline{\mathbf{h}}_w \right) = \frac{1}{2\pi\sigma_{\mathbf{h},w}^2} \exp \left( \frac{\underline{\mathbf{h}}_w^* \underline{\mathbf{h}}_w}{2\sigma_{\mathbf{h},w}^2} \right) \quad (2.40)$$

of the components  $\underline{\mathbf{h}}_w$  of  $\underline{\mathbf{h}}$  of (2.38). The vector

$$\boldsymbol{\sigma}_{\mathbf{h}}^2 = \left( \sigma_{\mathbf{h},1}^2 \cdots \sigma_{\mathbf{h},w}^2 \cdots \sigma_{\mathbf{h},W}^2 \overbrace{0 \cdots 0}^{N_F - W} \right)^T \quad (2.41)$$

is termed the power delay profile (PDP) of the radio channel [Pät02]. Due to the independence of the components  $\underline{\mathbf{h}}_w$ , the covariance matrix of  $\underline{\mathbf{h}}$  of (2.38), which we term CIR covariance matrix, is the diagonal matrix

$$\mathbf{R}_{\mathbf{h}} = \mathbb{E} \left( \underline{\mathbf{h}} \underline{\mathbf{h}}^H \right) = 2 \text{diag} \left( \boldsymbol{\sigma}_{\mathbf{h}}^2 \right) = 2 \begin{pmatrix} \sigma_{\mathbf{h},1}^2 & 0 & \cdots & \cdots & \cdots & \cdots & \cdots & \cdots & 0 \\ 0 & \ddots & & & & & & & \vdots \\ \vdots & & \sigma_{\mathbf{h},w}^2 & & & & & & \vdots \\ \vdots & & & \ddots & & & & & \vdots \\ \vdots & & & & \sigma_{\mathbf{h},W}^2 & & & & \vdots \\ \vdots & & & & & 0 & & & \vdots \\ \vdots & & & & & & \ddots & & \vdots \\ 0 & \cdots & \cdots & \cdots & \cdots & \cdots & \cdots & \cdots & 0 \end{pmatrix} \in \mathbb{C}^{N_F \times N_F}. \quad (2.42)$$

The elements of  $\boldsymbol{\sigma}_{\mathbf{h}}^2$  of (2.41) have the mean

$$\sigma_{\mathbf{h}}^2 = \frac{1}{W} \sum_{w=1}^W \sigma_{\mathbf{h},w}^2. \quad (2.43)$$

As a measure of the total attenuation of the radio channel, the quantity  $1/(2W\sigma_{\mathbf{h}}^2)$  is suited. In the bandpass domain the impulse response of the Rayleigh fading radio channel has the mean energy  $2W\sigma_{\mathbf{h}}^2$ . Therefore,  $2W\sigma_{\mathbf{h}}^2$  is also known as channel energy. In the case of a uniform PDP, each one of the  $W$  variances  $2\sigma_{\mathbf{h},w}^2$  of (2.39) takes on the value  $2\sigma_{\mathbf{h}}^2$ .

The larger the parameter  $W$  in  $\underline{\mathbf{h}}$  of (2.38), the more the radio channel spreads the transmitted signal along the delay axis. The generally accepted quantitative measure for this effect is the delay spread of the radio channel [Pät02], which with

$$P_M = \sum_{w=1}^W \sigma_{\mathbf{h},w}^2 \quad (2.44)$$

and

$$\mu_{2M} = \frac{1}{P_M} \sum_{w=1}^W w^2 \sigma_{\mathbf{h},w}^2 - \left[ \frac{1}{P_M} \sum_{w=1}^W w \sigma_{\mathbf{h},w}^2 \right]^2 \quad (2.45)$$

is given by

$$T_M = 2\sqrt{\mu_{2M}}. \quad (2.46)$$

$T_M$  of (2.46) is a dimensionless quantity. With the OFDM symbol duration  $T$ , we obtain from  $T_M$  the delay spread

$$T'_M = \frac{T}{N_F} T_M \quad (2.47)$$

in time units. In the case of a uniform PDP, (2.44) to (2.46) yield the delay spread

$$T_M = \sqrt{\frac{W^2 - 1}{3}}. \quad (2.48)$$

Due to (2.48), for  $W$  larger than one the delay spread  $T_M$  is virtually proportional to  $W$ , which is a plausible result.

### 2.3.3 Channel transfer function (CTF) vector and CTF matrix

In Subsections 2.3.1 and 2.3.2 we modelled the radio channel in the delay domain. However, in OFDM transmission we are primarily interested in the channel transfer function (CTF) values  $\underline{h}_{n_F}$ ,  $n_F = 1 \cdots N_F$ , of the radio channel for the  $N_F$  frequencies of the different OFDM subcarriers. This means that we, setting out from the delay domain channel model of Subsections 2.3.1 and 2.3.2, have to generate a frequency domain channel model.

We stack the CTF values  $\underline{h}_{n_F}$  in the CTF vector, which results by Fourier transformation of the CIR vector  $\underline{\mathbf{h}}$  of (2.38) with the  $N_F \times N_F$  Fourier matrix  $\underline{\mathbf{F}}^{N_F \times N_F}$  as

$$\underline{\mathbf{h}} = (\underline{h}_1 \cdots \underline{h}_{n_F} \cdots \underline{h}_{N_F})^T = \underline{\mathbf{F}}^{N_F \times N_F} \underline{\mathbf{h}}. \quad (2.49)$$

Like the CIR vector  $\underline{\mathbf{h}}$  of (2.38), the CTF vector  $\underline{\mathbf{h}}$  of (2.49) is subjected to fading. Within the individual OFDM symbol,  $\underline{\mathbf{h}}$  is, like  $\underline{\mathbf{h}}$  of (2.38), considered constant. However, the realizations of  $\underline{\mathbf{h}}$  for time instants more than the OFDM symbol duration  $T$  apart may differ from each other more or less. Snapshots of  $\underline{\mathbf{h}}$  sufficiently distant from each other

along the time axis are independent.

With the CTF vector  $\underline{\mathbf{h}}$  of (2.49) we can form the CTF matrix

$$\underline{\mathbf{H}} = \text{diag}(\underline{\mathbf{h}}) \in \mathbb{C}^{N_F \times N_F}. \quad (2.50)$$

In what follows, we aspire to express the CTF covariance matrix

$$\underline{\mathbf{R}}_{\mathbf{h}} = \text{E} \{ \underline{\mathbf{h}} \underline{\mathbf{h}}^H \} \quad (2.51)$$

of  $\underline{\mathbf{h}}$  of (2.49) by the delay domain quantities introduced in Subsection 2.3.2. To this end we substitute  $\underline{\mathbf{h}}$  of (2.49) in (2.51) and obtain with the CIR covariance matrix  $\underline{\mathbf{R}}_{\mathbf{h}}$  of (2.42)

$$\underline{\mathbf{R}}_{\mathbf{h}} = \text{E} \{ \underline{\mathbf{h}} \underline{\mathbf{h}}^H \} = \underline{\mathbf{F}}^{N_F \times N_F} \underline{\mathbf{R}}_{\mathbf{h}} (\underline{\mathbf{F}}^{N_F \times N_F})^H. \quad (2.52)$$

With the Fourier transform

$$\underline{\boldsymbol{\kappa}} = (\underline{\kappa}_1 \cdots \underline{\kappa}_{N_F})^T = \underline{\mathbf{F}}^{N_F \times N_F} \boldsymbol{\sigma}_{\mathbf{h}}^2 \quad (2.53)$$

of the PDP  $\boldsymbol{\sigma}_{\mathbf{h}}^2$  of (2.41) we can rewrite  $\underline{\mathbf{R}}_{\mathbf{h}}$  of (2.52) and obtain the Hermitean Toeplitz matrix

$$\underline{\mathbf{R}}_{\mathbf{h}} = \text{E} \{ \underline{\mathbf{h}} \underline{\mathbf{h}}^H \} = \frac{2}{\sqrt{N_F}} \begin{pmatrix} \kappa_1 & \underline{\kappa}_2^* & \underline{\kappa}_3^* & \cdots & \cdots & \underline{\kappa}_{N_F}^* \\ \underline{\kappa}_2 & \kappa_1 & \underline{\kappa}_2^* & \underline{\kappa}_3^* & \ddots & \vdots \\ \underline{\kappa}_3 & \underline{\kappa}_2 & \kappa_1 & \underline{\kappa}_2^* & \ddots & \vdots \\ \vdots & \underline{\kappa}_3 & \underline{\kappa}_2 & \kappa_1 & \ddots & \underline{\kappa}_3^* \\ \vdots & \vdots & \ddots & \ddots & \ddots & \underline{\kappa}_2^* \\ \underline{\kappa}_{N_F} & \underline{\kappa}_{N_F-1} & \cdots & \underline{\kappa}_3 & \underline{\kappa}_2 & \kappa_1 \end{pmatrix}. \quad (2.54)$$

According to (2.54), the variances of all  $N_F$  elements  $\underline{h}_{n_F}$  of  $\underline{\mathbf{h}}$  of (2.49) take the same value. With  $\boldsymbol{\sigma}_{\mathbf{h}}^2$  of (2.43) we can express this value as

$$2\sigma_{\mathbf{h}}^2 = \text{E} \{ \underline{h}_{n_F}^* \underline{h}_{n_F} \} = \frac{2}{\sqrt{N_F}} \kappa_1 = 2 \frac{W}{N_F} \sigma_{\mathbf{h}}^2. \quad (2.55)$$

We observe from (2.55) that the channel energy expressed as  $2N_F\sigma_{\mathbf{h}}^2$  in the frequency domain equals the channel energy expressed as  $2W\sigma_{\mathbf{h}}^2$  in the delay domain.

In the case of a uniform PDP and  $W$  equal to  $N_F$ ,  $\underline{\mathbf{R}}_{\mathbf{h}}$  of (2.54) becomes a diagonal matrix, which means that the CTF values  $\underline{h}_{n_F}$  of different OFDM subcarriers are uncorrelated. The more  $\boldsymbol{\sigma}_{\mathbf{h}}^2$  of (2.41) deviates from uniformity and the smaller  $W$ , the larger the correlations of the CTF values  $\underline{h}_{n_F}$ . As a rule, the correlation decreases with increasing frequency difference. A measure of the frequency difference for which the correlation

becomes negligibly small is the coherence bandwidth  $B_{\text{coh}}$ , which can be approximated with  $T'_M$  of (2.47) as [Pät02]

$$B_{\text{coh}} = \frac{1}{T'_M}. \quad (2.56)$$

## 2.4 Noise

The noise introduced by the noise adder in the model of Fig. 2.1 is characterized by the white bivariate Gaussian vector

$$\underline{\mathbf{n}}_{\text{Rx}} = (\underline{n}_{\text{Rx},1} \cdots \underline{n}_{\text{Rx},n_F} \cdots \underline{n}_{\text{Rx},N_F})^T, \quad \mathbb{E} \left( |\underline{n}_{\text{Rx},n_F}|^2 \right) = 2\sigma^2. \quad (2.57)$$

We term the realizations of  $\underline{\mathbf{n}}_{\text{Rx}}$  sometimes noise snapshots. The bandpass equivalent of  $\underline{\mathbf{n}}_{\text{Rx}}$  of (2.57) has the energy  $\sigma^2$  [SJ67].

## 2.5 Disturbed receive vector, data detection and demapping

With the transmit vector  $\underline{\mathbf{t}}$  of (2.5) and with the CTF vector  $\underline{\mathbf{h}}$  of (2.49) we obtain at the output of the radio channel in the model of Fig. 2.1 the undisturbed receive vector

$$\underline{\mathbf{e}} = \underline{\mathbf{h}} \odot \underline{\mathbf{t}}. \quad (2.58)$$

Addition of the noise vector  $\underline{\mathbf{n}}_{\text{Rx}}$  of (2.57) to  $\underline{\mathbf{e}}$  of (2.58) in the noise adder yields at the input of the phase equalizer the vector

$$\underline{\mathbf{r}}_{\text{Rx}} = \underline{\mathbf{h}} \odot \underline{\mathbf{t}} + \underline{\mathbf{n}}_{\text{Rx}}. \quad (2.59)$$

We assume throughout this thesis that the receiver has gained the knowledge of  $\underline{\mathbf{h}}$  by means of channel estimation [OA07]. With  $\underline{\mathbf{h}}$  of (2.49) we form the vector

$$\underline{\boldsymbol{\varphi}} = \left( \exp(-j \arg(\underline{h}_1)) \cdots \exp(-j \arg(\underline{h}_{n_F})) \cdots \exp(-j \arg(\underline{h}_{N_F})) \right)^T. \quad (2.60)$$

In the phase equalizer,  $\underline{\mathbf{r}}_{\text{Rx}}$  of (2.59) is elementwise multiplied with this vector. This multiplication yields with the CTF magnitude vector

$$\underline{\mathbf{h}} = (|\underline{h}_1| \cdots |\underline{h}_{n_F}| \cdots |\underline{h}_{N_F}|)^T = (h_1 \cdots h_{n_F} \cdots h_{N_F})^T \quad (2.61)$$

the vector

$$\underline{\mathbf{r}} = (\underline{r}_1 \cdots \underline{r}_{n_F} \cdots \underline{r}_{N_F})^T = \underline{\mathbf{h}} \odot \underline{\mathbf{t}} + \underline{\boldsymbol{\varphi}} \odot \underline{\mathbf{n}}_{\text{Rx}} \quad (2.62)$$



at the output of the phase equalizer. We term this vector the disturbed receive vector. With

$$\underline{\mathbf{n}} = \underline{\boldsymbol{\varphi}} \odot \underline{\mathbf{n}}_{\text{Rx}} \quad (2.63)$$

we can write (2.62) as

$$\underline{\mathbf{r}} = (\underline{r}_1 \cdots \underline{r}_{n_F} \cdots \underline{r}_{N_F})^T = \mathbf{h} \odot \underline{\mathbf{t}} + \underline{\mathbf{n}}. \quad (2.64)$$

The magnitudes of the elements of  $\underline{\boldsymbol{\varphi}}$  of (2.60) are one. Therefore, like the noise vector  $\underline{\mathbf{n}}_{\text{Rx}}$  of (2.57), also the noise vector  $\underline{\mathbf{n}}$  of (2.63) is bivariate Gaussian and white and can be displayed as

$$\underline{\mathbf{n}} = (\underline{n}_1 \cdots \underline{n}_{n_F} \cdots \underline{n}_{N_F})^T, \quad \text{E} \left( |\underline{n}_{n_F}|^2 \right) = 2\sigma^2. \quad (2.65)$$

In the receiver,  $\underline{\mathbf{r}}$  and  $\mathbf{h}$  are known, whereas  $\underline{\mathbf{t}}$  and  $\underline{\mathbf{n}}$  are unknown.

In the detector in the model of Fig. 2.1,  $\underline{\mathbf{r}}$  of (2.64) is subjected to the detection operation  $\mathcal{D}(\cdot)$ , which determines under consideration of  $\mathbf{h}$  of (2.61) the complex discrete valued estimate

$$\hat{\underline{\mathbf{t}}} = (\hat{t}_1 \cdots \hat{t}_{n_F} \cdots \hat{t}_{N_F})^T = \mathcal{D}(\underline{\mathbf{r}}) \quad (2.66)$$

of  $\underline{\mathbf{t}}$  of (2.5), which, with  $\tilde{Q}$  of (2.13), equals one of the  $\tilde{Q}$  realizations  $\underline{\mathbf{t}}^{\{\tilde{q}\}}$ ,  $\tilde{q} = 1 \cdots \tilde{Q}$ , of  $\underline{\mathbf{t}}$ . We term this realization  $\underline{\mathbf{t}}^{\{\tilde{q}'\}}$ .

The optimum detection operation would be Maximum Likelihood (ML) detection [Wha71], which yields the ML estimate

$$\begin{aligned} \hat{\underline{\mathbf{t}}} = \mathcal{D}(\underline{\mathbf{r}}) &= (\hat{t}_1 \cdots \hat{t}_{n_F} \cdots \hat{t}_{N_F})^T = \underline{\mathbf{t}}^{\{\tilde{q}'\}} = \left( \underline{t}_1^{\{\tilde{q}'\}} \cdots \underline{t}_{n_F}^{\{\tilde{q}'\}} \cdots \underline{t}_{N_F}^{\{\tilde{q}'\}} \right)^T, \\ \tilde{q}' &= \arg \min_{\tilde{q}=1 \cdots \tilde{Q}} \left\{ |\mathbf{h} \odot \underline{\mathbf{t}}^{\{\tilde{q}\}} - \underline{\mathbf{r}}| \right\}, \end{aligned} \quad (2.67)$$

of  $\underline{\mathbf{t}}$ . With the real and imaginary part vectors

$$\mathbf{r}_R = \text{Re}(\underline{\mathbf{r}}) = (r_{R,1} \cdots r_{R,n_F} \cdots r_{R,N_F})^T, \quad \mathbf{r}_I = \text{Im}(\underline{\mathbf{r}}) = (r_{I,1} \cdots r_{I,n_F} \cdots r_{I,N_F})^T, \quad (2.68)$$

of  $\underline{\mathbf{r}}$  of (2.64), with the  $Q$  equal  $M^{N_F}$  realizations  $\mathbf{x}^{\{q_x\}}$ ,  $q_x = 1 \cdots Q$ , of the real part vector  $\mathbf{x}$ , and with the  $Q$  equal  $M^{N_F}$  realizations  $\mathbf{y}^{\{q_y\}}$ ,  $q_y = 1 \cdots Q$ , of the imaginary part vector  $\mathbf{y}$ , we can split up (2.67) into a real part ML detector

$$\begin{aligned} \hat{\mathbf{x}} = \mathcal{D}(\mathbf{r}_R) &= (\hat{x}_1 \cdots \hat{x}_{n_F} \cdots \hat{x}_{N_F})^T = \mathbf{x}^{\{q'_x\}} = \left( x_1^{\{q'_x\}} \cdots x_{n_F}^{\{q'_x\}} \cdots x_{N_F}^{\{q'_x\}} \right)^T, \\ q'_x &= \arg \min_{q_x=1 \cdots Q} \left\{ |\mathbf{h} \odot \mathbf{x}^{\{q_x\}} - \mathbf{r}_R| \right\}, \end{aligned} \quad (2.69)$$

and an imaginary part ML detector

$$\hat{\mathbf{y}} = \mathcal{D}(\mathbf{r}_I) = (\hat{y}_1 \cdots \hat{y}_{n_F} \cdots \hat{y}_{N_F})^T = \mathbf{y}^{\{q'_y\}} = \left( y_1^{\{q'_y\}} \cdots y_{n_F}^{\{q'_y\}} \cdots y_{N_F}^{\{q'_y\}} \right)^T, \quad (2.70)$$

$$q'_y = \arg \min_{q_y=1 \cdots Q} \{ |\mathbf{h} \odot \mathbf{y}^{\{q_y\}} - \mathbf{r}_I| \}.$$

With  $v_m$  of (2.9), we can further disintegrate (2.69) and (2.70) into the  $2N_F$  one dimensional ML detectors

$$\begin{aligned} \hat{x}_{n_F} &= v_{m'_x}, \\ m'_x &= \arg \min_{m=1 \cdots M} \{ |h_{n_F} v_m - r_{R, n_F}| \}, \\ n_F &= 1 \cdots N_F, \end{aligned} \quad (2.71)$$

and

$$\begin{aligned} \hat{y}_{n_F} &= v_{m'_y}, \\ m'_y &= \arg \min_{m=1 \cdots M} \{ |h_{n_F} v_m - r_{I, n_F}| \}, \\ n_F &= 1 \cdots N_F. \end{aligned} \quad (2.72)$$

Obviously, ML detection becomes very inexpensive in this case.

The demapper in the model of Fig. 2.1 has the task to generate from the estimate  $\hat{\mathbf{t}}$  of (2.67) with the inverse  $\mathcal{M}^{-1}(\cdot)$  of the mapping operator  $\mathcal{M}(\cdot)$  of (2.5) an estimate

$$\hat{\mathbf{u}} = \mathcal{M}^{-1}(\hat{\mathbf{t}}) = (\hat{u}_1 \cdots \hat{u}_{n_u} \cdots \hat{u}_{N_u})^T \quad (2.73)$$

of the transmitted information vector  $\mathbf{u}$  of (2.2).

## 2.6 Bit error probabilities

The quality of the transmission can be characterized by bit error probabilities. Quite generally, these are defined as the probabilities  $P_b$  of the events that the components  $\hat{u}_{n_u}$  of the estimate  $\hat{\mathbf{u}}$  of (2.73) differ from the corresponding components  $u_{n_u}$  of the transmitted information vector  $\mathbf{u}$  of (2.2). When determining these probabilities, different modes of averaging can be chosen, which are listed in Table 2.3. In this table the subscripts of  $E\{\cdot\}$  indicate over which vectors averaging is performed. In Table 2.3 we also list the corresponding signal-to-noise ratios (SNR). In column six of Table 2.3 we show how these SNRs are determined by the chosen modulation scheme as well as by the characteristics of the radio channel and the received noise. In the case of the last row of Table 2.3, we have the SNR

$$\gamma_o = \frac{2\sigma_t^2 \sigma_h^2}{\sigma^2}. \quad (2.74)$$

This is the gross mean SNR. With the size  $M$  of the set  $\mathbb{V}$  of (2.9), the corresponding gross mean SNR per bit would be

$$\gamma_b = \frac{1}{2 \log_2 M} \gamma_o = \frac{1}{\log_2 M} \frac{\sigma_t^2 \sigma_h^2}{\sigma^2}. \quad (2.75)$$

$P_b$  depends on the chosen detection operator  $\mathcal{D}(\cdot)$  and decreases with growing SNR  $\gamma_b$ . In order to characterize the overall performance of our transmission systems, we resort in the later simulations to the case of the last row of Table 2.3. This means that we will determine

$$P_b = \frac{1}{N_u} \mathbb{E}_{\mathbf{n}, \mathbf{u}, \mathbf{h}} \left\{ (\hat{\mathbf{u}} - \mathbf{u})^T (\hat{\mathbf{u}} - \mathbf{u}) \right\} \quad (2.76)$$

depending on  $\gamma_b$  of (2.75).

	averaging over				$P_b$	SNR
	$u_{n_u}$	$\mathbf{n}$	$\mathbf{u}$	$\mathbf{h}$		
1	×				$\frac{1}{N_u} (\hat{\mathbf{u}} - \mathbf{u})^T (\hat{\mathbf{u}} - \mathbf{u})$	$\frac{\sum_{n_F=1}^{N_F}  t_{n_F} ^2 h_{n_F}^2}{\sum_{n_F=1}^{N_F}  n_{\text{Rx}, n_F} ^2}$
2	×	×			$\frac{1}{N_u} \mathbb{E}_{\mathbf{n}} \left\{ (\hat{\mathbf{u}} - \mathbf{u})^T (\hat{\mathbf{u}} - \mathbf{u}) \right\}$	$\frac{\sum_{n_F=1}^{N_F}  t_{n_F} ^2 h_{n_F}^2}{2 N_F \sigma^2}$
3	×	×	×		$\frac{1}{N_u} \mathbb{E}_{\mathbf{u}} \left\{ (\hat{\mathbf{u}} - \mathbf{u})^T (\hat{\mathbf{u}} - \mathbf{u}) \right\}$	$\frac{\sigma_t^2 \sum_{n_F=1}^{N_F} h_{n_F}^2}{N_F \sigma^2}$
4	×	×	×	×	$\frac{1}{N_u} \mathbb{E}_{\mathbf{n}, \mathbf{u}, \mathbf{h}} \left\{ (\hat{\mathbf{u}} - \mathbf{u})^T (\hat{\mathbf{u}} - \mathbf{u}) \right\}$	$\frac{2 \sigma_t^2 \sigma_h^2}{\sigma^2}$

Table 2.3. Definitions of bit error probabilities  $P_b$  and SNRs

## 2.7 Continuous time representation of OFDM symbols in the equivalent low pass domain

In this section we present an expression for the continuous time complex envelopes  $\underline{\mathbf{s}}(t)$  of the OFDM symbols. With the  $N_F \times N_F$  Fourier matrix

$$\underline{\mathbf{F}}^{N_F \times N_F} \in \mathbb{C}^{N_F \times N_F}, \quad (2.77)$$

$\underline{\mathbf{t}}$  of (2.5) yields the discrete time representation

$$\underline{\mathbf{s}} = (\underline{s}_1 \cdots \underline{s}_{n_F} \cdots \underline{s}_{N_F})^T = (\mathbf{F}^{N_F \times N_F})^{-1} \underline{\mathbf{t}} \quad (2.78)$$

of the complex envelope. With the duration  $T$  of the OFDM symbols given by (2.36) and under the assumption of a sufficiently large OFDM subcarrier number  $N_F$ , the complex envelope  $\underline{s}(t)$  rapidly decays to zero for  $|t|$  larger than  $T/2$ . Then, with the components  $\underline{s}_{n_F}$  of  $\underline{\mathbf{s}}$  of (2.78) and  $\Delta\tau$  of (2.29) the complex envelope can be expressed as

$$\underline{s}(t) = \text{rect}\left(\frac{t}{T}\right) \sum_{n_F=1}^{N_F} \underline{s}_{n_F} \frac{\sin\left(\frac{\pi}{\Delta\tau}(t - (n_F - 1)\Delta\tau)\right)}{\frac{\pi}{\Delta\tau}(t - (n_F - 1)\Delta\tau)}. \quad (2.79)$$

# Chapter 3

## Combating frequency selectivity of radio channels by partial data spreading

### 3.1 Preliminary remarks

#### 3.1.1 Impact of Rayleigh fading

In order to illustrate the detrimental impact of Rayleigh fading, we consider as examples OFDM transmission with QPSK data modulation over an AWGN radio channel on the one side and over a Rayleigh fading radio channel on the other side. We assume that, with  $\sigma_b^2$  of (2.43), both channels have the same channel energy  $2W\sigma_b^2$ . Then, the (constant) SNR per bit of the AWGN radio channel becomes equal to the (average) SNR per bit  $\gamma_b$  of (2.75) of the Rayleigh fading radio channel. In the technically interesting region of low bit error probabilities  $P_b$ , the dependence of these probabilities on  $\gamma_b$  for the transmissions over said two channels is well approximated by [Pro00]

$$P_b = \begin{cases} \frac{1}{2} \operatorname{erfc}(\sqrt{\gamma_b}) & \text{(AWGN channel),} \\ \frac{1}{2} \left[ 1 - \sqrt{\frac{\gamma_b}{1 + \gamma_b}} \right] & \text{(Rayleigh fading channel).} \end{cases} \quad (3.1)$$

Fig. 3.1 shows  $P_b$  of (3.1) versus  $\gamma_b$ , and it becomes evident that Rayleigh fading substantially impairs the transmission quality. In the present Chapter 3 we aspire to mitigate the impact of Rayleigh fading by data spreading for uncoded OFDM transmission. In Chapter 4 the combination of PDS with FEC encoding is dealt with.

#### 3.1.2 Frequency diversity by data spreading

A well known measure against the detrimental impact of frequency selectivity consists in transmitting one and the same data in parallel on different frequencies over the frequency selective channel [Pro00]. If for these frequencies the variations of the CTF values of the channel are sufficiently independent, then the receiver can improve the transmission quality by averaging over the different transmissions. This approach to combating the detrimental impact of frequency selectivity is termed frequency diversity. In the context of OFDM transmission it was proposed [WZZ10] to achieve frequency diversity by spreading each one of the  $N_F$  components  $t_{n_F}$  of the transmit vector  $\mathbf{t}$  of (2.5) occurring at the output of the the mapper over all  $N_F$  OFDM subcarriers. Because in this case all  $N_F$

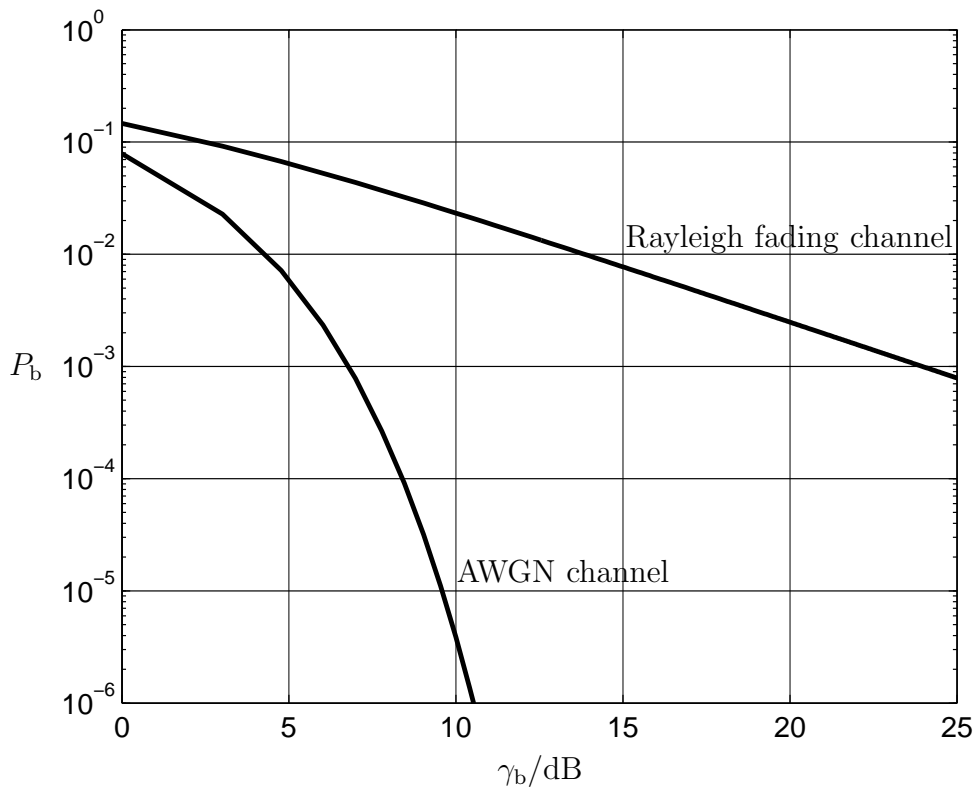


Fig. 3.1.  $P_b$  of (3.1) versus  $\gamma_b$  for the AWGN channel and the Rayleigh fading channel

OFDM subcarriers are employed for each component  $\underline{t}_{n_F}$ , we term this approach Full Data Spreading (FDS). The more independent the components  $\underline{h}_{n_F}$  of the CTF vector  $\underline{\mathbf{h}}$  of (2.49), that is the larger  $W$  in (2.38) and the delay spread  $T_M$  of (2.48), the larger the frequency diversity benefit to be expected from data spreading. Therefore,  $W$  can be considered a measure of the frequency diversity potential of the radio channel. In the case  $W$  equal one, according to (2.53) to (2.55) the components  $\underline{h}_{n_F}$  of  $\underline{\mathbf{h}}$  of (2.49) are fully correlated so that data spreading does not offer any frequency diversity advantage.

In order to perform FDS, we extend the generic model of Fig. 2.1 as shown in Fig. 3.2 by a block termed spreader. This block is characterized by an in general complex valued spreading matrix

$$\underline{\mathbf{S}} \in \mathbb{C}^{N_F \times N_F} \quad (3.2)$$

and transforms the original transmit vector  $\underline{\mathbf{t}}$  of (2.5) into the transmit vector

$$\tilde{\underline{\mathbf{t}}} = \underline{\mathbf{S}} \underline{\mathbf{t}}, \quad (3.3)$$

which we term spread transmit vector, and which is then fed into the radio channel. With a view to achieve FDS,  $\underline{\mathbf{S}}$  has to be a full matrix, because only then each component  $\underline{t}_{n_F}$  of  $\underline{\mathbf{t}}$  of (2.5) is spread over all  $N_F$  OFDM subcarriers. The columns of the spreading matrix

$\underline{\mathbf{S}}$  have the role of signatures assigned to the individual components  $\underline{t}_{n_F}$ . The signatures of different components  $\underline{t}_{n_F}$  should be as different as possible from each other. Therefore, it is advisable that  $\underline{\mathbf{S}}$  is unitary, and an  $N_F \times N_F$  Walsh-Hadamard matrix  $\mathbf{W}^{N_F \times N_F}$  would be an obvious choice for  $\underline{\mathbf{S}}$  [WZZ10]. In this case, the spreading matrix would be real valued. The concept of FDS can be considered a special version of code division multiple access (CDMA) as described in [Kle96].

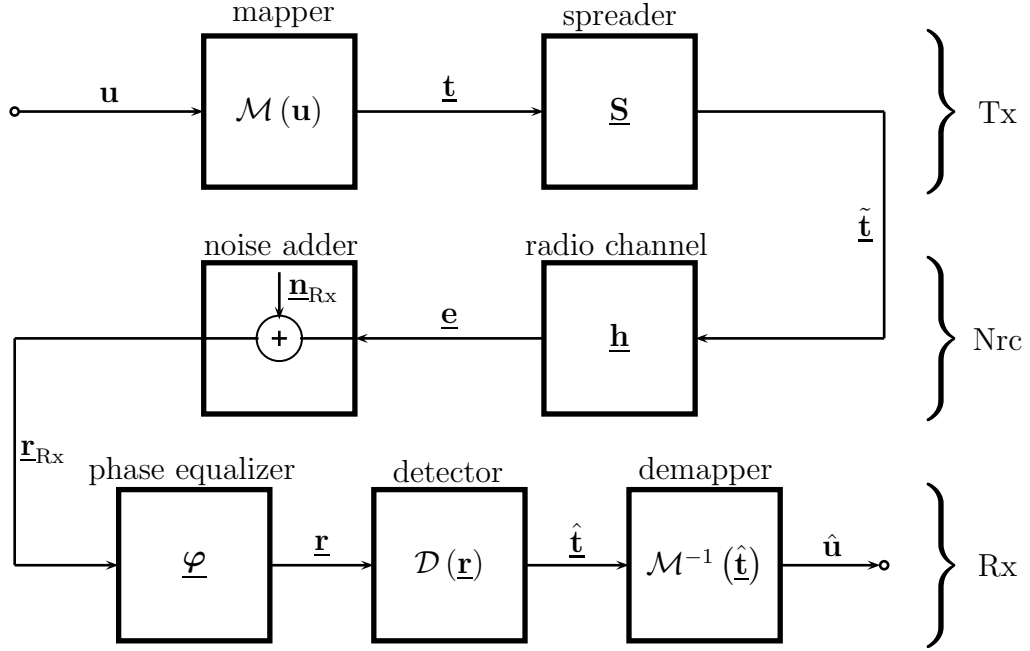


Fig. 3.2. Model of OFDM transmission with FDS

With the exception of the spreader, the transmission models of Figs. 2.1 and 3.2 are identical. However, in the case of Fig. 3.2 the detection operator  $\mathcal{D}(\cdot)$  not only needs the knowledge of the CTF magnitude vector  $\mathbf{h}$  of (2.61), but also of the employed spreading matrix  $\underline{\mathbf{S}}$  in order to enable detection. In the case of FDS, we obtain for the disturbed receive vector instead of (2.64) now

$$\underline{\mathbf{r}} = \mathbf{h} \odot \underline{\tilde{\mathbf{t}}} + \underline{\mathbf{n}} = \text{diag}(\mathbf{h}) \underline{\mathbf{S}} \underline{\mathbf{t}} + \underline{\mathbf{n}}, \quad (3.4)$$

and instead of (2.67) the ML estimate would now read

$$\begin{aligned} \mathcal{D}(\underline{\mathbf{r}}) = \hat{\underline{\mathbf{t}}} &= (\hat{t}_1 \cdots \hat{t}_{n_F} \cdots \hat{t}_{N_F})^T = \underline{\mathbf{t}}^{\{\hat{q}'\}} = \left( \hat{t}_1^{\{\hat{q}'\}} \cdots \hat{t}_{n_F}^{\{\hat{q}'\}} \cdots \hat{t}_{N_F}^{\{\hat{q}'\}} \right)^T, \\ \hat{q}' &= \arg \min_{\tilde{q}=1 \cdots \tilde{Q}} \{ |\text{diag}(\mathbf{h}) \underline{\mathbf{S}} \underline{\mathbf{t}}^{\{\tilde{q}\}} - \underline{\mathbf{r}}| \}. \end{aligned} \quad (3.5)$$

In (2.67)  $\underline{\mathbf{t}}^{\{\hat{q}'\}}$  is componentwise multiplied with the CTF magnitude vector  $\mathbf{h}$ , whereas

in (3.5)  $\underline{\mathbf{t}}^{\{\tilde{q}\}}$  has to be multiplied to the matrix  $\text{diag}(\mathbf{h})\underline{\mathbf{S}}$ , which is a full and in general complex valued matrix. Therefore, in contrast to (2.69) to (2.72), we cannot split up (3.5) correspondingly. This means that ML detection would be quite complex. In the case of larger subcarrier numbers  $N_F$ , even suboptimum linear detection of  $\underline{\mathbf{r}}$  of (3.4) by the Zero Forcing (ZF) or Minimum Mean Square Error (MMSE) schemes [Wha71, Kle96] would still be prohibitively expensive. If we choose, as above mentioned, the Walsh-Hadamard matrix  $\mathbf{W}^{N_F \times N_F}$  as a in this case real valued spreading matrix, then the matrix  $\text{diag}(\mathbf{h})\underline{\mathbf{S}}$  in (3.5) would be real valued, and ML estimation could at least be split up in analogy to (2.69) and (2.70) into one ML estimator each for the real part and imaginary part vectors  $\mathbf{x}$  and  $\mathbf{y}$  of (2.7) and (2.8), respectively; this would somewhat reduce the computational expense of ML detection in the case of FDS.

(3.5) describes the detection operator  $\mathcal{D}(\cdot)$  of the ML detector in the structure of Fig. 3.2. This operator compares the  $Q$  spread and channel distorted transmit vectors  $\underline{\mathbf{t}}$  with the disturbed receive vector  $\underline{\mathbf{r}}$  of (3.4). Instead of (3.5) three equivalent alternative inner structures of the ML detector marked by the subscripts eq, ds, and eq,ds are possible. In the case of the first alternative, we subject the disturbed receive vector  $\underline{\mathbf{r}}$  of (3.4) prior to detection to channel equalization. This yields the vector

$$\underline{\mathbf{r}}_{\text{eq}} = (\text{diag}(\mathbf{h}))^{-1} \underline{\mathbf{r}} = \underline{\mathbf{S}} \underline{\mathbf{t}} + \underbrace{(\text{diag}(\mathbf{h}))^{-1} \underline{\mathbf{n}}}_{\underline{\mathbf{n}}_{\text{eq}}}. \quad (3.6)$$

The covariance matrix of the noise vector  $\underline{\mathbf{n}}_{\text{eq}}$  in (3.6) reads

$$\underline{\mathbf{R}}_{\underline{\mathbf{n}}_{\text{eq}}} = \begin{pmatrix} \frac{2\sigma^2}{h_1^2} & 0 & \cdots & \cdots & 0 \\ 0 & \ddots & & & \vdots \\ \vdots & & \frac{2\sigma^2}{h_{n_F}^2} & & \vdots \\ \vdots & & & \ddots & 0 \\ 0 & \cdots & \cdots & 0 & \frac{2\sigma^2}{h_{N_F}^2} \end{pmatrix} \quad (3.7)$$

and is a diagonal matrix with in general unequal diagonal elements. Then, ML detection of  $\underline{\mathbf{r}}_{\text{eq}}$  of (3.6) is given by [Wha71]

$$\mathcal{D}_{\text{eq}}(\underline{\mathbf{r}}_{\text{eq}}) = \hat{\underline{\mathbf{t}}}_{\text{eq}} = (\hat{t}_{\text{eq},1} \cdots \hat{t}_{\text{eq},n_F} \cdots \hat{t}_{\text{eq},N_F})^T = \underline{\mathbf{t}}^{\{\tilde{q}'\}} = \left( \hat{t}_1^{\{\tilde{q}'\}} \cdots \hat{t}_{n_F}^{\{\tilde{q}'\}} \cdots \hat{t}_{N_F}^{\{\tilde{q}'\}} \right)^T, \quad (3.8)$$

$$\tilde{q}' = \arg \min_{\tilde{q}=1 \cdots \tilde{Q}} \left\{ (\underline{\mathbf{S}} \underline{\mathbf{t}}^{\{\tilde{q}\}} - \underline{\mathbf{r}}_{\text{eq}})^H \underline{\mathbf{R}}_{\underline{\mathbf{n}}_{\text{eq}}}^{-1} (\underline{\mathbf{S}} \underline{\mathbf{t}}^{\{\tilde{q}\}} - \underline{\mathbf{r}}_{\text{eq}}) \right\}.$$

In the case of the second alternative, we subject the disturbed receive vector  $\underline{\mathbf{r}}$  of (3.4)



prior to detection to despreading, which yields the despread receive vector

$$\mathbf{r}_{\text{ds}} = \underline{\mathbf{S}}^{-1} \mathbf{r} = \underline{\mathbf{S}}^{-1} \text{diag}(\mathbf{h}) \underline{\mathbf{S}} \mathbf{t} + \underbrace{\underline{\mathbf{S}}^{-1} \mathbf{n}}_{\mathbf{n}_{\text{ds}}}. \quad (3.9)$$

Because the spreading matrix  $\underline{\mathbf{S}}$  is unitary, the covariance matrix of noise vector  $\mathbf{n}_{\text{ds}}$  in (3.9) reads

$$\underline{\mathbf{R}}_{\mathbf{n}_{\text{ds}}} = 2\sigma^2 \mathbf{I}^{N_{\text{F}} \times N_{\text{F}}} \quad (3.10)$$

and is proportional to the unit matrix. Consequently, in analogy to (3.5) the ML estimate would now read

$$\begin{aligned} \mathcal{D}_{\text{ds}}(\mathbf{r}_{\text{ds}}) = \hat{\mathbf{t}}_{\text{ds}} &= (\hat{t}_{\text{ds},1} \cdots \hat{t}_{\text{ds},n_{\text{F}}} \cdots \hat{t}_{\text{ds},N_{\text{F}}})^{\text{T}} = \mathbf{t}^{\{\tilde{q}'\}} = \left( t_1^{\{\tilde{q}'\}} \cdots t_{n_{\text{F}}}^{\{\tilde{q}'\}} \cdots t_{N_{\text{F}}}^{\{\tilde{q}'\}} \right)^{\text{T}}, \\ \tilde{q}' &= \arg \min_{\tilde{q}=1 \cdots \tilde{Q}} \left\{ \left| \underline{\mathbf{S}}^{-1} \text{diag}(\mathbf{h}) \underline{\mathbf{S}} \mathbf{t}^{\{\tilde{q}\}} - \mathbf{r}_{\text{ds}} \right| \right\}. \end{aligned} \quad (3.11)$$

In the case of the third alternative, the disturbed receive vector  $\mathbf{r}$  of (3.4) is channel equalized and despread prior to detection, which yields the vector

$$\mathbf{r}_{\text{eq,ds}} = \underline{\mathbf{S}}^{-1} (\text{diag}(\mathbf{h}))^{-1} \mathbf{r} = \mathbf{t} + \underbrace{\underline{\mathbf{S}}^{-1} (\text{diag}(\mathbf{h}))^{-1} \mathbf{n}}_{\mathbf{n}_{\text{eq,ds}}}. \quad (3.12)$$

The covariance matrix of noise vector  $\mathbf{n}_{\text{eq,ds}}$  in (3.12) becomes

$$\underline{\mathbf{R}}_{\mathbf{n}_{\text{eq,ds}}} = (\underline{\mathbf{S}}^{-1}) \begin{pmatrix} \frac{2\sigma^2}{h_1^2} & 0 & \cdots & \cdots & 0 \\ 0 & \ddots & & & \vdots \\ \vdots & & \frac{2\sigma^2}{h_{n_{\text{F}}}^2} & & \vdots \\ \vdots & & & \ddots & 0 \\ 0 & \cdots & \cdots & 0 & \frac{2\sigma^2}{h_{N_{\text{F}}}^2} \end{pmatrix} (\underline{\mathbf{S}}^{-1})^{\text{H}}, \quad (3.13)$$

which is a full matrix. Now, the ML estimate would read similarly to (3.8)

$$\begin{aligned} \mathcal{D}_{\text{eq,ds}}(\mathbf{r}_{\text{eq,ds}}) = \hat{\mathbf{t}}_{\text{eq,ds}} &= (\hat{t}_{\text{eq,ds},1} \cdots \hat{t}_{\text{eq,ds},n_{\text{F}}} \cdots \hat{t}_{\text{eq,ds},N_{\text{F}}})^{\text{T}} = \mathbf{t}^{\{\tilde{q}'\}} = \left( t_1^{\{\tilde{q}'\}} \cdots t_{n_{\text{F}}}^{\{\tilde{q}'\}} \cdots t_{N_{\text{F}}}^{\{\tilde{q}'\}} \right)^{\text{T}}, \\ \tilde{q}' &= \arg \min_{\tilde{q}=1 \cdots \tilde{Q}} \left\{ \left( \mathbf{t}^{\{\tilde{q}\}} - \mathbf{r}_{\text{eq,ds}} \right)^{\text{H}} \underline{\mathbf{R}}_{\mathbf{n}_{\text{eq,ds}}}^{-1} \left( \mathbf{t}^{\{\tilde{q}\}} - \mathbf{r}_{\text{eq,ds}} \right) \right\}. \end{aligned} \quad (3.14)$$

These three alternatives lead to the same system performance. As a topic of future research, these alternatives could be evaluated with respect to their computational complexity. In what follows, we rely on the ML estimator of (3.5).

## 3.2 Concept of partial data spreading (PDS)

In order to overcome the complexity problem of FDS pointed out in the last section and to yet affordably seize the advantage of frequency diversity by data spreading, we revisit and further intensively investigate in this chapter the scheme of Partial Data Spreading (PDS), the basics of which can be found in [ARDK07]. As the crux of PDS, we use instead of a full spreading matrix  $\underline{\mathbf{S}}$  typical of FDS a block diagonal spreading matrix. With  $Z$  of (1.1) we choose  $Z$  diagonal blocks of dimensions  $N \times N$  each. For said blocks we propose the  $N \times N$  Walsh-Hadamard matrix  $\mathbf{W}^{N \times N}$  so that we arrive with the  $Z \times Z$  unit matrix  $\mathbf{I}^{Z \times Z}$  at the real valued spreading matrix

$$\underline{\mathbf{S}} = \mathbf{I}^{Z \times Z} \otimes \mathbf{W}^{N \times N}. \quad (3.15)$$

We term  $\mathbf{W}^{N \times N}$  partial spreading matrix. Each of the  $Z$  blocks of  $\underline{\mathbf{S}}$  spreads a subvector

$$\begin{aligned} \underline{\mathbf{t}}^{(z)} = \mathbf{x}^{(z)} + \mathbf{j}\mathbf{y}^{(z)} &= \left( \underline{t}_1^{(z)} \cdots \underline{t}_n^{(z)} \cdots \underline{t}_N^{(z)} \right)^T, \\ \underline{t}_n^{(z)} &= t_{n+(z-1)N}, \\ z &= 1 \cdots Z, \end{aligned} \quad (3.16)$$

of  $\underline{\mathbf{t}}$  of (2.5) termed partial transmit vector into a vector

$$\tilde{\underline{\mathbf{t}}}^{(z)} = \left( \tilde{t}_1^{(z)} \cdots \tilde{t}_n^{(z)} \cdots \tilde{t}_N^{(z)} \right)^T = \mathbf{W}^{N \times N} \underline{\mathbf{t}}^{(z)}, \quad z = 1 \cdots Z, \quad (3.17)$$

which we term partial spread transmit vector. We designate the parameter  $N$  in (3.15) to (3.17) as spreading factor, and we assume that  $N$  is a power of two. Due to (3.15), the spreading operation of (3.3) now disintegrates into  $Z$  partial spreading operations, and hence we term this approach PDS. The  $Z$  partial spread transmit vectors  $\tilde{\underline{\mathbf{t}}}^{(z)}$  of (3.17) yield the total spread transmit vector

$$\tilde{\underline{\mathbf{t}}} = \left( \tilde{\underline{\mathbf{t}}}^{(1)T} \cdots \tilde{\underline{\mathbf{t}}}^{(z)T} \cdots \tilde{\underline{\mathbf{t}}}^{(Z)T} \right)^T. \quad (3.18)$$

## 3.3 Transmission model

The transmission model of PDS is depicted in Fig. 3.3. This model is obtained by supplementing the transmission model of Fig. 3.2 by an interleaver on the transmit side and by a corresponding deinterleaver on the receive side. By interleaving we aspire that the  $N$  components  $\tilde{t}_n^{(z)}$  of each partial spread transmit vector  $\tilde{\underline{\mathbf{t}}}^{(z)}$  of (3.17) are commonly transmitted by  $N$  OFDM subcarriers with frequencies as far apart from each other as possible. In this way each partial spread transmit vector  $\tilde{\underline{\mathbf{t}}}^{(z)}$  attains maximum benefit

of frequency diversity. In the present Section 3.3 we consider the interleaver and the deinterleaver quite generally by the operators  $\mathcal{I}^{(N,Z)}(\cdot)$  and  $(\mathcal{I}^{(N,Z)})^{-1}(\cdot)$ , respectively. We indicate by the superscripts  $(N, Z)$  that the interleaving operator depends on the chosen spreading factor  $N$  and on the parameter  $Z$ , the latter resulting with  $N$  and  $N_F$  from (1.1). In the following Section 3.4 the operators  $\mathcal{I}^{(N,Z)}(\cdot)$  and  $(\mathcal{I}^{(N,Z)})^{-1}(\cdot)$  will be specified in detail.

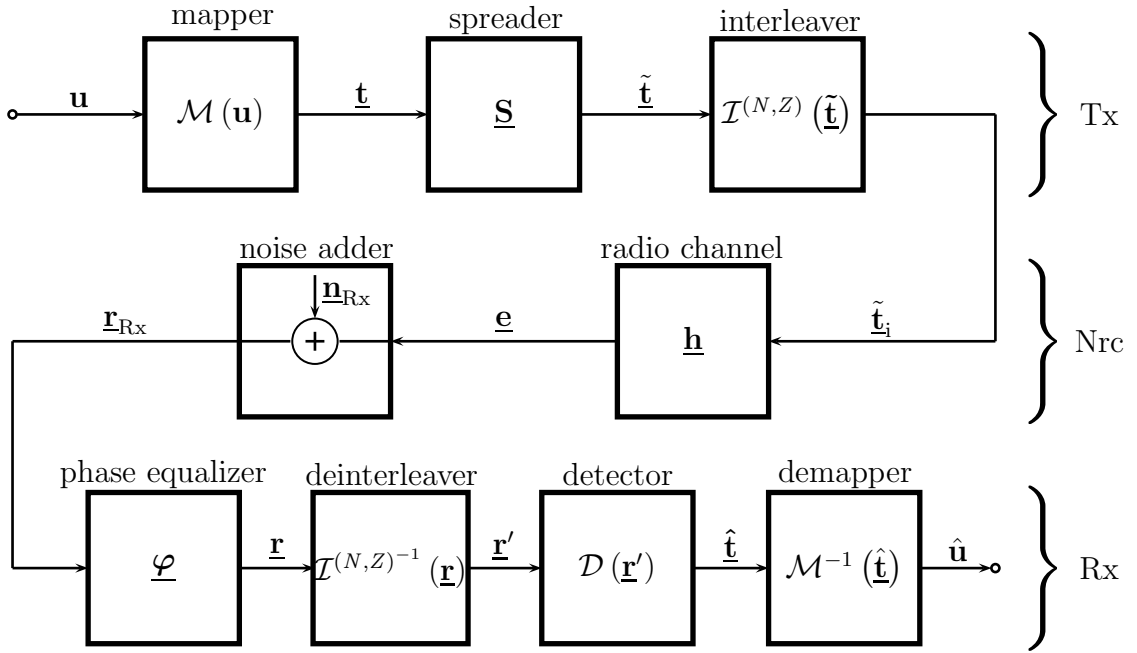


Fig. 3.3. OFDM transmission model incorporating PDS

The interleaver transforms the spread transmit vector  $\tilde{\mathbf{t}}$  of (3.18) into the interleaved spread transmit vector

$$\tilde{\mathbf{t}}_i = (\tilde{t}_{i,1} \cdots \tilde{t}_{i,n_F} \cdots \tilde{t}_{i,N_F})^T = \mathcal{I}^{(N,Z)}(\tilde{\mathbf{t}}) = \mathcal{I}^{(N,Z)}(\mathbf{S}\mathbf{t}). \quad (3.19)$$

With this vector, we obtain for the disturbed receive vector instead of (3.4) now

$$\mathbf{r} = \mathbf{h} \odot \tilde{\mathbf{t}}_i + \mathbf{n} = \mathbf{h} \odot \mathcal{I}^{(N,Z)}(\tilde{\mathbf{t}}) + \mathbf{n} = \mathbf{h} \odot \mathcal{I}^{(N,Z)}(\mathbf{S}\mathbf{t}) + \mathbf{n}. \quad (3.20)$$

$\mathbf{r}$  of (3.20) is fed into the deinterleaver, which yields at its output the “deinterleaved”

version

$$\begin{aligned} \mathbf{r}' &= \mathcal{I}^{(N,Z)^{-1}}(\mathbf{r}) = \\ \mathcal{I}^{(N,Z)^{-1}}(\mathbf{h}) \odot \mathcal{I}^{(N,Z)^{-1}}\left(\mathcal{I}^{(N,Z)}(\tilde{\mathbf{t}})\right) + \mathcal{I}^{(N,Z)^{-1}}(\mathbf{n}) &= \\ \mathcal{I}^{(N,Z)^{-1}}(\mathbf{h}) \odot \tilde{\mathbf{t}} + \mathcal{I}^{(N,Z)^{-1}}(\mathbf{n}) & \end{aligned} \quad (3.21)$$

of  $\mathbf{r}$  of (3.20). We recognize that in (3.21) the “deinterleaved” versions

$$\mathbf{h}' = (h'_{i,1} \cdots h'_{i,n_F} \cdots h'_{i,N_F})^T = \mathcal{I}^{(N,Z)^{-1}}(\mathbf{h}) \quad (3.22)$$

of the CTF magnitude vector  $\mathbf{h}$  of (2.61) and

$$\mathbf{n}' = \mathcal{I}^{(N,Z)^{-1}}(\mathbf{n}) \quad (3.23)$$

of the noise vector  $\mathbf{n}$  of (2.65) occur. With these, (3.21) can be rewritten as

$$\mathbf{r}' = \mathbf{h}' \odot \tilde{\mathbf{t}} + \mathbf{n}' = \text{diag}(\mathbf{h}') \underline{\mathbf{S}} \mathbf{t} + \mathbf{n}'. \quad (3.24)$$

The application of PDS has also implications for the detection operator  $\mathcal{D}(\cdot)$ , which will be specified in Section 3.5.

### 3.4 Interleaver and deinterleaver

We now specify the interleaving and deinterleaving operators  $\mathcal{I}^{(N,Z)}(\cdot)$  and  $(\mathcal{I}^{(N,Z)})^{-1}(\cdot)$ , respectively, introduced in Section 3.3. To this end we consider the vector

$$\mathbf{x} = (\underline{x}_1 \cdots \underline{x}_{n_F} \cdots \underline{x}_{N_F})^T \quad (3.25)$$

and arrange its  $N_F$  elements in the  $N \times Z$  matrix

$$\underline{\mathbf{X}} = \begin{pmatrix} \underline{x}_1 & \underline{x}_2 & \underline{x}_3 & \cdots & \underline{x}_Z \\ \underline{x}_{Z+1} & \underline{x}_{Z+2} & \underline{x}_{Z+3} & \cdots & \underline{x}_{2Z} \\ \underline{x}_{2Z+1} & \underline{x}_{2Z+2} & \underline{x}_{2Z+3} & \cdots & \underline{x}_{3Z} \\ \vdots & \vdots & \vdots & \ddots & \vdots \\ \underline{x}_{(N-1)Z+1} & \underline{x}_{(N-1)Z+2} & \underline{x}_{(N-1)Z+3} & \cdots & \underline{x}_{N_F} \end{pmatrix}, \quad (3.26)$$

where  $N$  and  $Z$  fulfil (1.1). Then, we take as the interleaved version of  $\mathbf{x}$  the vector

$$\underline{\mathbf{x}}_i = (\underline{x}_{i,1} \cdots \underline{x}_{i,n_F} \cdots \underline{x}_{i,N_F})^T = \mathcal{I}^{(N,Z)}(\mathbf{x}) = \text{vec}(\underline{\mathbf{X}}). \quad (3.27)$$

For deinterleaving, we arrange the  $N_F$  elements of the interleaved vector  $\underline{\mathbf{x}}_i$  of (3.27) in the  $Z \times N$  matrix

$$\underline{\mathbf{X}}_i = \begin{pmatrix} \underline{x}_{i,1} & \underline{x}_{i,Z+1} & \underline{x}_{i,2Z+1} & \cdots & \underline{x}_{i,(N-1)Z+1} \\ \underline{x}_{i,2} & \underline{x}_{i,Z+2} & \underline{x}_{i,Z+2} & \cdots & \underline{x}_{i,(N-1)Z+2} \\ \underline{x}_{i,3} & \underline{x}_{i,2Z+3} & \underline{x}_{i,2Z+3} & \cdots & \underline{x}_{i,(N-1)Z+3} \\ \vdots & \vdots & \vdots & \ddots & \vdots \\ \underline{x}_{i,Z} & \underline{x}_{i,2Z} & \underline{x}_{i,3Z} & \cdots & \underline{x}_{i,N_F} \end{pmatrix}, \quad (3.28)$$

and then obtain the deinterleaved version

$$\underline{\mathbf{x}} = (\mathcal{I}^{(N,Z)})^{-1} (\underline{\mathbf{x}}_i) = \text{vec} (\underline{\mathbf{X}}_i) \quad (3.29)$$

of  $\underline{\mathbf{x}}_i$ .

In order to improve understandability, we visualize in Fig. 3.4 the process of PDS and interleaving. The parameters chosen in this figure are  $N_F$  equal 32 and  $N$  equal four.

## 3.5 Data detection

### 3.5.1 Introduction of partial vectors in the receiver, and partial detection

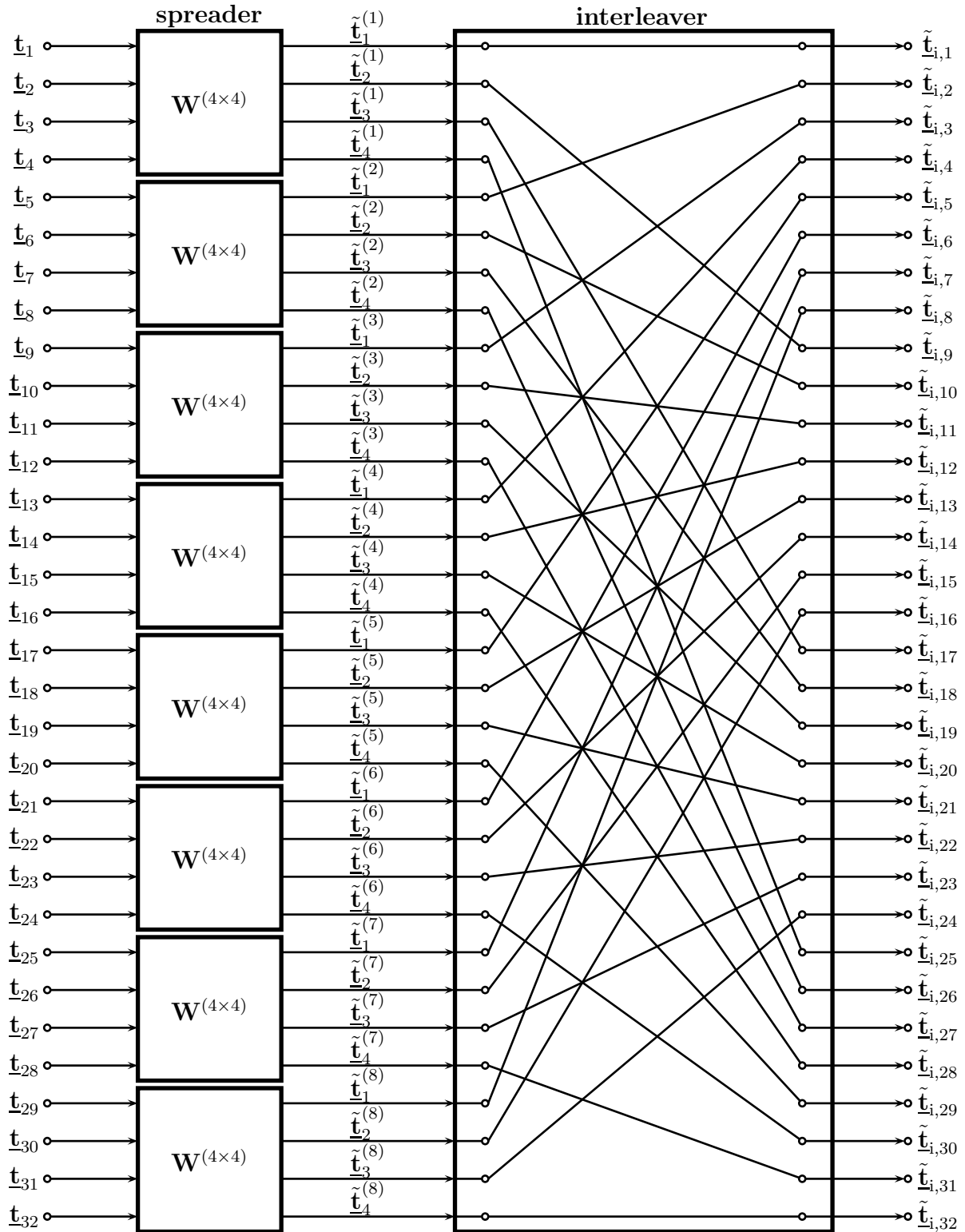
In (3.16) we split up the transmit vector  $\underline{\mathbf{t}}$  of (2.5) into  $Z$  partial transmit vectors  $\underline{\mathbf{t}}^{(z)}$ . Analogously, the vectors  $\underline{\mathbf{r}}'$ ,  $\underline{\mathbf{h}}'$ ,  $\tilde{\underline{\mathbf{t}}}$  and  $\underline{\mathbf{n}}'$  occurring in (3.24) can be split up into  $Z$  partial vectors

$$\begin{aligned} \underline{\mathbf{r}}'^{(z)} &= \left( \underline{r}'_1{}^{(z)} \cdots \underline{r}'_n{}^{(z)} \cdots \underline{r}'_N{}^{(z)} \right)^T, \\ \underline{r}'_n{}^{(z)} &= \underline{r}'_{n+(z-1)N}, \\ z &= 1 \cdots Z, \end{aligned} \quad (3.30)$$

$$\begin{aligned} \underline{\mathbf{h}}'^{(z)} &= \left( h'_1{}^{(z)} \cdots h'_n{}^{(z)} \cdots h'_N{}^{(z)} \right)^T, \\ h'_n{}^{(z)} &= h'_{n+(z-1)N}, \\ z &= 1 \cdots Z, \end{aligned} \quad (3.31)$$

$$\begin{aligned} \tilde{\underline{\mathbf{t}}}^{(z)} &= \left( \tilde{t}_1{}^{(z)} \cdots \tilde{t}_n{}^{(z)} \cdots \tilde{t}_N{}^{(z)} \right)^T, \\ \tilde{t}_n{}^{(z)} &= \tilde{t}_{n+(z-1)N}, \\ z &= 1 \cdots Z, \end{aligned} \quad (3.32)$$

and

Fig. 3.4. Visualization of PDS and interleaving,  $N_F = 32$ ,  $N = 4$

$$\begin{aligned}\underline{\mathbf{n}}^{(z)} &= \left( \underline{\mathbf{n}}_1^{(z)} \cdots \underline{\mathbf{n}}_n^{(z)} \cdots \underline{\mathbf{n}}_N^{(z)} \right)^T, \\ \underline{\mathbf{n}}_n^{(z)} &= \underline{\mathbf{n}}_{n+(z-1)N}^{(z)}, \\ z &= 1 \cdots Z,\end{aligned}\tag{3.33}$$

respectively. With these and under consideration of (3.15), (3.24) falls apart into  $Z$  partial equations

$$\underline{\mathbf{r}}^{(z)} = \mathbf{h}^{(z)} \odot \tilde{\underline{\mathbf{t}}}^{(z)} + \underline{\mathbf{n}}^{(z)} = \text{diag} \left( \mathbf{h}^{(z)} \right) \mathbf{W}^{N \times N} \underline{\mathbf{t}}^{(z)} + \underline{\mathbf{n}}^{(z)}, \quad z = 1 \cdots Z.\tag{3.34}$$

With the real valued matrix

$$\begin{aligned}\mathbf{A}^{(z)} &= \begin{pmatrix} a_{1,1} & \cdots & a_{1,n} & \cdots & a_{1,N} \\ \vdots & \ddots & & & \vdots \\ a_{n,1} & & a_{n,n} & & a_{n,N} \\ \vdots & & & \ddots & \vdots \\ a_{N,1} & \cdots & a_{N,n} & \cdots & a_{N,N} \end{pmatrix} = \text{diag} \left( \mathbf{h}^{(z)} \right) \mathbf{W}^{N \times N} = \\ &\quad \begin{pmatrix} h_1^{(z)} & 0 & \cdots & \cdots & 0 \\ 0 & \ddots & & & \vdots \\ \vdots & & h_n^{(z)} & & \vdots \\ \vdots & & & \ddots & 0 \\ 0 & \cdots & \cdots & 0 & h_N^{(z)} \end{pmatrix} \mathbf{W}^{N \times N},\end{aligned}\tag{3.35}$$

which we term partial system matrix, (3.34) can be rewritten as

$$\underline{\mathbf{r}}^{(z)} = \mathbf{h}^{(z)} \odot \tilde{\underline{\mathbf{t}}}^{(z)} + \underline{\mathbf{n}}^{(z)} = \mathbf{A}^{(z)} \underline{\mathbf{t}}^{(z)} + \underline{\mathbf{n}}^{(z)}, \quad z = 1 \cdots Z.\tag{3.36}$$

From each partial receive vector  $\underline{\mathbf{r}}^{(z)}$  of (3.36), an estimate

$$\hat{\underline{\mathbf{t}}}^{(z)} = \left( \hat{t}_1^{(z)} \cdots \hat{t}_n^{(z)} \cdots \hat{t}_N^{(z)} \right)^T\tag{3.37}$$

of the corresponding partial transmit vector  $\underline{\mathbf{t}}^{(z)}$  of (3.16) has to be determined. Keeping this partitioning in mind, the detector in the model of Fig. 3.3 has to be given the inner structure shown in Fig. 3.5. This structure consists of the three blocks splitter, partial detector, and desplitter. The splitter has the task to split up the vector  $\underline{\mathbf{r}}'$  of (3.24) into the  $Z$  partial vectors  $\underline{\mathbf{r}}^{(z)}$  of (3.30). As indicated in Fig. 3.5, the block partial detector occurs, with  $Z$  of (1.1), in a  $Z$ -fold multitude. With the size  $M$  of the set  $\mathbb{V}$  of (2.9), each of the  $Z$  partial transmit vectors  $\underline{\mathbf{t}}^{(z)}$  of (3.16) can assume

$$R = M^{2N} \quad (3.38)$$

different realizations  $\underline{\mathbf{t}}^{(z)\{r\}}$ ,  $r = 1 \cdots R$ . The  $z^{\text{th}}$  partial detector performing the detection operation  $\mathcal{D}^{(z)}(\cdot)$  has the task to determine out of the  $R$  realizations  $\underline{\mathbf{t}}^{(z)\{r\}}$ ,  $r = 1 \cdots R$ , an estimate  $\hat{\underline{\mathbf{t}}}^{(z)}$  of the sent partial transmit vector  $\underline{\mathbf{t}}^{(z)}$ .

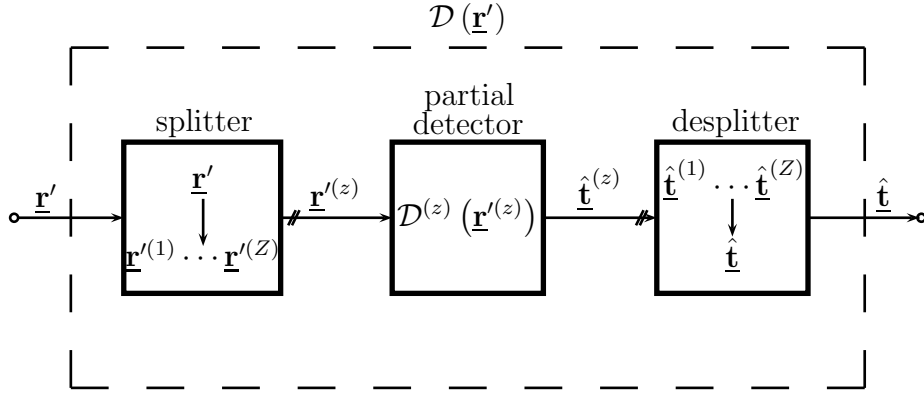


Fig. 3.5. Inner structure of detector in the OFDM transmission model of Fig. 3.3

In the desplitter, the  $Z$  estimates  $\hat{\underline{\mathbf{t}}}^{(z)}$  are composed to the estimate

$$\hat{\underline{\mathbf{t}}} = \left( \hat{\underline{\mathbf{t}}}^{(1)\text{T}} \cdots \hat{\underline{\mathbf{t}}}^{(z)\text{T}} \cdots \hat{\underline{\mathbf{t}}}^{(Z)\text{T}} \right)^{\text{T}} \quad (3.39)$$

of  $\underline{\mathbf{t}}$  of (2.5). Finally, by demapping we obtain the estimate

$$\hat{\mathbf{u}} = \mathcal{M}^{-1}(\hat{\underline{\mathbf{t}}}) \quad (3.40)$$

of the transmitted information vector  $\mathbf{u}$  of (2.2).

Analogously to (3.16), the information vector  $\mathbf{u}$  of (2.2) and its estimate  $\hat{\mathbf{u}}$  of (3.40) can be split up into the  $Z$  partial vectors

$$\begin{aligned} \mathbf{u}^{(z)} &= \left( u_1^{(z)} \cdots u_{n'}^{(z)} \cdots u_{N'}^{(z)} \right)^{\text{T}}, \\ N' &= N_u/Z, \\ u_{n'}^{(z)} &= u_{n'+(z-1)N'}, \\ z &= 1 \cdots Z, \end{aligned} \quad (3.41)$$

and



$$\begin{aligned}
 \hat{\mathbf{u}}^{(z)} &= \left( \hat{u}_1^{(z)} \cdots \hat{u}_{n'}^{(z)} \cdots \hat{u}_{N'}^{(z)} \right)^T, \\
 N' &= N_u/Z, \\
 \hat{u}_{n'}^{(z)} &= \hat{u}_{n'+(z-1)N'}, \\
 z &= 1 \cdots Z,
 \end{aligned} \tag{3.42}$$

respectively. As already indicated in connexion with (2.76), the bit error probability results by averaging. In the case of PDS with uncoded transmission over Rayleigh fading channels, the bit error probabilities  $P_b^{(z)}$  of all  $Z$  partial estimates  $\hat{\mathbf{u}}^{(z)}$  take the same value  $P_b$ , that is

$$P_b^{(z)} = P_b, \quad z = 1 \cdots Z. \tag{3.43}$$

Due to this insight, it is sufficient to consider in the simulations only one of the  $Z$  partial transmission chains from  $\mathbf{u}^{(z)}$  of (3.41) to the estimate  $\hat{\mathbf{u}}^{(z)}$  of (3.42). In this way the expense of the simulations can be significantly reduced.

In what follows we consider three different detection schemes, namely Maximum Likelihood (ML), Minimum Mean Square Error (MMSE) and Zero Forcing (ZF) detection [Wha71, Kle96, Pro00]. In order to discern the estimates obtained for the different detection schemes, we mark these estimates by the subscripts ML, MMSE and ZF, respectively.

### 3.5.2 ML detection

In order to obtain the ML estimate  $\hat{\mathbf{t}}_{\text{ML}}^{(z)}$  of  $\mathbf{t}^{(z)}$  of (3.16),  $\mathbf{r}'^{(z)}$  of (3.36) has to be checked against all  $R$  possible realizations  $\mathbf{t}^{(z)\{r\}}$ ,  $r = 1 \cdots R$ , of  $\mathbf{t}^{(z)}$ . With  $\mathbf{A}^{(z)}$  of (3.35) the realization  $\mathbf{t}^{(z)\{r'\}}$  chosen as the ML estimate is determined by [Wha71]

$$\begin{aligned}
 \hat{\mathbf{t}}_{\text{ML}}^{(z)} &= \left( \hat{t}_{\text{ML},1}^{(z)} \cdots \hat{t}_{\text{ML},n}^{(z)} \cdots \hat{t}_{\text{ML},N}^{(z)} \right)^T = \mathbf{t}^{(z)\{r'\}}, \\
 r' &= \arg \min_{r=1 \cdots R} \left\{ \left| \mathbf{A}^{(z)} \mathbf{t}^{(z)\{r\}} - \mathbf{r}'^{(z)} \right| \right\}.
 \end{aligned} \tag{3.44}$$

Because the system matrix  $\mathbf{A}^{(z)}$  in (3.44) is real valued, we can in analogy to (2.69) and (2.70) split up the ML detector of (3.44) into an real and imaginary part ML detector. We introduce the real and imaginary part vectors

$$\begin{aligned}
 \mathbf{r}'_{\text{R}}^{(z)} &= \left( r'_{\text{R},1}^{(z)} \cdots r'_{\text{R},n}^{(z)} \cdots r'_{\text{R},N}^{(z)} \right)^T = \\
 \text{Re} \left( \mathbf{r}'^{(z)} \right) &= \mathbf{A}^{(z)} \mathbf{x}^{(z)} + \text{Re} \left( \mathbf{u}^{(z)} \right),
 \end{aligned} \tag{3.45}$$

and

$$\begin{aligned} \mathbf{r}'_I(z) &= \left( r'_{I,1}(z) \cdots r'_{I,n}(z) \cdots r'_{I,N}(z) \right)^T = \\ \text{Im} \left( \underline{\mathbf{r}}'(z) \right) &= \mathbf{A}^{(z)} \mathbf{y}^{(z)} + \text{Im} \left( \underline{\mathbf{r}}'(z) \right), \end{aligned} \quad (3.46)$$

of  $\underline{\mathbf{r}}'(z)$  of (3.36) and the number

$$S = M^N \quad (3.47)$$

possible realizations  $\mathbf{x}^{(z)\{s_x\}}$ ,  $s_x = 1 \cdots S$ , and  $\mathbf{y}^{(z)\{s_y\}}$ ,  $s_y = 1 \cdots S$ , of the real and imaginary part vectors  $\mathbf{x}^{(z)}$  and  $\mathbf{y}^{(z)}$  of  $\underline{\mathbf{t}}^{(z)}$  of (3.16). Then, (3.44) can be split up into two ML detectors which yield the estimates

$$\begin{aligned} \hat{\mathbf{x}}_{\text{ML}}^{(z)} &= \mathcal{D} \left( \mathbf{r}_R^{(z)} \right) = \mathcal{D} \left( r_{R,1}^{(z)} \cdots r_{R,n}^{(z)} \cdots r_{R,N}^{(z)} \right)^T = \\ \mathbf{x}^{(z)\{s'_x\}} &= \left( x_1^{(z)\{s'_x\}} \cdots x_n^{(z)\{s'_x\}} \cdots x_N^{(z)\{s'_x\}} \right)^T, \\ s'_x &= \arg \min_{s_x=1 \cdots S} \left\{ \left| \mathbf{A}^{(z)} \mathbf{x}^{(z)\{s_x\}} - \mathbf{r}_R^{(z)} \right| \right\}, \end{aligned} \quad (3.48)$$

and

$$\begin{aligned} \hat{\mathbf{y}}_{\text{ML}}^{(z)} &= \mathcal{D} \left( \mathbf{r}_I^{(z)} \right) = \mathcal{D} \left( r_{I,1}^{(z)} \cdots r_{I,n}^{(z)} \cdots r_{I,N}^{(z)} \right)^T = \\ \mathbf{y}^{(z)\{s'_y\}} &= \left( y_1^{(z)\{s'_y\}} \cdots y_n^{(z)\{s'_y\}} \cdots y_N^{(z)\{s'_y\}} \right)^T, \\ s'_y &= \arg \min_{s_y=1 \cdots S} \left\{ \left| \mathbf{A}^{(z)} \mathbf{y}^{(z)\{s_y\}} - \mathbf{r}_I^{(z)} \right| \right\}, \end{aligned} \quad (3.49)$$

of  $\mathbf{x}^{(z)}$  and  $\mathbf{y}^{(z)}$ , respectively.

ML detection as described above immediately gives discrete valued estimates of the  $Z$  partial transmit vectors  $\underline{\mathbf{t}}^{(z)}$ , which then, by desplitting and demapping, give the estimate  $\hat{\mathbf{u}}$  of  $\mathbf{u}$  of (2.2). In the case of PDS, ML detection is less expensive than in the case of FDS. Nevertheless, ML detection encounters computational limits also in the case of PDS for larger spreading factors  $N$ . For  $N$  equal  $N_F$ , PDS would turn into FDS.

### 3.5.3 MMSE detection

The computational limits of PDS with ML detection mentioned above do not exist if we resort to PDS with MMSE detection. MMSE detection is a linear scheme, which has to be followed by quantization. We now adapt the scheme of MMSE detection [Kle96] to our OFDM transmission concept with PDS. Like in the case of ML detection, see (3.48) and (3.49), also the MMSE detector could be split up into real and imaginary part detectors. However, this obvious aspect will not be set forth in what follows.

We introduce the covariance matrix

$$\underline{\mathbf{R}}_{\mathbf{t}}^{(z)} = \mathbb{E} \left\{ \underline{\mathbf{t}}^{(z)} \underline{\mathbf{t}}^{(z)\text{H}} \right\} \quad (3.50)$$

of the partial transmit vector  $\underline{\mathbf{t}}^{(z)}$  of (3.16), and

$$\underline{\mathbf{R}}_{\mathbf{n}'}^{(z)} = \mathbb{E} \left\{ \underline{\mathbf{n}}'^{(z)} \underline{\mathbf{n}}'^{(z)\text{H}} \right\} \quad (3.51)$$

of the partial noise vector  $\underline{\mathbf{n}}'^{(z)}$  of (3.33). The averaging  $\mathbb{E}\{\cdot\}$  has to be performed in (3.50) over many realizations of the partial transmit vector  $\underline{\mathbf{t}}^{(z)}$  of (3.16), and in (3.51) over many snapshots of the partial noise vector  $\underline{\mathbf{n}}'^{(z)}$  of (3.33).

In a first step, MMSE detection yields with  $\underline{\mathbf{r}}^{(z)}$  of (3.36),  $\underline{\mathbf{R}}_{\mathbf{t}}^{(z)}$  of (3.50) and  $\underline{\mathbf{R}}_{\mathbf{n}'}^{(z)}$  of (3.51) the continuous valued estimate [Wha71, Kle96]

$$\hat{\underline{\mathbf{t}}}_{\text{MMSE,cont}}^{(z)} = \left( \hat{\underline{\mathbf{t}}}_{\text{MMSE,cont},1}^{(z)} \cdots \hat{\underline{\mathbf{t}}}_{\text{MMSE,cont},n}^{(z)} \cdots \hat{\underline{\mathbf{t}}}_{\text{MMSE,cont},N}^{(z)} \right)^{\text{T}} = \left( \mathbf{A}^{(z)\text{T}} \underline{\mathbf{R}}_{\mathbf{n}'}^{(z)-1} \mathbf{A}^{(z)} + \underline{\mathbf{R}}_{\mathbf{t}}^{(z)-1} \right)^{-1} \mathbf{A}^{(z)\text{T}} \underline{\mathbf{R}}_{\mathbf{n}'}^{(z)-1} \underline{\mathbf{r}}^{(z)} \quad (3.52)$$

of the partial transmit vector  $\underline{\mathbf{t}}^{(z)}$  of (3.16). Substitution of  $\underline{\mathbf{r}}^{(z)}$  of (3.36) in (3.52) yields

$$\begin{aligned} \hat{\underline{\mathbf{t}}}_{\text{MMSE,cont}}^{(z)} &= \\ & \left( \mathbf{A}^{(z)\text{T}} \underline{\mathbf{R}}_{\mathbf{n}'}^{(z)-1} \mathbf{A}^{(z)} + \underline{\mathbf{R}}_{\mathbf{t}}^{(z)-1} \right)^{-1} \mathbf{A}^{(z)\text{T}} \underline{\mathbf{R}}_{\mathbf{n}'}^{(z)-1} \left( \mathbf{A}^{(z)} \underline{\mathbf{t}}^{(z)} + \underline{\mathbf{n}}'^{(z)} \right) = \\ & \left( \mathbf{A}^{(z)\text{T}} \underline{\mathbf{R}}_{\mathbf{n}'}^{(z)-1} \mathbf{A}^{(z)} + \underline{\mathbf{R}}_{\mathbf{t}}^{(z)-1} \right)^{-1} \mathbf{A}^{(z)\text{T}} \underline{\mathbf{R}}_{\mathbf{n}'}^{(z)-1} \mathbf{A}^{(z)} \underline{\mathbf{t}}^{(z)} + \\ & \left( \mathbf{A}^{(z)\text{T}} \underline{\mathbf{R}}_{\mathbf{n}'}^{(z)-1} \mathbf{A}^{(z)} + \underline{\mathbf{R}}_{\mathbf{t}}^{(z)-1} \right)^{-1} \mathbf{A}^{(z)\text{T}} \underline{\mathbf{R}}_{\mathbf{n}'}^{(z)-1} \underline{\mathbf{n}}'^{(z)}. \end{aligned} \quad (3.53)$$

For the matrix expression in the third row of (3.53) we now write

$$\left( \mathbf{A}^{(z)\text{T}} \underline{\mathbf{R}}_{\mathbf{n}'}^{(z)-1} \mathbf{A}^{(z)} + \underline{\mathbf{R}}_{\mathbf{t}}^{(z)-1} \right)^{-1} \mathbf{A}^{(z)\text{T}} \underline{\mathbf{R}}_{\mathbf{n}'}^{(z)-1} \mathbf{A}^{(z)} = \underline{\mathbf{T}}^{(z)}. \quad (3.54)$$

We further rewrite the matrix expression in the last row of (3.53) under consideration of (3.54) as

$$\begin{aligned} \left( \mathbf{A}^{(z)\text{T}} \underline{\mathbf{R}}_{\mathbf{n}'}^{(z)-1} \mathbf{A}^{(z)} + \underline{\mathbf{R}}_{\mathbf{t}}^{(z)-1} \right)^{-1} \mathbf{A}^{(z)\text{T}} \underline{\mathbf{R}}_{\mathbf{n}'}^{(z)-1} &= \\ \underline{\mathbf{T}}^{(z)} \mathbf{A}^{(z)-1} &= \underline{\mathbf{N}}^{(z)}. \end{aligned} \quad (3.55)$$

With (3.54) and (3.55) we can rewrite (3.53) as [Kle96]

$$\hat{\underline{\mathbf{t}}}_{\text{MMSE,cont}}^{(z)} = \underline{\mathbf{T}}^{(z)} \underline{\mathbf{t}}^{(z)} + \underline{\mathbf{N}}^{(z)} \underline{\mathbf{n}}'^{(z)} = \underbrace{\text{dg} \left( \underline{\mathbf{T}}^{(z)} \right) \underline{\mathbf{t}}^{(z)}}_{\underline{\mathbf{t}}_{\text{u}}^{(z)}} + \underbrace{\overline{\text{dg}} \left( \underline{\mathbf{T}}^{(z)} \right) \underline{\mathbf{t}}^{(z)}}_{\underline{\mathbf{i}}^{(z)}} + \underbrace{\underline{\mathbf{N}}^{(z)} \underline{\mathbf{n}}'^{(z)}}_{\underline{\mathbf{n}}_{\text{e}}^{(z)}}. \quad (3.56)$$

In (3.56) we indicate that the estimate  $\hat{\underline{\mathbf{t}}}_{\text{MMSE,cont}}^{(z)}$  is constituted by three continuous valued vectorial components, namely the vector

$$\underline{\mathbf{t}}_{\text{u}}^{(z)} = \text{dg} \left( \underline{\mathbf{T}}^{(z)} \right) \underline{\mathbf{t}}^{(z)}, \quad (3.57)$$

which is the useful content of  $\hat{\underline{\mathbf{t}}}_{\text{MMSE,cont}}^{(z)}$ , the vector

$$\underline{\mathbf{i}}^{(z)} = \overline{\text{dg}} \left( \underline{\mathbf{T}}^{(z)} \right) \underline{\mathbf{t}}^{(z)}, \quad (3.58)$$

which represents the interference contained in  $\hat{\underline{\mathbf{t}}}_{\text{MMSE,cont}}^{(z)}$ , and the vector

$$\underline{\mathbf{n}}_{\text{e}}^{(z)} = \underline{\mathbf{N}}^{(z)} \underline{\mathbf{n}}'^{(z)}, \quad (3.59)$$

which stands for the effective noise in the estimate  $\hat{\underline{\mathbf{t}}}_{\text{MMSE,cont}}^{(z)}$  of (3.56) [Kle96].

In the context of this thesis, we assume that the  $N$  components  $\underline{t}_n^{(z)}$  of the partial transmit vector  $\underline{\mathbf{t}}^{(z)}$  are independent so that the covariance matrix of (3.50) becomes with  $\sigma_{\text{t}}$  of (2.10)

$$\underline{\mathbf{R}}_{\text{t}}^{(z)} = 2\sigma_{\text{t}}^2 \mathbf{I}^{N \times N}. \quad (3.60)$$

The operation  $\mathcal{I}^{(N,Z)^{-1}}(\underline{\mathbf{n}})$  with  $\mathcal{I}^{(N,Z)^{-1}}(\cdot)$  of (3.28) and (3.29) does not alter the statistical properties of the bivariate white Gaussian noise vector  $\underline{\mathbf{n}}$  of (2.65). Therefore, we can assume that the covariance matrix of (3.51) reads

$$\underline{\mathbf{R}}_{\text{n}'}^{(z)} = 2\sigma^2 \mathbf{I}^{N \times N}. \quad (3.61)$$

With the covariance matrices of (3.60) and (3.61) the expressions (3.54) and (3.55) can be simplified as follows:

$$\underline{\mathbf{T}}^{(z)} = \left( \mathbf{A}^{(z)\text{T}} \mathbf{A}^{(z)} + \frac{\sigma^2}{\sigma_{\text{t}}^2} \mathbf{I}^{N \times N} \right)^{-1} \mathbf{A}^{(z)\text{T}} \mathbf{A}^{(z)} \quad (3.62)$$

and

$$\underline{\mathbf{N}}^{(z)} = \underline{\mathbf{T}}^{(z)} \mathbf{A}^{(z)^{-1}} = \left( \mathbf{A}^{(z)\text{T}} \mathbf{A}^{(z)} + \frac{\sigma^2}{\sigma_{\text{t}}^2} \mathbf{I}^{N \times N} \right)^{-1} \mathbf{A}^{(z)\text{T}}. \quad (3.63)$$

By substituting of  $\mathbf{A}^{(z)}$  of (3.35) in (3.62) and invoking the principle of Eigenvalue decomposition (EVD) [Mar87], we obtain

$$\begin{aligned}
\underline{\mathbf{T}}^{(z)} = & \left( \mathbf{W}^{N \times N} \left( \begin{array}{cccccc} h_1'^{(z)^2} + \frac{\sigma^2}{\sigma_t^2} & 0 & \cdots & \cdots & 0 & \\ 0 & \ddots & & & \vdots & \\ \vdots & & h_n'^{(z)^2} + \frac{\sigma^2}{\sigma_t^2} & & \vdots & \\ \vdots & & & \ddots & 0 & \\ 0 & \cdots & \cdots & 0 & h_N'^{(z)^2} + \frac{\sigma^2}{\sigma_t^2} & \end{array} \right) \mathbf{W}^{N \times N} \right)^{-1} \times \\
& \mathbf{W}^{N \times N} \left( \begin{array}{cccccc} h_1^{(z)} & 0 & \cdots & \cdots & 0 & \\ 0 & \ddots & & & \vdots & \\ \vdots & & h_n^{(z)} & & \vdots & \\ \vdots & & & \ddots & 0 & \\ 0 & \cdots & \cdots & 0 & h_N^{(z)} & \end{array} \right) \mathbf{W}^{N \times N} = \\
& \mathbf{W}^{N \times N} \left( \begin{array}{cccccc} \frac{h_1'^{(z)^2}}{h_1'^{(z)^2} + \frac{\sigma^2}{\sigma_t^2}} & 0 & \cdots & \cdots & 0 & \\ \frac{h_1'^{(z)^2}}{h_1'^{(z)^2} + \frac{\sigma^2}{\sigma_t^2}} & 0 & \cdots & \cdots & 0 & \\ 0 & \ddots & & & \vdots & \\ \vdots & & \frac{h_n'^{(z)^2}}{h_n'^{(z)^2} + \frac{\sigma^2}{\sigma_t^2}} & & \vdots & \\ \vdots & & \frac{h_n'^{(z)^2}}{h_n'^{(z)^2} + \frac{\sigma^2}{\sigma_t^2}} & & \vdots & \\ \vdots & & & \ddots & 0 & \\ 0 & \cdots & \cdots & 0 & \frac{h_N'^{(z)^2}}{h_N'^{(z)^2} + \frac{\sigma^2}{\sigma_t^2}} & \end{array} \right) \mathbf{W}^{N \times N}.
\end{aligned} \tag{3.64}$$

For (3.63) we get with the system matrix  $\mathbf{A}^{(z)}$  of (3.35) and  $\mathbf{T}^{(z)}$  of (3.64)

$$\begin{aligned}
 \underline{\mathbf{N}}^{(z)} = \mathbf{W}^{N \times N} & \begin{pmatrix} \frac{h_1'^{(z)^2}}{h_1'^{(z)^2} + \frac{\sigma^2}{\sigma_t^2}} & 0 & \cdots & \cdots & 0 \\ 0 & \ddots & & & \vdots \\ \vdots & & \frac{h_n'^{(z)^2}}{h_n'^{(z)^2} + \frac{\sigma^2}{\sigma_t^2}} & & \vdots \\ \vdots & & & \ddots & 0 \\ 0 & \cdots & \cdots & 0 & \frac{h_N'^{(z)^2}}{h_N'^{(z)^2} + \frac{\sigma^2}{\sigma_t^2}} \end{pmatrix} \mathbf{W}^{N \times N} \times \\
 & \mathbf{W}^{N \times N} \begin{pmatrix} h_1^{(z)} & 0 & \cdots & \cdots & 0 \\ 0 & \ddots & & & \vdots \\ \vdots & & h_n^{(z)} & & \vdots \\ \vdots & & & \ddots & 0 \\ 0 & \cdots & \cdots & 0 & h_N^{(z)} \end{pmatrix}^{-1} = \quad (3.65) \\
 & \mathbf{W}^{N \times N} \begin{pmatrix} \frac{h_1^{(z)}}{h_1'^{(z)^2} + \frac{\sigma^2}{\sigma_t^2}} & 0 & \cdots & \cdots & 0 \\ 0 & \ddots & & & \vdots \\ \vdots & & \frac{h_n^{(z)}}{h_n'^{(z)^2} + \frac{\sigma^2}{\sigma_t^2}} & & \vdots \\ \vdots & & & \ddots & 0 \\ 0 & \cdots & \cdots & 0 & \frac{h_N^{(z)}}{h_N'^{(z)^2} + \frac{\sigma^2}{\sigma_t^2}} \end{pmatrix} .
 \end{aligned}$$

In what follows, we will show that the useful partial vector of (3.57) can be written with a real valued positive scalar  $a^{(z)}$  as

$$\underline{\mathbf{t}}_{\mathbf{u}}^{(z)} = \text{dg} \left( \underline{\mathbf{T}}^{(z)} \right) \underline{\mathbf{t}}^{(z)} = a^{(z)} \underline{\mathbf{t}}^{(z)}. \quad (3.66)$$

We will further show that the diagonal matrix consisting of the diagonal elements of the covariance matrix of the interference vector  $\underline{\mathbf{i}}^{(z)}$  of (3.58) can be expressed with the interference variance  $\sigma_{\mathbf{i}}^{(z)^2}$  as

$$\begin{aligned} & \text{dg} \left( \mathbb{E} \left\{ \underline{\mathbf{i}}^{(z)} \underline{\mathbf{i}}^{(z)\text{H}} \right\} \right) = \\ & \text{dg} \left( \overline{\text{dg}} \left( \underline{\mathbf{T}}^{(z)} \right) \mathbb{E} \left\{ \underline{\mathbf{t}}^{(z)} \underline{\mathbf{t}}^{(z)\text{H}} \right\} \overline{\text{dg}} \left( \underline{\mathbf{T}}^{(z)\text{H}} \right) \right) = \\ & 2\sigma_{\mathbf{t}}^2 \text{dg} \left( \overline{\text{dg}} \left( \underline{\mathbf{T}}^{(z)} \right) \overline{\text{dg}} \left( \underline{\mathbf{T}}^{(z)\text{H}} \right) \right) = 2\sigma_{\mathbf{i}}^{(z)^2} \mathbf{I}^{N \times N}. \end{aligned} \quad (3.67)$$

Finally, we will show that the diagonal matrix consisting of the diagonal elements of the covariance matrix of the effective noise vector  $\underline{\mathbf{n}}_{\mathbf{e}}^{(z)}$  of (3.59) can be expressed with the noise variance  $\sigma_{\mathbf{n}_e}^{(z)^2}$  as

$$\begin{aligned} & \text{dg} \left( \mathbb{E} \left\{ \underline{\mathbf{n}}_{\mathbf{e}}^{(z)} \underline{\mathbf{n}}_{\mathbf{e}}^{(z)\text{H}} \right\} \right) = \\ & \text{dg} \left( \underline{\mathbf{N}}^{(z)} \mathbb{E} \left\{ \underline{\mathbf{n}}'^{(z)} \underline{\mathbf{n}}'^{(z)\text{H}} \right\} \underline{\mathbf{N}}^{(z)\text{H}} \right) = 2\sigma^2 \text{dg} \left( \underline{\mathbf{N}}^{(z)} \underline{\mathbf{N}}^{(z)\text{H}} \right) = 2\sigma_{\mathbf{n}_e}^{(z)^2} \mathbf{I}^{N \times N}. \end{aligned} \quad (3.68)$$

In what follows, we derive expressions for the determination of the three quantities  $a^{(z)}$ ,  $\sigma_{\mathbf{i}}^{(z)^2}$  and  $\sigma_{\mathbf{n}_e}^{(z)^2}$  occurring in (3.66), (3.67) and (3.68), respectively.

First, we address the determination of  $a^{(z)}$  in (3.66). Inspection of (3.64) reveals that all  $N$  diagonal elements of the matrix  $\underline{\mathbf{T}}^{(z)}$  take the same real value  $\frac{1}{N} \sum_{n=1}^N \frac{h'_n{}^{(z)^2}}{h_n'^{(z)^2} + \sigma^2/\sigma_{\mathbf{t}}^2}$  so that we can rewrite (3.66) as

$$\underline{\mathbf{t}}_{\mathbf{u}}^{(z)} = \frac{1}{N} \sum_{n=1}^N \frac{h'_n{}^{(z)^2}}{h_n'^{(z)^2} + \sigma^2/\sigma_{\mathbf{t}}^2} \underline{\mathbf{t}}^{(z)} \quad (3.69)$$

and obtain

$$a^{(z)} = \frac{1}{N} \sum_{n=1}^N \frac{h'_n{}^{(z)^2}}{h_n'^{(z)^2} + \sigma^2/\sigma_{\mathbf{t}}^2}. \quad (3.70)$$

Concerning the determination of  $\sigma_{\mathbf{i}}^{(z)^2}$  in (3.67), we write with  $\underline{\mathbf{T}}^{(z)}$  of (3.64) and  $a^{(z)}$  of (3.70)

$$\begin{aligned}
\overline{\text{dg}}\left(\mathbf{T}^{(z)}\right) &= \mathbf{T}^{(z)} - \text{dg}\left(\mathbf{T}^{(z)}\right) = \mathbf{T}^{(z)} - a^{(z)}\mathbf{I}^{N \times N} = \mathbf{W}^{N \times N} \times \\
&\left( \begin{array}{cccccc}
\frac{h_1^{(z)^2}}{h_1^{(z)^2} + \frac{\sigma^2}{\sigma_t^2}} - a^{(z)} & 0 & \dots & \dots & 0 \\
0 & \ddots & & & \vdots \\
\vdots & & \frac{h_n^{(z)^2}}{h_n^{(z)^2} + \frac{\sigma^2}{\sigma_t^2}} - a^{(z)} & & \vdots \\
\vdots & & & \ddots & 0 \\
0 & \dots & \dots & 0 & \frac{h_N^{(z)^2}}{h_N^{(z)^2} + \frac{\sigma^2}{\sigma_t^2}} - a^{(z)}
\end{array} \right) \mathbf{W}^{N \times N} = \\
&\mathbf{W}^{N \times N} \times \\
&\left( \begin{array}{cccccc}
\frac{(1 - a^{(z)}) h_1^{(z)^2} - a^{(z)} \frac{\sigma^2}{\sigma_t^2}}{h_1^{(z)^2} + \frac{\sigma^2}{\sigma_t^2}} & 0 & \dots & \dots & 0 \\
0 & \ddots & & & \vdots \\
\vdots & & \frac{(1 - a^{(z)}) h_n^{(z)^2} - a^{(z)} \frac{\sigma^2}{\sigma_t^2}}{h_n^{(z)^2} + \frac{\sigma^2}{\sigma_t^2}} & 0 & \vdots \\
\vdots & & & \ddots & 0 \\
0 & \dots & \dots & 0 & \frac{(1 - a^{(z)}) h_N^{(z)^2} - a^{(z)} \frac{\sigma^2}{\sigma_t^2}}{h_N^{(z)^2} + \frac{\sigma^2}{\sigma_t^2}}
\end{array} \right) \times \\
&\mathbf{W}^{N \times N}.
\end{aligned} \tag{3.71}$$

With  $\overline{\text{dg}}\left(\mathbf{T}^{(z)}\right)$  of (3.71) we can write in (3.67)

$$\text{dg}\left(\overline{\text{dg}}\left(\mathbf{T}^{(z)}\right)\overline{\text{dg}}\left(\mathbf{T}^{(z)\text{H}}\right)\right) = \frac{1}{N} \sum_{n=1}^N \left( \frac{(1 - a^{(z)}) h_n^{(z)^2} - a^{(z)} \sigma^2 / \sigma_t^2}{h_n^{(z)^2} + \sigma^2 / \sigma_t^2} \right)^2 \mathbf{I}^{N \times N} \tag{3.72}$$



so that we obtain

$$\sigma_i^{(z)^2} = \sigma_t^2 \frac{1}{N} \sum_{n=1}^N \left( \frac{(1 - a^{(z)}) h_n'^{(z)^2} - a^{(z)} \sigma^2 / \sigma_t^2}{h_n'^{(z)^2} + \sigma^2 / \sigma_t^2} \right)^2. \quad (3.73)$$

With  $\underline{\mathbf{N}}^{(z)}$  of (3.65) we can write in (3.68)

$$\mathbf{W}^{N \times N} \left( \underline{\mathbf{N}}^{(z)} \underline{\mathbf{N}}^{(z)H} = \begin{pmatrix} \frac{h_1'^{(z)}}{h_1'^{(z)^2} + \sigma^2 / \sigma_t^2} & 0 & \dots & \dots & 0 \\ 0 & \ddots & & & \vdots \\ \vdots & & \frac{h_n'^{(z)}}{h_n'^{(z)^2} + \sigma^2 / \sigma_t^2} & & \vdots \\ \vdots & & & \ddots & 0 \\ 0 & \dots & \dots & 0 & \frac{h_N'^{(z)}}{h_N'^{(z)^2} + \sigma^2 / \sigma_t^2} \end{pmatrix} \right)^2 \mathbf{W}^{N \times N}. \quad (3.74)$$

All diagonal elements of this matrix assume the same value  $\frac{1}{N} \sum_{n=1}^N \left( \frac{h_n'^{(z)}}{h_n'^{(z)^2} + \sigma^2 / \sigma_t^2} \right)^2$ .

Therefore, we obtain from (3.68) with (3.74)

$$\sigma_{ne}^{(z)^2} = \sigma^2 \frac{1}{N} \sum_{n=1}^N \left( \frac{h_n'^{(z)}}{h_n'^{(z)^2} + \sigma^2 / \sigma_t^2} \right)^2. \quad (3.75)$$

$a^{(z)}$  of (3.70) is in general not equal one. Therefore, the useful constituent  $\underline{\mathbf{t}}_u^{(z)}$  of (3.66) of the estimate  $\hat{\underline{\mathbf{t}}}_{\text{MMSE,cont}}^{(z)}$  is biased. By scaling of  $\underline{\mathbf{t}}_u^{(z)}$  with  $a^{(z)}$  of (3.70) we arrive at the unbiased continuous valued version

$$\underline{\mathbf{t}}_{u,\text{unbiased}}^{(z)} = \underline{\mathbf{t}}_u^{(z)} / a^{(z)} \quad (3.76)$$

of  $\underline{\mathbf{t}}_u^{(z)}$ . Finally, quantization of  $\underline{\mathbf{t}}_{u,\text{unbiased}}^{(z)}$  of (3.76) with the quantization operator  $\mathcal{Q}(\cdot)$  determined by the Voronoi regions [FJ89] given by the set  $\mathbb{V}$  of (2.9) yields the discrete valued estimate

$$\hat{\underline{\mathbf{t}}}^{(z)} = \mathcal{Q} \left( \underline{\mathbf{t}}_{u,\text{unbiased}}^{(z)} \right) \quad (3.77)$$

of  $\underline{\mathbf{t}}^{(z)}$  of (3.16). In the special case of QPSK data modulation, the scaling of (3.76) would not be necessary, because only the signs of the real and imaginary parts of the components of  $\underline{\mathbf{t}}_{u,\text{unbiased}}^{(z)}$  play a role.

$\sigma_t$  of (2.10),  $a^{(z)}$  of (3.70),  $\sigma_i^{(z)^2}$  of (3.73) and  $\sigma_{ne}^{(z)^2}$  of (3.75) yield the effective signal-

to-noise-plus-interference ratio (SNIR) [Kle96]

$$\gamma_{\text{MMSE,effect}}^{(z)} = \frac{a^{(z)^2} \sigma_t^2}{\sigma_{n_e}^{(z)^2} + \sigma_i^{(z)^2}} \quad (3.78)$$

of the components  $\hat{\mathbf{t}}_{\text{MMSE,cont},n}^{(z)}$  of the estimate  $\hat{\mathbf{t}}_{\text{MMSE,cont}}^{(z)}$  of (3.52). From (3.78) results with the size  $M$  of the set  $\mathbb{V}$  of (2.9) the effective SNIR

$$\gamma_{\text{b,MMSE,effect}}^{(z)} = \frac{1}{2 \log_2 M} \cdot \frac{a^{(z)^2} \sigma_t^2}{\sigma_{n_e}^{(z)^2} + \sigma_i^{(z)^2}} \quad (3.79)$$

per bit. By the attribute ‘‘effect’’ in the subscripts of the SNIRs of (3.78) and (3.79), we indicate that these SNIRs determine the error probabilities.

Under the assumptions that the interference vector  $\mathbf{i}^{(z)}$  of (3.58) is bivariate Gaussian and that the effective SNIR per bit of (3.79) is sufficiently large, we obtain for the bit error probabilities the expressions [HCC<sup>+</sup>01]

$$P_b^{(z)} \left( \gamma_{\text{b,MMSE,effect}}^{(z)} \right) = \begin{cases} \frac{1}{2} \text{erfc} \left( \sqrt{\gamma_{\text{b,MMSE,effect}}^{(z)}} \right) & \text{for QPSK,} \\ \frac{3}{8} \text{erfc} \left( \sqrt{0.4 \gamma_{\text{b,MMSE,effect}}^{(z)}} \right) & \text{for 16QAM.} \end{cases} \quad (3.80)$$

The assumption of a Gaussian  $\mathbf{i}^{(z)}$  is not exactly fulfilled, because the partial data vectors  $\mathbf{t}^{(z)}$  of (3.16) are discrete valued. However, in Subsubsection 3.6.3.1 we will show by a simulation example that this assumption is justified.

$\gamma_{\text{b,MMSE,effect}}^{(z)}$  of (3.79), and, therefore, the bit error probability  $P_b^{(z)} \left( \gamma_{\text{b,MMSE,effect}}^{(z)} \right)$  of (3.80) hold for the case of averaging over many snapshots of  $\mathbf{t}^{(z)}$  and of  $\mathbf{u}^{(z)}$  for a given snapshot of the CTF magnitude vector  $\mathbf{h}'^{(z)}$  of (3.31). Therefore, (3.79) and (3.80) correspond to the case of row three of Table 2.3. In the case of Rayleigh fading radio channels considered in this thesis, averaging of  $P_b^{(z)} \left( \gamma_{\text{b,MMSE,effect}}^{(z)} \right)$  of (3.80) over sufficiently many snapshots of the CTF magnitude vector  $\mathbf{h}'^{(z)}$  yields, with the pdf  $p_{\gamma_b} \left( \gamma_{\text{b,MMSE,effect}}^{(z)} \right)$  of  $\gamma_{\text{b,MMSE,effect}}^{(z)}$  of (3.79), the mean bit error probability

$$P_b = \int_0^\infty P_b^{(z)} \left( \gamma_{\text{b,MMSE,effect}}^{(z)} \right) p_{\gamma_b} \left( \gamma_{\text{b,MMSE,effect}}^{(z)} \right) d \left( \gamma_{\text{b,MMSE,effect}}^{(z)} \right). \quad (3.81)$$

Following the argument presented at the end of Subsection 3.5.1, and as indicated by omitting the superscript  $(z)$  of  $P_b$ , of (3.81) holds likewise for all  $Z$  partial information vectors  $\mathbf{u}^{(z)}$  of (3.41) and, in order to describe the system performance, should be depicted

versus the mean SNIR per bit

$$\gamma_b = \int_0^\infty p_{\gamma_b} \left( \gamma_{b,\text{MMSE}}^{(z)} \right) d \left( \gamma_{b,\text{MMSE}}^{(z)} \right). \quad (3.82)$$

The pdf  $p_{\gamma_b} \left( \gamma_{b,\text{MMSE,effct}}^{(z)} \right)$  in (3.81) is determined by the chosen modulation scheme as well as by the parameters  $W$  in (2.38) and  $\gamma_o$  of (2.74).

### 3.5.4 ZF detection

In order to obtain the continuous valued ZF estimate of  $\underline{\mathbf{t}}^{(z)}$ , we have to omit in (3.52) the matrix  $\underline{\mathbf{R}}_{\mathbf{t}}^{(z)-1}$ , which yields with  $\underline{\mathbf{r}}'^{(z)}$  of (3.34)

$$\begin{aligned} \hat{\underline{\mathbf{t}}}_{\text{ZF,cont}}^{(z)} &= \left( \hat{t}_{\text{ZF,cont},1}^{(z)} \cdots \hat{t}_{\text{ZF,cont},n}^{(z)} \cdots \hat{t}_{\text{ZF,cont},N}^{(z)} \right)^{\text{T}} = \\ &\left( \mathbf{A}^{(z)\text{T}} \underline{\mathbf{R}}_{\mathbf{r}'}^{(z)-1} \mathbf{A}^{(z)} \right)^{-1} \mathbf{A}^{(z)\text{T}} \underline{\mathbf{R}}_{\mathbf{r}'}^{(z)-1} \underline{\mathbf{r}}'^{(z)} = \\ &\mathbf{A}^{(z)-1} \underline{\mathbf{r}}'^{(z)} = \underline{\mathbf{t}}^{(z)} + \mathbf{A}^{(z)-1} \underline{\mathbf{n}}'^{(z)}, \end{aligned} \quad (3.83)$$

and we recognize that the continuous valued ZF estimate is free of interference. Therefore, we obtain instead of (3.62) and (3.70)

$$\underline{\mathbf{T}}^{(z)} = \mathbf{I}^{N \times N} \quad (3.84)$$

and

$$a^{(z)} = 1, \quad (3.85)$$

respectively. Further, (3.65) yields

$$\underline{\mathbf{N}}^{(z)} = \mathbf{W}^{N \times N} \begin{pmatrix} \frac{1}{h_1'^{(z)}} & 0 & \cdots & \cdots & 0 \\ 0 & \ddots & & & \vdots \\ \vdots & & \frac{1}{h_n'^{(z)}} & & \vdots \\ \vdots & & & \ddots & 0 \\ 0 & \cdots & \cdots & 0 & \frac{1}{h_N'^{(z)}} \end{pmatrix}, \quad (3.86)$$

and we get instead of (3.74)

$$\mathbf{W}^{N \times N} \left( \begin{array}{ccccc} \frac{1}{h_1^{(z)}} & 0 & \cdots & \cdots & 0 \\ 0 & \ddots & & & \vdots \\ \vdots & & \frac{1}{h_n^{(z)}} & & \vdots \\ \vdots & & & \ddots & 0 \\ 0 & \cdots & \cdots & 0 & \frac{1}{h_N^{(z)}} \end{array} \right)^2 \mathbf{W}^{N \times N}. \quad (3.87)$$

All diagonal elements of this matrix assume the value  $\frac{1}{N} \sum_{n=1}^{\infty} \frac{1}{h_n^{(z)^2}}$ . Then, we obtain instead of (3.75) now

$$\sigma_{\text{ne}}^{(z)^2} = \sigma^2 \frac{1}{N} \sum_{n=1}^N \frac{1}{h_n^{(z)^2}}. \quad (3.88)$$

Finally, with  $a^{(z)}$  of (3.85) and  $\sigma_{\text{ne}}^{(z)}$  of (3.88) the effective SNRs

$$\gamma_{\text{ZF, effect}}^{(z)} = \frac{\sigma_t^2}{\sigma_{\text{ne}}^{(z)^2}} \quad (3.89)$$

and

$$\gamma_{\text{b,ZF, effect}}^{(z)} = \frac{1}{2 \log_2 M} \cdot \frac{\sigma_t^2}{\sigma_{\text{ne}}^{(z)^2}} \quad (3.90)$$

follow. With  $\gamma_{\text{b,ZF, effect}}^{(z)}$  of (3.90) the calculation of the bit error probabilities  $P_b^{(z)}(\gamma_{\text{b,ZF, effect}}^{(z)})$  and  $P_b$  can be performed as outlined in the last two paragraphs of Subsection 3.5.3.

It is well known [Kle96] that the MMSE detector boils down to the ZF detector for a sufficiently small noise variance  $\sigma^2$ . In our case “sufficiently small” means that in (3.70), (3.73) and (3.75)

$$\sigma^2 / \sigma_t^2 \ll h_n^{(z)^2} \text{ for all } n = 1 \cdots N \quad (3.91)$$

should hold. Then, (3.70) and (3.75) turn into (3.85) and (3.88), respectively, and  $\sigma_i^{(z)^2}$  (3.73) characterizing the interference vanishes. Even if  $\sigma^2 / \sigma_t^2$  is so small that, when averaging over many channel snapshots of  $\mathbf{h}^{(z)}$  of (3.31), (3.91) is fulfilled, then in the case of the assumed Rayleigh fading radio channels, channel snapshots with component values  $h_n^{(z)^2}$  far below this average may occur. This has the effect that for those channel snapshots the equivalence of MMSE and ZF detection would come about only at particularly small values of  $\sigma^2 / \sigma_t^2$ .

### 3.5.5 Matched Filter (MF) bound

PDS has the benefit that the frequency diversity offered by the radio channel can be cost efficiently exploited. However, the signal separation required in the receiver when using PDS has a negative impact on the system performance. In the present section we aspire, in a theoretical study, to separate out this negative impact so that only the benefit of frequency diversity offered by PDS remains. The adequate approach is the determination of the MF bound [VB00].

We consider the detection of the  $N$  components  $x_n^{(z)}$  of the real part vector  $\mathbf{x}^{(z)}$  and  $y_n^{(z)}$  of the imaginary part vector  $\mathbf{y}^{(z)}$  of  $\underline{\mathbf{t}}^{(z)}$  of (3.16). In general, the bit error probabilities of practical detection schemes lie above the MF bound. This bound is obtained by considering the receive vectors caused by each of the  $N$  components  $x_n^{(z)}$  of  $\mathbf{x}^{(z)}$  and  $y_n^{(z)}$  of  $\mathbf{y}^{(z)}$  of  $\underline{\mathbf{t}}^{(z)}$  of (3.16) separately, and by feeding each of these vectors into a matched filter. We express the system matrix of (3.35) by its  $N$  column vectors as

$$\begin{aligned} \mathbf{A}^{(z)} &= \left( \mathbf{a}_1^{(z)} \cdots \mathbf{a}_n^{(z)} \cdots \mathbf{a}_N^{(z)} \right), \\ \mathbf{a}_n^{(z)} &= \left( a_{1,n}^{(z)} \cdots a_{n,n}^{(z)} \cdots a_{N,n}^{(z)} \right)^T. \end{aligned} \quad (3.92)$$

Then, we can write the real part receive vector caused by the component  $x_n^{(z)}$  as

$$\mathbf{r}'_{R,n}{}^{(z)} = \mathbf{a}_n^{(z)} x_n^{(z)} + \text{Re} \left( \underline{\mathbf{n}}'^{(z)} \right), \quad (3.93)$$

and the imaginary part receive vector caused by the component  $y_n^{(z)}$  as

$$\mathbf{r}'_{I,n}{}^{(z)} = \mathbf{a}_n^{(z)} y_n^{(z)} + \text{Im} \left( \underline{\mathbf{n}}'^{(z)} \right). \quad (3.94)$$

With these two vectors we obtain for the components  $x_n^{(z)}$  and  $y_n^{(z)}$  the continuous valued MF estimates

$$\begin{aligned} \hat{x}_{\text{MF,cont},n}^{(z)} &= \left( \mathbf{a}_n^{(z)T} \mathbf{a}_n^{(z)} \right)^{-1} \mathbf{a}_n^{(z)T} \mathbf{r}'_{R,n}{}^{(z)} = \left( \mathbf{a}_n^{(z)T} \mathbf{a}_n^{(z)} \right)^{-1} \mathbf{a}_n^{(z)T} \left( \mathbf{a}_n^{(z)} x_n^{(z)} + \text{Re} \left( \underline{\mathbf{n}}'^{(z)} \right) \right) = \\ &= x_n^{(z)} + \left( \mathbf{a}_n^{(z)T} \mathbf{a}_n^{(z)} \right)^{-1} \mathbf{a}_n^{(z)T} \text{Re} \left( \underline{\mathbf{n}}'^{(z)} \right) \end{aligned} \quad (3.95)$$

and

$$\begin{aligned} \hat{y}_{\text{MF,cont},n}^{(z)} &= \left( \mathbf{a}_n^{(z)T} \mathbf{a}_n^{(z)} \right)^{-1} \mathbf{a}_n^{(z)T} \mathbf{r}'_{I,n}{}^{(z)} = \left( \mathbf{a}_n^{(z)T} \mathbf{a}_n^{(z)} \right)^{-1} \mathbf{a}_n^{(z)T} \left( \mathbf{a}_n^{(z)} y_n^{(z)} + \text{Im} \left( \underline{\mathbf{n}}'^{(z)} \right) \right) = \\ &= y_n^{(z)} + \left( \mathbf{a}_n^{(z)T} \mathbf{a}_n^{(z)} \right)^{-1} \mathbf{a}_n^{(z)T} \text{Im} \left( \underline{\mathbf{n}}'^{(z)} \right), \end{aligned} \quad (3.96)$$

respectively. Quantization of  $\hat{x}_{\text{MF,cont},n}^{(z)}$  of (3.95) and  $\hat{y}_{\text{MF,cont},n}^{(z)}$  of (3.96) with the quantization operator  $\mathcal{Q}(\cdot)$  determined by the Voronoi regions [FJ89] given by the set  $\mathbb{V}$  of

(2.9) yields the discrete valued estimates  $\hat{x}_{\text{MF},n}^{(z)}$  and  $\hat{y}_{\text{MF},n}^{(z)}$  of the components  $x_n^{(z)}$  and  $y_n^{(z)}$ , respectively.

With the components  $h_n^{(z)}$  of the partial CTF vector  $\mathbf{h}'^{(z)}$  of (3.31) we can determine the quantity

$$\alpha_{\mathbf{h}}^{(z)^2} = \frac{1}{N} \sum_{n=1}^N \left( h_n^{(z)} \right)^2, \quad (3.97)$$

which with  $\sigma^2$  of (2.57) yields the variance

$$\sigma_{\text{MF}}^{(z)^2} = \frac{\sigma^2}{\alpha_{\mathbf{h}}^{(z)^2}} \quad (3.98)$$

of the noise terms  $\left( \mathbf{a}_n^{(z)\text{T}} \mathbf{a}_n^{(z)} \right)^{-1} \mathbf{a}_n^{(z)\text{T}} \text{Re} \left( \underline{\mathbf{n}}'^{(z)} \right)$  and  $\left( \mathbf{a}_n^{(z)\text{T}} \mathbf{a}_n^{(z)} \right)^{-1} \mathbf{a}_n^{(z)\text{T}} \text{Im} \left( \underline{\mathbf{n}}'^{(z)} \right)$  in (3.95) and (3.96), respectively. Finally, with  $\sigma_{\text{t}}^2$  of (2.10) and  $\sigma_{\text{MF}}^{(z)^2}$  of (3.98) the SNR becomes

$$\gamma_{\text{MF}}^{(z)} = \frac{\sigma_{\text{t}}^2}{\sigma_{\text{MF}}^{(z)^2}}. \quad (3.99)$$

With  $\gamma_{\text{MF}}^{(z)}$  of (3.99) the calculation of the bit error probabilities  $P_{\text{b}}^{(z)} \left( \gamma_{\text{MF}}^{(z)} \right)$  and  $P_{\text{b}}$  can be performed as outlined in the last two paragraphs of Subsection 3.5.3.

### 3.5.6 Unspread transmission

As a reference system for our scheme OFDM transmission with PDS we consider in Section 3.6 also the bit error probability  $P_{\text{b}}$  of unspread OFDM transmission over the Rayleigh fading radio channel; PDS degenerates to unspread transmission if we set the spreading factor  $N$  equal one. We will choose QPSK modulation, and then we can, with the SNR  $\gamma_{\text{b}}$  per bit of (2.75), immediately resort to row two of (3.1).

## 3.6 Quantitative evaluations

### 3.6.1 Preliminary remarks

In the present section we verify and illustrate the performance of OFDM transmission with PDS for the above introduced schemes of ML, MMSE and ZF detection by the results of computer simulations. The simulations are performed for QPSK modulation as defined by (2.18) to (2.22) and for

$$N_{\text{F}} = 128 \quad (3.100)$$

OFDM subcarriers. In the simulations we set out from given parameter values  $\gamma_b$  of (2.75) and from sufficiently many realizations of the information vector  $\mathbf{u}$  of (2.2) and of the CTF vector  $\underline{\mathbf{h}}$  of (2.49).

### 3.6.2 Performance comparison of the schemes ML, MMSE and ZF detection

In Fig. 3.6 we depict  $P_b$  of (3.81) versus  $\gamma_b$  of (3.82) for the case of PDS with ML detection as described by (3.44) with the spreading factor  $N$  equal four. For ML detection Figs. 3.6a and 3.6b show two curves each, namely curves marked with WH-PDS, which stands for Walsh-Hadamard PDS, and curves marked with F-PDS, which stands for Fourier PDS. At the moment only the curves marked with WH-PDS are of interest. In Section 3.8 we will return to the curves marked with F-PDS.

The channel parameter  $W$  introduced in (2.38) is given the value four in Fig. 3.6a and 128 in Fig. 3.6b. In Fig. 3.6 we consider as references also unspread transmission as well as PDS with MMSE and ZF detection, and the MF bound for PDS. As to be expected, the curves for all four schemes lie above the MF bound. Unexpectedly, PDS with ZF detection performs worse than unspread transmission. ML detection gives the best result, however, it is only marginally superior to MMSE detection. In the case  $W$  equal four of Fig. 3.6a the radio channel has a lower diversity potential than in the case  $W$  equal 128 of Fig. 3.6b, and, therefore, one would expect that in the latter case the performance would be better. However, we recognize that the curves in Figs. 3.6a and 3.6b are virtually identical; this means that with the spreading factor  $N$  equal four the diversity potential of the case  $W$  equal 128 cannot be fully utilized by PDS.

In the case of the MF bound in Fig 3.6, the mutual interference is neglected. Therefore, the inclination of the curve of the MF bound fits together with the corresponding diversity order equal four. However, in the cases of ZF, MMSE and ML detections, a loss of diversity gain occurs because a price has to be paid for dealing with the mutual interference. In Section 3.7 the diversity gains of PDS and conventional diversity characterized by independent interference-free channels are compared.

### 3.6.3 Detailed investigation of MMSE and ZF detection

#### 3.6.3.1 SNIR and SNR

In a first step, we illustrate in Figs. 3.7a to p the performance of the schemes MMSE and ZF detection based on the cdf of the SN(I)R  $\gamma_{\text{MMSE, effect}}$  of (3.78) and  $\gamma_{\text{ZF, effect}}$  of (3.89) for  $W$  equal 128 and for the parameter values  $N$  and  $\gamma_o$  of (2.74) listed in Table 3.1. We omit the superscript ( $z$ ), because the cdf is identical for all values  $z = 1 \dots Z$ . As a reference

we include in Fig. 3.7 also the cdf of the SNR for the case of unspread transmission. With a view to achieving good system performance, the variance of the SN(I)R should be small, and the mean SN(I)R should be large. In Fig. 3.7, a small variance of the SN(I)R manifests itself in a steep slope of the cdf, and the more the cdf is situated to the right, the larger the mean of the SN(I)R. By inspection of Figs. 3.7a to p we recognize the following tendencies, which become more explicit with increasing spreading factor  $N$ :

- The variance of the SN(I)R is smallest for PDS with MMSE detection and largest for unspread transmission, whereas PDS with ZF detection lies in the middle.
- The mean SN(I)R is smallest for PDS with ZF detection and largest for unspread transmission, whereas PDS with MMSE detection has a position in between.

Fig. 3.7	a	b	c	d	e	f	g	h
$N$	2				8			
$\gamma_o/\text{dB}$	7	10	13	16	7	10	13	16
Fig. 3.7	i	j	k	l	m	n	o	p
$N$	32				128			
$\gamma_o/\text{dB}$	7	10	13	16	7	10	13	16

Table 3.1. Parameters  $N$  and  $\gamma_o$  chosen in Figs. 3.7a to p

When using  $\gamma_{b,\text{MMSE,eff}}^{(z)}$  of (3.79) for determining the bit error probability  $P_b^{(z)}\left(\gamma_{b,\text{MMSE,eff}}^{(z)}\right)$  of (3.80), we assume that the interference vector  $\mathbf{i}^{(z)}$  of (3.58) is bivariate Gaussian. In Fig. 3.8 we depict as an example the pdf  $p_{i^{(z)}}\left(\left|\mathbf{i}^{(z)}\right|\right)$  of  $\left|\mathbf{i}^{(z)}\right|$  obtained by computer simulation for the parameters  $W$  equal 128,  $N$  equal eight and  $\gamma_o$  equal 10 dB; this pdf has a variance  $\sigma_i^{(z)^2}$  equal to 0.0058. In the same figure we also show a Rayleigh pdf with the same variance 0.0058. We observe that both curves differ only marginally so that the assumption of a bivariate Gaussian  $\mathbf{i}^{(z)}$  is justified.

### 3.6.3.2 Bit error probability $P_b$

In view of the good performance of MMSE data detection, we now focus on this detection scheme in detail and investigate, how  $P_b$  of (3.81) depends on  $N$  for a given  $\gamma_b$  of (3.82) and given parameter values  $W$  in (2.38). Fig. 3.9 illustrates for the example  $\gamma_b$  equal 16 dB that  $P_b$  decreases with increasing  $W$  and  $N$ . However, for values  $N$  going beyond  $4W$ ,  $P_b$  remains virtually constant. Therefore, we term

$$N_{\max} = 4W \quad (3.101)$$

the maximum reasonable spreading factor.



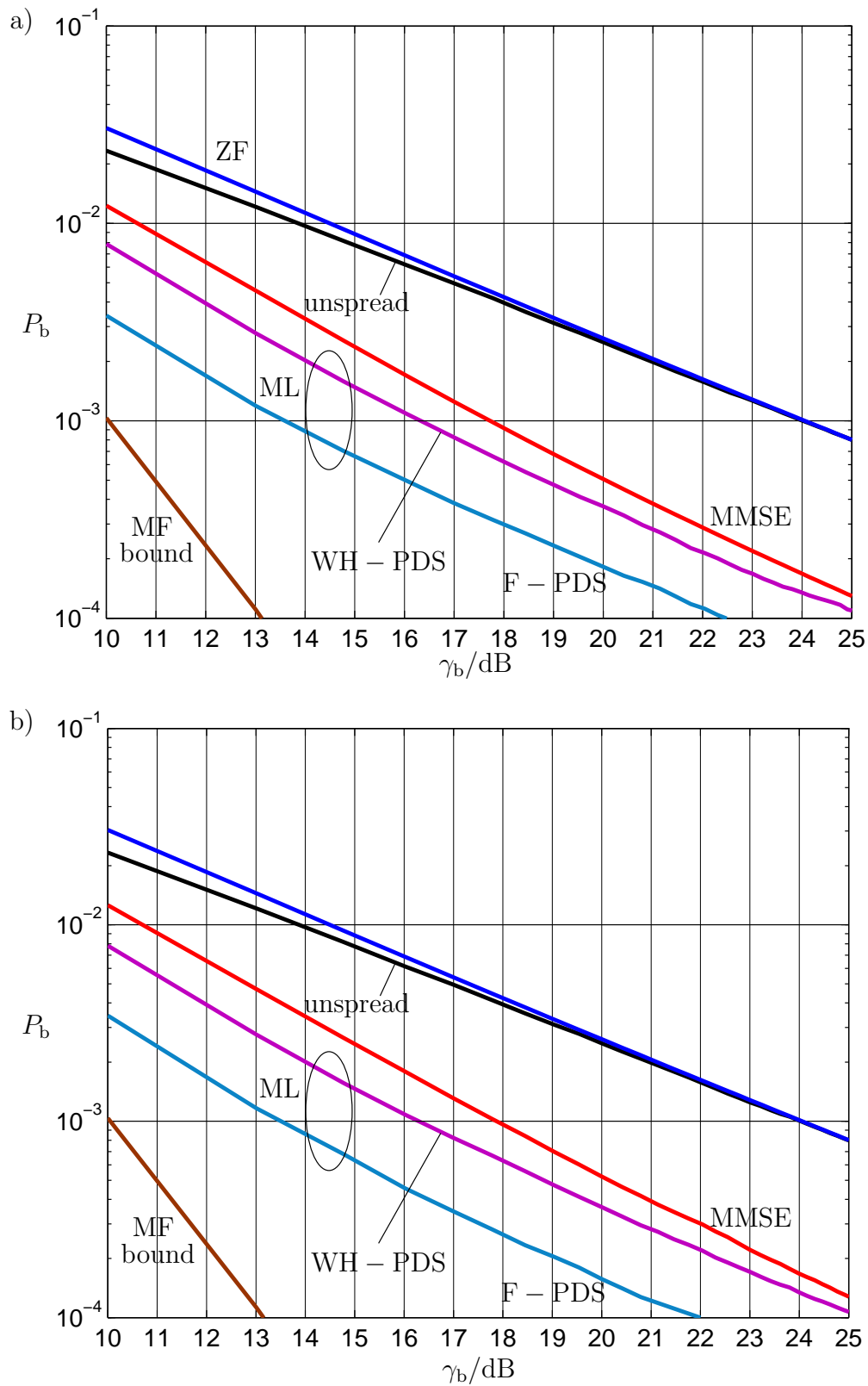
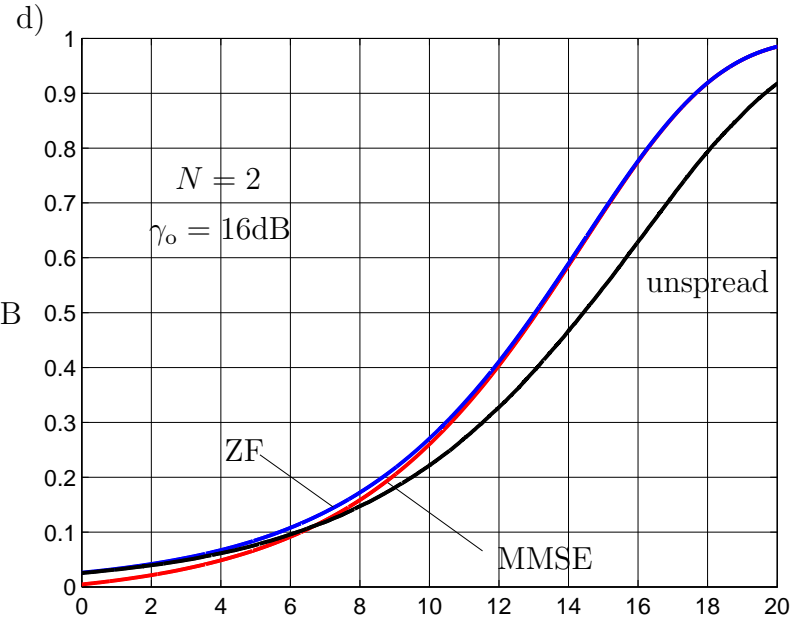
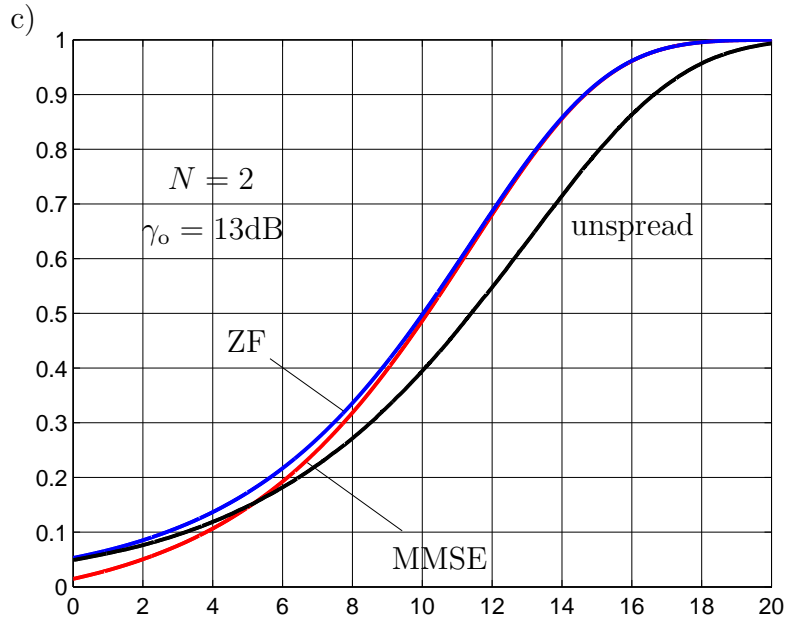
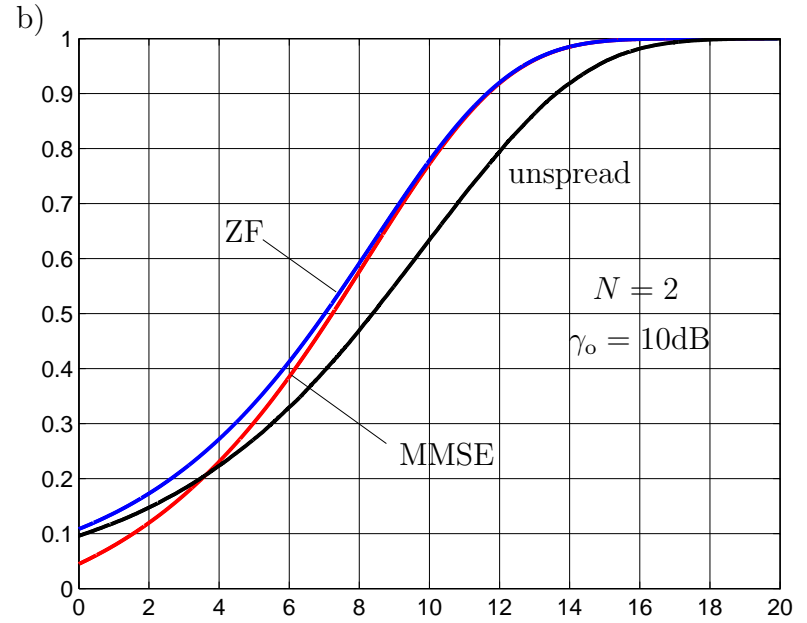
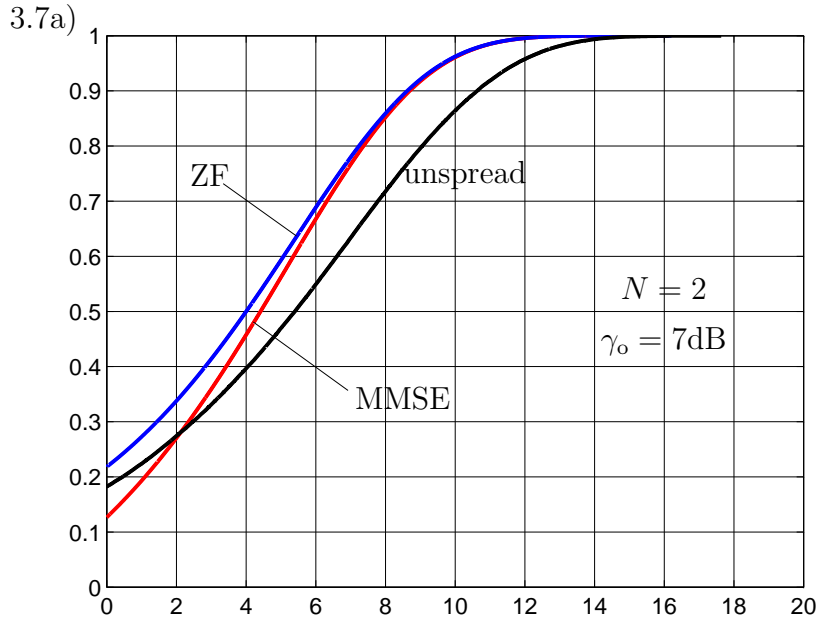
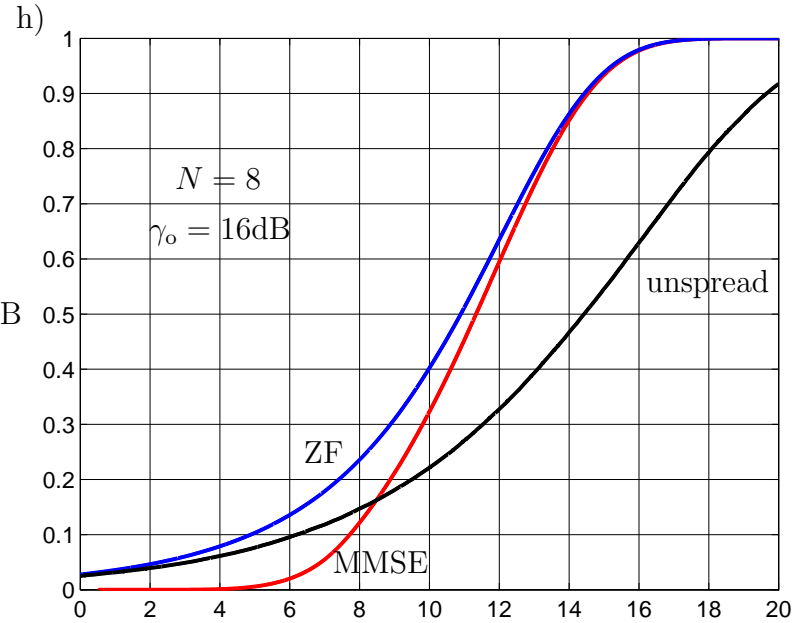
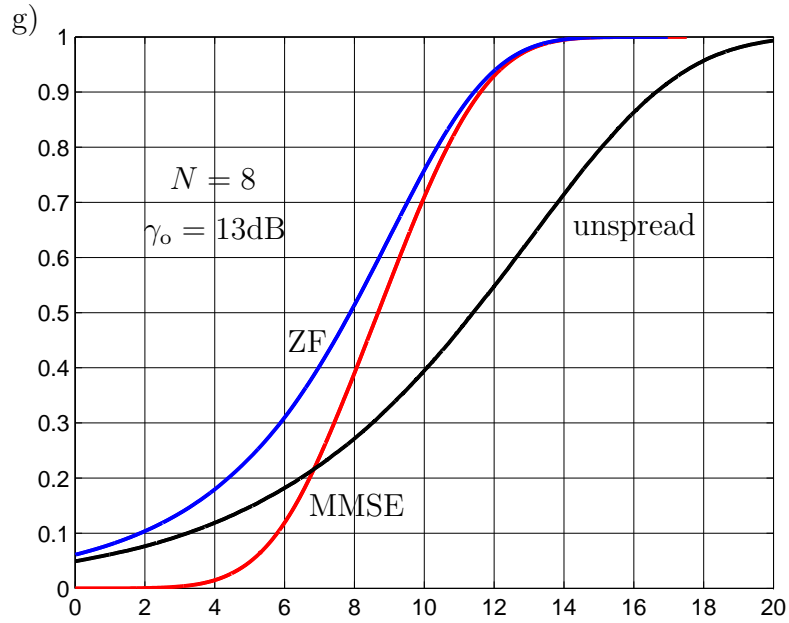
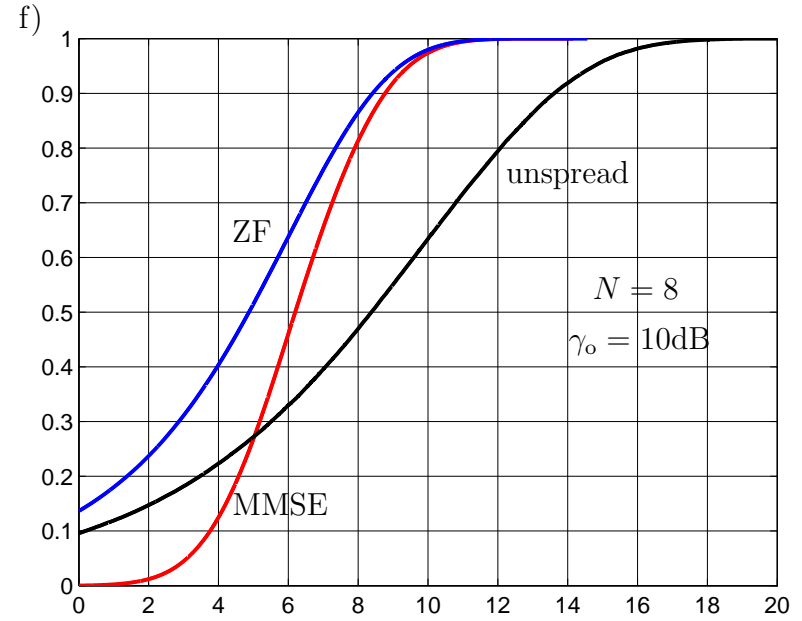
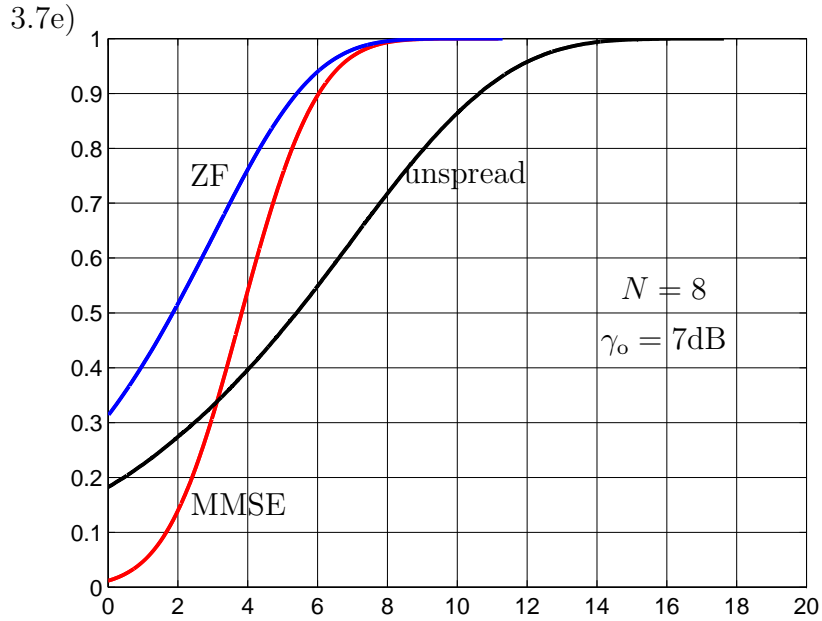


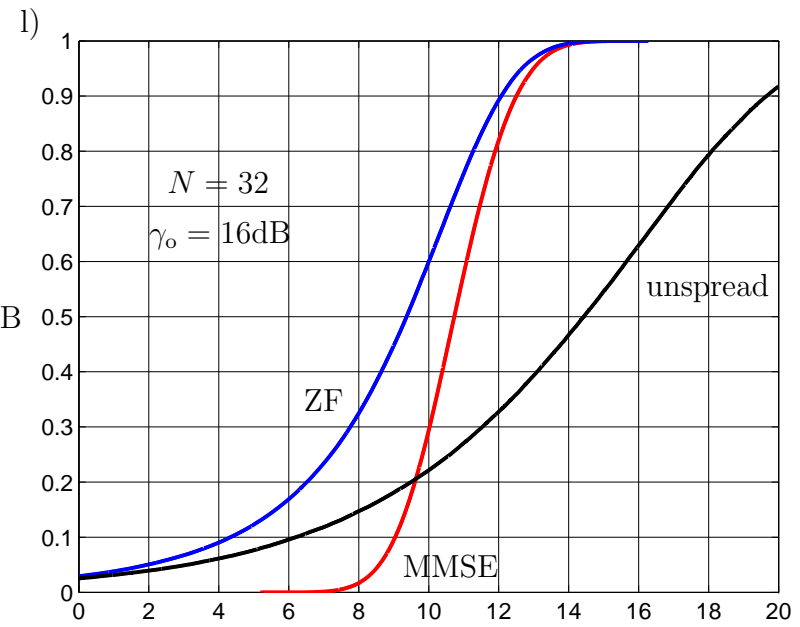
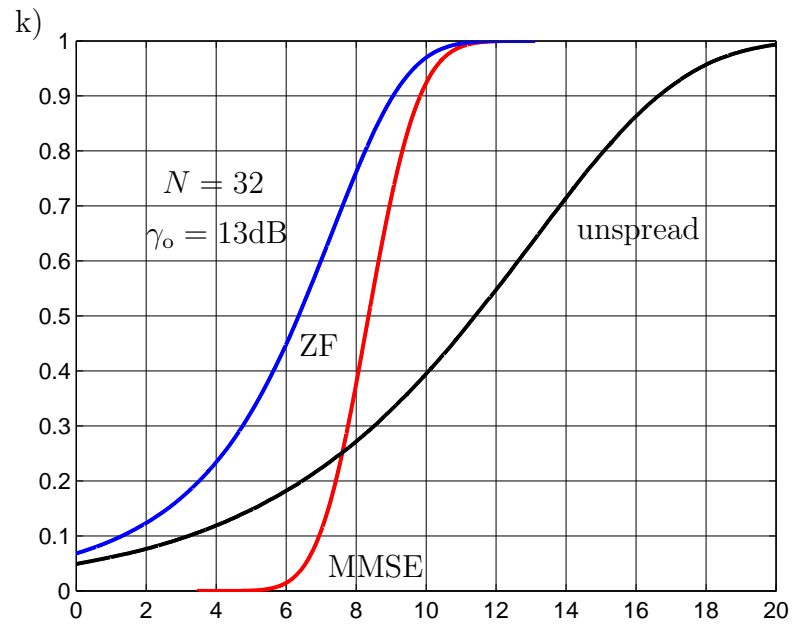
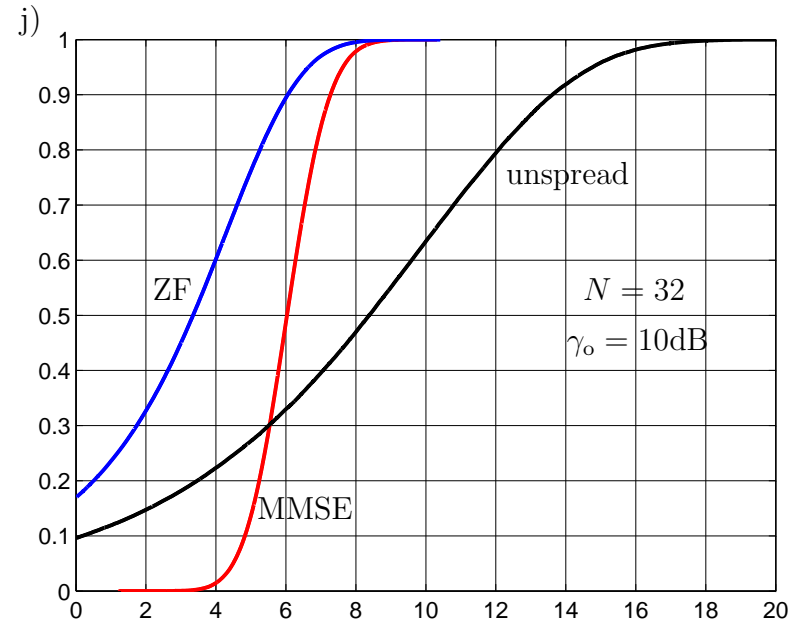
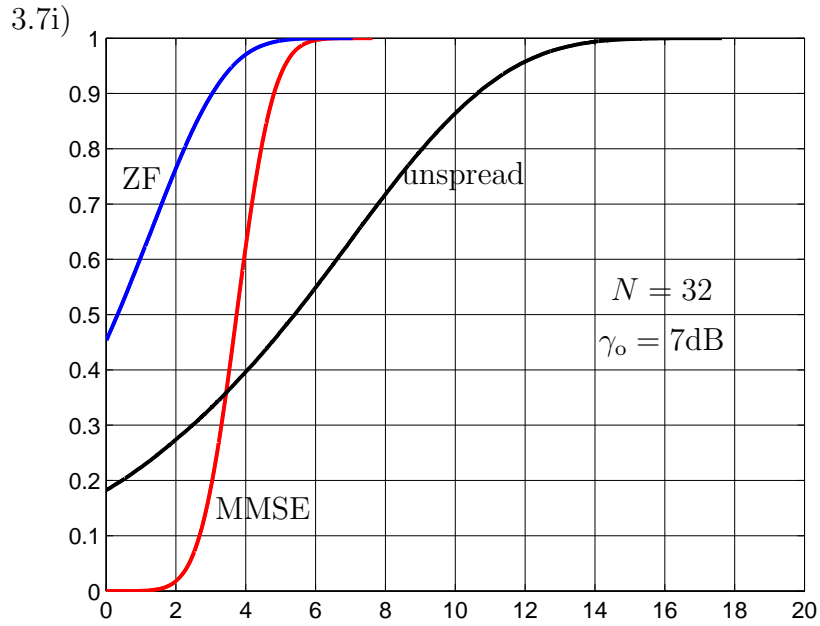
Fig. 3.6.  $P_b$  versus  $\gamma_b$  for different detection schemes, and MF bound;  
 $N_F = 128$ , PDS with  $N = 4$   
 a)  $W = 4$   
 b)  $W = 128$



→ dB



→ dB



↑

→ dB

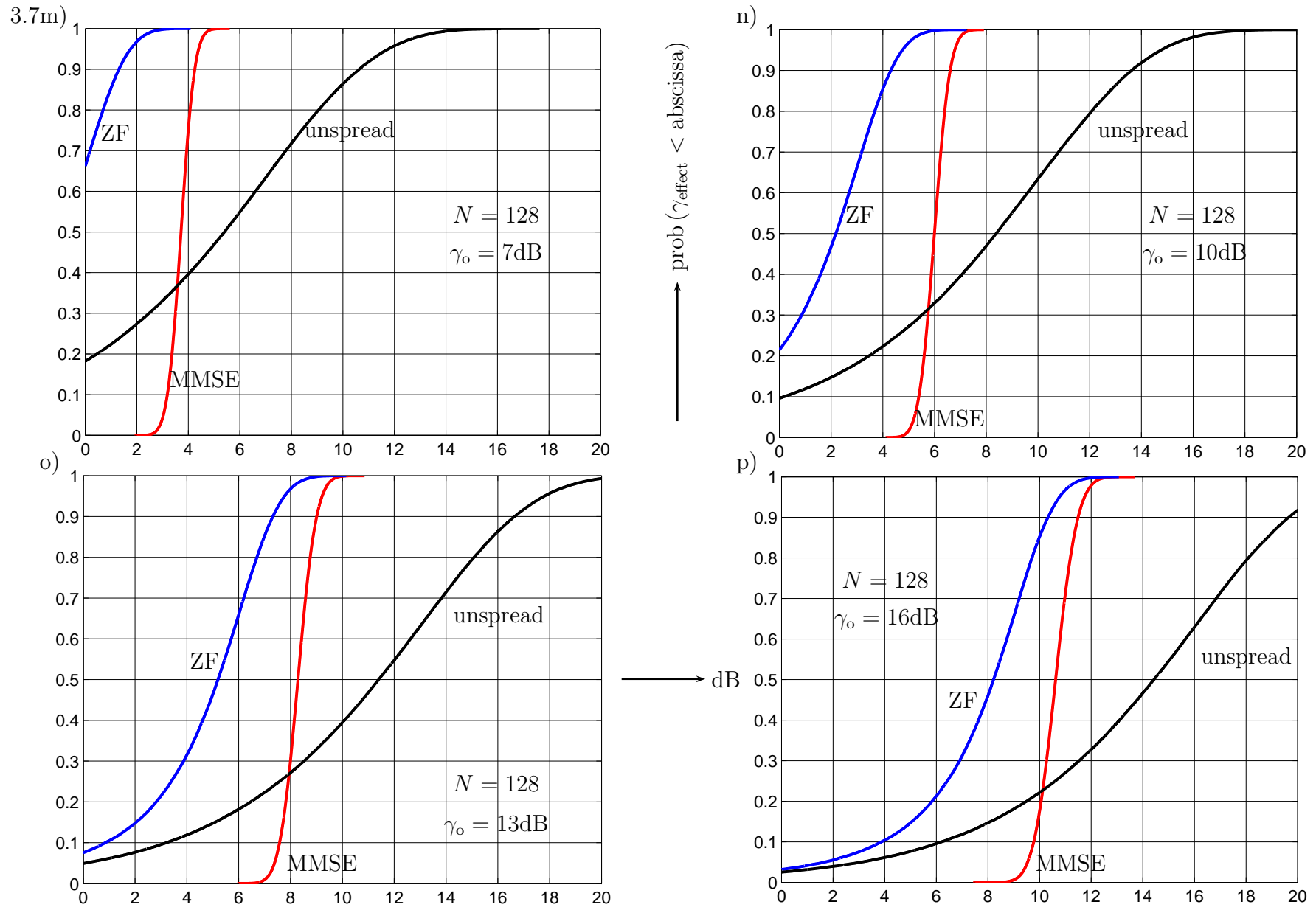


Fig. 3.7. CDF of  $\gamma_{\text{MMSE}}$ ,  $\gamma_{\text{ZF}}$  and  $\gamma$  with  $\gamma_0$  and  $N$  as parameters;  $W = N_F = 128$

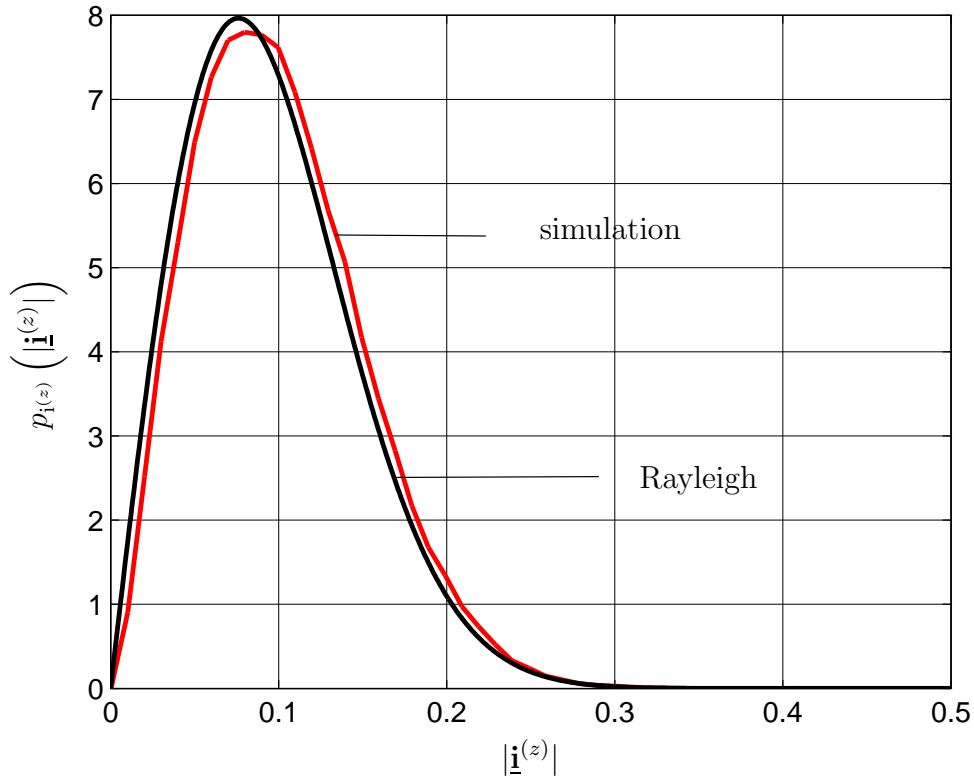


Fig. 3.8. pdf  $p_{i^{(z)}}(|i^{(z)}|)$  of  $|i^{(z)}|$ ;  $N = 8$ ,  $W = 128$ ,  $\gamma_o = 10\text{dB}$

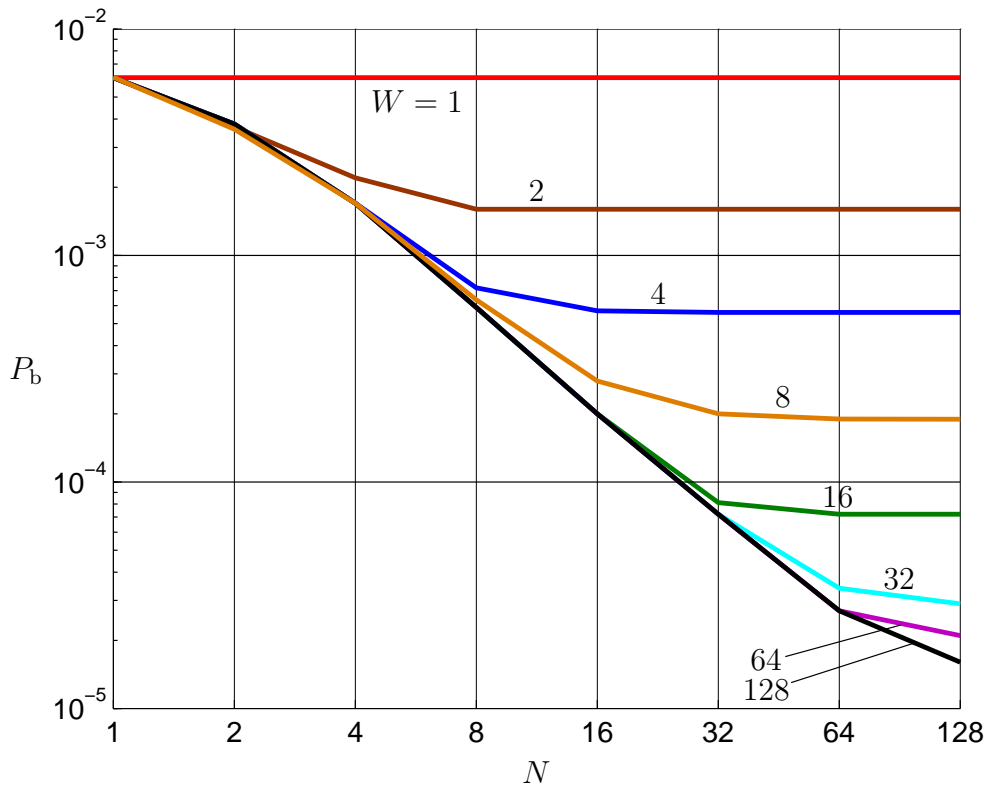


Fig. 3.9.  $P_b$  versus  $N$  for PDS with MMSE detection;  $\gamma_b = 16\text{dB}$ , with  $W$  as parameter

In Fig. 3.10 we depict  $P_b$  versus  $\gamma_b$  with  $W$  as the curve parameter. We choose  $N$  equal  $4W$  with exception of the curves for  $W$  equal one and 128, where we choose  $N$  equal  $W$ ; for  $W$  equal 64, where we choose  $N$  equal  $2W$ . The curve with the parameter value  $W$  equal one in Fig. 3.10 describes also the performance of unspread transmission for any value of  $W$  from one to 128. We recognize that PDS only bears fruit for  $W$  larger than one, and that the benefit of PDS increases with  $W$ , that is with an increasing diversity potential of the radio channel.

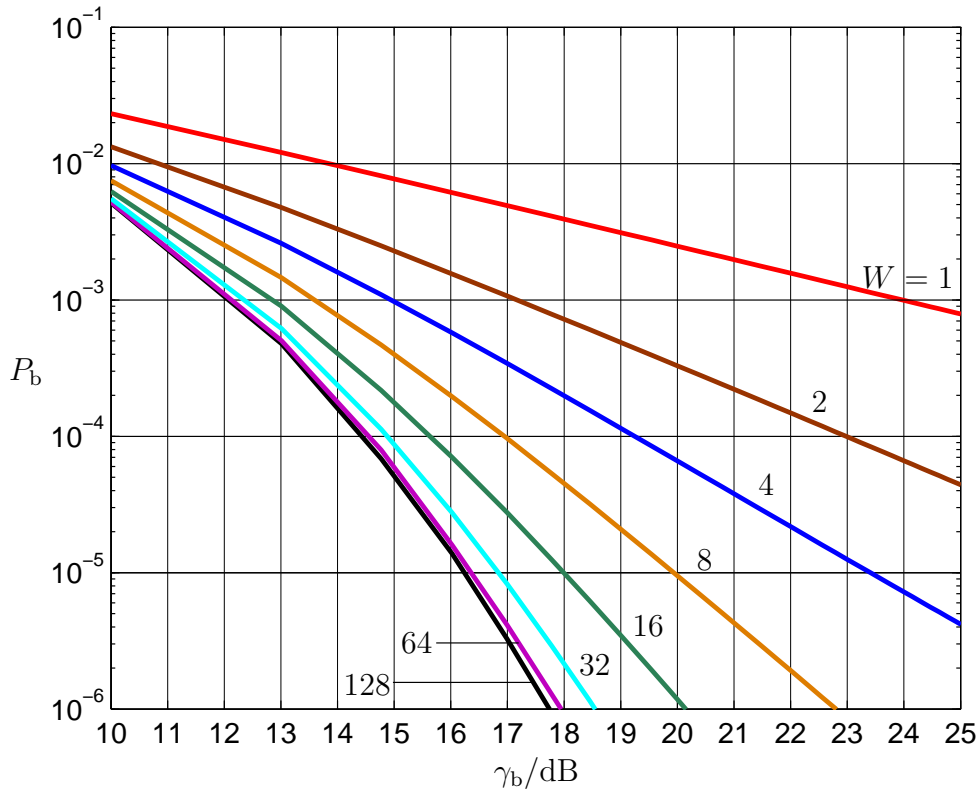


Fig. 3.10.  $P_b$  versus  $\gamma_b$  with  $W$  as parameter for PDS with MMSE detection,  $N_F = 128$ ;  $W = 1$  and  $W = 128$ :  $N = W$ ;  $W = 64$ :  $N = 2W$ ; else  $N = 4W$

### 3.6.3.3 Plausibility explanation of the maximum reasonable spreading factor

With the components of the  $N_F \times N_F$  Fourier matrix

$$\underline{\mathbf{F}} = \frac{1}{\sqrt{N_F}} \begin{pmatrix} 1 & 1 & 1 & \dots & 1 \\ 1 & e^{-j\frac{2\pi}{N_F}} & e^{-j2\frac{2\pi}{N_F}} & \dots & e^{-j(N_F-1)\frac{2\pi}{N_F}} \\ 1 & e^{-j2\frac{2\pi}{N_F}} & e^{-j4\frac{2\pi}{N_F}} & \dots & \vdots \\ \vdots & \vdots & \vdots & \ddots & \vdots \\ 1 & e^{-j(N_F-1)\frac{2\pi}{N_F}} & \dots & \dots & e^{-j(N_F-1)^2\frac{2\pi}{N_F}} \end{pmatrix}. \quad (3.102)$$

and the components  $\underline{h}_w$  of the CIR vector  $\underline{h}$  of (2.38), the components of the CTF vector  $\underline{h}$  follow from (2.49) as

$$\underline{h}_{n_F} = \sum_{w=1}^W \underline{h}_w e^{-j\frac{2\pi}{N_F}(w-1)n_F}, \quad n_F = 1 \cdots N_F. \quad (3.103)$$

In (3.103) the subcarrier indices  $n_F$  can be considered discrete valued subcarrier frequencies. To (3.103) corresponds with the continuous valued frequency  $\nu$  the CTF

$$\underline{h}(\nu) = \sum_{w=1}^W \underline{h}_w e^{-j\frac{2\pi}{N_F}(w-1)\nu}, \quad \nu \in [0, N_F]. \quad (3.104)$$

From this CTF we obtain the components of the CTF vector  $\underline{h}$  according to

$$\underline{h}_{n_F} = \underline{h}(\nu) \Big|_{\nu=n_F-1}, \quad n_F = 1 \cdots N_F. \quad (3.105)$$

In the expressions (3.70), (3.73), and (3.75) for  $a^{(z)}$ ,  $\sigma_i^{(z)^2}$ , and  $\sigma_{n_e}^{(z)^2}$ , respectively, the magnitude squares  $h_{n_F}^2$  occur. To the sequence of values  $h_{n_F}^2$ ,  $n_F = 1 \dots N_F$ , corresponds the function

$$\begin{aligned} h^2(\nu) = & \\ & \left( \sum_{w=1}^W \left( \mathfrak{h}_{r,w} \cos \left( \frac{2\pi}{N_F} (w-1)\nu \right) + \mathfrak{h}_{i,w} \sin \left( \frac{2\pi}{N_F} (w-1)\nu \right) \right) \right)^2 + \\ & \left( \sum_{w=1}^W \left( \mathfrak{h}_{r,w} \sin \left( \frac{2\pi}{N_F} (w-1)\nu \right) + \mathfrak{h}_{i,w} \cos \left( \frac{2\pi}{N_F} (w-1)\nu \right) \right) \right)^2. \end{aligned} \quad (3.106)$$

As approximations of said expressions for  $a^{(z)}$ ,  $\sigma_i^{(z)^2}$  and  $\sigma_{n_e}^{(z)^2}$ , we can substitute the summations in (3.70), (3.73), and (3.75) by integrals, which for instance in the case of  $z$  equal one yields

$$\begin{aligned} a^{(1)} = & \frac{1}{N} \sum_{n=1}^N \frac{h_n^{(1)^2}}{h_n^{(1)^2} + \sigma^2/\sigma_t^2} \approx \\ & \int_0^{N_F} \frac{h^2(\nu)}{h^2(\nu) + \sigma^2/\sigma_t^2} d\nu, \end{aligned} \quad (3.107)$$

$$\begin{aligned} \sigma_i^{(1)^2} = & \sigma_t^2 \frac{1}{N} \sum_{n=1}^N \left( \frac{(1 - a^{(1)}) h_n^{(1)^2} - a^{(1)} \sigma^2/\sigma_t^2}{h_n^{(1)^2} + \sigma^2/\sigma_t^2} \right)^2 \approx \\ & \sigma_t^2 \int_0^{N_F} \left( \frac{(1 - a^{(1)}) h^2(\nu) - a^{(1)} \sigma^2/\sigma_t^2}{h^2(\nu) + \sigma^2/\sigma_t^2} \right)^2 d\nu \end{aligned} \quad (3.108)$$

and



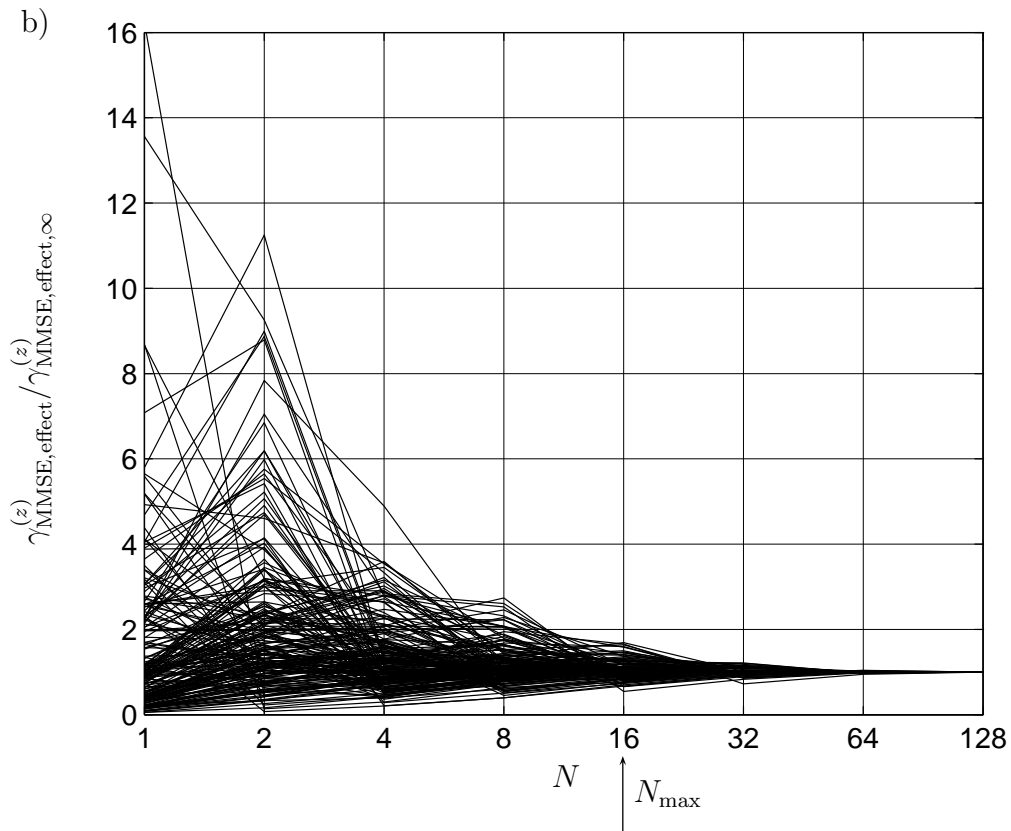
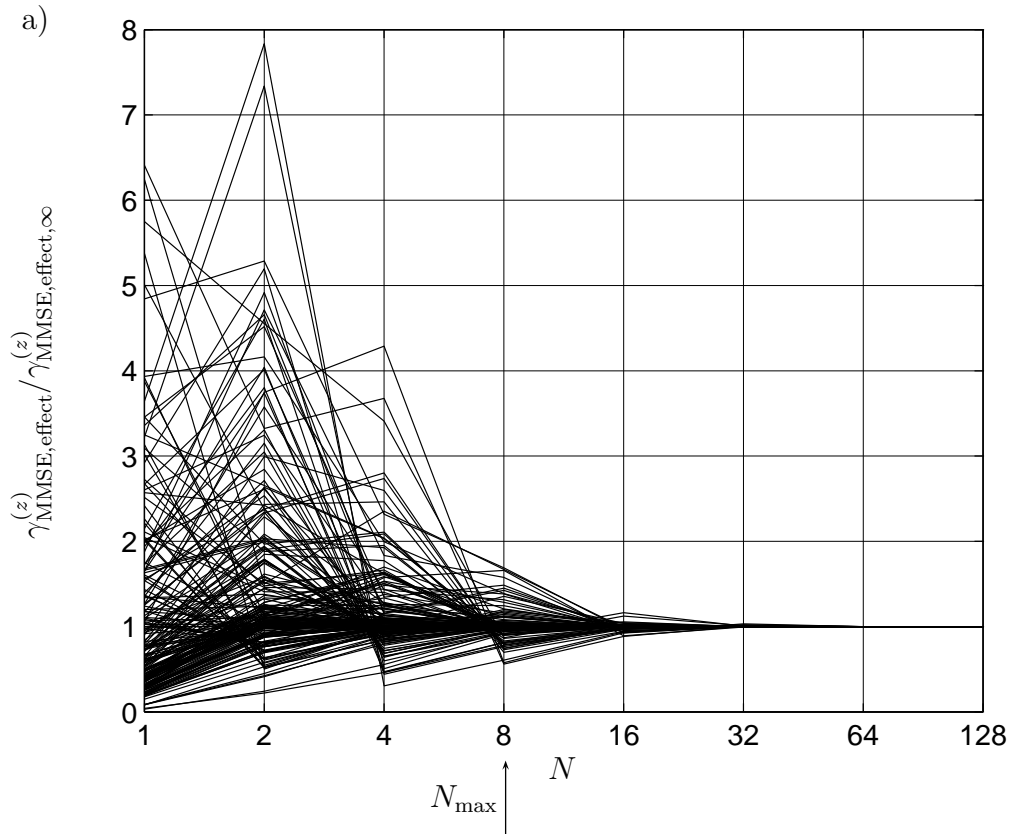


Fig. 3.11.  $\gamma_{\text{MMSE, effect}}^{(z)} / \gamma_{\text{MMSE, effect, } \infty}^{(z)}$  versus  $N$ ;  $N_{\text{F}} = 128$ ,  $\gamma_{\text{b}} = 16\text{dB}$

a)  $W = 2$

b)  $W = 4$

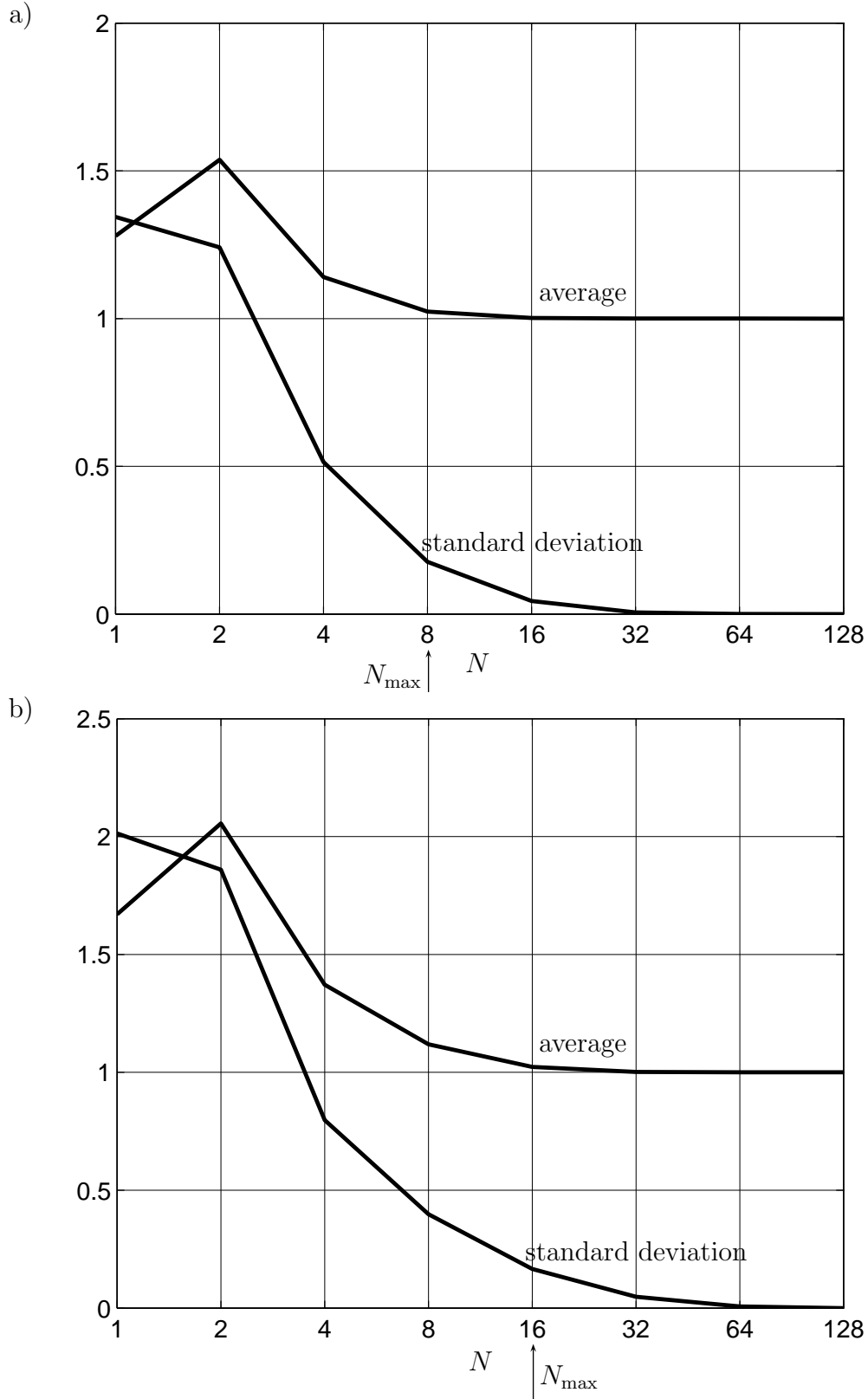


Fig. 3.12. Average and standard deviation of  $\gamma_{\text{MMSE, effect}}^{(z)} / \gamma_{\text{MMSE, effect, \infty}}^{(z)}$  versus  $N$ ;  
 $N_{\text{F}} = 128$ ,  $\gamma_{\text{b}} = 16\text{dB}$   
 a)  $W = 2$   
 b)  $W = 4$

$$\begin{aligned}\sigma_{n_e}^{(1)2} &= \sigma^2 \frac{1}{N} \sum_{n=1}^N \left( \frac{h'_n{}^{(1)}}{h_n'^{(1)2} + \sigma^2/\sigma_t^2} \right)^2 \approx \\ &\sigma^2 \int_0^{N_F} \left( \frac{h(\nu)}{h^2(\nu) + \sigma^2/\sigma_t^2} \right)^2 d\nu.\end{aligned}\quad (3.109)$$

With increasing  $N$  the differences between the summation results and the corresponding integrals of (3.107) to (3.109) decrease. If  $N$  goes beyond the maximum reasonable spreading factor  $N_{\max}$  introduced in Subsubsection 3.6.3.2, the differences becomes negligible.  $N_{\max}$  depends on the fine structure of the function  $h^2(\nu)$  of (3.106). The larger  $W$ , the more explicit this fine structure, and the larger  $N_{\max}$ . For  $N$  equal to or larger than  $N_{\max}$ , the SNIR  $\gamma_{\text{MMSE, effect}}^{(z)}$  of (3.78) converges to the value  $\gamma_{\text{MMSE, effect, } \infty}^{(z)}$ .

In Fig. 3.11 we depict  $\gamma_{\text{MMSE, effect}}^{(z)}/\gamma_{\text{MMSE, effect, } \infty}^{(z)}$  versus  $N$  for a large ensemble of channel snapshots, where we choose  $N_F$  equal 128 and  $\gamma_b$  equal 16 dB. Fig. 3.11a holds for  $W$  equal two and Fig. 3.11b for  $W$  equal four. For  $N$  smaller than  $N_{\max}$ , the ratio  $\gamma_{\text{MMSE, effect}}^{(z)}/\gamma_{\text{MMSE, effect, } \infty}^{(z)}$  is far away from one, and it converges to one when  $N$  approaches  $N_{\max}$ . This statement is corroborated by Fig. 3.12, which shows the average and standard deviation of  $\gamma_{\text{MMSE, effect}}^{(z)}/\gamma_{\text{MMSE, effect, } \infty}^{(z)}$  versus  $N$  with the same parameters as in Fig 3.11. Fig. 3.12a holds for  $W$  equal two and Fig. 3.12b for  $W$  equal four.

To conclude, the value  $N_{\max}$  of (3.101) observed in Fig. 3.9 can be plausibly explained by the above argument.

### 3.6.4 Error statistics

In Figs. 3.6, 3.9 and 3.10 we consider the mean bit error probability  $P_b$  of (2.76) versus the mean SNR per bit of  $\gamma_b$  of (2.75). As explained in Section 2.6, for obtaining these results averaging has to be performed over many snapshots of the information vector  $\mathbf{u}$  of (2.2) and the CTF vector  $\mathbf{h}$  of (2.49).

We now address the quality of data detection in an OFDM transmission system with PDS for a single snapshot of the CTF vector  $\mathbf{h}$  of (2.49). For such a snapshot, the  $Z$  partial system matrices  $\mathbf{A}^{(z)}$  of (3.35) occurring in (3.44), (3.52) and (3.83) play an important role. The farther away these matrices from singularity, that is the smaller their Eigenvalue spread [HJ85], the better the quality of detection [Kle96]. Partial system matrices  $\mathbf{A}^{(z)}$  far from/close to singularity are termed well/ill conditioned.

Let us now consider the estimate  $\hat{\mathbf{u}}^{(z)}$  of the partial information vector  $\mathbf{u}^{(z)}$  averaged over many snapshots of  $\mathbf{u}$  and  $\mathbf{h}$ . In the case of PDS, all  $N_u$  components  $\hat{u}_{n_u}^{(z)}$  of the estimate  $\hat{\mathbf{u}}^{(z)}$  benefit or suffer more or less equally from the well or ill conditioned partial system matrix  $\mathbf{A}^{(z)}$ . Therefore, the bit errors of the estimate  $\hat{\mathbf{u}}^{(z)}$ , if there are any, are prone to occur in bursts. This burstyness is illustrated in Table 3.2 by an example. This example

holds for  $N_F$  equal 128,  $N$  equal four,  $W$  equal 128,  $\gamma_b$  equal 10 dB, and ML detection. In the table we show the probabilities

$$p_e(e) = \text{Prob}(\hat{\mathbf{u}}^{(z)} \text{ contains } e \text{ bit errors}) \quad (3.110)$$

observed for unspread transmission and transmission with PDS. The values in Table 3.2 yield for the bit error probability

$$P_b = \frac{1}{8} \sum_{e=1}^8 e \cdot p_e(e) \quad (3.111)$$

in the case of unspread transmission the value 0.0231 and in the case of PDS the considerably smaller value 0.0077, which clearly shows the benefit of PDS. However, a closer inspection of Table 3.2 reveals that in the case of unspread transmission the probabilities  $p_e(e)$  of (3.110) monotonously decrease with increasing  $e$ , which is not true in the case of PDS. The fact that the probability  $p_e(e)$  may increase with decreasing  $e$  is a manifestation of the bursty error behavior of PDS.

number $e$ of bit errors in $\mathbf{u}^{(z)}$	probability $p_e(e)$	
	unspread	PDS
0	0.8425	0.9722
1	0.1322	0.0067
2	0.0231	0.0147
3	0.0020	6.5832e-004
4	1.6875e-004	0.0054
5	1.0313e-005	6.9219e-005
6	3.1250e-007	1.5832e-004
7	0	4.6094e-006
8	0	5.4062e-005

Table 3.2.  $p_e(e)$  of (3.110) for unspread transmission and PDS;  $N_F = 128$ ,  $N = 4$ ,  $W = 128$ ,  $\gamma_b = 10\text{dB}$

### 3.7 PDS versus conventional diversity

We consider QPSK transmission over  $L$  independent parallel Rayleigh fading radio channels without mutual interference [Pro00]. With the mean SNR  $\gamma_b$  per channel output and bit we form the quantity

$$\mu = \sqrt{\frac{\gamma_b}{1 + \gamma_b}}. \quad (3.112)$$

Then, the average bit error probability becomes [Pro00]

$$P_b = \left(\frac{1-\mu}{2}\right)^L \sum_{l=0}^{L-1} \binom{L-1+l}{l} \left(\frac{1+\mu}{2}\right)^l. \quad (3.113)$$

Fig. 3.13 shows  $P_b$  of (3.81) versus  $\gamma_b$  of (3.82) for  $W$  equal 128 with the spreading factor  $N$  equal one to 128 as the curve parameter for the case of MMSE detection. As a reference,  $P_b$  of (3.113) with  $L$  equal one to eight as the curve parameter is also included. As expected,  $P_b$  decreases with increasing values  $N$  and  $L$ . However, for the same values  $N$  and  $L$  conventional diversity performs better than PDS, because PDS is degraded by the necessity to deal with mutual interference.

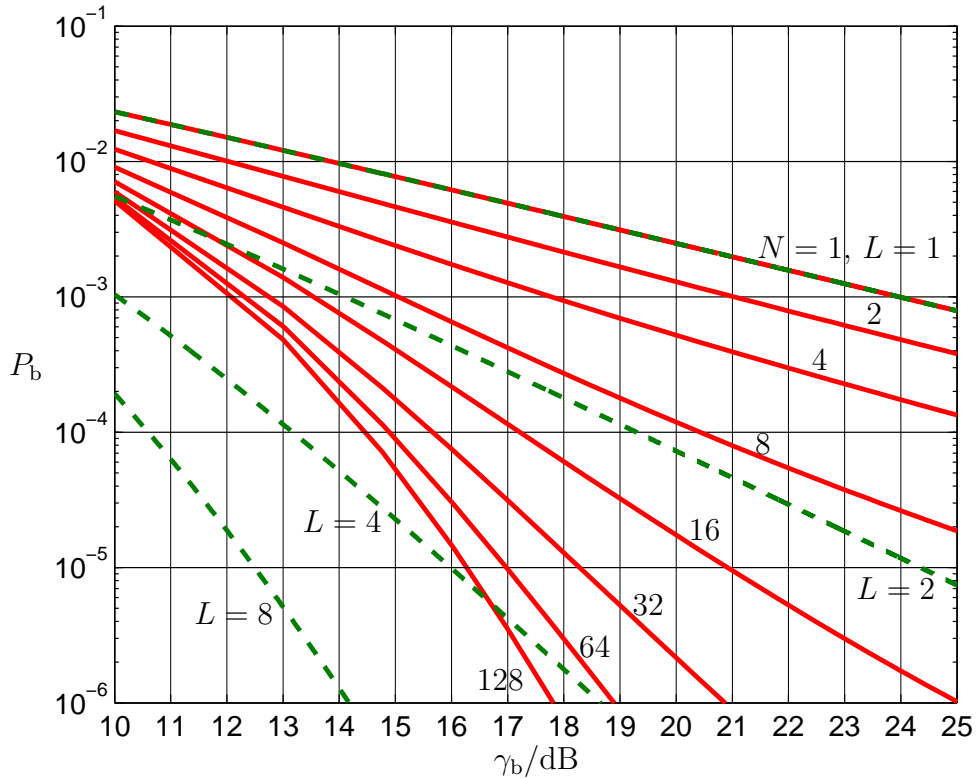


Fig. 3.13.  $P_b$  versus  $\gamma_b$   
 — MMSE detection with  $N$  as parameter  
 - - - conventional diversity with  $L$  as parameter

### 3.8 Generalization to other partial spreading matrices

The Walsh-Hadamard matrix  $\mathbf{W}^{N \times N}$  employed in (3.17) as the partial spreading matrix for PDS has the following two properties:

1. The matrix is unitary,
2. All  $N^2$  matrix elements have the same magnitude  $1/\sqrt{N}$ .

If we would substitute in (3.17) as the partial spreading matrix another  $N \times N$  matrix featuring the just mentioned two properties, then also for this spreading matrix all the

results obtained in Sections 3.5 and 3.6 for MMSE and ZF detection would hold. This would even be true if the elements of this other matrix would be complex valued. In this case, we would obtain instead of the real valued partial system matrix  $\mathbf{A}^{(z)}$  of (3.35) now a complex valued partial system matrix  $\underline{\mathbf{A}}^{(z)}$ , and whenever in the expressions in Section 3.5 the matrix  $\mathbf{A}^{(z)}$  occurs, we now should write  $\underline{\mathbf{A}}^{(z)}$ . An example of an alternative partial spreading matrix exhibiting the two above mentioned properties would be the  $N \times N$  Fourier matrix  $\underline{\mathbf{F}}^{N \times N}$  [BEL03, Myu07]. We term the two cases of employing the Walsh-Hadamard matrix  $\mathbf{W}^{N \times N}$  or the Fourier matrix  $\underline{\mathbf{F}}^{N \times N}$  as partial spreading matrices for PDS briefly as WH-PDS or F-PDS, respectively. Because the Walsh-Hadamard matrix is a real-valued matrix with all its elements being  $\pm 1/\sqrt{N}$ , it is particularly suited for a low-complexity implementation, which made it the most common spreading matrix for multi-carrier spread spectrum (MC-SS) transmission systems.

Whereas WH-PDS and F-PDS perform equivalently in the cases of MMSE and ZF detection, we found that this is not true in the case of ML detection in combination with QPSK modulation. Rather, in this case WH-PDS performs significantly worse than F-PDS. This is illustrated in Fig. 3.6. The reason for this poorer performance of WH-PDS is the following: With a certain probability partial transmit vectors  $\underline{\mathbf{t}}^{(z)}$  of (3.16) occur, which are orthogonal to all but one row of the partial spreading matrix  $\mathbf{W}^{N \times N}$  of WH-PDS. Such partial transmit vectors  $\underline{\mathbf{t}}^{(z)}$  lead to spread partial transmit vectors  $\tilde{\underline{\mathbf{t}}}^{(z)}$  of (3.17) having only one non-zero component, and, therefore, being radiated with a very low transmit energy. Such a low transmit energy entails a high bit error probability  $P_b$ .

### 3.9 Computational complexity

Adapting the argumentation of [OA07] to PDS with QPSK modulation for the cases of ML and MMSE detection yields the computational complexities  $O(\frac{N_F}{N}4^N)$  and  $O(N_F N^2)$ , respectively. These are depicted versus  $N$  in Fig. 3.14. Obviously, for larger values of the spreading factor  $N$  the complexity of ML detection by far exceeds the complexity of MMSE detection.

The Walsh-Hadamard and Fourier transformations can be implemented as fast Hadamard transformation (FHT) and fast Fourier transformation (FFT), respectively. By adapting the argumentations of [CT65, FA76] to PDS, Walsh-Hadamard PDS only requires  $N_F \log_2 N$  complex additions, whereas Fourier PDS requires  $2N_F \log_2 N$  complex additions and  $N_F \log_2 N$  complex multiplications. Therefore, the additionally required arithmetic operations of Fourier PDS amount to  $N_F \log_2 N$  complex additions and  $N_F \log_2 N$  complex multiplications. In Fig. 3.15 we depict the number of these additional operations versus the spreading factor  $N$  for QPSK modulation and  $N_F$  equal 128.

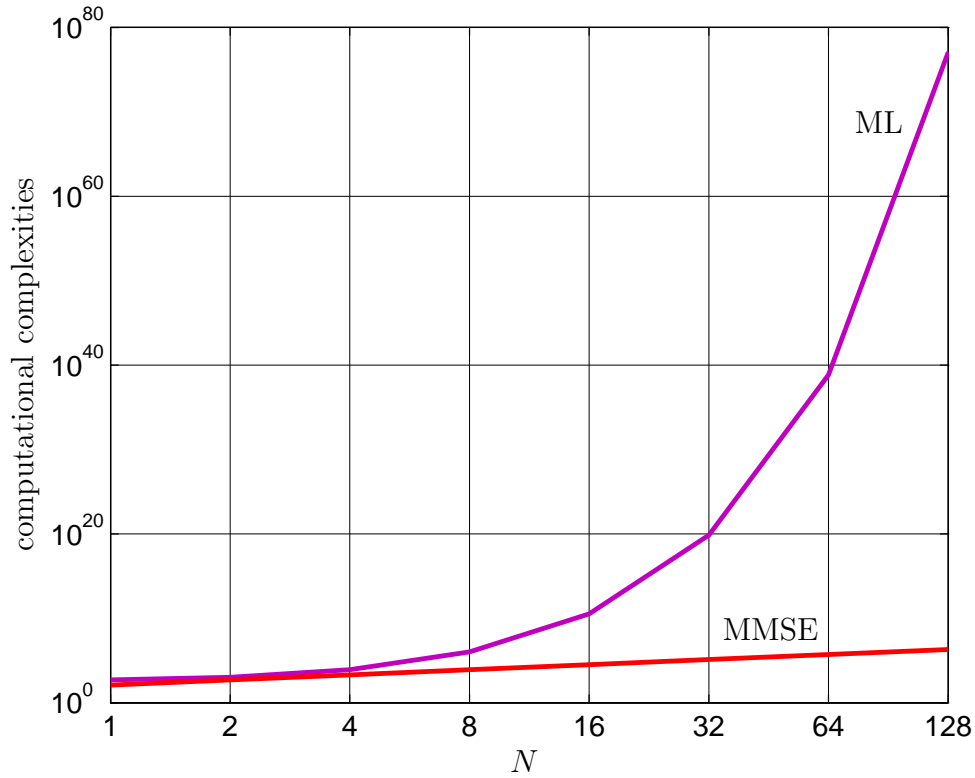


Fig. 3.14. Computational complexities  $O\left(\frac{N_F}{N}4^N\right)$  of PDS with ML detection and  $O(N_F N^2)$  of PDS with MMSE detection; QPSK,  $N_F = 128$

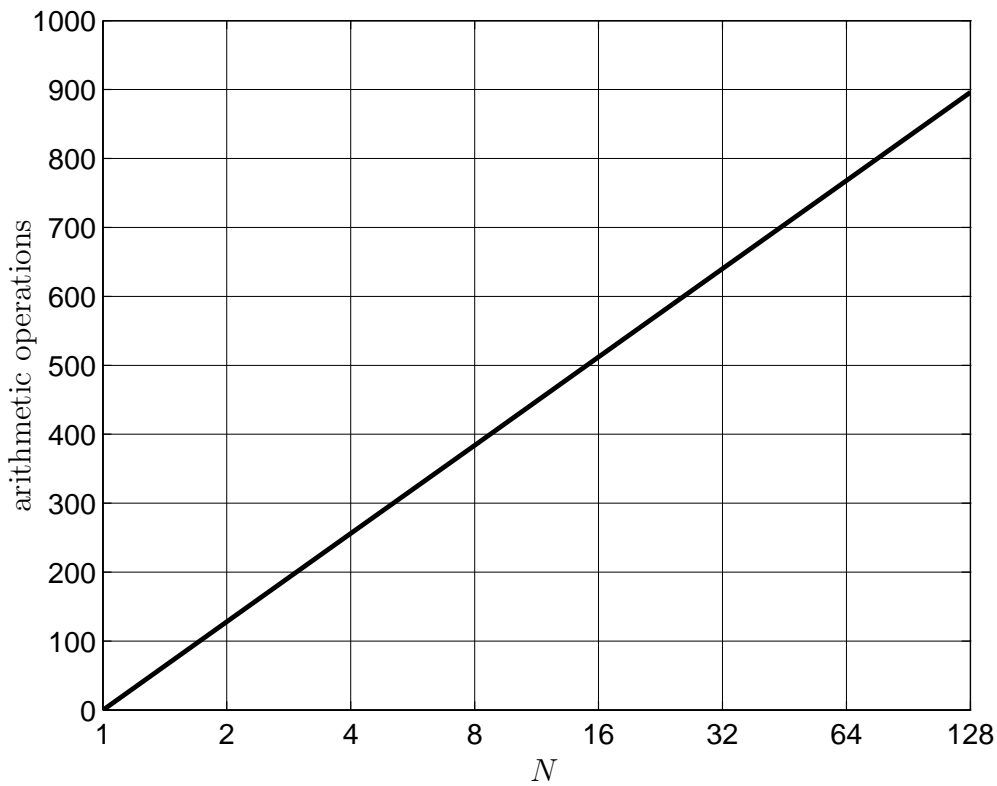


Fig. 3.15. Additional arithmetic operations of Fourier PDS :  $N_F \log_2 N$  complex additions and  $N_F \log_2 N$  complex multiplications;  $N_F = 128$

# Chapter 4

## Combination of PDS with FEC encoding

### 4.1 Preliminary remarks

In Chapter 3 we consider OFDM transmission utilizing PDS without FEC encoding. In the present Chapter 4 we extend the concept of OFDM transmission with PDS by the inclusion of FEC encoding. As a particularly interesting aspect of the following investigations, we address the beneficial utilization of reliability information [Fri95, GB10] in a soft input FEC decoder [Fri95, GB10] of the receiver, and we show by means of an example how this information can be generated.

### 4.2 System model

In what follows, we assume the reader to be familiar with the contents of Chapter 3 and go into particulars only as far as additional aspects play a role. In order to include FEC encoding, we supplement the system model of Fig. 3.3 as shown in Fig. 4.1 by an FEC encoder and a code interleaver on the transmit side, and by a code deinterleaver and an FEC decoder on the receive side.

The FEC encoder in the model of Fig. 4.1 is characterized by the coding operator  $\mathcal{C}(\cdot)$  and transforms the binary information vector  $\mathbf{u}$  of (2.2) into the binary code vector

$$\mathbf{c} = (c_1 \cdots c_{n_c} \cdots c_{N_c})^T = \mathcal{C}(\mathbf{u}), \quad c_{n_c} \in \{\pm 0.5\}, \quad (4.1)$$

of dimension  $N_c$ , which we assume to be a power of two. The components  $u_{n_u}$  of the information vector  $\mathbf{u}$  of (2.2) stem from the set  $\{0, 1\}$ . With a view to generate reliability information in the receiver and to utilize it in a soft input FEC decoder as will be later explained in this chapter, we take the components  $c_{n_c}$  of the code vector  $\mathbf{c}$  of (4.1) from the binary set  $\{\pm 0.5\}$ .

With the coding rate  $R_c$  of the FEC code, the dimensions  $N_u$  of  $\mathbf{u}$  of (2.2) and  $N_c$  of  $\mathbf{c}$  of (4.1) are related by

$$N_c = N_u / R_c. \quad (4.2)$$

Concerning the gross mean SNR per bit, we now obtain with the coding rate  $R_c$  instead of (2.75)

$$\gamma_b = \frac{1}{R_c \log_2 M} \frac{\sigma_t^2 \sigma_h^2}{\sigma^2}. \quad (4.3)$$



The number of possible realizations of the code vector  $\mathbf{c}$  of (4.1) is

$$Q_c = 2^{N_c}, \quad (4.4)$$

and we term these realizations  $\mathbf{c}^{\{q_c\}}$ ,  $q_c = 1 \cdots Q_c$ . In order to introduce redundancy, the coding operator  $\mathcal{C}(\cdot)$  employs only a subset of these possible realizations of  $\mathbf{c}$ .

We assume that  $Q_c$  of (4.4) equals the number  $\tilde{Q}$  of (2.13) of possible realizations of the transmit vector  $\underline{\mathbf{t}}$  of (2.5), that is we have

$$\begin{aligned} Q_c = 2^{N_c} = \tilde{Q} &= M^{2N_F}, \\ N_c &= 2N_F \log_2 M. \end{aligned} \quad (4.5)$$

Prior to being mapped onto the transmit vector  $\underline{\mathbf{t}}$ , we subject the code vector  $\mathbf{c}$  of (4.1) to a code interleaving operation. With the number  $Z$  of PDS subsets and the dimension  $N_c$  of  $\mathbf{c}$  of (4.1) we introduce in analogy to (1.1) the relation

$$Z = N_c / N_z, \quad (4.6)$$

which determines for given values  $Z$  and  $N_c$  the integer  $N_z$ . The code interleaver in the model of Fig. 4.1 is characterized by the code interleaving operator  $\mathcal{I}_c^{(N_z, Z)}(\cdot)$ . This operator transforms the code vector  $\mathbf{c}$  into the interleaved code vector  $\mathbf{c}_i$  according to the scheme

$$\begin{aligned} \mathbf{C} &= \begin{pmatrix} c_1 & c_2 & c_3 & \cdots & c_{2Z} \\ c_{2Z+1} & c_{2Z+2} & c_{2Z+3} & \cdots & c_{4Z} \\ c_{4Z+1} & c_{4Z+2} & c_{4Z+3} & \cdots & c_{6Z} \\ \vdots & \vdots & \vdots & \ddots & \vdots \\ c_{(N_z-2)Z+1} & c_{(N_z-2)Z+2} & c_{(N_z-2)Z+3} & \cdots & c_{N_c} \end{pmatrix}, \\ \mathbf{c}_i &= (c_{i,1} \cdots c_{i,n_c} \cdots c_{i,N_c})^T = \mathcal{I}_c^{(N_z, Z)}(\mathbf{c}) = \text{vec}(\mathbf{C}). \end{aligned} \quad (4.7)$$

To each possible realization  $\mathbf{c}^{\{q_c\}}$  of  $\mathbf{c}$  of (4.1) corresponds a realization  $\mathbf{c}_i^{\{q_c\}}$  of  $\mathbf{c}_i$  of (4.7).

Concerning the further signal processing, the interleaved code vector  $\mathbf{c}_i$  takes in the model of Fig. 4.1 the same position as the information vector  $\mathbf{u}$  in the model of Fig. 3.3. In the mapper of the model of Fig. 4.1,  $\mathbf{c}_i$  of (4.7) is mapped on the transmit vector  $\underline{\mathbf{t}}$  by applying the procedures introduced in (2.18) to (2.22) for QPSK modulation, and in (2.23) to (2.27) for 16QAM modulation.

With a view to perform PDS, as already shown in (3.16),  $\underline{\mathbf{t}}$  is split up into  $Z$  partial transmit vectors  $\underline{\mathbf{t}}^{(z)}$ . To each of these corresponds with  $\mathbf{c}_i$  of (4.7) a partial interleaved code vector

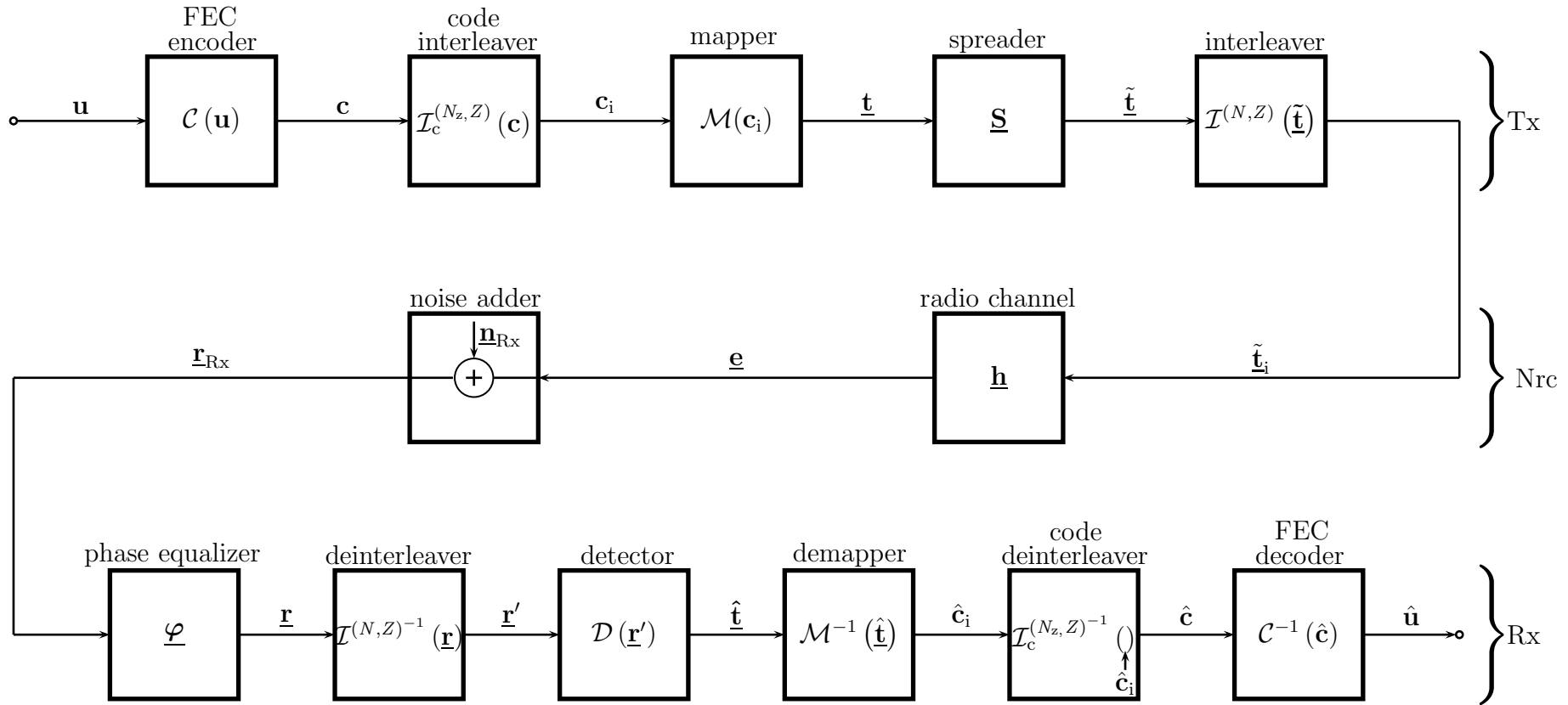


Fig. 4.1. OFDM transmission model incorporating PDS and FEC encoding

$$\mathbf{c}_i^{(z)} = \left( c_{i,1}^{(z)} \cdots c_{i,n_z}^{(z)} \cdots c_{i,N_z}^{(z)} \right)^T, \quad N_z = N_c/Z,$$

$$c_{i,n_z}^{(z)} = \begin{cases} c_{i,n_z+(z-1)N_z/2} & \text{for } n_z \leq N_z/2, \\ c_{i,n_z+(z-2)N_z/2+N_c/2} & \text{for } n_z > N_z/2 \end{cases}, \quad (4.8)$$

$$z = 1 \cdots Z.$$

In the receiver, estimates

$$\hat{\mathbf{c}}_i^{(z)} = \left( \hat{c}_{i,1}^{(z)} \cdots \hat{c}_{i,n_z}^{(z)} \cdots \hat{c}_{i,N_z}^{(z)} \right)^T \quad (4.9)$$

of the partial interleaved code vectors  $\mathbf{c}_i^{(z)}$  of (4.8) are determined by resorting to ML, MMSE or ZF detection as shown in Section 3.5. From the estimates  $\hat{\mathbf{c}}_i^{(z)}$  of (4.9) results the estimate

$$\hat{\mathbf{c}}_i = \left( \hat{\mathbf{c}}_i^{(1)T} \cdots \hat{\mathbf{c}}_i^{(z)T} \cdots \hat{\mathbf{c}}_i^{(Z)T} \right)^T \quad (4.10)$$

of  $\mathbf{c}_i$  of (4.7). Finally, as indicated in the model of Fig. 4.1, code deinterleaving and FEC decoding yield the estimate  $\hat{\mathbf{u}}$  of the transmitted information vector  $\mathbf{u}$  of (2.2).

An issue not yet addressed up to now are the above described inclusions of an FEC code interleaver in the transmitter and of an FEC code deinterleaver in the receiver in the model of Fig. 4.1. As explained in Subsection 3.6.4, all  $N$  components of the estimate  $\hat{\mathbf{t}}^{(z)}$  of the partial transmit vector  $\mathbf{t}^{(z)}$  are equally affected by the good or ill condition of the corresponding partial system matrix  $\mathbf{A}^{(z)}$  of (3.35). Therefore, as shown by an example in Table 3.2, the bit errors associated with the estimate  $\hat{\mathbf{t}}^{(z)}$  tend to be bursty. It is well known that certain FEC encoding schemes are particularly sensitive to burst errors [Fri95]. In order to break up such burst errors, as shown in the system model of Fig. 4.1, the code vector  $\mathbf{c}$  of (4.1) is subjected to the code interleaving of (4.7) before being fed into the mapper.

For each of the  $N_c$  components  $\hat{c}_{i,n_c}$  of the estimate  $\hat{\mathbf{c}}_i$  of (4.10) delivered by the demapper in the system model of Fig. 4.1, we can introduce the probability

$$p_{n_c} = \text{Prob}(\hat{c}_{i,n_c} \neq c_{i,n_c}), \quad n_c = 1 \cdots N_c, \quad (4.11)$$

of the event that the estimated component  $\hat{c}_{i,n_c}$  differs from the transmitted component  $c_{i,n_c}$ . With these probabilities, which have the character of error probabilities, we can form the vector [HH89, Fri95, GB10]

$$\mathbf{w} = (w_1 \cdots w_{n_c} \cdots w_{N_c})^T,$$

$$w_{n_c} = \ln \left( \frac{1 - p_{n_c}}{p_{n_c}} \right), \quad n_c = 1 \cdots N_c, \quad (4.12)$$

which we term reliability vector. With this vector, the hard decided estimate  $\hat{\mathbf{c}}_i$  occurring at the demapper output can be transformed by a soft bit generator, as shown in the system model of Fig. 4.2, into the soft estimate [HH89, Fri95, GB10]

$$\hat{\mathbf{c}}_{i,\text{soft}} = (\hat{c}_{i,\text{soft},1} \cdots \hat{c}_{i,\text{soft},n_c} \cdots \hat{c}_{i,\text{soft},N_c})^T = \mathbf{w} \odot \hat{\mathbf{c}}_i \quad (4.13)$$

of  $\mathbf{c}_i$  of (4.7). Deinterleaving of  $\hat{\mathbf{c}}_{i,\text{soft}}$  of (4.13) yields the soft estimate

$$\hat{\mathbf{c}}_{\text{soft}} = (\hat{c}_{\text{soft},1} \cdots \hat{c}_{\text{soft},n_c} \cdots \hat{c}_{\text{soft},N_c})^T = \mathcal{I}_c^{(N_z, Z)^{-1}}(\hat{\mathbf{c}}_{i,\text{soft}}), \quad \hat{c}_{\text{soft},n_c} \in \mathbb{R}, \quad (4.14)$$

of  $\mathbf{c}$  of (4.1), which then is forwarded to the soft input FEC decoder [Fri95, GB10] in order to deliver the estimate  $\hat{\mathbf{u}}$  of  $\mathbf{u}$  of (2.2).

It should be mentioned that the reliability vector  $\mathbf{w}$  of (4.12) depends on the outcome of the individual estimation of  $\mathbf{c}_i$  and is not, like for example the bit error probability  $P_b$  of (2.76), a quantity characterizing the mean overall system performance.

## 4.3 Case study

### 4.3.1 System characteristics and parameters

In order to verify and illustrate the scheme of OFDM transmission with PDS and FEC encoding, we perform computer simulations. We consider a system with the following characteristics:

- QPSK modulation given by (2.18) to (2.22),
- number of OFDM subcarriers

$$N_F = 128, \quad (4.15)$$

- channel parameter introduced in (2.38)

$$1 \leq W \leq 128, \quad (4.16)$$

- number of PDS subsets

$$Z = 32, \quad (4.17)$$

- ML detection of (3.44) complemented by the generation of reliability information as explained in Section 4.2,

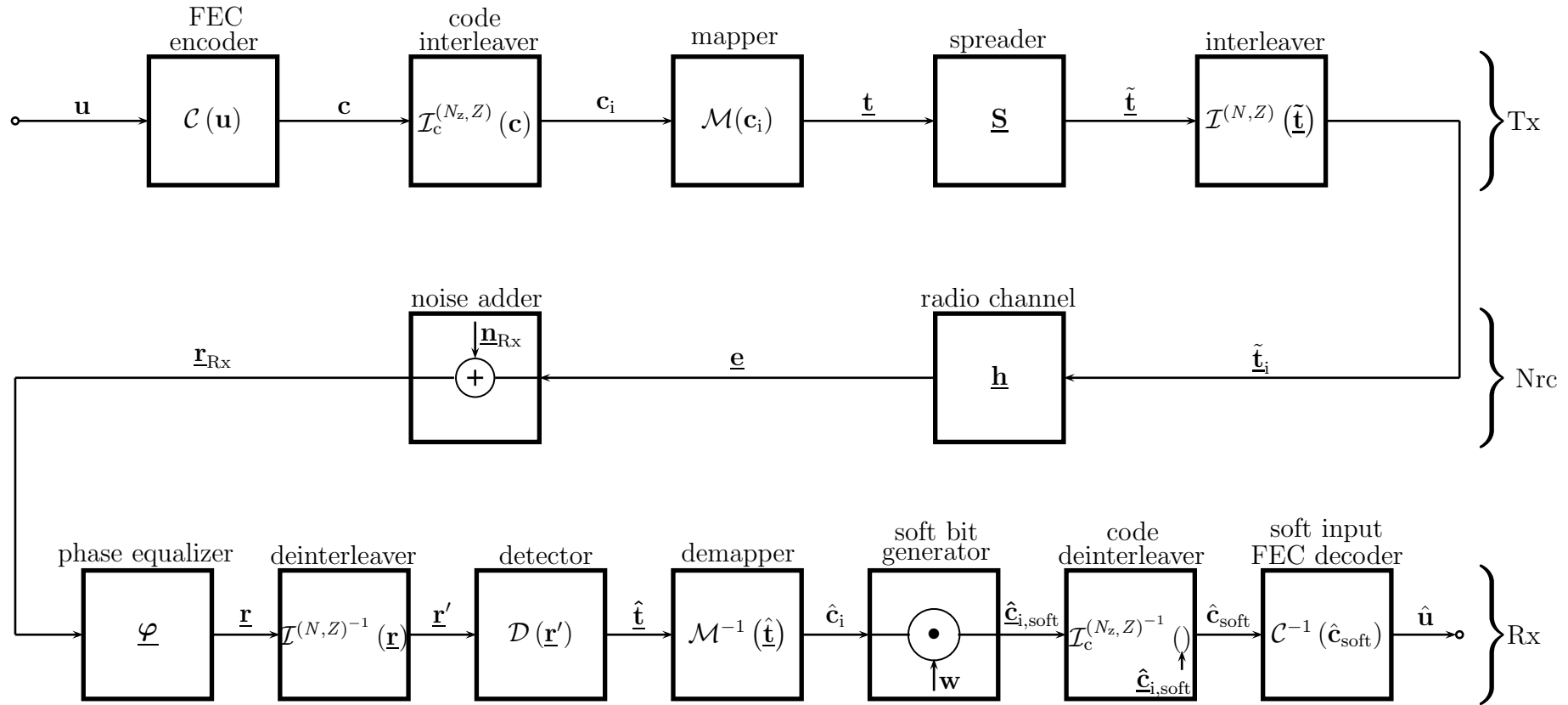


Fig. 4.2. OFDM transmission model incorporating PDS, FEC encoding and soft input FEC decoding

- terminated convolutional FEC encoding [VO79, Fri95] with the code rate

$$R_c = \frac{1}{2} \quad (4.18)$$

and with the generator polynomials

$$\begin{aligned} g_1(x) &= 1 + x + x^2, \\ g_2(x) &= 1 + x^2, \end{aligned} \quad (4.19)$$

and

- soft input Viterbi FEC decoding [Fri95, GB10] .

With the above system characteristics, we obtain the system parameters listed in Table 4.1.

designation	quantity
dimension of $\mathbf{u}$	$N_u = 2N_F \log_2 M = 256$
number of occurring realizations of $\mathbf{u}$	$Q_u = 2^{N_u} = 2^{256}$
dimension of $\underline{\mathbf{t}}, \mathbf{x}, \mathbf{y}, \underline{\mathbf{h}}, \underline{\mathbf{h}}$	$N_F = 128$
size of set $\mathbb{V}$	$M = 2$
number of possible realizations of $\underline{\mathbf{t}}$ ,	$\tilde{Q} = M^{2N_F} = 2^{256}$
number of possible realizations of $\mathbf{x}, \mathbf{y}$	$Q = M^{N_F} = 2^{128}$
number of PDS subsets	$Z = N_F/N = 32$
dimension of $\underline{\mathbf{t}}^{(z)}, \mathbf{x}^{(z)}, \mathbf{y}^{(z)}$	$N = 4$
number of possible realizations of $\underline{\mathbf{t}}^{(z)}$	$M^{2N} = 256$
number of possible realizations of $\mathbf{x}^{(z)}, \mathbf{y}^{(z)}$	$S = M^N = 16$
dimension of $\mathbf{c}$	$N_c = 2N_F \log_2 M = 256$
number of possible realizations of $\mathbf{c}$	$Q_c = 2^{N_c} = 2^{256}$
dimension of $\mathbf{c}^{(z)}$	$N_z = N_c/Z = 8$
number of possible realizations of $\mathbf{c}^{(z)}$	$M^{N_z} = 256$

Table 4.1. System parameters used in the case study

### 4.3.2 Mathematical description

The gross average SNR per bit of (4.3) becomes with the system characteristics and parameters introduced in Subsection 4.3.1

$$\gamma_b = \frac{1}{R_c \log_2 M} \frac{\sigma_t^2 \sigma_h^2}{\sigma^2} = \frac{2\sigma_t^2 \sigma_h^2}{\sigma^2}. \quad (4.20)$$

The real and imaginary part vectors  $\mathbf{x}^{(z)}$  and  $\mathbf{y}^{(z)}$  of the partial transmit vector  $\underline{\mathbf{t}}^{(z)}$  of (3.16) have the  $S$  equal 16 possible realizations

$$\mathbf{x}^{(z)\{s_x\}} = \begin{pmatrix} x_1^{(z)\{s_x\}} \\ x_2^{(z)\{s_x\}} \\ x_3^{(z)\{s_x\}} \\ x_4^{(z)\{s_x\}} \end{pmatrix} = -0.5 \times \begin{pmatrix} (-1)^{\text{floor}(s_x/(8+1))} \\ (-1)^{\text{floor}(2s_x/(8+\frac{1}{2}))} \\ (-1)^{\text{floor}(4s_x/(8+\frac{1}{4}))} \\ (-1)^{\text{floor}(8s_x/(8+\frac{1}{8}))} \end{pmatrix}, \quad s_x = 1 \cdots 16, \quad (4.21)$$

and

$$\mathbf{y}^{(z)\{s_y\}} = \begin{pmatrix} y_1^{(z)\{s_y\}} \\ y_2^{(z)\{s_y\}} \\ y_3^{(z)\{s_y\}} \\ y_4^{(z)\{s_y\}} \end{pmatrix} = -0.5 \times \begin{pmatrix} (-1)^{\text{floor}(s_y/(8+1))} \\ (-1)^{\text{floor}(2s_y/(8+\frac{1}{2}))} \\ (-1)^{\text{floor}(4s_y/(8+\frac{1}{4}))} \\ (-1)^{\text{floor}(8s_y/(8+\frac{1}{8}))} \end{pmatrix}, \quad s_y = 1 \cdots 16, \quad (4.22)$$

respectively. By (4.21) and (4.22), to each superscript  $s_x$  or  $s_y$  the corresponding realizations of the real and imaginary part vectors  $\mathbf{x}^{(z)}$  and  $\mathbf{y}^{(z)}$ , respectively, are determined.

ML detection as described in (3.48) and (3.49) yields the estimate  $\mathbf{x}^{(z)\{s'_x\}}$  of the transmitted real part vector  $\mathbf{x}^{(z)\{s_x\}}$  and the estimate  $\mathbf{y}^{(z)\{s'_y\}}$  of the transmitted imaginary part vector  $\mathbf{y}^{(z)\{s_y\}}$ . For a given  $\mathbf{r}'_{\text{R}}^{(z)}$  of (3.45) observed in the receiver, we obtain with

$$P_{\text{x}}^{(z)} = \frac{1}{4\pi^2\sigma^4} \sum_{s_x=1}^{16} \exp\left(-\frac{|\mathbf{r}'_{\text{R}}^{(z)} - \mathbf{h}'^{(z)} \odot (\mathbf{W}^{4 \times 4} \mathbf{x}^{(z)\{s_x\}})|^2}{2\sigma^2}\right) \quad (4.23)$$

the probability

$$p_{\text{x},s_x}^{(z)} = \frac{1}{P_{\text{x}}} p_{\mathbf{r}'_{\text{R}}^{(z)} | \mathbf{x}^{(z)\{s_x\}} \left( \mathbf{r}'_{\text{R}}^{(z)} | \mathbf{x}^{(z)\{s_x\}} \right) = \frac{1}{P_{\text{x}}} \frac{1}{4\pi^2\sigma^4} \exp\left(-\frac{|\mathbf{r}'_{\text{R}}^{(z)} - \mathbf{h}'^{(z)} \odot (\mathbf{W}^{4 \times 4} \mathbf{x}^{(z)\{s_x\}})|^2}{2\sigma^2}\right), \quad s_x = 1 \cdots 16, \quad (4.24)$$

of the event that the transmitted realization of the real part transmit vector  $\mathbf{x}^{(z)}$  is  $\mathbf{x}^{(z)\{s_x\}}$ . Analogously, we obtain for a given  $\mathbf{r}'_{\text{I}}^{(z)}$  of (3.46) observed in the receiver with

$$P_{\text{y}}^{(z)} = \frac{1}{4\pi^2\sigma^4} \sum_{s=1}^{16} \exp\left(-\frac{|\mathbf{r}'_{\text{I}}^{(z)} - \mathbf{h}'^{(z)} \odot (\mathbf{W}^{4 \times 4} \mathbf{y}^{(z)\{s_y\}})|^2}{2\sigma^2}\right) \quad (4.25)$$

the probability

$$p_{y, s_y}^{(z)} = \frac{1}{P_y^{(z)}} p_{\mathbf{r}'_R(z) | \mathbf{y}^{(z)\{s_y\}}} \left( \mathbf{r}'_R(z) \mid \mathbf{y}^{(z)\{s_y\}} \right) =$$

$$\frac{1}{P_y^{(z)}} \frac{1}{4\pi^2 \sigma^4} \exp \left( - \frac{|\mathbf{r}'_R(z) - \mathbf{h}'(z) \odot (\mathbf{W}^{4 \times 4} \mathbf{y}^{(z)\{s_y\}})|^2}{2\sigma^2} \right), \quad s_y = 1 \cdots 16, \quad (4.26)$$

of the event that the transmitted realization of the imaginary part vector  $\mathbf{y}^{(z)}$  is  $\mathbf{y}^{(z)\{s_y\}}$ .

If we compare the real and imaginary part vectors  $\mathbf{x}^{(z)\{s'_x\}}$  and  $\mathbf{y}^{(z)\{s'_y\}}$  obtained by ML detection following (3.48) and (3.49) with the transmitted real and imaginary part vectors  $\mathbf{x}^{(z)\{s_x\}}$  and  $\mathbf{y}^{(z)\{s_y\}}$ , then zero, one, two, three of four elements of the estimates  $\mathbf{x}^{(z)\{s'_x\}}$  and  $\mathbf{y}^{(z)\{s'_y\}}$  may be erroneous. In order to quantitatively describe the error situation, we introduce the error coefficients

$$f_n(s'_x, s_x) = \left[ \text{floor} \left( \frac{s'_x}{17 \cdot 2^{-n}} \right) + \text{floor} \left( \frac{s_x}{17 \cdot 2^{-n}} \right) \right] \bmod 2 =$$

$$\begin{cases} 0, & \text{if component } x_n^{(z)\{s'_x\}} \text{ of } \mathbf{x}^{(z)\{s'_x\}} \text{ is correct,} \\ 1 & \text{else,} \end{cases} \quad (4.27)$$

$$n = 1 \cdots 4,$$

and

$$g_n(s'_y, s_y) = \left[ \text{floor} \left( \frac{s'_y}{17 \cdot 2^{-n}} \right) + \text{floor} \left( \frac{s_y}{17 \cdot 2^{-n}} \right) \right] \bmod 2 =$$

$$\begin{cases} 0, & \text{if component } y_n^{(z)\{s'_y\}} \text{ of } \mathbf{y}^{(z)\{s'_y\}} \text{ is correct,} \\ 1 & \text{else,} \end{cases} \quad (4.28)$$

$$n = 1 \cdots 4.$$

For illustration we list in Table 4.2  $f_n(s'_x, s_x)$  of (4.27) versus  $s'_x$  and  $s_x$ ; for instance, in the case  $s'_x$  equal 11 and  $s_x$  equal 14 the elements  $x_2^{(z)\{s'_x\}}$ ,  $x_3^{(z)\{s'_x\}}$  and  $x_4^{(z)\{s'_x\}}$  of the estimate  $\mathbf{x}^{(z)\{s'_x\}}$  would be in error. Now, with the error coefficients  $f_n(s'_x, s_x)$  of (4.27) and  $g_n(s'_y, s_y)$  of (4.28) we obtain the partial error probabilities

$$p_{x, n}^{(z)} = \text{Prob} \left( x_n^{(z)\{s'_x\}} \neq x_n^{(z)\{s_x\}} \right) = \frac{1}{P_x} \sum_{s_x=1}^{16} f_n(s'_x, s_x) p_{\mathbf{r}'_R(z) | \mathbf{x}^{(z)\{s_x\}}} \left( \mathbf{r}'_R(z) \mid \mathbf{x}^{(z)\{s_x\}} \right), \quad n = 1 \cdots 4, \quad (4.29)$$

and

$$p_{y, n}^{(z)} = \text{Prob} \left( y_n^{(z)\{s'_y\}} \neq y_n^{(z)\{s_y\}} \right) = \frac{1}{P_y} \sum_{s_y=1}^{16} g_n(s'_y, s_y) p_{\mathbf{r}'_I(z) | \mathbf{y}^{(z)\{s_y\}}} \left( \mathbf{r}'_I(z) \mid \mathbf{y}^{(z)\{s_y\}} \right), \quad n = 1 \cdots 4. \quad (4.30)$$



$s_x \backslash s'_x$	1	2	3	4	5	6	7	8
1	0,0,0,0	0,0,0,1	0,0,1,0	0,0,1,1	0,1,0,0	0,1,0,1	0,1,1,0	0,1,1,1
2	0,0,0,1	0,0,0,0	0,0,1,1	0,0,1,0	0,1,0,1	0,1,0,0	0,1,1,1	0,1,1,0
3	0,0,1,0	0,0,1,1	0,0,0,0	0,0,0,1	0,1,1,0	0,1,1,1	0,1,0,0	0,1,0,1
4	0,0,1,1	0,0,1,0	0,0,0,1	0,0,0,0	0,1,1,1	0,1,1,0	0,1,0,1	0,1,0,0
5	0,1,0,0	0,1,0,1	0,1,1,0	0,1,1,1	0,0,0,0	0,0,0,1	0,0,1,0	0,0,1,1
6	0,1,0,1	0,1,0,0	0,1,1,1	0,1,1,0	0,0,0,1	0,0,0,0	0,0,1,1	0,0,1,0
7	0,1,1,0	0,1,1,1	0,1,0,0	0,1,0,1	0,0,1,0	0,0,1,1	0,0,0,0	0,0,0,1
8	0,1,1,1	0,1,1,0	0,1,0,1	0,1,0,0	0,0,1,1	0,0,1,0	0,0,0,1	0,0,0,0
9	1,0,0,0	1,0,0,1	1,0,1,0	1,0,1,1	1,1,0,0	1,1,0,1	1,1,1,0	1,1,1,1
10	1,0,0,1	1,0,0,0	1,0,1,1	1,0,1,0	1,1,0,1	1,1,0,0	1,1,1,1	1,1,1,0
11	1,0,1,0	1,0,1,1	1,0,0,0	1,0,0,1	1,1,1,0	1,1,1,1	1,1,0,0	1,1,0,1
12	1,0,1,1	1,0,1,0	1,0,0,1	1,0,0,0	1,1,1,1	1,1,1,0	1,1,0,1	1,1,0,0
13	1,1,0,0	1,1,0,1	1,1,1,0	1,1,1,1	1,0,0,0	1,0,0,1	1,0,1,0	1,0,1,1
14	1,1,0,1	1,1,0,0	1,1,1,1	1,1,1,0	1,0,0,1	1,0,0,0	1,0,1,1	1,0,1,0
15	1,1,1,0	1,1,1,1	1,1,0,0	1,1,0,1	1,0,1,0	1,0,1,1	1,0,0,0	1,0,0,1
16	1,1,1,1	1,1,1,0	1,1,0,1	1,1,0,0	1,0,1,1	1,0,1,0	1,0,0,1	1,0,0,0

$s_x \backslash s'_x$	9	10	11	12	13	14	15	16
1	1,0,0,0	1,0,0,1	1,0,1,0	1,0,1,1	1,1,0,0	1,1,0,1	1,1,1,0	1,1,1,1
2	1,0,0,1	1,0,0,0	1,0,1,1	1,0,1,0	1,1,0,1	1,1,0,0	1,1,1,1	1,1,1,0
3	1,0,1,0	1,0,1,1	1,0,0,0	1,0,0,1	1,1,1,0	1,1,1,1	1,1,0,0	1,1,0,1
4	1,0,1,1	1,0,1,0	1,0,0,1	1,0,0,0	1,1,1,1	1,1,1,0	1,1,0,1	1,1,0,0
5	1,1,0,0	1,1,0,1	1,1,1,0	1,1,1,1	1,0,0,0	1,0,0,1	1,0,1,0	1,0,1,1
6	1,1,0,1	1,1,0,0	1,1,1,1	1,1,1,0	1,0,0,1	1,0,0,0	1,0,1,1	1,0,1,0
7	1,1,1,0	1,1,1,1	1,1,0,0	1,1,0,1	1,0,1,0	1,0,1,1	1,0,0,0	1,0,0,1
8	1,1,1,1	1,1,1,0	1,1,0,1	1,1,0,0	1,0,1,1	1,0,1,0	1,0,0,1	1,0,0,0
9	0,0,0,0	0,0,0,1	0,0,1,0	0,0,1,1	0,1,0,0	0,1,0,1	0,1,1,0	0,1,1,1
10	0,0,0,1	0,0,0,0	0,0,1,1	0,0,1,0	0,1,0,1	0,1,0,0	0,1,1,1	0,1,1,0
11	0,0,1,0	0,0,1,1	0,0,0,0	0,0,0,1	0,1,1,0	0,1,1,1	0,1,0,0	0,1,0,1
12	0,0,1,1	0,0,1,0	0,0,0,1	0,0,0,0	0,1,1,1	0,1,1,0	0,1,0,1	0,1,0,0
13	0,1,0,0	0,1,0,1	0,1,1,0	0,1,1,1	0,0,0,0	0,0,0,1	0,0,1,0	0,0,1,1
14	0,1,0,1	0,1,0,0	0,1,1,1	0,1,1,0	0,0,0,1	0,0,0,0	0,0,1,1	0,0,1,0
15	0,1,1,0	0,1,1,1	0,1,0,0	0,1,0,1	0,0,1,0	0,0,1,1	0,0,0,0	0,0,0,1
16	0,1,1,1	0,1,1,0	0,1,0,1	0,1,0,0	0,0,1,1	0,0,1,0	0,0,0,1	0,0,0,0

Table 4.2. Visualization of the error coefficients  $f_1(s'_x, s_x)$ ,  $f_2(s'_x, s_x)$ ,  $f_3(s'_x, s_x)$ ,  $f_4(s'_x, s_x)$  and  $g_1(s'_y, s_y)$ ,  $g_2(s'_y, s_y)$ ,  $g_3(s'_y, s_y)$ ,  $g_4(s'_y, s_y)$

In order to introduce PDS, the interleaved code vector  $\mathbf{c}_i$  of (4.7) is according to (4.8) split up into  $Z$  equal 32 partial interleaved code vectors

$$\mathbf{c}_i^{(z)} = \left( c_{i,1}^{(z)}, c_{i,2}^{(z)}, c_{i,3}^{(z)}, c_{i,4}^{(z)}, c_{i,5}^{(z)}, c_{i,6}^{(z)}, c_{i,7}^{(z)}, c_{i,8}^{(z)} \right)^T, \quad z = 1 \cdots 32, \quad (4.31)$$

of dimension  $N_z$  equal eight each. In the case of the chosen modulation scheme QPSK, the components of the real and imaginary part vectors  $\mathbf{x}^{(z)}$  and  $\mathbf{y}^{(z)}$  are related to the components of the partial interleaved code vector  $\mathbf{c}_i^{(z)}$  of (4.31) according to

$$\mathbf{x}^{(z)} = \begin{pmatrix} x_1^{(z)} \\ x_2^{(z)} \\ x_3^{(z)} \\ x_4^{(z)} \end{pmatrix} = \begin{pmatrix} c_{i,1}^{(z)} \\ c_{i,2}^{(z)} \\ c_{i,3}^{(z)} \\ c_{i,4}^{(z)} \end{pmatrix} \quad (4.32)$$

and

$$\mathbf{y}^{(z)} = \begin{pmatrix} y_1^{(z)} \\ y_2^{(z)} \\ y_3^{(z)} \\ y_4^{(z)} \end{pmatrix} = \begin{pmatrix} c_{i,5}^{(z)} \\ c_{i,6}^{(z)} \\ c_{i,7}^{(z)} \\ c_{i,8}^{(z)} \end{pmatrix}. \quad (4.33)$$

Due to (4.32) and (4.33), we obtain with the error probabilities  $p_{x,n}^{(z)}$  and  $p_{y,n}^{(z)}$  of (4.29) and (4.30), respectively, the error probabilities

$$p_{n_z}^{(z)} = \text{Prob} \left( \hat{c}_{i,n_z}^{(z)} \neq c_{i,n_z}^{(z)} \right) = p_{x,n_z}^{(z)}, \quad n_z = 1 \cdots 4, \quad (4.34)$$

and

$$p_{n_z}^{(z)} = \text{Prob} \left( \hat{c}_{i,n_z}^{(z)} \neq c_{i,n_z}^{(z)} \right) = p_{y,n_z-4}^{(z)}, \quad n_z = 5 \cdots 8, \quad (4.35)$$

of the eight components  $\hat{c}_{i,n_z}^{(z)}$  of the estimate  $\hat{\mathbf{c}}_i^{(z)}$  of  $\mathbf{c}_i^{(z)}$ . With these error probabilities, we can determine the partial reliability vector [GB10]

$$\mathbf{w}^{(z)} = \left( w_1^{(z)} \cdots w_{n_z}^{(z)} \cdots w_{N_z}^{(z)} \right)^T, \quad (4.36)$$

$$w_{n_z}^{(z)} = \ln \left( \frac{1 - p_{n_z}^{(z)}}{p_{n_z}^{(z)}} \right), \quad n_z = 1 \cdots N_z, \quad N_z = 8.$$

Finally, the  $Z$  partial reliability vectors  $\mathbf{w}^{(z)}$  of (4.36) are composed to the total reliability vector

$$\mathbf{w} = \left( \mathbf{w}^{(1)T} \cdots \mathbf{w}^{(z)T} \cdots \mathbf{w}^{(Z)T} \right)^T \quad (4.37)$$

to be used in (4.13).

We also determine the MF bound for the case of FEC encoded OFDM transmission with PDS and utilization of reliability information. In doing so, we refer to the considerations made in Subsection 3.5.5. With the elements  $v_m$  of the set  $\mathbb{V}$  of (2.9) we designate the transmitted component of  $\mathbf{x}^{(z)}$  as

$$x_n^{(z)\{m_x\}} = v_{m_x} \quad (4.38)$$

and the MF estimate of this component as

$$\hat{x}_{\text{MF},n}^{(z)} = v_{m'_x}. \quad (4.39)$$

With  $\sigma_{\text{MF}}^{(z)}$  of (3.98) and  $\mathbf{r}'_{\text{R},n}^{(z)}$  of (3.93) we introduce

$$P_{\mathbf{x},n}^{(z)} = \frac{1}{\sqrt{2\pi}\sigma_{\text{MF}}^{(z)}} \sum_{m=1}^2 \exp\left(-\frac{|\mathbf{r}'_{\text{R},n}^{(z)} - \mathbf{a}_n^{(z)} v_m|^2}{2\sigma_{\text{MF}}^{(z)2}}\right), \quad (4.40)$$

and then obtain the error probability

$$p_{\mathbf{x},n}^{(z)} = \text{Prob}\left(\hat{x}_{\text{MF},n}^{(z)} \neq x_n^{(z)\{m_x\}}\right) = \frac{1}{P_{\mathbf{x},n}^{(z)}} \frac{1}{\sqrt{2\pi}\sigma_{\text{MF}}^{(z)}} \exp\left(-\frac{|\mathbf{r}'_{\text{R},n}^{(z)} - \mathbf{a}_n^{(z)} v_{m_x}|^2}{2\sigma_{\text{MF}}^{(z)2}}\right). \quad (4.41)$$

In analogy to (4.38) to (4.41) we can write with  $\mathbf{r}'_{\text{I},n}^{(z)}$  of (3.94)

$$y_n^{(z)\{m_y\}} = v_{m_y}, \quad (4.42)$$

$$\hat{y}_{\text{MF},n}^{(z)} = v_{m'_y}, \quad (4.43)$$

$$P_{\mathbf{y},n}^{(z)} = \frac{1}{\sqrt{2\pi}\sigma_{\text{MF}}^{(z)}} \sum_{m=1}^2 \exp\left(-\frac{|\mathbf{r}'_{\text{I},n}^{(z)} - \mathbf{a}_n^{(z)} v_m|^2}{2\sigma_{\text{MF}}^{(z)2}}\right), \quad (4.44)$$

and

$$p_{\mathbf{y},n}^{(z)} = \text{Prob}\left(\hat{y}_{\text{MF},n}^{(z)} \neq y_n^{(z)\{m_y\}}\right) = \frac{1}{P_{\mathbf{y},n}^{(z)}} \frac{1}{\sqrt{2\pi}\sigma_{\text{MF}}^{(z)}} \exp\left(-\frac{|\mathbf{r}'_{\text{I},n}^{(z)} - \mathbf{a}_n^{(z)} v_{m_y}|^2}{2\sigma_{\text{MF}}^{(z)2}}\right). \quad (4.45)$$

Now, with the error probabilities  $p_{\mathbf{x},n}^{(z)}$  of (4.41) and  $p_{\mathbf{y},n}^{(z)}$  of (4.45) we can determine the reliability vector  $\mathbf{w}$  following the expressions (4.34) to (4.37).

### 4.3.3 Simulation results

In order to verify the proposed scheme of OFDM transmission with PDS, FEC encoding and ML detection, we determine the bit error probability  $P_b$  of (2.76) depending on the mean gross SNR per bit  $\gamma_b$  of (4.20). We resort to Walsh-Hadamard PDS.

Fig. 4.3 holds for the normalized delay spread  $W$  equal 128, and we demonstrate the benefits of the proposed measures code interleaving (CI) and utilization of reliability information (URI). We see a curve each for the four cases

- No CI, no URI (case 1).
- No CI, but URI (case 2).
- CI, but no URI (case 3).
- CI & URI (case 4).

Case 4 concerns our proposed transmission scheme, and we recognize in Fig. 4.3 that in this case the performance is the best. Case 1 exhibits the worst performance, and the other two cases perform in between of the worst and the best case. For  $P_b$  equal  $10^{-5}$ , the best case shows an impressive superiority of more than 5 dB over the second best case.

In Fig. 4.4 we depict  $P_b$  versus  $\gamma_b$  with the normalized delay spread  $W$  of (2.38) as the curve parameter. We use CI & URI. For  $W$  equal 16 and 128, the solid curves apply for PDS, and the dashed curves for unspread transmission. We recognize that, for such relatively large values of  $W$ , PDS offers a distinct advantage over unspread transmission. For example, this advantage amounts to 3 dB for  $W$  equal 128 at  $P_b$  equal  $10^{-6}$ . For smaller values  $W$  as for instance four or one, transmission with PDS and unspread transmission show virtually the same performance, see the dash-dotted curves in Fig. 4.4. From the simulation results shown in Fig. 4.4 we can conclude that PDS is advantageous as long as  $W$  is significantly above the spreading factor  $N$ , whereas this advantage vanishes more and more if  $W$  approaches  $N$ . In order to further illustrate this situation, we refer to Fig. 4.5. In this figure we depict the value  $\gamma_b$  of (4.20) required to achieve the bit error probability  $P_b$  equal  $10^{-6}$  versus the channel parameter  $W$  for transmission with PDS and for unspread transmission. The benefit offered by PDS in the case of larger values  $W$  is obvious.

In Fig. 4.6 we depict the MF bound of FEC encoded OFDM transmission with PDS and URI with the curve parameter  $W$ . As indicated in Fig. 4.6, the simulations reveal that, for a given  $W$ , all curves for  $N$  equal to or larger than  $W$  coincide. This is due to the fact that by  $N$  equal  $W$  the diversity potential of the radio channel is fully exploited so that a further increase of  $N$  beyond  $W$  would not bear fruit. Finally, we show in

Fig. 4.7 the MF bound of FEC encoded OFDM transmission with URI and with the curve parameter  $W$  for the two cases PDS with  $N$  equal four and unspread transmission. The comparison of Figs. 4.4 and 4.7 shows that PDS with ML detection outperforms unspread transmission only if  $N$  is larger than  $W$ , whereas in the case of the MF bound, PDS outperforms unspread transmission already for  $N$  equal  $W$ , because in this case the mutual interference is neglected.

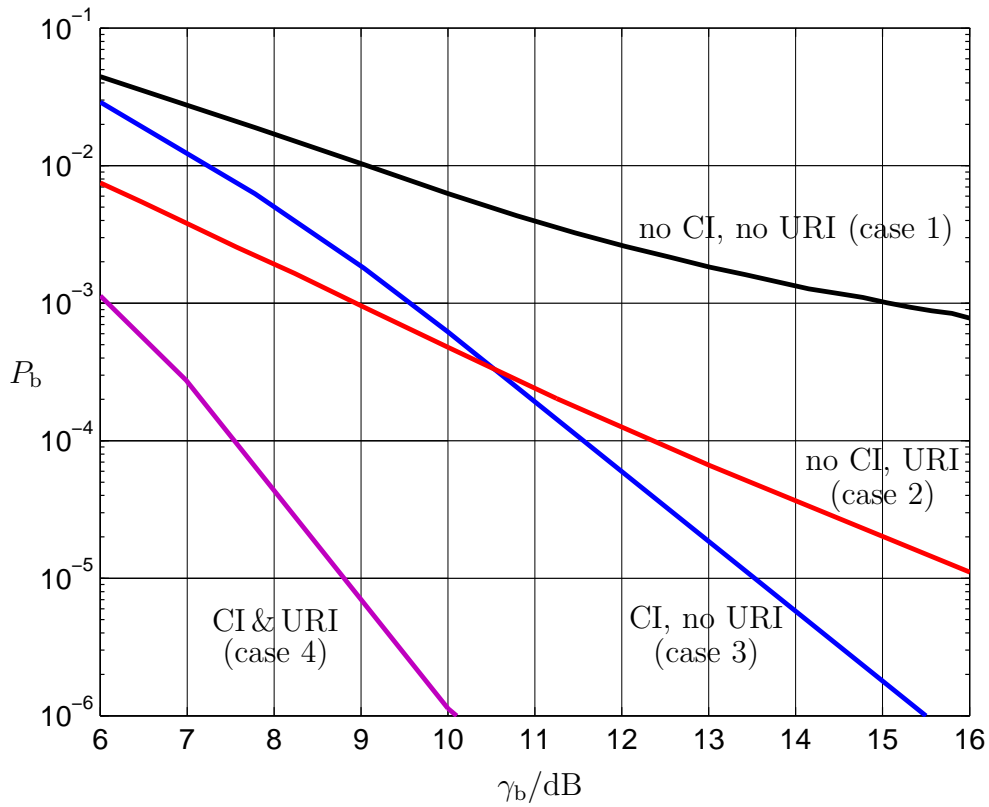


Fig. 4.3.  $P_b$  versus SNR  $\gamma_b$ , influence of CI and URI;  $W = 128$ ,  $N = 4$

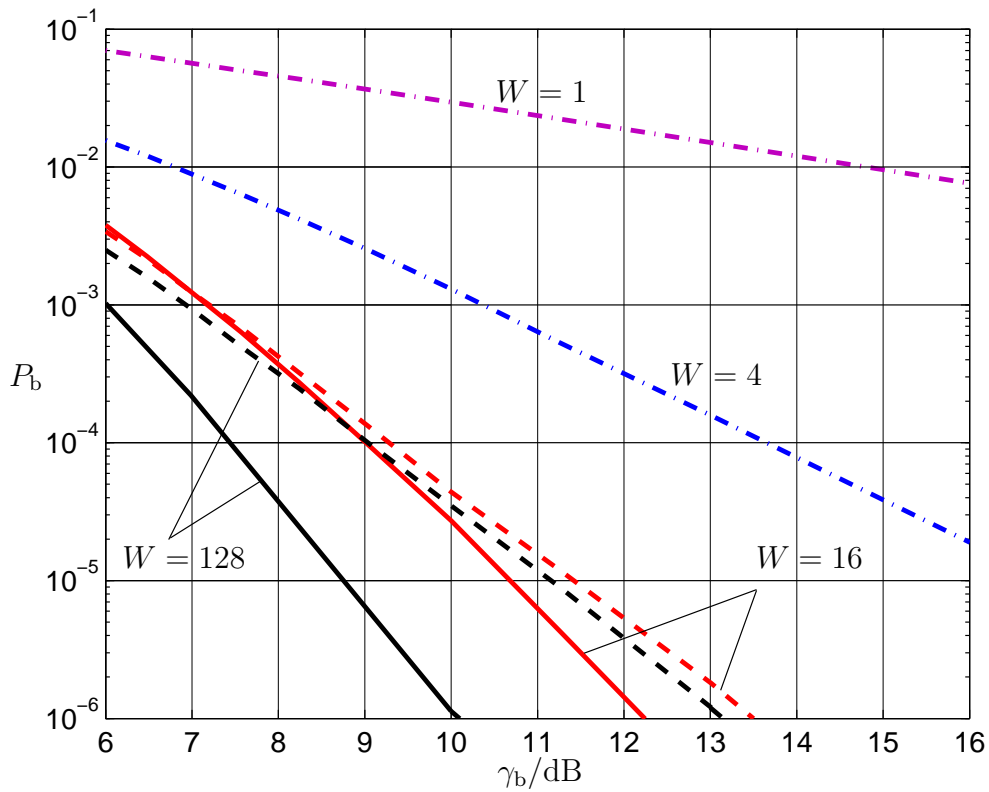


Fig. 4.4.  $P_b$  versus the SNR  $\gamma_b$ ; CI & URI; ML detection; parameter  $W$ ;  $N = 4$   
 ——— PDS    - - - unspread    - · - · - PDS and unspread

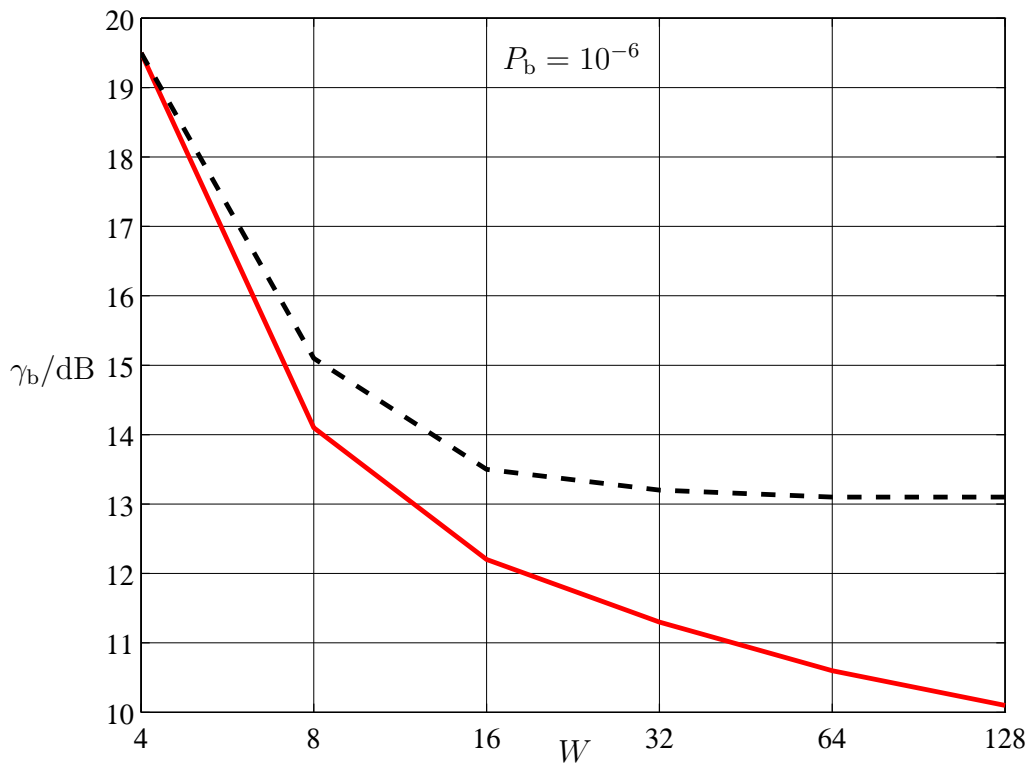


Fig. 4.5. SNR  $\gamma_b$  required to achieve  $P_b = 10^{-6}$  versus parameter  $W$ ;  $N = 4$   
 ——— PDS    - - - unspread

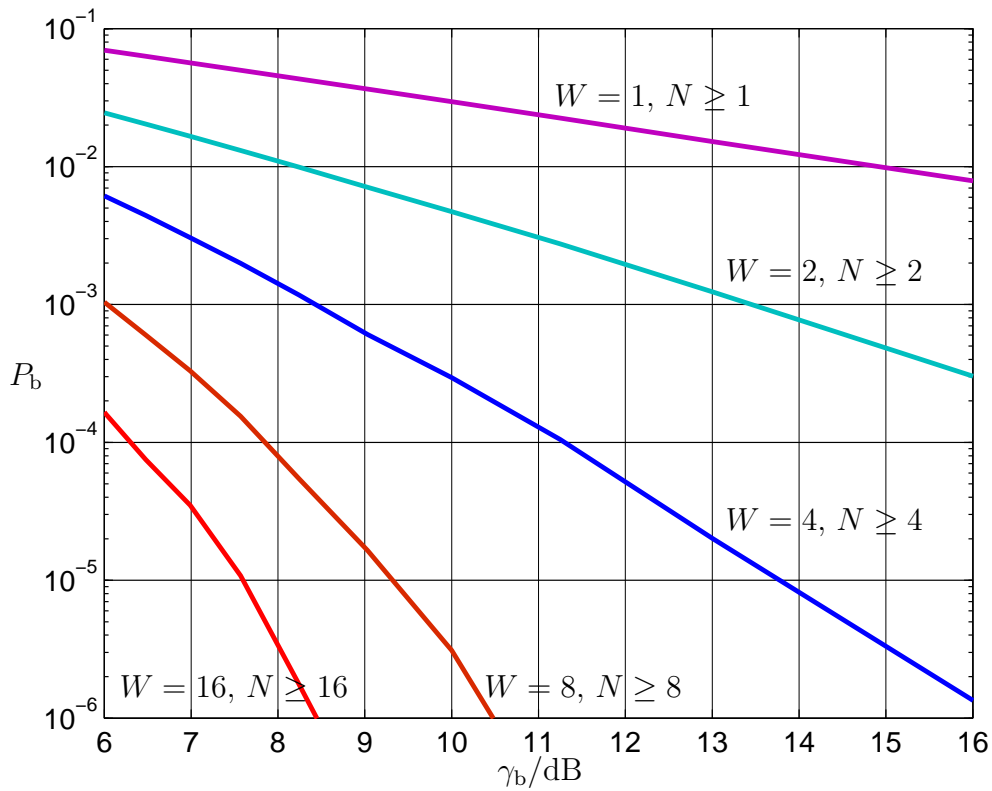


Fig. 4.6. MF bound of  $P_b$  versus SNR  $\gamma_b$ ; parameter  $W$ ; CI & URI

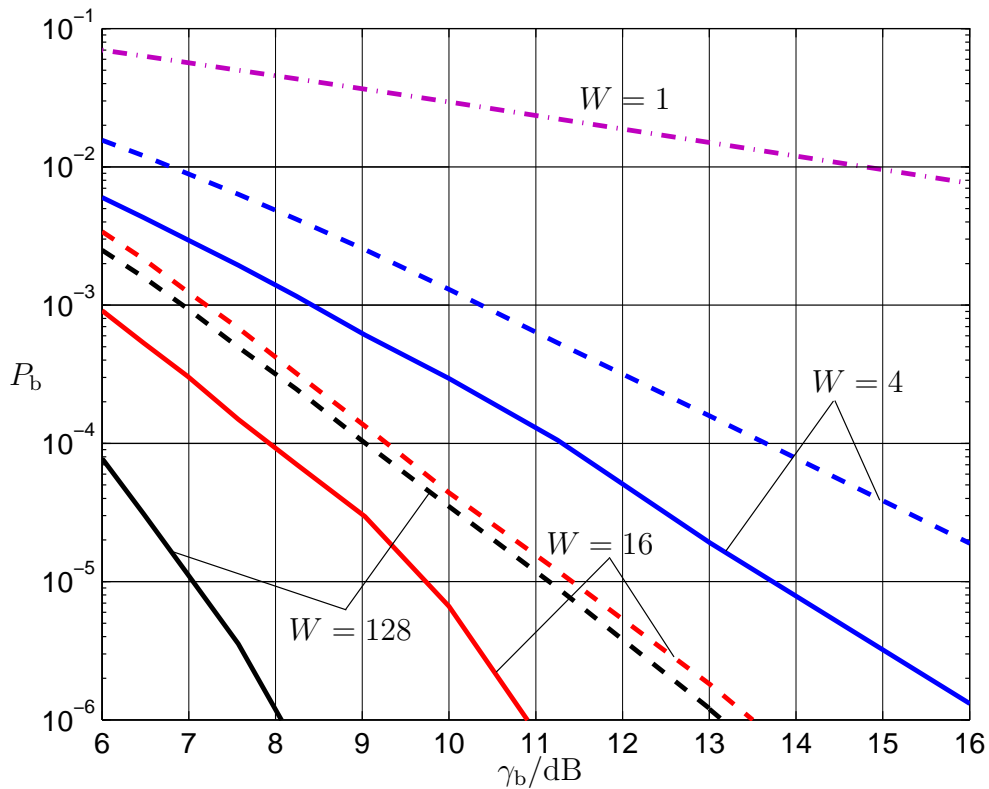


Fig. 4.7. MF bound of  $P_b$  versus SNR  $\gamma_b$ ; parameter  $W$ ; CI & URI;  $N = 4$   
 — PDS    - - - unspread    - · - · - PDS and unspread

# Chapter 5

## PAPR reduction by combining Partial Data Spreading with Selective Data Mapping (SDM)

### 5.1 Preliminary remarks

As already mentioned in Chapter 1, the channel access scheme OFDM has a number of advantages [vNP00]. However, the large PAPR of the OFDM symbols hampers the applicability of power efficient transmit amplifiers, which usually are non-linear, and, therefore, should be operated with signals of low PAPR in order to avoid distortions. In the transmission model of Fig. 2.1 the complex envelope  $\underline{s}(t)$  of an OFDM symbol is given by (2.79), and its PAPR is defined as

$$p_o = \frac{\max_{t \in \{-T/2 \dots T/2\}} (|\underline{s}(t)|^2)}{\frac{1}{T} \int_{-T/2}^{T/2} |\underline{s}(t)|^2 dt}. \quad (5.1)$$

In order to express  $p_o$  of (5.1) by the transmit vector  $\underline{\mathbf{t}}$  of (2.5), this vector is subjected to a  $k_o$  – fold oversampled inverse fast Fourier transformation (IFFT) with the  $(k_o N_F) \times (k_o N_F)$  Fourier matrix

$$\underline{\mathbf{F}}^{(k_o N_F) \times (k_o N_F)} \in \mathbb{C}^{(k_o N_F) \times (k_o N_F)}. \quad (5.2)$$

This yields the discrete time low pass equivalent

$$\underline{\mathbf{s}} = (\underline{s}_1 \cdots \underline{s}_{k_o n_F} \cdots \underline{s}_{k_o N_F})^T = \left( \underline{\mathbf{F}}^{(k_o N_F) \times (k_o N_F)} \right)^{-1} \begin{pmatrix} \underline{\mathbf{t}}^T, & \underbrace{0 \dots 0}_{(k_o - 1) N_F \text{ zeros}} \end{pmatrix}^T \quad (5.3)$$

of the OFDM symbol corresponding to  $\underline{\mathbf{t}}$ . With a sufficiently large  $k_o$  we can express the PAPR of (5.1) by the components  $\underline{s}_{k_o n_F}$  of  $\underline{\mathbf{s}}$  of (5.3) as

$$p_o = k_o N_F \frac{\max_{n_s \in \{1 \dots k_o N_F\}} (|\underline{s}_{n_s}|^2)}{(\underline{\mathbf{s}})^H \underline{\mathbf{s}}}. \quad (5.4)$$

Our simulations revealed that an oversampling factor  $k_o$  equal to four would be sufficiently large in the sense that, with larger values of  $k_o$ , (5.3) and (5.4) would yield virtually the same PAPR as for  $k_o$  equal to four. Therefore, all the simulation results presented in this chapter are generated for

$$k_o = 4. \quad (5.5)$$



The vectors  $\underline{\mathbf{t}}$  and  $\underline{\mathbf{s}}$  of an OFDM symbol and, therefore, its PAPR  $p_o$  depend on the carried information vector  $\mathbf{u}$  of (2.2). In PAPR reduction research [HL05],  $p_o$  of (5.4) is determined for many realizations of  $\mathbf{u}$ . The Complementary Cumulative Distribution Function (CCDF) of the PAPR is used as the performance measure. For the simulations of this chapter, we consider QPSK modulation given by (2.18) to (2.22) and set  $N_F$  equal 128. Fig. 5.1 depicts the CCDF of  $p_o$  of (5.4). We recognize that the value at  $\text{Prob}(p_o \geq \text{abscissa}) = 10^{-3}$  is approximately 11 dB. This means that the power amplifier has to be operated with a severe back-off in order to avoid distortions, and, consequently, with a very low power efficiency  $\eta$ . In order to overcome this problem, in the last 15 years some schemes of PAPR reduction were proposed and investigated [HL05]. A promising one of these is Selective Data Mapping (SDM) [BFH96, MS96, OO03].

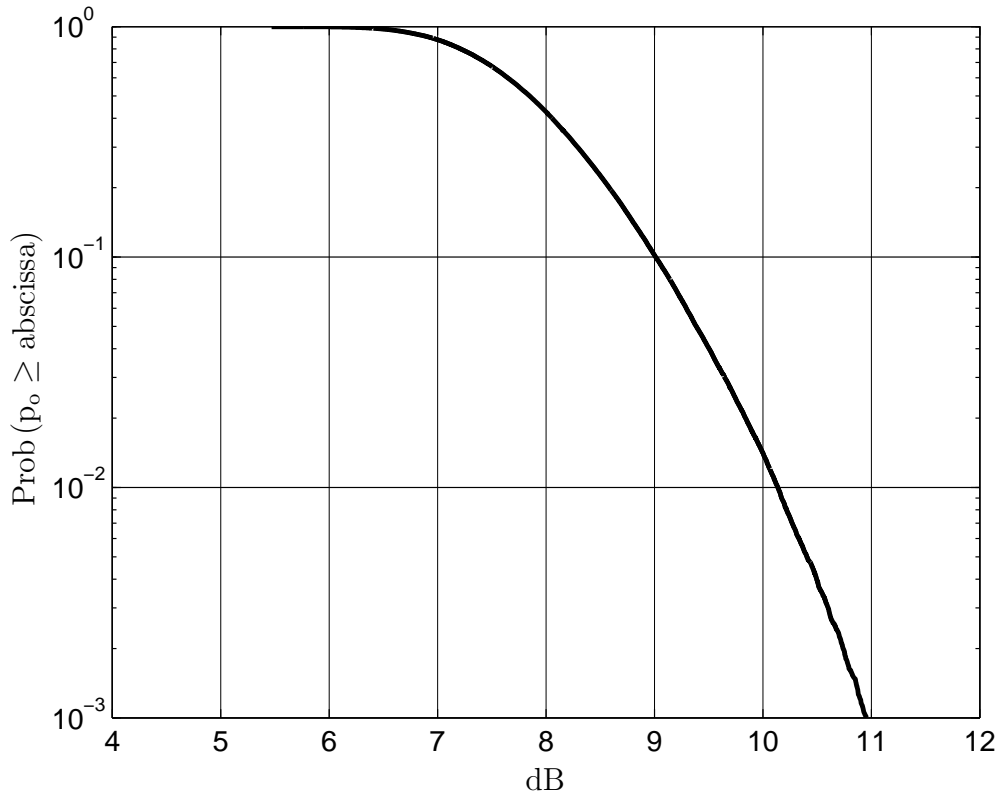


Fig. 5.1. CCDF of the PAPR  $p_o$  for the original OFDM symbols;  $N_F = 128$

In order to present conventional SDM [BFH96], we extend the transmission model of Fig. 2.1 on the transmit side by a phase factor set selector and a phase shifter, and on the receive side by an inverse phase shifter. Fig. 5.2 shows this extended transmission model.

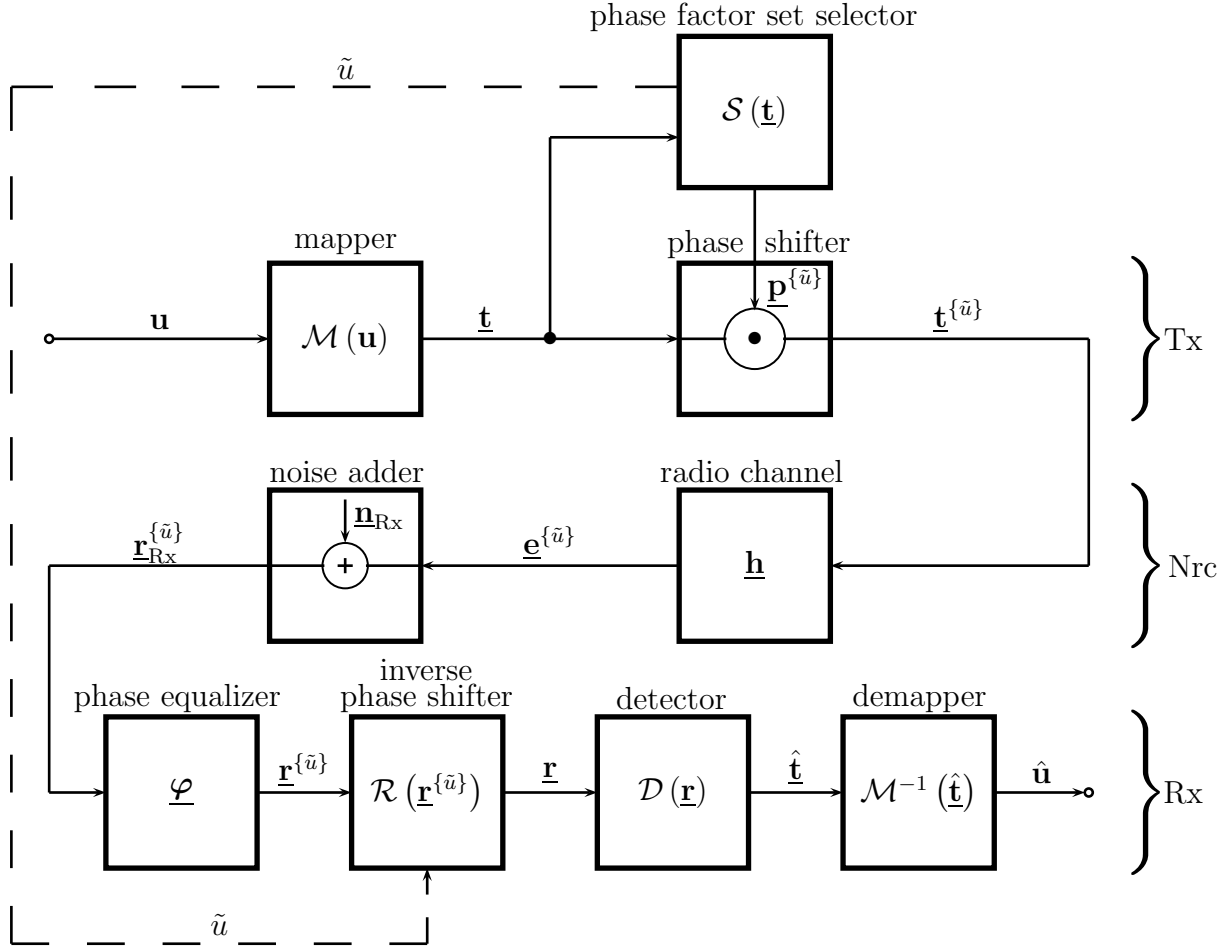


Fig. 5.2. OFDM transmission model with conventional SDM

SDM takes advantage of the fact that the PAPR of an OFDM signal is very sensitive to phase shifts of the OFDM subcarriers. PAPR reduction by SDM is achieved by applying a number of  $U$  vectorial sets

$$\underline{\mathbf{p}}^{\{u\}} = \left( p_1^{\{u\}} \cdots p_{n_F}^{\{u\}} \cdots p_{N_F}^{\{u\}} \right)^T, \quad |p_{n_F}^{\{u\}}| = 1, \quad u = 1 \cdots U, \quad (5.6)$$

of  $N_F$  phase factors  $p_{n_F}^{\{u\}}$  to the original OFDM subcarriers and determining the PAPR resulting for each of these sets. Then, the set yielding the lowest PAPR is selected for transmission. We term the  $U$  sets of phase factors briefly phase factor sets.

In the transmission model with conventional SDM of Fig. 5.2, the original transmit vector  $\underline{\mathbf{t}}$  of (2.5) is multiplied componentwise by all  $U$  phase factor sets  $\underline{\mathbf{p}}^{\{u\}}$  of (5.6) to yield the  $U$  alternative transmit vectors

$$\underline{\mathbf{t}}^{\{u\}} = \underline{\mathbf{p}}^{\{u\}} \odot \underline{\mathbf{t}}, \quad u = 1 \cdots U. \quad (5.7)$$

Each vector  $\underline{\mathbf{t}}^{\{u\}}$  of (5.7) is subjected to oversampled IFFT with the Fourier matrix

$\underline{\mathbf{F}}^{(k_o N_F) \times (k_o N_F)}$  of (5.2), which yields the  $U$  discrete time low pass equivalents

$$\underline{\mathbf{s}}^{\{u\}} = \left( \underline{s}_1^{\{u\}} \cdots \underline{s}_{k_o N_F}^{\{u\}} \right)^T = \left( \underline{\mathbf{F}}^{(k_o N_F) \times (k_o N_F)} \right)^{-1} \left( \underline{\mathbf{t}}^{\{u\}T}, \underbrace{0 \cdots 0}_{(k_o - 1)N_F \text{ zeros}} \right)^T, \quad u = 1 \cdots U, \quad (5.8)$$

of the  $U$  OFDM symbols corresponding to  $\underline{\mathbf{t}}$ . For each of the  $U$  discrete time low pass equivalents  $\underline{\mathbf{s}}^{\{u\}}$  of (5.8) we determine the PAPR

$$p^{\{u\}} = k_o N_F \frac{\max_{n_s \in \{1 \cdots k_o N_F\}} \left( \left| \underline{s}_{n_s}^{\{u\}} \right|^2 \right)}{\left( \underline{\mathbf{s}}^{\{u\}} \right)^H \underline{\mathbf{s}}^{\{u\}}}, \quad u = 1 \cdots U. \quad (5.9)$$

Finally, the phase factor set yielding the lowest PAPR is selected for transmission. We designate this set as

$$\underline{\mathbf{p}}^{\{\tilde{u}\}} = \left( \underline{p}_1^{\{\tilde{u}\}} \cdots \underline{p}_{n_F}^{\{\tilde{u}\}} \cdots \underline{p}_{N_F}^{\{\tilde{u}\}} \right)^T, \quad (5.10)$$

and with  $p^{\{u\}}$  of (5.9) its superscript is given by

$$\tilde{u} = \arg \min_{u=1 \cdots U} \{ p^{\{u\}} \}. \quad (5.11)$$

The key to the scheme SDM is how to generate the  $U$  phase factor sets  $\underline{\mathbf{p}}^{\{u\}}$  of (5.6) and select the optimum set  $\underline{\mathbf{p}}^{\{\tilde{u}\}}$  of (5.10) and (5.11). The phase factor set selector in the model of Fig. 5.2 has the task to determine and select the optimum phase factor set  $\underline{\mathbf{p}}^{\{\tilde{u}\}}$ . The inner structure of the phase factor set selector and its functionality become evident in a self-explanatory manner from Fig. 5.3. In this figure, the operators  $\mathcal{F}^{-1}(\cdot)$  and  $\mathcal{P}(\cdot)$  represent the inverse Fourier transformation and the determination of the PAPR, respectively.

In conventional SDM [BFH96], the  $N_F$  components  $\underline{p}_{n_F}^{\{u\}}$  of each of the  $U$  phase factor sets  $\underline{\mathbf{p}}^{\{u\}}$  are taken from the quaternary set

$$\underline{p}_{n_F}^{\{u\}} \in \{1, j, -1, -j\}. \quad (5.12)$$

Then, only integer multiples of  $\pi/2$  occur as phase shifts which has the advantage that the  $U$  phase factor sets  $\underline{\mathbf{p}}^{\{u\}}$  can be applied without any multiplications [BFH96]. With the components  $\underline{p}_{n_F}^{\{u\}}$  of the phase factor sets given by (5.12), in total

$$R_p = 4^{N_F} \quad (5.13)$$

different realizations of the phase factor sets are possible. With respect to system com-

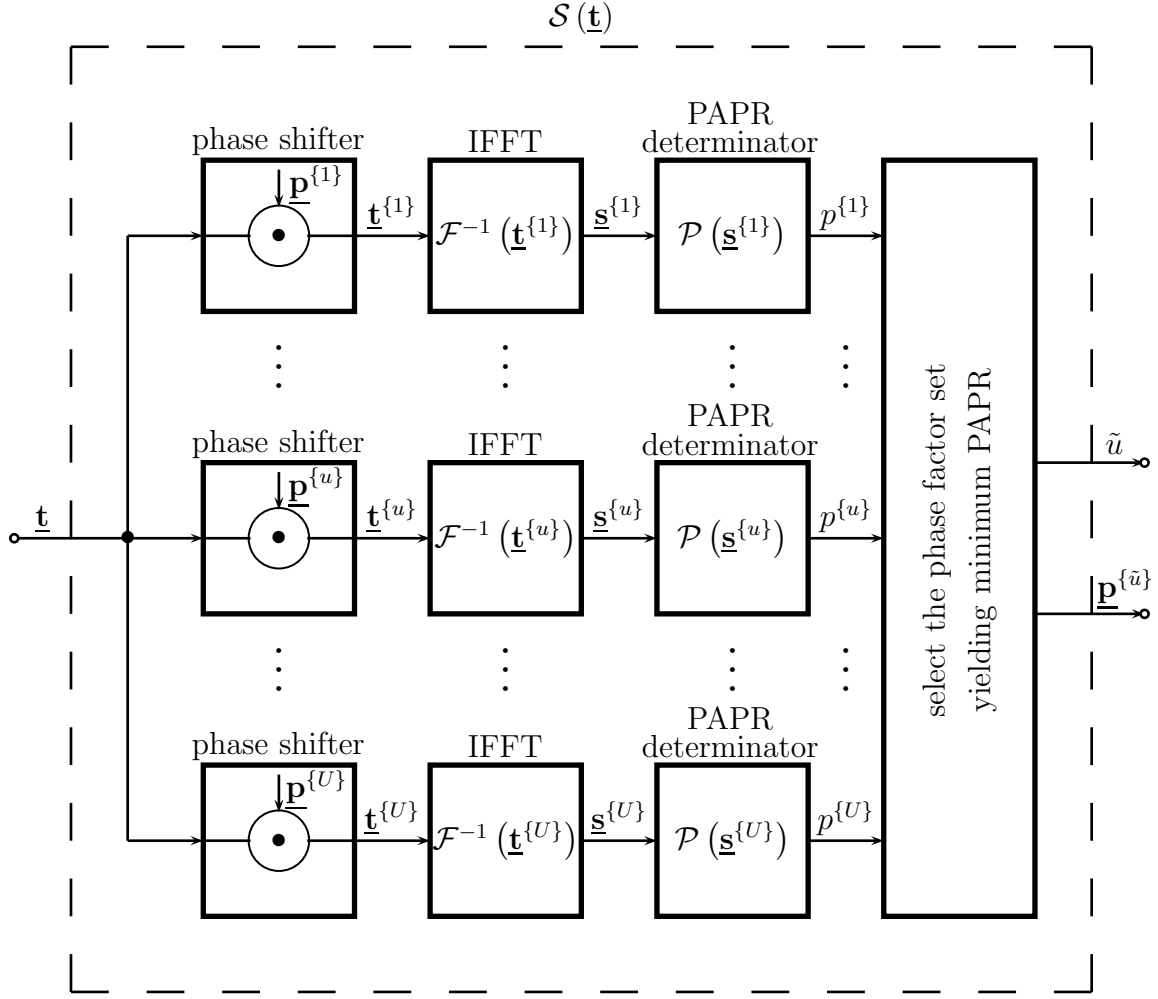


Fig. 5.3. Inner structure of phase factor set selector in the transmission model of Fig. 5.2

plexity, the number  $U$  of used phase factor sets has to be far below  $R_p$  of (5.13), that is

$$U \ll R_p. \quad (5.14)$$

In what follows, we choose the components  $p_{n_F}^{\{u\}}$  of each of the  $U$  considered phase factor sets  $\mathbf{p}^{\{u\}}$  randomly from the quaternary set (5.12).

In the model of Fig. 5.2, the inverse phase shifter on the receive side has to undo the phase shifts introduced by phase factor set  $\mathbf{p}^{\{\tilde{u}\}}$  in the transmitter. To this purpose, as indicated in the model of Fig. 5.2, the superscript  $\tilde{u}$  of (5.11) has to be signaled from the transmitter to the receiver. It is assumed that the receiver has the knowledge of all  $U$  possible phase factor sets  $\mathbf{p}^{\{u\}}$ . Then, the receiver can generate the inverse phase factor set  $\mathbf{p}^{\{\tilde{u}\}^{-1}}$ , which is then used in the inverse phase shifter to remove the phase shifts introduced in the transmitter. The inner structure of the inverse phase shifter is shown in Fig. 5.4.

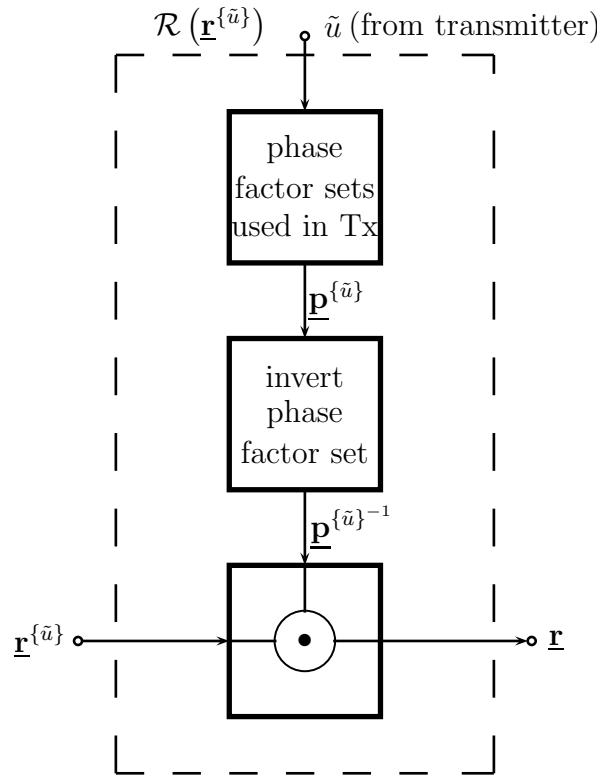


Fig. 5.4. Inner structure of inverse phase shifter in the transmission model of Fig. 5.2

In Fig. 5.5 we show the CCDF of the PAPR for conventional SDM [BFH96] with the parameter  $U$ . For  $U$  equal one, SDM is disabled, and we obtain the CCDF of  $p_o$  of (5.4) as shown in Fig. 5.1. For  $U$  equal 128, the PAPR performance is improved by about 4 dB as compared to  $p_o$  of (5.4). The larger the number  $U$  of employed phase factor sets  $\underline{\mathbf{p}}^{\{u\}}$ , the more the PAPR can be reduced. However, as already mentioned above,  $U$  cannot be chosen arbitrarily large, because the complexity of the OFDM transmission system increases with increasing  $U$ . In addition, with increasing  $U$  more and more transmission resources are consumed for signaling the superscript  $\tilde{u}$  of (5.11) to the receiver, which decreases the useful data rate.

## 5.2 PAPR reduction by PDS

In Chapter 3, PDS is introduced to enable frequency diversity similar to the one offered by spread spectrum techniques [BWW99]. In the present section we address the issue that PDS can, besides introducing frequency diversity, also offer a PAPR reduction.

We resort to the transmission model of Fig. 3.3. Under consideration of what is said in Section 3.8, we take into account in the present Section 5.2 and in the next Section 5.3 both Walsh-Hadamard PDS and Fourier PDS.

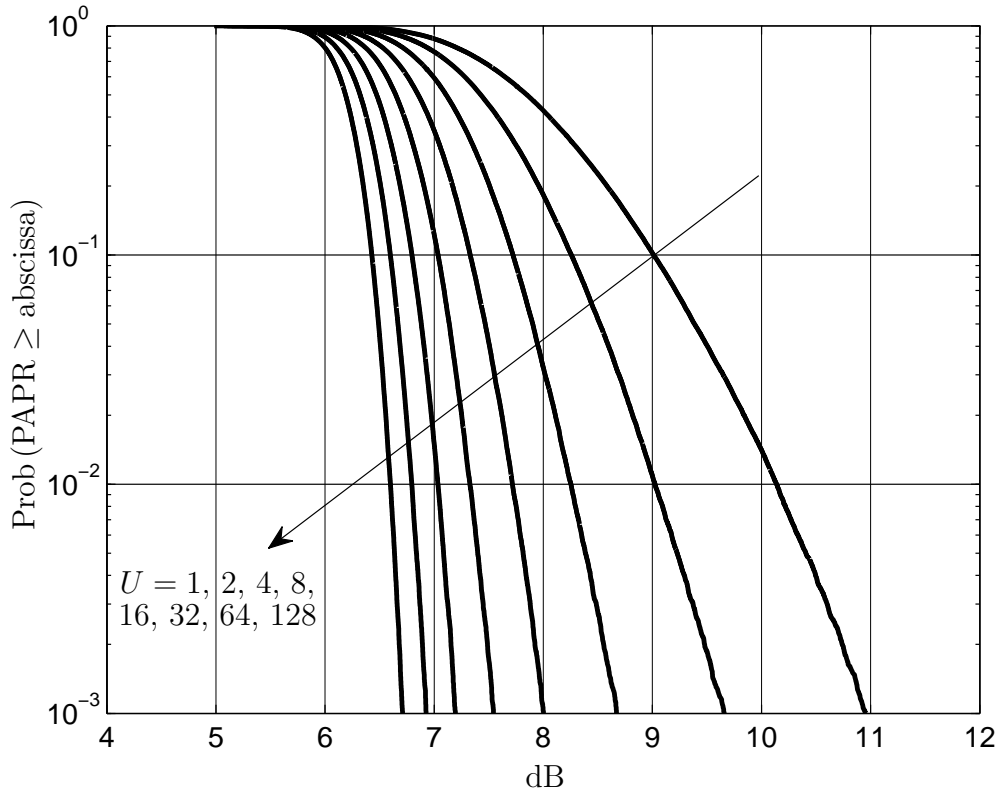


Fig. 5.5. CCDF of the PAPR for conventional SDM with parameter  $U$ ;  $N_F = 128$

Oversampled IFFT yields now with the interleaved spread transmit vector  $\tilde{\mathbf{t}}_i$  of (3.19) instead of (5.3) the discrete time low pass equivalent

$$\tilde{\mathbf{s}} = (\tilde{\mathbf{s}}_1 \cdots \tilde{\mathbf{s}}_{k_o N_F})^T = \left( \mathbf{F}^{(k_o N_F) \times (k_o N_F)} \right)^{-1} \begin{pmatrix} \tilde{\mathbf{t}}_i^T \\ \underbrace{0 \cdots 0}_{(k_o - 1) N_F \text{ zeros}} \end{pmatrix}^T. \quad (5.15)$$

Substituting  $\tilde{\mathbf{s}}$  of (5.15) in (5.4) yields the PAPR of OFDM transmission with PDS.

Figs. 5.6a and b depict the CCDF of the PAPR for OFDM transmission with Walsh-Hadamard PDS and Fourier PDS, respectively, with the spreading factor  $N$  as the curve parameter. For  $N$  equal one, PDS degenerates to the unspread case, which also represents the original OFDM signal, whereas PDS turns into FDS for  $N$  equal  $N_F$ . We observe that Walsh-Hadamard PDS and Fourier PDS offer a PAPR reduction of approximately 1 dB and 3.5 dB, respectively, as compared to the original OFDM signal, and that the PAPR performances improve with increasing  $N$ . The reason for this dependence on  $N$  is that high envelope peaks are more and more evened out, the more the spreading matrix  $\mathbf{S}$  goes from a block diagonal structure to a full matrix. Fourier PDS is superior over Walsh-Hadamard PDS. With increasing  $N$  this superiority increases because the OFDM symbols obtained by Fourier PDS become more and more similar to QPSK modulated OFDM symbols with their inherently low PAPR.

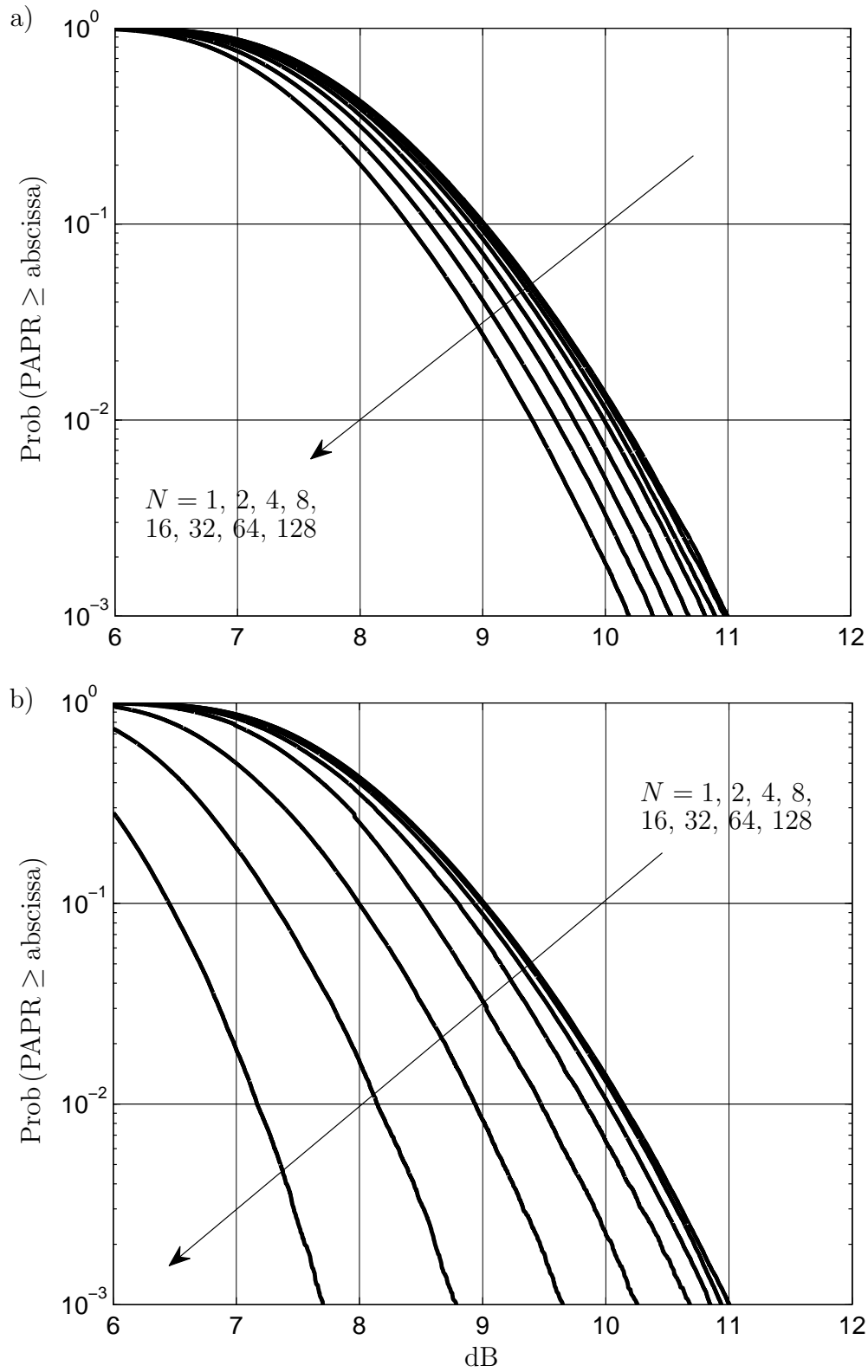


Fig. 5.6. CCDF of the PAPR for PDS with parameter  $N$ ;  $N_F = 128$   
 a) Walsh – Hadamard PDS  
 b) Fourier PDS

## 5.3 Combination of PDS with SDM

### 5.3.1 System model

Figs. 5.5 and 5.6 quantitatively show that the two conceptually totally different schemes SDM and PDS have the potential of a PAPR reduction. This observation raises the question if, by combining these two schemes, their PAPR reduction potentials could be simultaneously utilized in the sense of a synergy. In the present section we study such combinations, for which we coin the acronym PDS-SDM.

In order to obtain the scheme PDS-SDM, we extend the transmission model of Fig. 3.3 on the transmit side by a phase factor set selector and a phase shifter, and on the receive side by an inverse phase shifter. There are three different options where to place the phase shifter in the transmitter. These options are illustrated in Figs. 5.7 to 5.9, and we designate them as cases I, II and III.

With the  $U$  phase factor sets  $\underline{\mathbf{p}}^{\{u\}}$  of (5.6) we obtain at the input of the radio channel for said cases I, II and III instead of the interleaved spread transmit vector  $\tilde{\mathbf{t}}_i$  of (3.19) the  $U$  transmit vectors

$$\tilde{\mathbf{t}}_i^{\{u\}} = \begin{cases} \mathcal{I}^{(N,Z)}(\underline{\mathbf{S}}(\underline{\mathbf{p}}^{\{u\}} \odot \underline{\mathbf{t}})), & \text{case I,} \\ \mathcal{I}^{(N,Z)}((\underline{\mathbf{p}}^{\{u\}}) \odot (\underline{\mathbf{S}}\underline{\mathbf{t}})), & \text{case II,} \\ \underline{\mathbf{p}}^{\{u\}} \odot (\mathcal{I}^{(N,Z)}(\underline{\mathbf{S}}\underline{\mathbf{t}})), & \text{case III,} \end{cases} \quad u = 1 \cdots U. \quad (5.16)$$

For each of these transmit vectors we can determine in analogy to (5.8) and (5.9) a discrete time low pass equivalent  $\mathbf{s}^{\{u\}}$  and a PAPR  $p^{\{u\}}$ , respectively. Finally, we obtain the optimum phase factor set  $\underline{\mathbf{p}}^{\{\tilde{u}\}}$  according to (5.10) and (5.11).

### 5.3.2 Simulation results

In Fig. 5.10 we show the CCDF of the PAPR for the cases I, II and III introduced in Subsection 5.3.1 for  $N_F$  equal 128. Fig. 5.10a holds for Walsh-Hadamard PDS and Fig. 5.10b for Fourier PDS. The chosen parameter values are  $N$  equal 128 and  $U$  equal 128. As a reference we include in this figure also the curve for conventional SDM. We recognize that the PAPR performances of cases II, III and conventional SDM coincide, whereas case I for Walsh-Hadamard PDS and Fourier PDS outperforms the other two cases by approximately 0.5 dB and 2 dB, respectively. From this finding we conclude that the scheme PDS-SDM case I should be chosen by the system designer. Therefore, in the following simulation results we restrict ourselves to only considering PDS-SDM case I and do not explicitly mention this in the following.



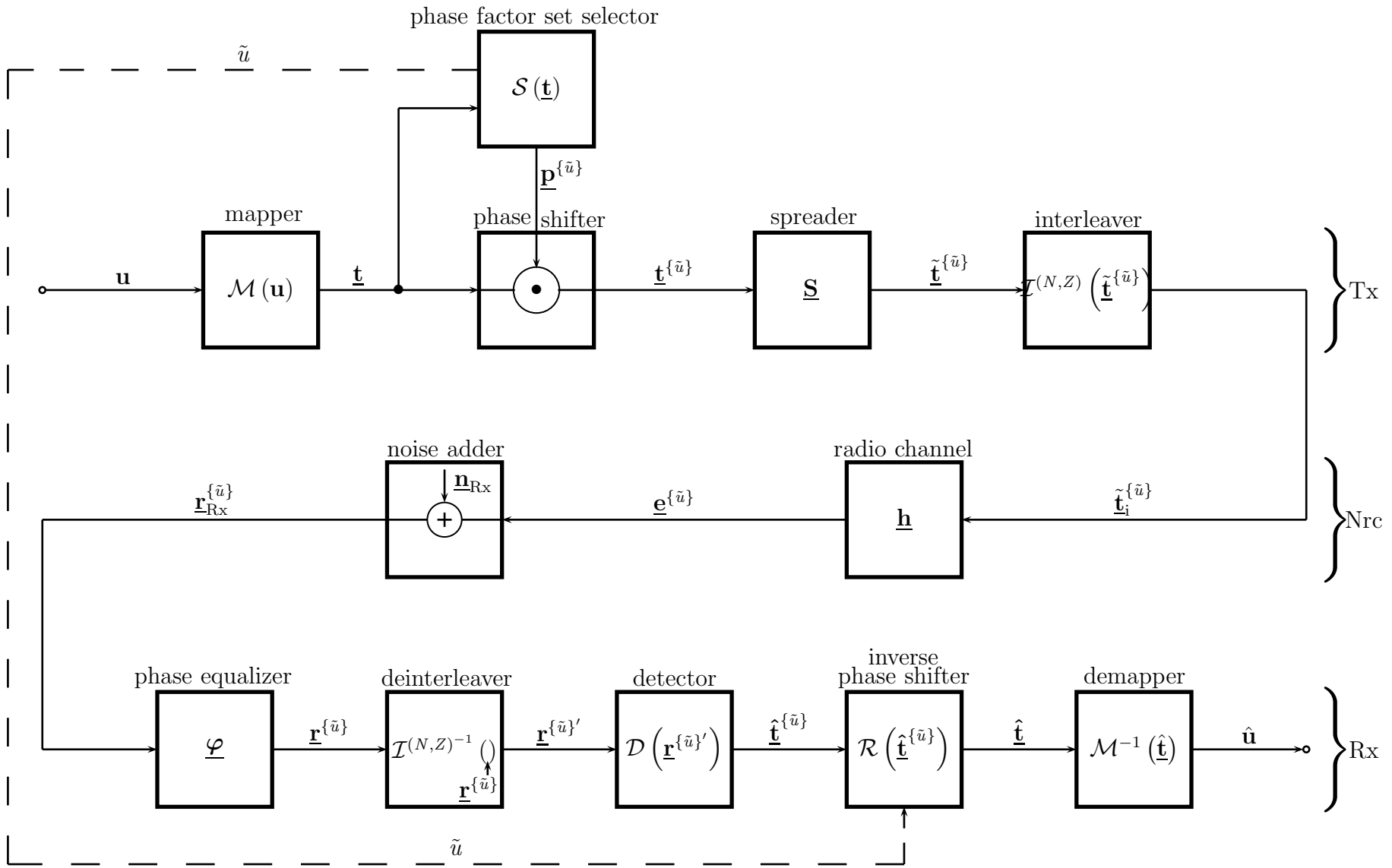


Fig. 5.7. Transmission model of PDS-SDM case I

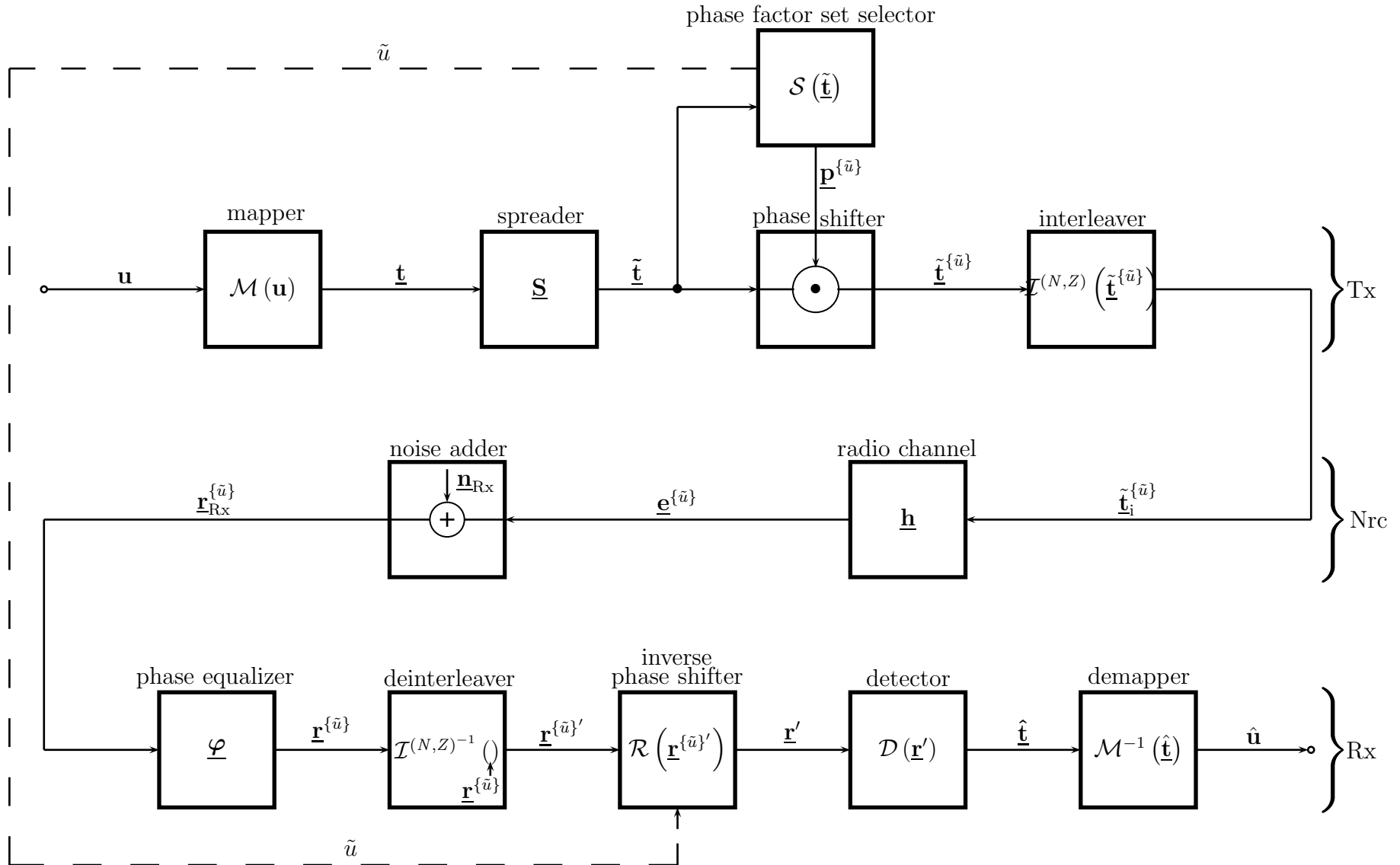


Fig. 5.8. Transmission model of PDS-SDM case II

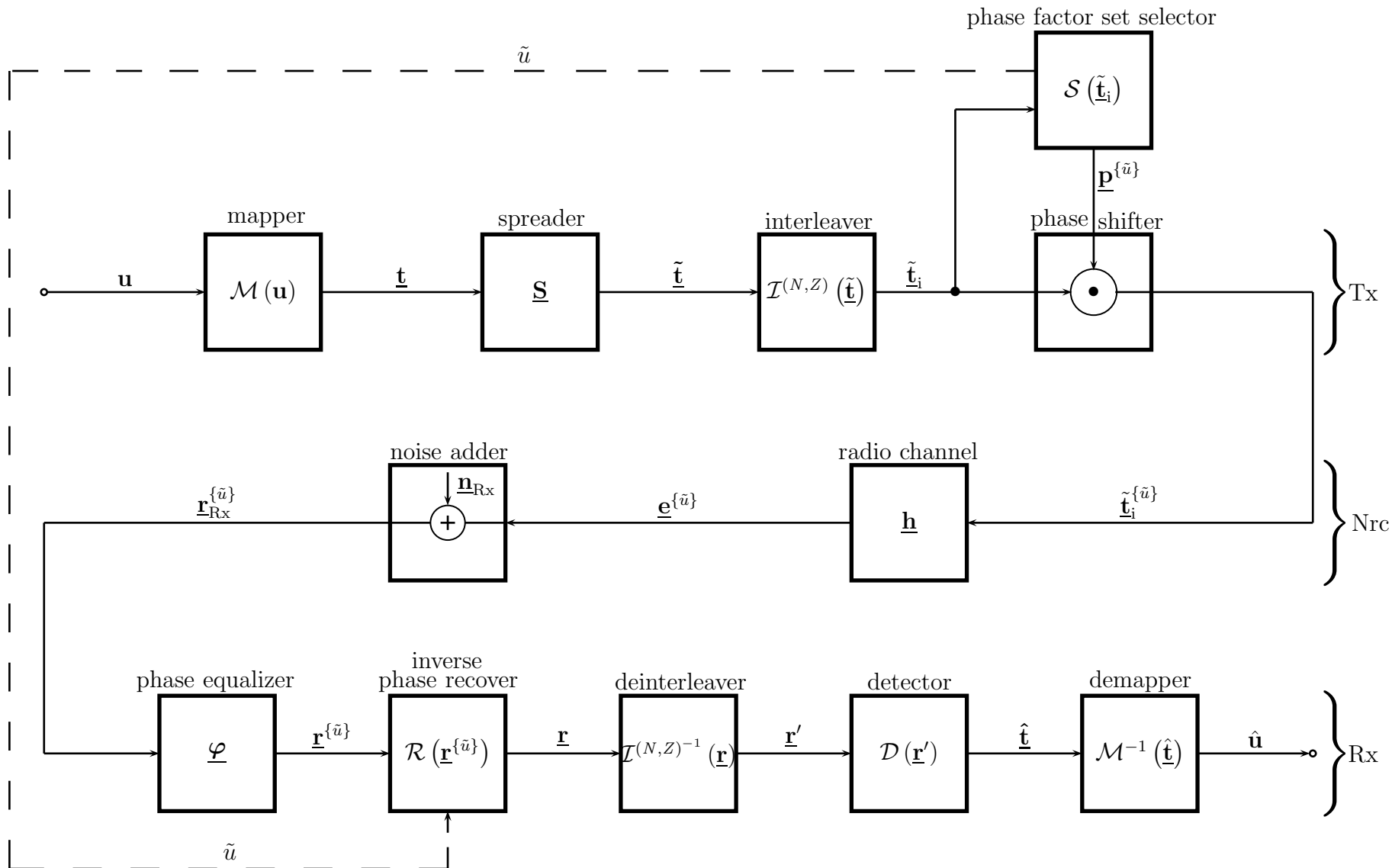


Fig. 5.9. Transmission model of PDS-SDM case III

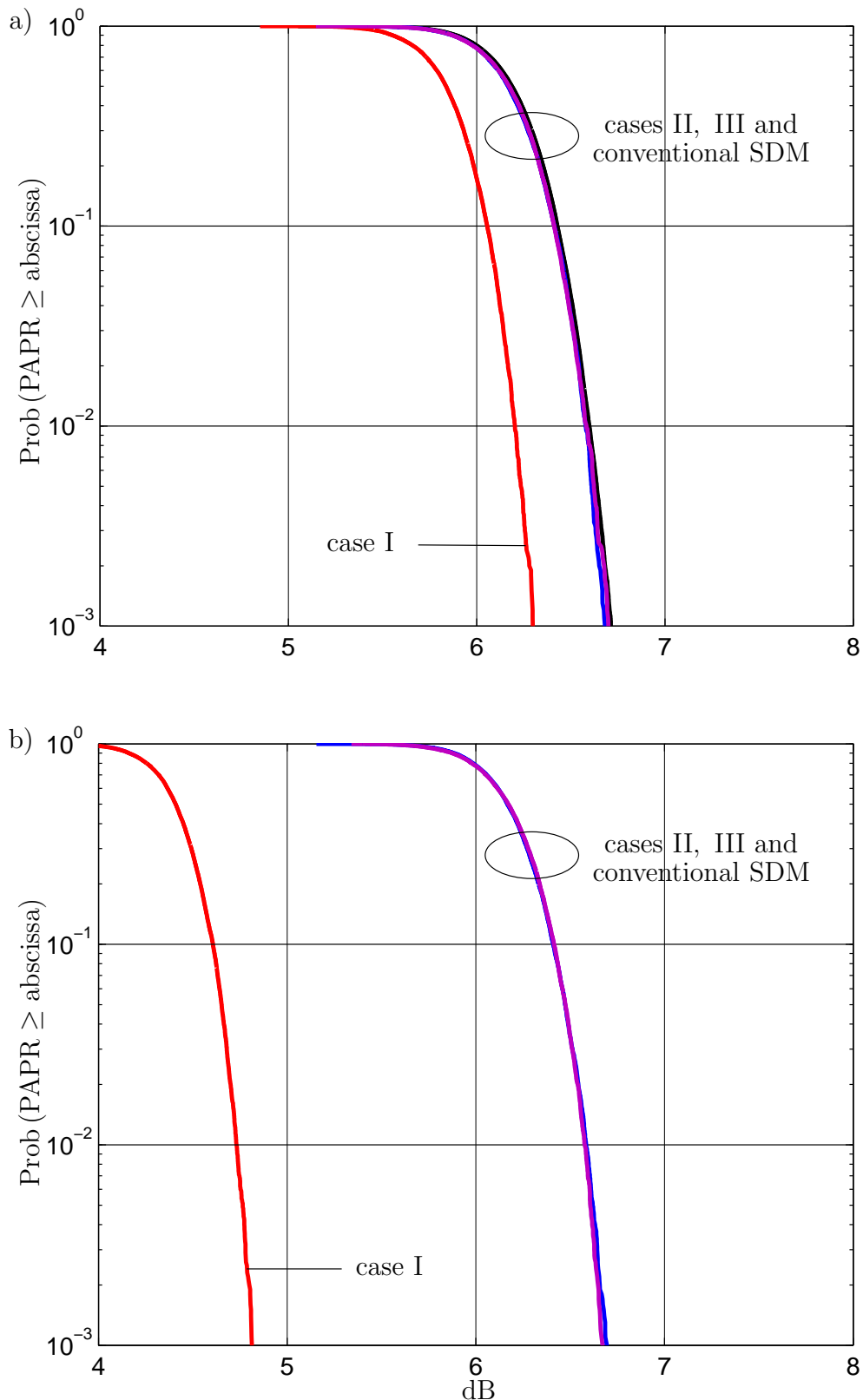


Fig. 5.10. CCDF of the PAPR for cases I, II and III of PDS – SDM, and for conventional SDM;  $N = 128$ ,  $N_F = 128$ ,  $U = 128$

- a) Walsh – Hadamard PDS
- b) Fourier PDS

In Figs. 5.11 and 5.12 we depict the CCDF of the PAPR for PDS-SDM and for conventional SDM with  $U$  as the parameter. Fig. 5.11 holds for  $N$  equal four and Fig. 5.12 for  $N$  equal 32. Figs. 5.11a and 5.12a concern the case of Walsh-Hadamard PDS, and Figs. 5.11b and 5.12b the case of Fourier PDS. Figs. 5.13a and b show the CCDF of the PAPR for the case of Walsh-Hadamard FDS-SDM and Fourier FDS-SDM, respectively; FDS results if we set  $N$  equal  $N_F$ . Also in Fig. 5.13 we include curves for conventional SDM.

Fig.	$N$	$U$
5.11	4	1,4,32,128
5.12	32	1,4,32,128
5.13	128	1,4,32,128

Table 5.1. Parameter values  $N$  and  $U$  in Figs. 5.11 to 5.13

By inspection of Figs. 5.11 to 5.13 we can draw the following conclusions concerning the PAPR performance:

- PDS-SDM and FDS-SDM outperform conventional SDM,
- this superiority of PDS-SDM and FDS-SDM increases with increasing spreading factor  $N$ ,
- the PAPR performance of PDS-SDM and FDS-SDM as well as conventional SDM improves with increasing parameter  $U$ ,
- the advantage of Fourier PDS-SDM over Walsh-Hadamard PDS-SDM increases with increasing spreading factor  $N$ .

Let us assume that the PAPR should not exceed a given value. Then, the curves in Figs. 5.11 to 5.13 show that in order to keep this value, PDS-SDM and FDS-SDM require a smaller parameter value  $U$  than conventional SDM. This is an advantage of PDS-SDM and FDS-SDM over conventional SDM. In PDS-SDM the number of IFFTs to be performed in the phase factor set selector of Fig. 5.3 as well as the transmission resources required to signal the chosen  $\tilde{u}$  to the receiver are smaller than in the case of conventional SDM. Additionally, as mentioned above, Fourier PDS can do with even smaller parameters than Walsh-Hadamard PDS because of the lower PAPR.

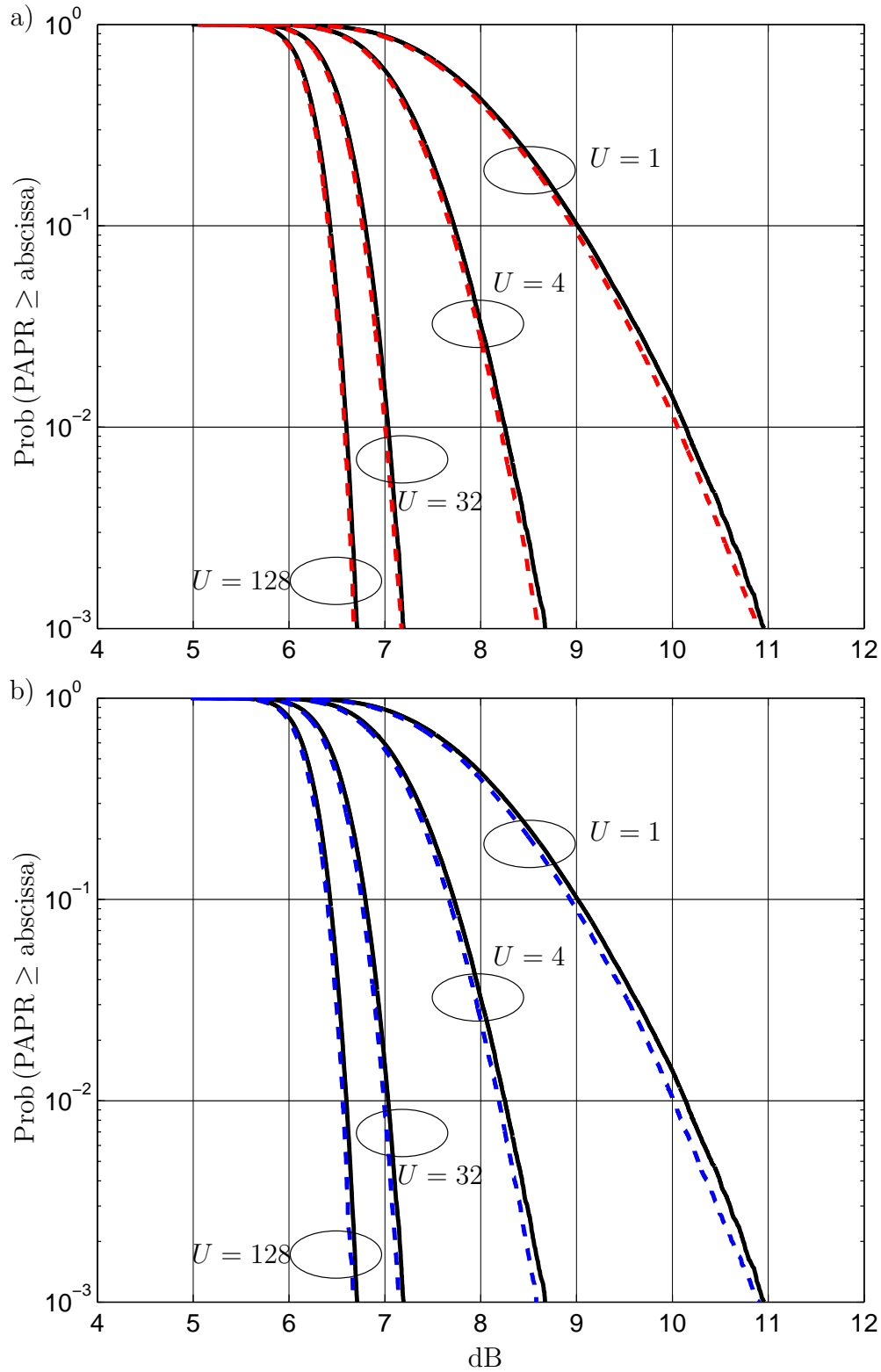


Fig. 5.11. CCDF of the PAPR for PDS – SDM and for conventional SDM with  $U$  as parameter;  $N = 4$ ,  $N_F = 128$

--- PDS-SDM case I      ——— conventional SDM

a) Walsh – Hadamard PDS

b) Fourier PDS

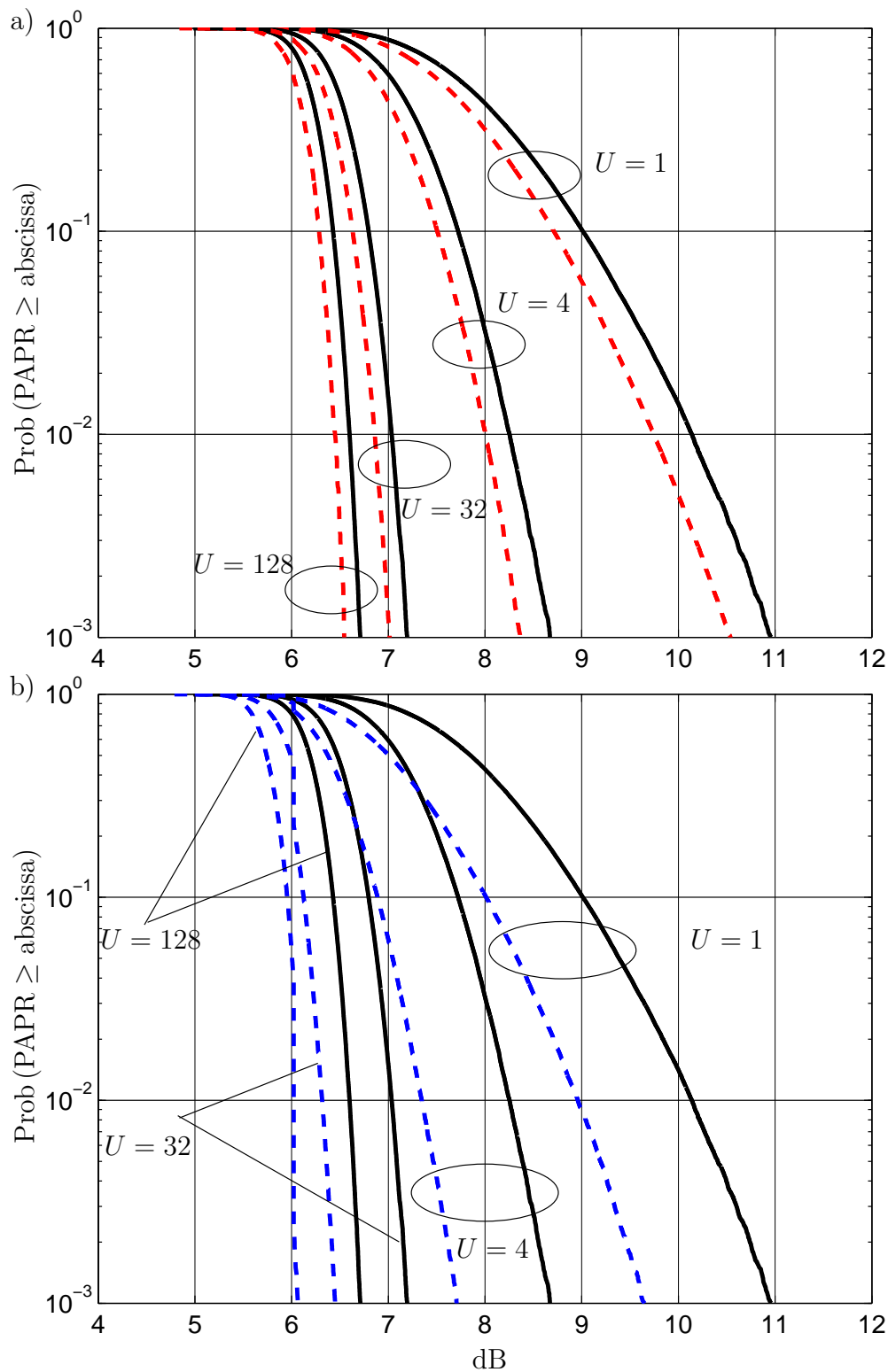


Fig. 5.12. CCDF of the PAPR for PDS – SDM and for conventional SDM with  $U$  as parameter;  $N = 32$ ,  $N_F = 128$

— — — PDS-SDM case I      ——— conventional SDM

a) Walsh – Hadamard PDS

b) Fourier PDS

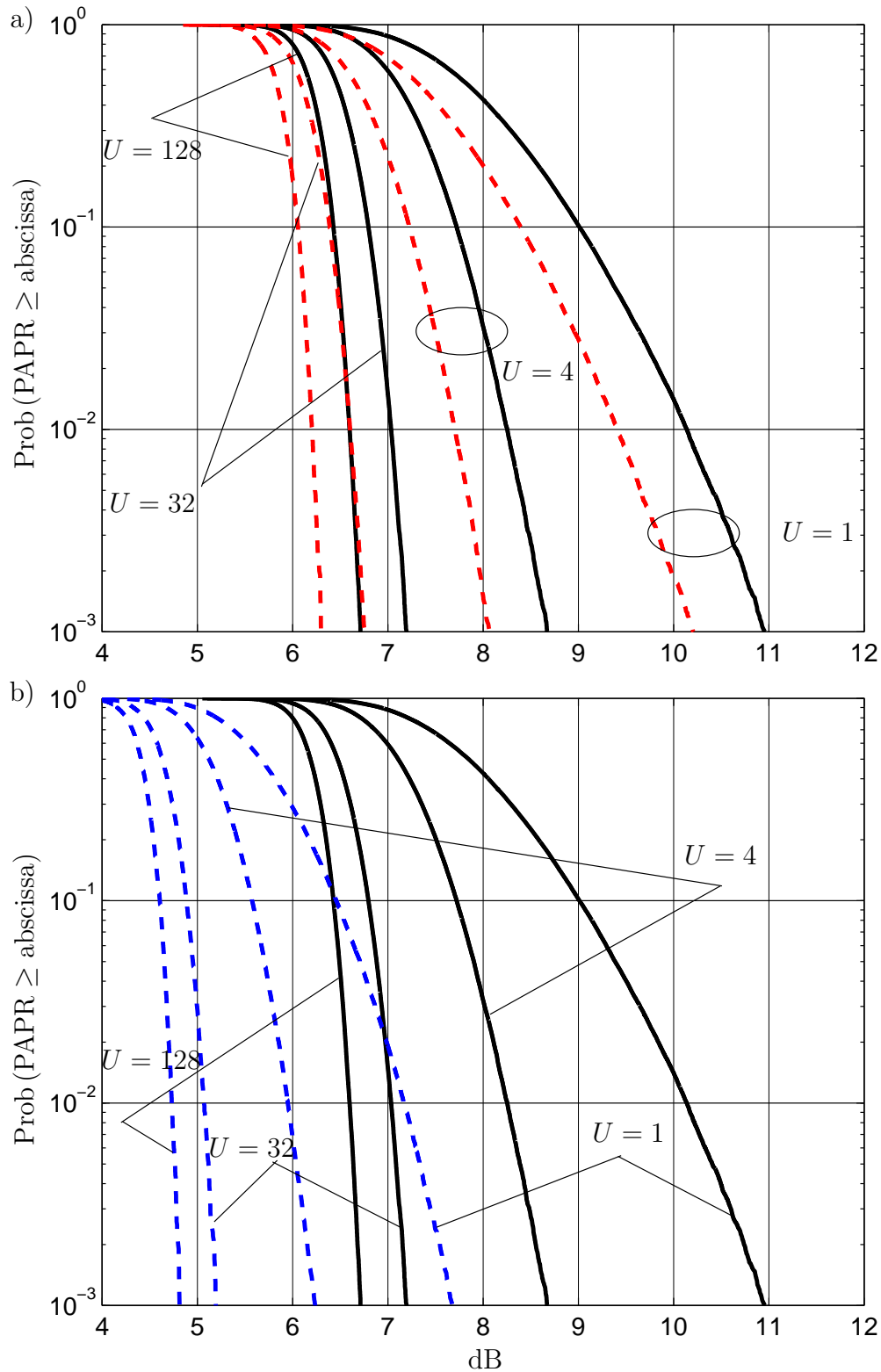


Fig. 5.13. CCDF of the PAPR for FDS – SDM and for conventional SDM with  $U$  as parameter;  $N = 128$ ,  $N_F = 128$

— — — FDS-SDM case I      ——— conventional SDM

a) Walsh – Hadamard FDS

b) Fourier FDS



### 5.3.3 Plausible explanations of the simulation results

In Sections 5.1 and 5.2 we found that the PAPR performance of OFDM transmission can be improved by conventional SDM and by PDS, respectively. In Subsection 5.3.1 we introduced the three different cases I, II and III of combining SDM with PDS. By simulations it turned out that PDS-SDM case I is beneficial, whereas PDS-SDM case II and III show no improvement as compared to conventional SDM. In the present subsection we support these findings by some plausible explanations. We only consider the Walsh-Hadamard PDS. To this purpose we determine for many snapshots of the information vector  $\mathbf{u}$  of (2.2) the PAPR  $p_o$  of (5.4) and the PAPRs

- $p_{\text{PDS}}$  of PDS,
- $p_{\text{SDM}}$  of conventional SDM, and
- $p_{\text{I,II,III}}$  of PDS-SDM cases I, II and III, respectively.

In Figs. 5.14 to 5.17 we represent each of said snapshots by a point in a Cartesian coordinate system, where the horizontal axis depicts  $p_o$  and the vertical axis depicts the appertaining values  $p_{\text{PDS}}$ ,  $p_{\text{SDM}}$  or  $p_{\text{I,II,III}}$ , respectively.

Fig. 5.14 concerns  $p_{\text{PDS}}$  for different parameter values  $N$ . We recognize that with increasing  $N$  the center of gravity of the clouds of points has the tendency to move more and more below the bisector line.

Figs. 5.15 to 5.17 hold for  $p_{\text{I,II,III}}$  and  $p_{\text{SDM}}$  for  $U$  equal 128 and  $N$  equal four, 32 and 128. We recognize that the center of gravity of the clouds of points with increasing  $N$  moves towards the horizontal axis, and that for PDS-SDM case I this center lies closest to the horizontal axis.

We now explain why the PAPR performances of conventional SDM and of PDS-SDM case II and III are virtually the same, whereas PDS-SDM case I shows a better PAPR performance. The reason is that in the cases of conventional SDM and PDS-SDM case II and III a number of  $U$  different versions of a quasi Gaussian signal are PAPR-wise evaluated, whereas in the case of PDS-SDM case I first the PAPR reduction offered by SDM as shown in Fig. 5.5 is exploited, and then, in addition, the PAPR is further decreased by PDS as shown in Fig. 5.6.

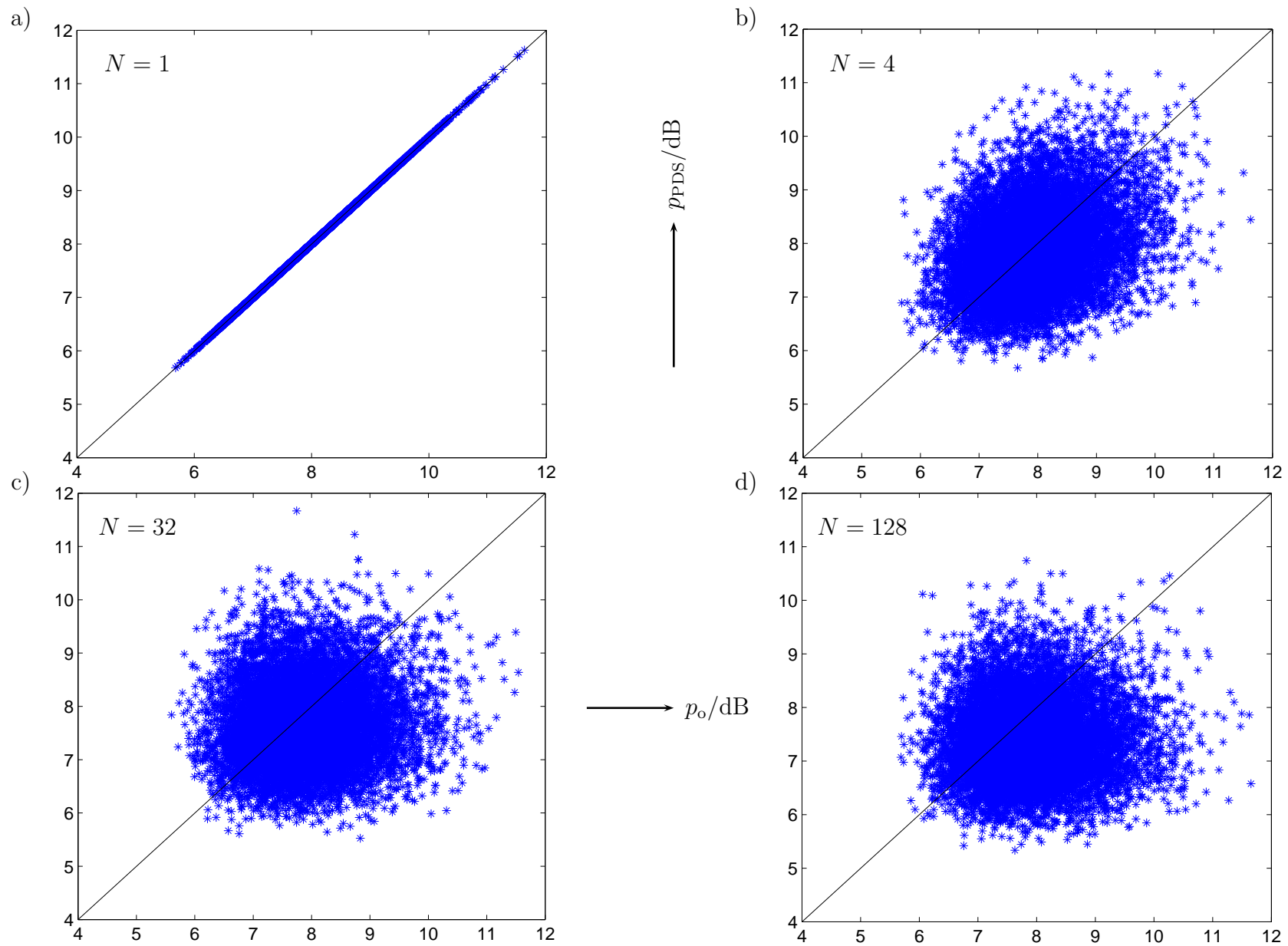


Fig. 5.14. PAPR  $p_{\text{PDS}}$  versus  $p_o$ ;  $N_{\text{F}} = 128$

a)  $N = 1$     b)  $N = 4$     c)  $N = 32$     d)  $N = 128$

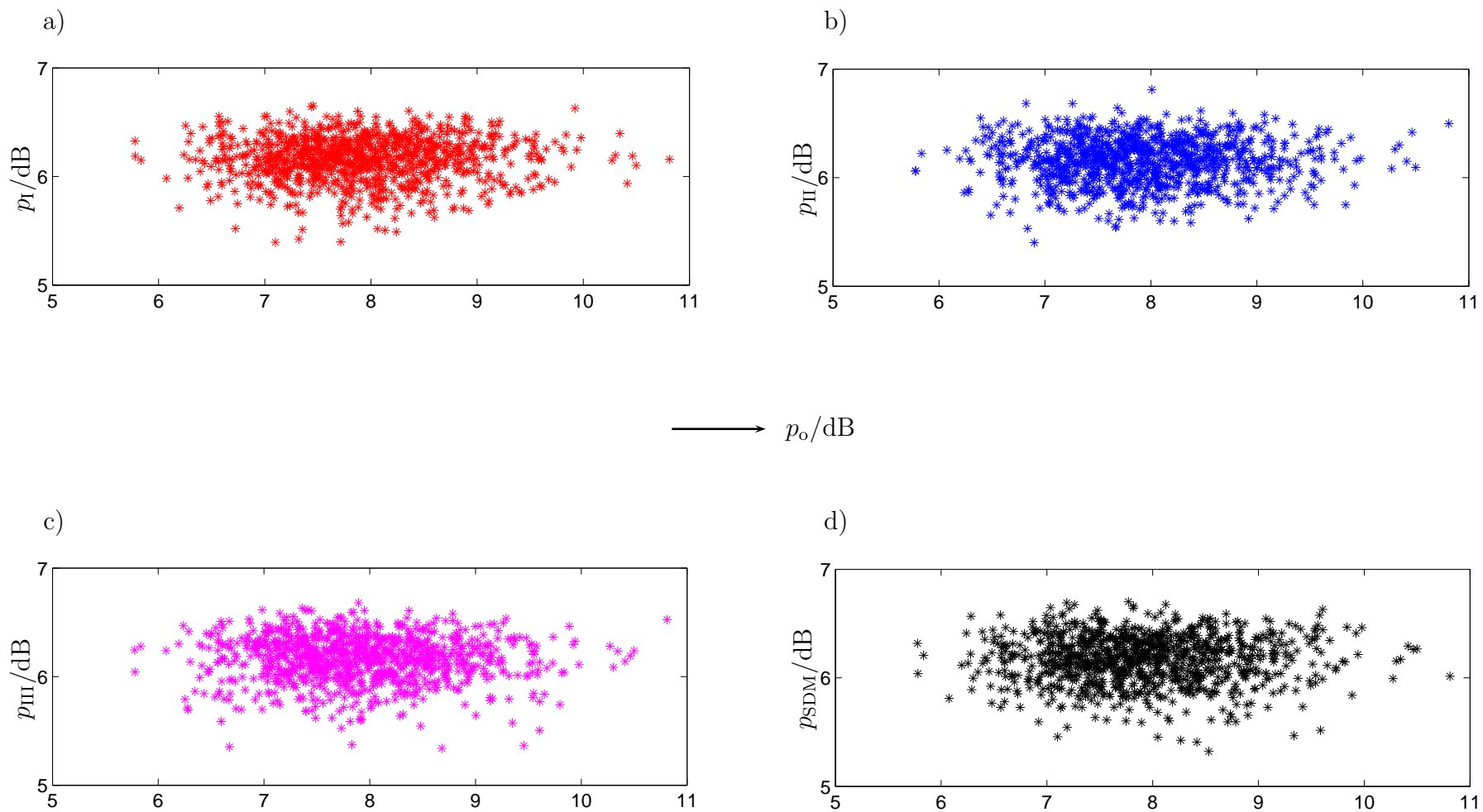


Fig. 5.15. PAPRs  $p_{I,II,III}$  and  $p_{SDM}$  versus  $p_o$ ;  $N = 4$ ;  $N_F = 128$ ,  $U = 128$

a)  $p_I$

b)  $p_{II}$

c)  $p_{III}$

d)  $p_{SDM}$

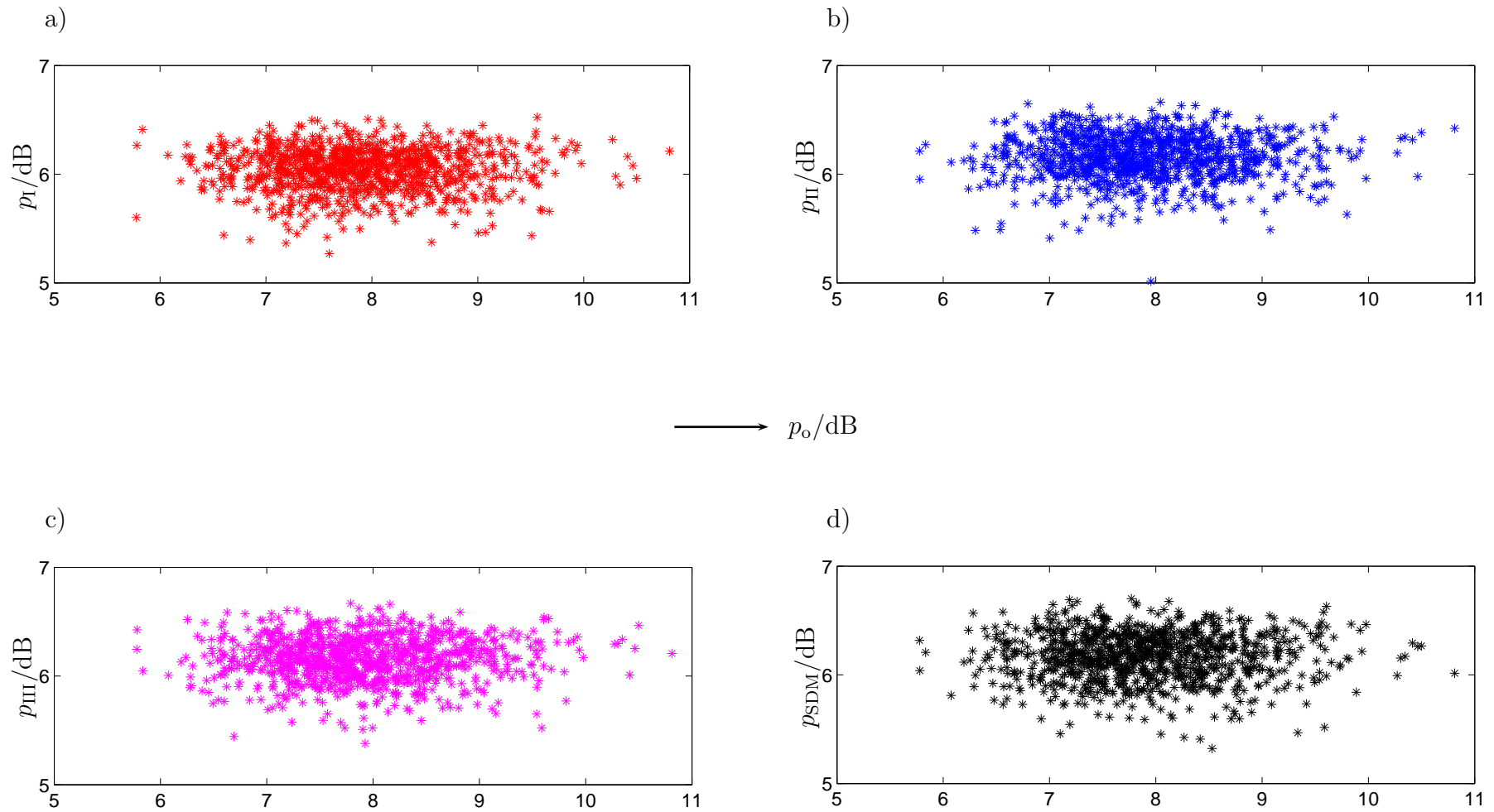


Fig. 5.16. PAPRs  $p_{I,II,III}$  and  $p_{SDM}$  versus  $p_o$ ;  $N = 32$ ;  $N_F = 128$ ,  $U = 128$   
 a)  $p_I$                       b)  $p_{II}$                       c)  $p_{III}$                       d)  $p_{SDM}$

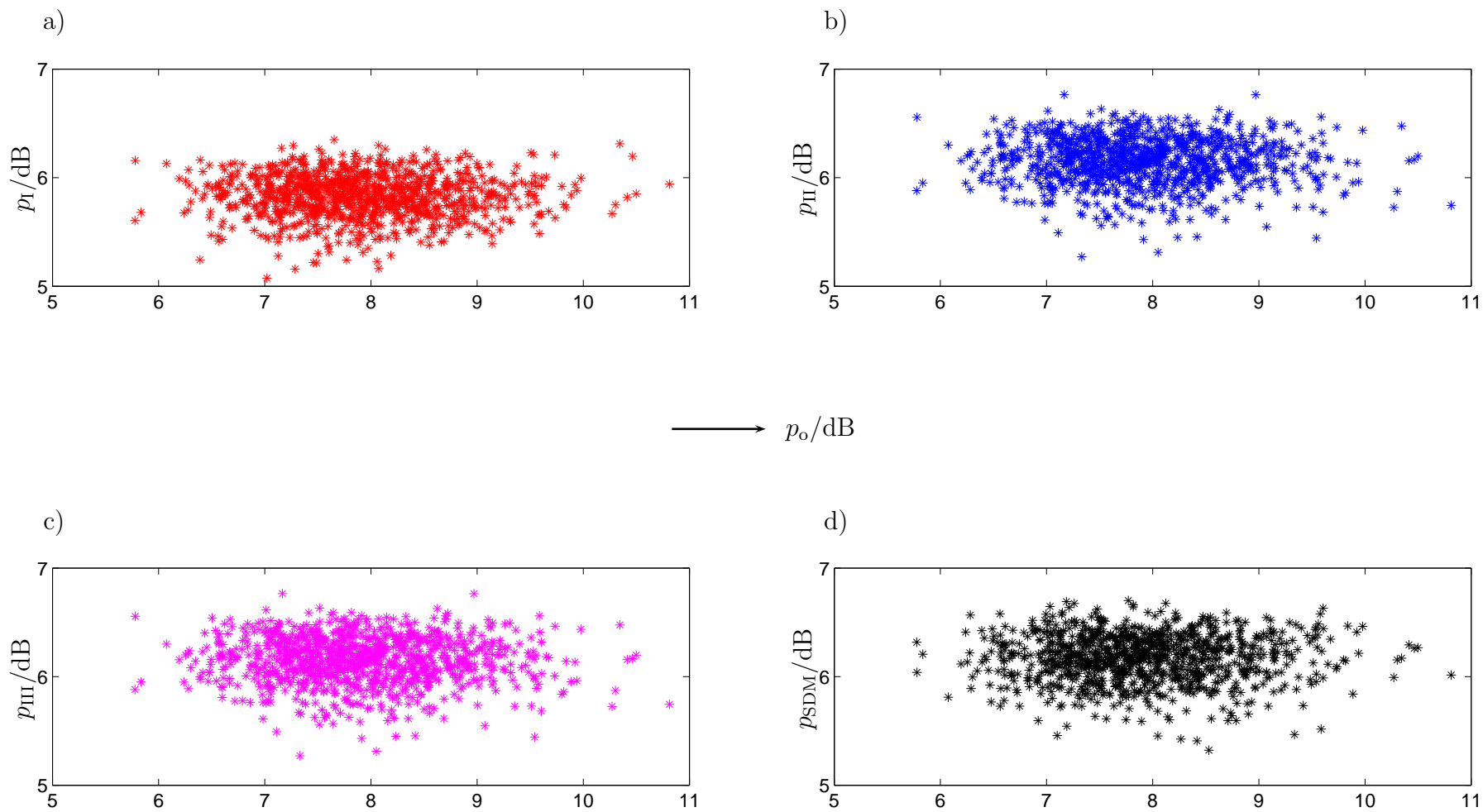


Fig. 5.17. PAPRs  $p_{I,II,III}$  and  $p_{SDM}$  versus  $p_o$ ;  $N = 128$ ;  $N_F = 128$ ,  $U = 128$

a)  $p_I$

b)  $p_{II}$

c)  $p_{III}$

d)  $p_{SDM}$

# Chapter 6

## Enhancing the power efficiency of transmit amplifiers by Optimum Clipping

### 6.1 Some fundamentals of transmit power amplifiers

An important component of each radio transmission system is its transmit power amplifier (PA), which can be characterized by its gain  $G$  and its power efficiency  $\eta$ . With the RF input power  $P_{\text{in}}$  and the RF output power  $P_{\text{out}}$  of the PA, the gain is defined as [RAC02]

$$G(P_{\text{in}}) = \frac{P_{\text{out}}}{P_{\text{in}}}. \quad (6.1)$$

In (6.1) we indicate that  $G$  in general depends on  $P_{\text{in}}$ . This means that the PA is non-linear, and, therefore, when signals of non-constant envelope are amplified, these are subjected to undesired distortions including the generation of out-of-band power [LCCP10]. However, having in mind the features of real world PAs [LvdTV01], we assume in our investigations that the PA is partly linear in the sense that  $G$  is constant as long as  $P_{\text{in}}$  does not exceed an upper limit  $P_{\text{sup}}$ . This partial linearity can be expressed as

$$G(P_{\text{in}}) = G_o = \text{const for } P_{\text{in}} \leq P_{\text{sup}}. \quad (6.2)$$

$G_o$  and  $P_{\text{sup}}$  are design parameters of the PA.

In order to produce a desired RF output power  $P_{\text{out}}$ , the PA requires a certain DC input power  $P_{\text{DC}}$ , which is only partly transformed into RF output power. The power efficiency of the PA is defined as the ratio [RAC02]

$$\eta(P_{\text{in}}) = \frac{P_{\text{out}}}{P_{\text{DC}}} = \frac{GP_{\text{in}}}{P_{\text{DC}}} \quad (6.3)$$

and should be as large as possible. In (6.3) we indicate that  $\eta$ , like  $G$  of (6.1), in general depends on  $P_{\text{in}}$ . However, whereas we assume a constant  $G$  equal  $G_o$  of (6.2) as long as  $P_{\text{in}}$  does not exceed  $P_{\text{sup}}$ , the power efficiency  $\eta(P_{\text{in}})$  of (6.3) is considered to depend on the input power  $P_{\text{in}}$  even if this power does not exceed  $P_{\text{sup}}$ . An alternative efficiency definition which we, however, do not consider in this thesis would be the power added efficiency (PAE) [LvdTV01]

$$\eta_{\text{PAE}}(P_{\text{in}}) = \frac{P_{\text{out}} - P_{\text{in}}}{P_{\text{DC}}}. \quad (6.4)$$

As important requirements in PA design, the linearity condition of (6.2) should be ful-

filled, and large values of  $\eta$  of (6.3) should be achieved. With a view to comply with these two requirements, a number of PA structures have been proposed [Bou08]. These include the PA schemes Envelope Elimination and Restoration (EER), Envelope Tracking (ET), Linear Amplification using Non-linear Components (LINC), as well as Doherty Modulation (DM). It is claimed that for the time being the Doherty PA is the most promising scheme [JW07, Bou08] for both handset devices and mobile radio base stations. Therefore, in the quantitative evaluations of the present chapter we choose a specific Doherty PA developed by Ansoft Corporation [KJS03] as an exemplary PA. In Fig. 6.1 we depict the gain  $G$  and the output power  $P_{\text{out}}$  of this PA versus its input power  $P_{\text{in}}$ . We recognize that the PA can be considered to perform linearly as long as

$$P_{\text{in}} \leq P_{\text{sup}} = 45 \text{ dBm} \quad (6.5)$$

holds. Fig. 6.2 shows the power efficiency  $\eta$  of said PA versus  $P_{\text{in}}$ , and we can state a strong dependence on  $P_{\text{in}}$  even if  $P_{\text{in}}$  does not exceed  $P_{\text{sup}}$ .

## 6.2 A scheme for clipping and scaling OFDM symbols

The complex envelopes  $\underline{s}(t)$  of (2.79) of the OFDM symbols depend on the carried information vector  $\mathbf{u}$  of (2.2) and, therefore, have different magnitude maxima. We pursue the idea to tailor the OFDM symbols [GB09b], prior to feeding them into the PA, in such a way that their complex envelopes obtain the same magnitude maximum  $s_{\text{max}}$ , which should lie in the linear range of the PA given by (6.2). We propose to achieve this tailoring by the three consecutive steps

1. Clipping the time domain representation of the OFDM symbol with a certain clipping level,
2. Filtering away the out-of-band power caused by clipping, and
3. Scaling the OFDM symbol obtained by filtering to the above mentioned envelope maximum  $s_{\text{max}}$ .

In order to investigate the effect of this tailoring, we reduce the OFDM transmission model of Fig. 2.1 to the model shown in Fig. 6.3. In this model the radio channel is of the type AWGN, and said tailoring is performed by a block clipper & scaler.

This block subjects the transmit vector  $\underline{\mathbf{t}}$  of (2.5) to the clipping & scaling operation  $\mathcal{CS}(\cdot)$ , and in this way produces the clipped and scaled version

$$\tilde{\underline{\mathbf{t}}} = \mathcal{CS}(\underline{\mathbf{t}}) \quad (6.6)$$

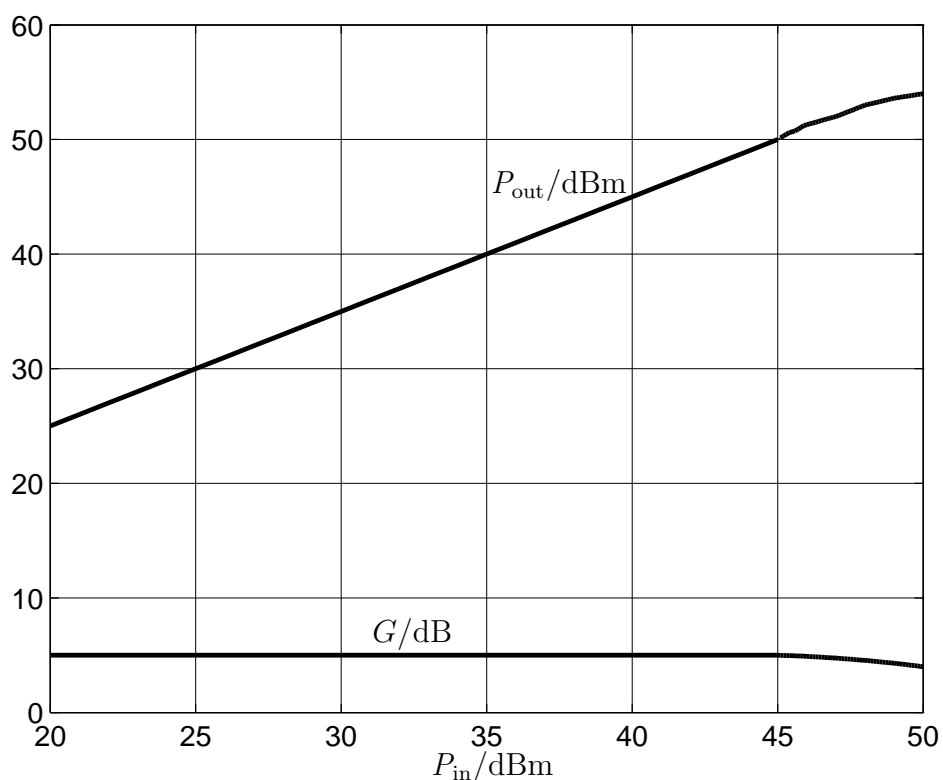


Fig. 6.1. Gain  $G$  and output power  $P_{out}$  of the considered Doherty PA versus input power  $P_{in}$

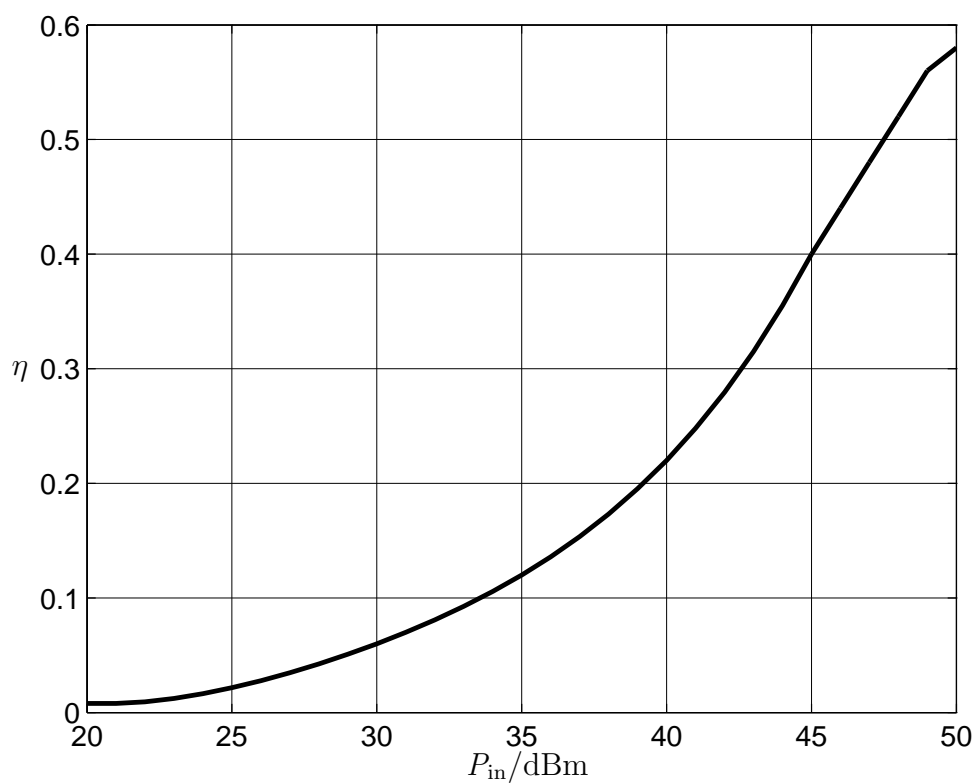


Fig. 6.2. Power efficiency  $\eta$  of the considered Doherty PA versus input power  $P_{in}$



of  $\underline{t}$ .

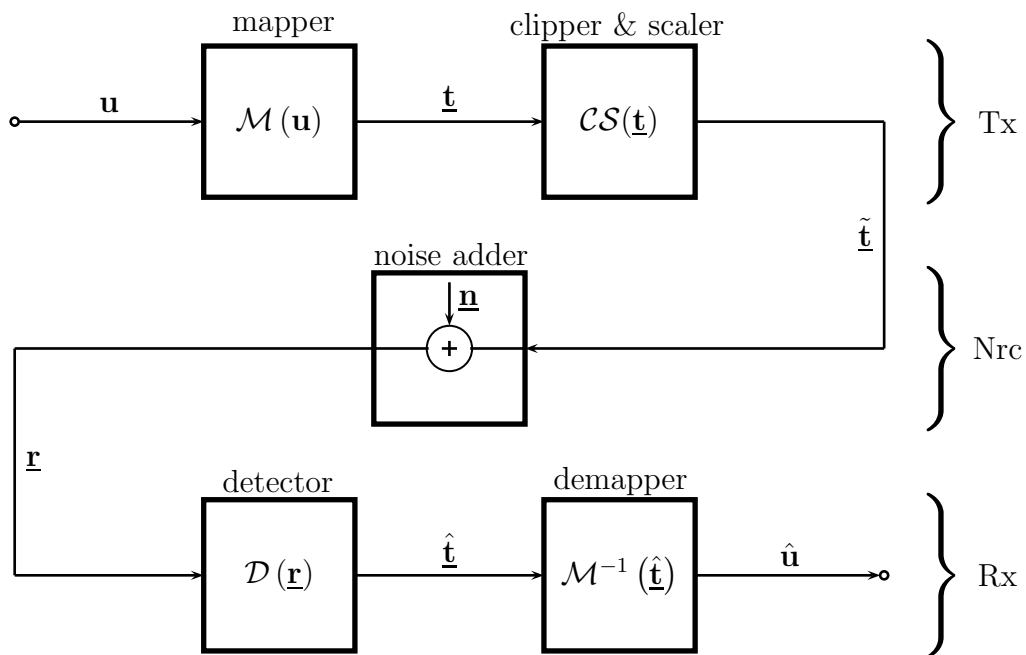


Fig. 6.3. OFDM transmission model incorporating clipping and scaling

In Fig. 6.4 we depict the inner structure of the block clipper & scaler, which is constituted by the seven blocks

- IFF transformer 1,
- clipper,
- FF transformer,
- filter,
- IFF transformer 2,
- scaling factor determinator, and
- scaler.

In the following we explain the operations performed by these blocks. The occurring Fourier operations are performed with  $k_o$ -fold oversampling. As stated in Section 5.1, by choosing  $k_o$  equal four the discrete time signal representations describe the time continuous signals with sufficient accuracy.

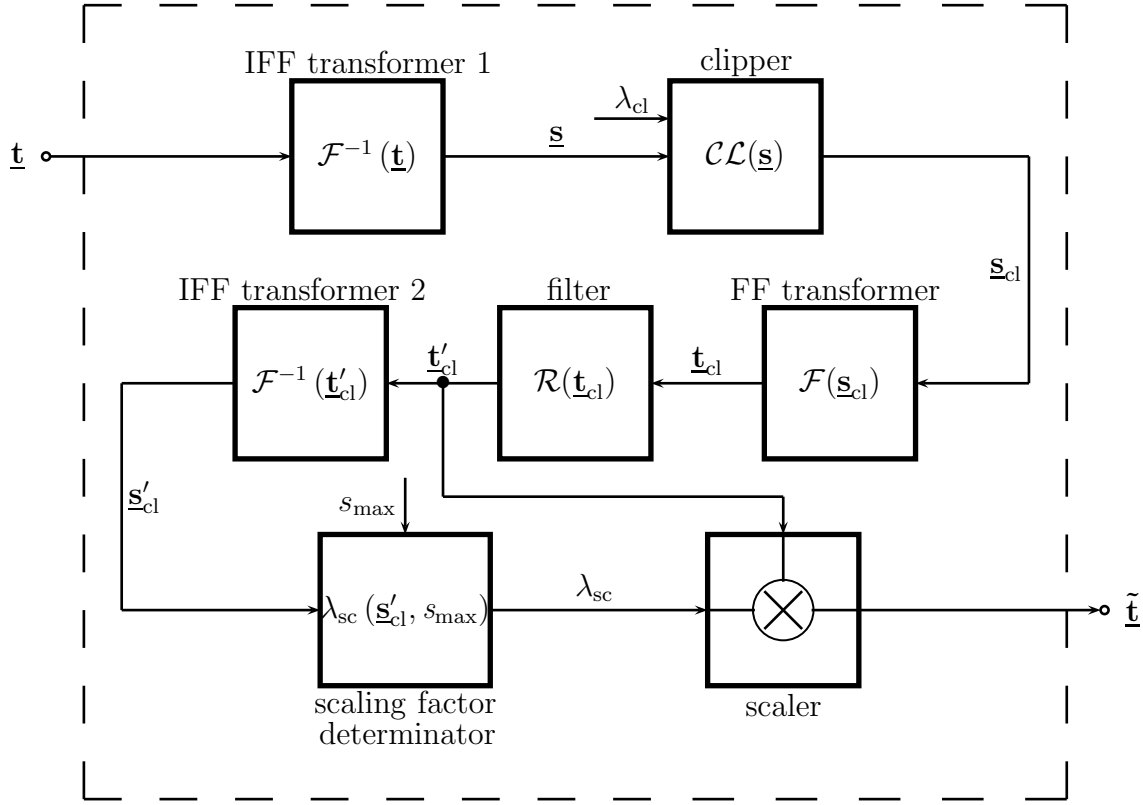


Fig. 6.4. Inner structure of the block clipper &amp; scaler

The block IFF transformer 1 subjects the transmit vector  $\underline{\mathbf{t}}$  of (2.5) to the IFF transformation  $\mathcal{F}^{-1}(\cdot)$  already introduced in (5.3), which yields the time domain representation

$$\underline{\mathbf{s}} = (\underline{s}_1 \cdots \underline{s}_{k_o n_F} \cdots \underline{s}_{k_o N_F})^T = \mathcal{F}^{-1}(\underline{\mathbf{t}}) = \left( \underline{\mathbf{F}}^{(k_o N_F) \times (k_o N_F)} \right)^{-1} \begin{pmatrix} \underline{\mathbf{t}}^T, & \underbrace{0 \cdots 0}_{(k_o - 1) N_F \text{ zeros}} \end{pmatrix}^T \in \mathbb{C}^{(k_o N_F) \times 1} \quad (6.7)$$

of the OFDM symbol. We designate the root mean square of the component magnitudes  $|\underline{s}_{k_o n_F}|$  of  $\underline{\mathbf{s}}$  obtained by averaging over the total ensemble of OFDM symbols as  $s_{av}$ . In the block clipper, with the clipping ratio  $\lambda_{cl}$  a clipped version

$$\underline{\mathbf{s}}_{cl} = \mathcal{CL}(\underline{\mathbf{s}}) = (\underline{s}_{cl,1} \cdots \underline{s}_{cl,k_o n_F} \cdots \underline{s}_{cl,k_o N_F})^T \in \mathbb{C}^{(k_o N_F) \times 1} \quad (6.8)$$

of  $\underline{\mathbf{s}}$  of (6.7) is produced by following to the rule

$$\underline{s}_{cl,k_o n_F} = \begin{cases} \underline{s}_{k_o n_F}, & \text{if } |\underline{s}_{k_o n_F}| \leq s_{av} \lambda_{cl}, \\ s_{av} \lambda_{cl} \cdot \exp(j \arg(\underline{s}_{k_o n_F})) & \text{else.} \end{cases} \quad (6.9)$$

The block FF transformer generates the frequency domain representation

$$\underline{\mathbf{t}}_{\text{cl}} = \mathcal{F}(\underline{\mathbf{s}}_{\text{cl}}) = (\underline{t}_{\text{cl},1} \cdots \underline{t}_{\text{cl},k_o n_F} \cdots \underline{t}_{\text{cl},k_o N_F})^T = \underline{\mathbf{F}}^{(k_o N_F) \times (k_o N_F)} \underline{\mathbf{s}}_{\text{cl}} \in \mathbb{C}^{(k_o N_F) \times 1} \quad (6.10)$$

of  $\underline{\mathbf{s}}_{\text{cl}}$  of (6.8) and (6.9). The block filter forms the vector

$$\underline{\mathbf{t}}'_{\text{cl}} = \mathcal{R}(\underline{\mathbf{t}}_{\text{cl}}) = (\underline{t}'_{\text{cl},1} \cdots \underline{t}'_{\text{cl},n_F} \cdots \underline{t}'_{\text{cl},N_F})^T = (\underline{t}_{\text{cl},1} \cdots \underline{t}_{\text{cl},n_F} \cdots \underline{t}_{\text{cl},N_F})^T \in \mathbb{C}^{N_F \times 1} \quad (6.11)$$

consisting of the first  $N_F$  components of  $\underline{\mathbf{t}}_{\text{cl}}$  of (6.10). The time domain representation

$$\underline{\mathbf{s}}'_{\text{cl}} = \mathcal{F}^{-1}(\underline{\mathbf{t}}'_{\text{cl}}) = (\underline{s}'_{\text{cl},1} \cdots \underline{s}'_{\text{cl},k_o n_F} \cdots \underline{s}'_{\text{cl},k_o N_F})^T = \left( \underline{\mathbf{F}}^{(k_o N_F) \times (k_o N_F)} \right)^{-1} \begin{pmatrix} (\underline{\mathbf{t}}'_{\text{cl}})^T \\ \underbrace{0 \cdots 0}_{(k_o - 1)N_F \text{ zeros}} \end{pmatrix} \in \mathbb{C}^{(k_o N_F) \times 1} \quad (6.12)$$

of this vector is produced in the block IFF transformer 2. The block scaling factor determinator has the task to calculate with the magnitude maximum  $s_{\text{max}}$  introduced above the scaling factor

$$\lambda_{\text{sc}} = \lambda_{\text{sc}}(\underline{\mathbf{s}}'_{\text{cl}}, s_{\text{max}}) = \frac{s_{\text{max}}}{\max_{n_s \in \{1 \cdots k_o N_F\}} \{|\underline{s}'_{\text{cl},n_s}|\}}. \quad (6.13)$$

Finally, the block scaler generates the scaled version

$$\underline{\tilde{\mathbf{t}}} = (\tilde{t}_1 \cdots \tilde{t}_{n_F} \cdots \tilde{t}_{N_F})^T = \lambda_{\text{sc}} \underline{\mathbf{t}}'_{\text{cl}} = \mathcal{CS}(\underline{\mathbf{t}}) \in \mathbb{C}^{N_F \times 1} \quad (6.14)$$

of  $\underline{\mathbf{t}}'_{\text{cl}}$  of (6.11).

It is true that signal distortions by the PA are avoided by tailoring the complex envelopes  $\underline{\mathbf{s}}(t)$  as described by (6.8) to (6.14). Unfortunately, this tailoring goes along with the undesired effect that signal distortions are introduced by the clipper & scaler itself, and these distortions increase with a decreasing clipping ratio  $\lambda_{\text{cl}}$  in (6.9). On the other side, for a given  $s_{\text{max}}$  the average transmit power increases with a decreasing  $\lambda_{\text{cl}}$ , which is beneficial. In the following we investigate if the detrimental generation of signal distortions by clipping & scaling and the beneficial effect of an increased transmit power can be balanced against each other by suitably choosing  $\lambda_{\text{cl}}$  with a view to optimize system performance.

## 6.3 Performance

### 6.3.1 Bit error probability

We choose  $N_F$  equal 128 OFDM subcarriers, the modulation scheme QPSK given by (2.18) to (2.22), and consider the transmission of the realization

$$\mathbf{u}^{\{q_u\}} = \left( u_1^{\{q_u\}} \dots u_{n_u}^{\{q_u\}} \dots u_{N_u}^{\{q_u\}} \right)^T, \quad u_{n_u}^{\{q_u\}} \in \{0, 1\}, \quad (6.15)$$

of the information vector  $\mathbf{u}$  of (2.2). With (2.22) and (6.14),  $\mathbf{u}^{\{q_u\}}$  of (6.15) yields the realization

$$\tilde{\mathbf{t}}^{\{q_u\}} = \mathcal{CS}(\mathbf{t}^{\{q_u\}}) = \mathcal{CS}(\mathcal{M}(\mathbf{u}^{\{q_u\}})) \quad (6.16)$$

of the clipped and scaled transmit vector. With the noise vector

$$\mathbf{n} = (\underline{n}_1 \dots \underline{n}_{n_F} \dots \underline{n}_{N_F})^T, \quad \mathbb{E}(|\underline{n}_{n_F}|^2) = 2\sigma^2, \quad (6.17)$$

we obtain the receive vector

$$\mathbf{r}^{\{q_u\}} = \left( \underline{r}_1^{\{q_u\}} \dots \underline{r}_{n_F}^{\{q_u\}} \dots \underline{r}_{N_F}^{\{q_u\}} \right)^T = \mathbf{r}_R^{\{q_u\}} + \mathbf{j}\mathbf{r}_I^{\{q_u\}} = \tilde{\mathbf{t}}^{\{q_u\}} + \mathbf{n} \quad (6.18)$$

with its real and imaginary part vectors

$$\begin{aligned} \mathbf{r}_R^{\{q_u\}} &= \text{Re}(\mathbf{r}^{\{q_u\}}) = \left( r_{R,1}^{\{q_u\}} \dots r_{R,n_F}^{\{q_u\}} \dots r_{R,N_F}^{\{q_u\}} \right)^T, \\ \mathbf{r}_I^{\{q_u\}} &= \text{Im}(\mathbf{r}^{\{q_u\}}) = \left( r_{I,1}^{\{q_u\}} \dots r_{I,n_F}^{\{q_u\}} \dots r_{I,N_F}^{\{q_u\}} \right)^T. \end{aligned} \quad (6.19)$$

From (6.19) follow with (2.22) the components

$$\hat{u}_{n_u} = \begin{cases} 0.5 \text{sign}(r_{R,n_u}^{\{q_u\}}) & \text{for } 1 \leq n_u \leq N_F, \\ 0.5 \text{sign}(r_{I,n_u-N_F}^{\{q_u\}}) & \text{for } N_F+1 \leq n_u \leq N_u, \end{cases} \quad (6.20)$$

of the estimate  $\hat{\mathbf{u}}$  of the transmitted realization  $\mathbf{u}^{\{q_u\}}$  of the information vector  $\mathbf{u}$ . By determining  $\hat{\mathbf{u}}$  for many snapshots of the noise vector  $\mathbf{n}$  of (6.17) we can obtain the bit error probability

$$P_b^{\{q_u\}}(\sigma^2, \lambda_{cl}) = \frac{1}{N_u} \sum_{n_u=1}^{N_u} \text{Prob}(\hat{u}_{n_u} \neq u_{n_u}^{\{q_u\}}) \quad (6.21)$$

valid for the transmitted realization  $\mathbf{u}^{\{q_u\}}$  of  $\mathbf{u}$ . In (6.21) we indicate that this bit error probability depends on the noise variance  $\sigma^2$  and on the chosen clipping ratio  $\lambda_{cl}$ .

With  $\tilde{\mathbf{t}}^{\{q_u\}}$  of (6.16) and  $\sigma^2$  of (6.17) the SNR per bit observed at the receiver input becomes

$$\gamma_b^{\{q_u\}}(\sigma^2, \lambda_{cl}) = \frac{\left(\tilde{\mathbf{t}}^{\{q_u\}}\right)^H \tilde{\mathbf{t}}^{\{q_u\}}}{4\sigma^2 N_F}, \quad (6.22)$$

where we, like in (6.21), indicate the dependence on  $\sigma^2$  and  $\lambda_{cl}$ .

Let us consider a specific value of  $\sigma^2$ . For this value, (6.21) and (6.22) yield certain values  $P_b^{\{q_u\}}(\sigma^2, \lambda_{cl})$  and  $\gamma_b^{\{q_u\}}(\sigma^2, \lambda_{cl})$ , respectively. By averaging these values over sufficiently many realizations  $\mathbf{u}^{\{q_u\}}$  of  $\mathbf{u}$  of (2.2), we obtain

$$P_b = P_b(\sigma^2, \lambda_{cl}) \quad (6.23)$$

and

$$\gamma_b = \gamma_b(\sigma^2, \lambda_{cl}). \quad (6.24)$$

(6.23) and (6.24) implicitly express the dependence

$$P_b = P_b(\gamma_b, \lambda_{cl}) \quad (6.25)$$

of the bit error probability on the SNR per bit  $\gamma_b$  with the parameter  $\lambda_{cl}$ .

In Fig. 6.5 we depict  $P_b$  of (6.25) versus  $\gamma_b$  for different parameter values  $\lambda_{cl}$ . We recognize that, starting with a clipping ratio  $\lambda_{cl}$  as low as 0.1 and then increasing  $\lambda_{cl}$ , the bit error performance first improves until  $\lambda_{cl}$  equal 2.1 is reached. If  $\lambda_{cl}$  goes beyond this value, the bit error performance again degrades. This performance is also illustrated in Fig. 6.6, in which we depict the bit error probability  $P_b$  versus  $\lambda_{cl}$  with  $\gamma_b$  as the curve parameter. Independently of  $\gamma_b$  the bit error probability  $P_b$  becomes minimum if we choose  $\lambda_{cl}$  equal 2.1. The dashed curve in Fig. 6.5 concerns the case of infinite  $\lambda_{cl}$ ; in this case no clipping occurs, however, nevertheless all OFDM symbols are scaled to the envelope maximum  $s_{max}$  introduced above. We term  $\lambda_{cl}$  equal 2.1 the optimum clipping ratio, and clipping & scaling with this clipping ratio optimum clipping (OC). In Fig. 6.7 we consider OFDM transmission over the AWGN radio channel for the ideal case of absent clipping & scaling, and for the case of OC. We recognize that OC performs only marginally inferior to the ideal case, even though the envelope maximum is given the value  $s_{max}$  for all OFDM symbols.

The above considerations of this subsection are normalized in such a way that the chosen value  $s_{max}$  is irrelevant, as long as it is within the linear range of the PA given by (6.2). However,  $s_{max}$  would play a role if the power amplification shall be adapted to different channel attenuations resulting for instance from different distances between transmitter and receiver.

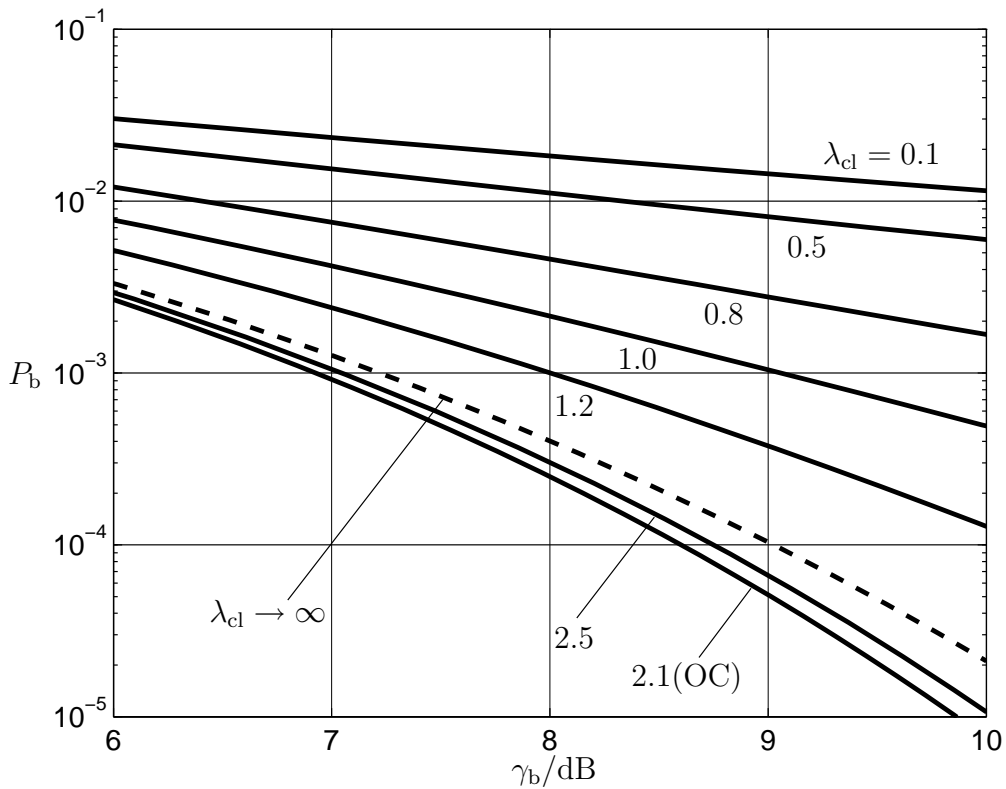


Fig. 6.5. Bit error probability  $P_b$  versus the SNR  $\gamma_b$  with the clipping ratio  $\lambda_{cl}$  as curve parameter

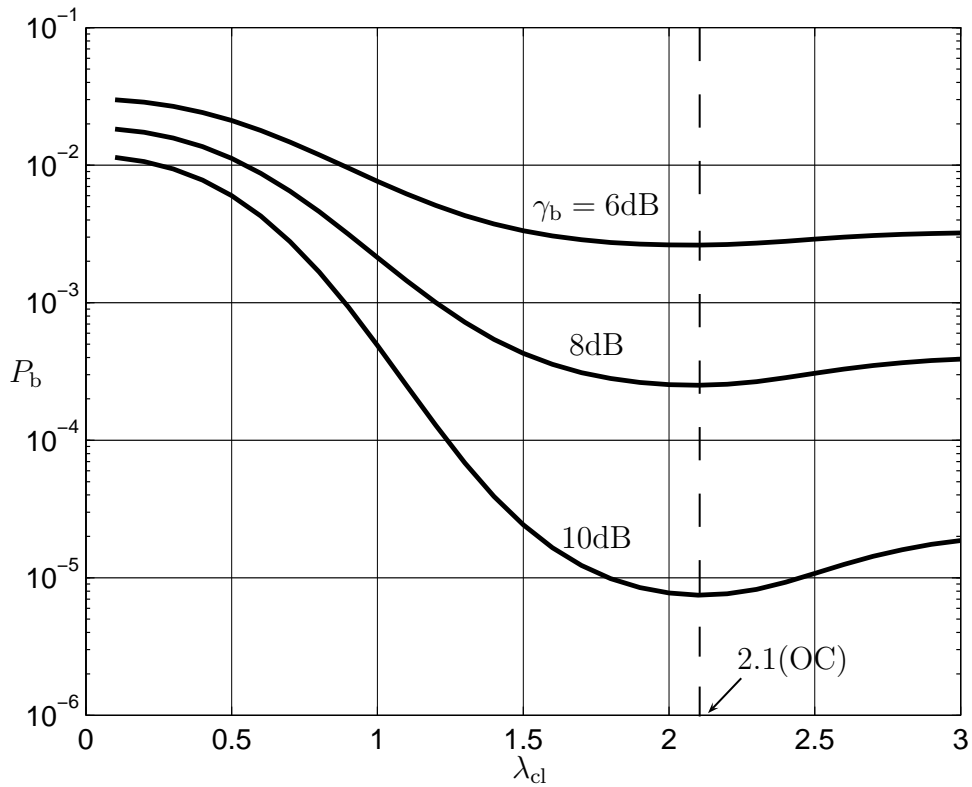


Fig. 6.6. Bit error probability  $P_b$  versus the clipping ratio  $\lambda_{cl}$  with the SNR  $\gamma_b$  as curve parameter

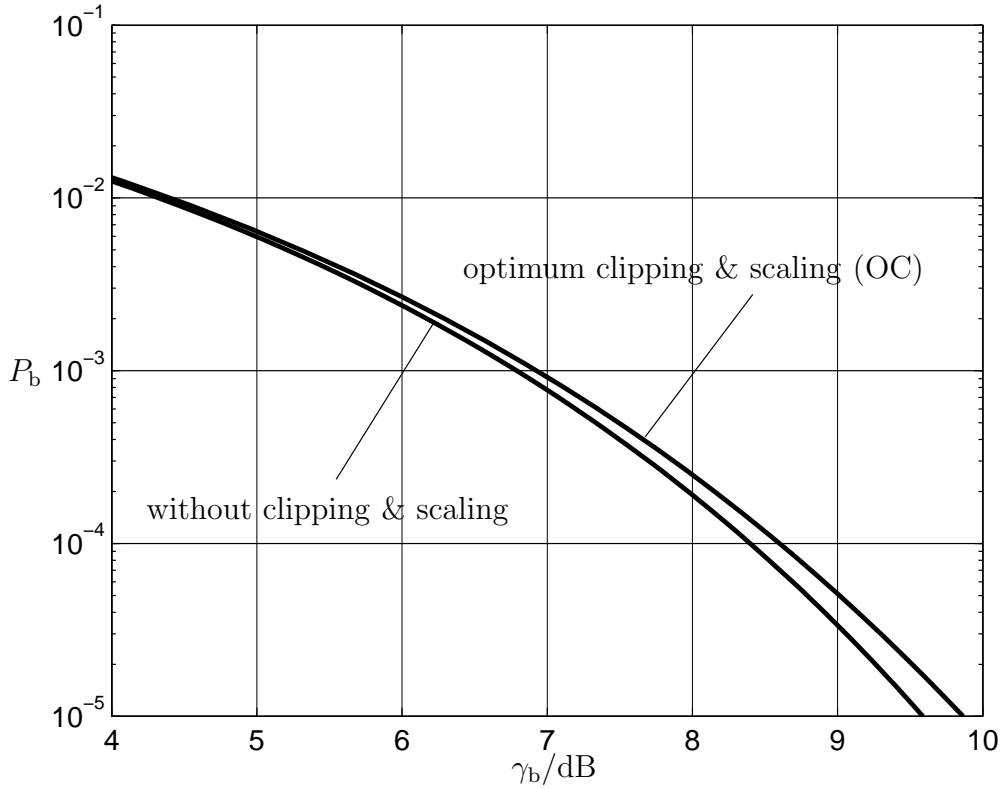


Fig. 6.7. Bit error performance of OFDM transmission over the AWGN radio channel

### 6.3.2 Required DC power

We assume that the PA is operated in such a way that each OFDM symbol feeds the maximum instantaneous RF power  $P_{\text{in,max}}$  into the PA. This power is a parameter of the PA operation and should not exceed  $P_{\text{sup}}$  of (6.2). To each component  $\underline{s}'_{\text{cl},k_0 n_F}$  of the time domain representation  $\underline{s}'_{\text{cl}}$  of (6.12) of the OFDM symbol corresponds an instantaneous RF power

$$P_{\text{in},k_0 n_F} = \frac{P_{\text{in,max}}}{\max_{n_s \in \{1 \dots k_0 N_F\}} \{|\underline{s}'_{\text{cl},n_s}|^2\}} |\underline{s}'_{\text{cl},k_0 n_F}|^2 \quad (6.26)$$

fed into the PA, and an instantaneous DC power

$$P_{\text{DC},k_0 n_F} = \frac{G_o}{\eta(P_{\text{in},k_0 N_F})} P_{\text{in},k_0 n_F} \quad (6.27)$$

drawn by the PA from the power supply. The instantaneous DC powers of (6.27) yield the average DC power

$$P_{\text{DC}}(P_{\text{in,max}}, \lambda_{\text{cl}}, \mathbf{u}^{\{q_u\}}) = \frac{1}{k_o N_F} \sum_{n_s=1}^{k_o N_F} P_{\text{DC},n_s} \quad (6.28)$$

required by the PA in order to amplify the OFDM symbol. In (6.28) we indicate that this power depends on the maximum  $P_{\text{in,max}}$  of the instantaneous RF input power  $P_{\text{in}}$ , on the clipping ratio  $\lambda_{\text{cl}}$ , and on the transmitted realization  $\mathbf{u}^{\{q_u\}}$  of the information vector  $\mathbf{u}$  of (2.2). By averaging over the ensemble of possible realizations  $\mathbf{u}^{\{q_u\}}$  we obtain the DC power  $P_{\text{DC}}(P_{\text{in,max}}, \lambda_{\text{cl}})$  which only depends on  $P_{\text{in,max}}$  and  $\lambda_{\text{cl}}$ .

In Fig. 6.8 we depict  $P_{\text{DC}}(P_{\text{in,max}}, \lambda_{\text{cl}})$  versus  $P_{\text{in,max}}$  with  $\lambda_{\text{cl}}$  as the curve parameter for the exemplary PA introduced in Section 6.1. We recognize that

- $P_{\text{DC}}$  increases with  $P_{\text{in,max}}$  increasing, what is plausible,
- $P_{\text{DC}}$  is smallest for  $\lambda_{\text{cl}} \rightarrow \infty$ , and
- $P_{\text{DC}}$  observed for OC is almost as low as  $P_{\text{DC}}$  for  $\lambda_{\text{cl}} \rightarrow \infty$ .

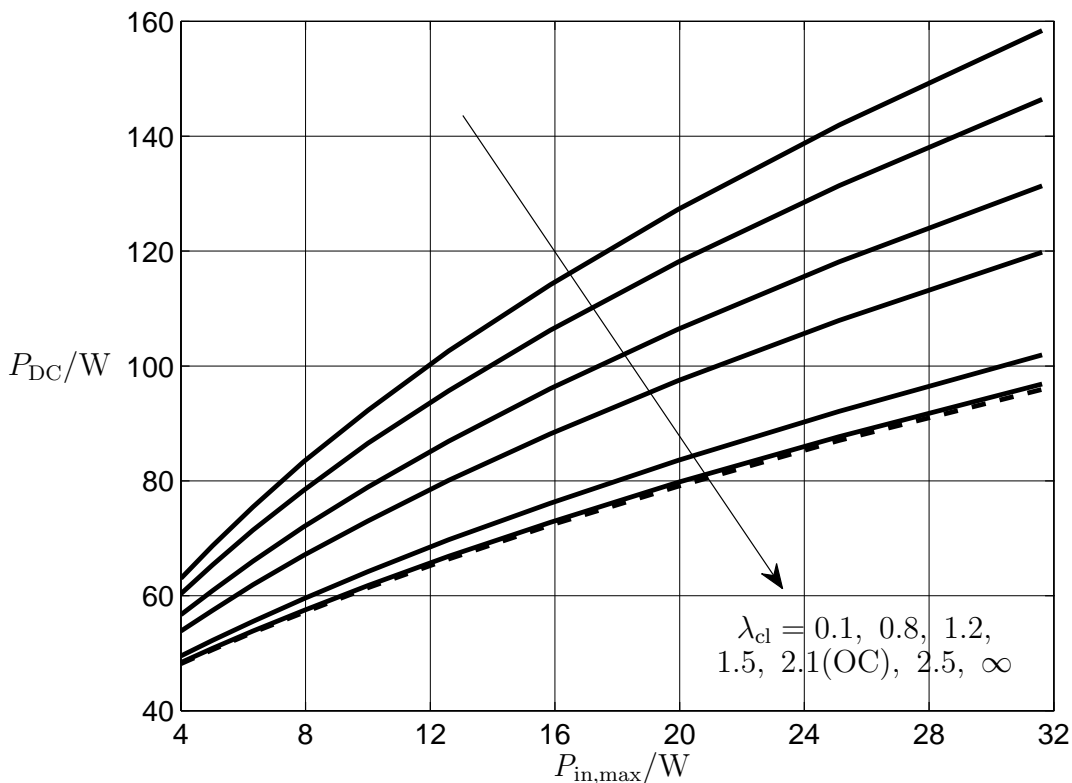


Fig. 6.8. Required DC power  $P_{\text{DC}}$  versus  $P_{\text{in,max}}$  with the clipping ratio  $\lambda_{\text{cl}}$  as curve parameter



## Chapter 7

# Joint optimization of pilot based channel estimation and data detection

### 7.1 Introduction

As already mentioned in Section 1.3, signal demodulation in the OFDM receiver requires the knowledge of the CTF vector  $\underline{\mathbf{h}}$  of (2.49). This knowledge, the utilization of which is termed channel equalization, has to be gained by channel estimation relying on the sufficiently frequent radiation of a certain number of the  $N_F$  OFDM subcarriers as pilots [OA07, HYW<sup>+</sup>09]. The investigations performed in the previous chapters are based on the assumption that channel estimation has been successfully accomplished so that  $\underline{\mathbf{h}}$  is known in the receiver. In the present Chapter 7 we address the problem of channel estimation. We consider the case of mobile stations placed in cars or trains which move so fast that the CTF vector  $\underline{\mathbf{h}}$  estimated for a certain OFDM symbol is already outdated when the next OFDM symbol is received. Therefore, the CTF vector  $\underline{\mathbf{h}}$  has to be estimated for each OFDM symbol anew with the consequence that in each OFDM symbol a certain number of the  $N_F$  subcarriers have to be sacrificed as pilots [GB09a]. This situation poses the problem how, with an energy partitioning coefficient  $v_E$  in the range

$$0 \leq v_E \leq 1, \quad (7.1)$$

the total transmit energy  $E$  provided for each OFDM symbol should be subdivided into partial energies

$$E_t = v_E E \quad (7.2)$$

and

$$E_p = (1 - v_E) E \quad (7.3)$$

for the data and pilot subcarriers, respectively, with a view to optimize system performance.

We present an approximate closed form solution to this problem, which, by simulations, proves sufficiently accurate for practical applications. Our solution is based on jointly considering the impact of the channel estimation and data detection errors. Such a joint consideration can be found in prior papers, see for instance [SK93, SBNS04, Lin08, ZL10]. Reviewing the state of the art contained in these papers reveals that the problem of fast fading radio channels is addressed, however, not the aspect of optimum energy partition-

ing.

Our optimization criterion is the symbol error probability  $P$ . The considered modulation alphabets are QPSK and 16QAM as outlined in Section 2.2. As in the preceding chapters of this thesis, we omit the Fourier operations on the transmit and receive sides as well as the insertion of the cyclic prefix. Our considerations will be performed in the frequency domain low pass regime as already introduced in Fig. 2.1.

Basically, for a given system bandwidth  $B$  pilot transmission in each one of the OFDM symbols could be avoided in said very fast varying radio channels by reducing the duration  $T$  of the OFDM symbols and the number  $N_F$  of subcarriers under consideration of (2.1). However, this would leave the required duration  $T_s$  of (2.36) of the cyclic prefix unaltered, because  $T_s$  is solely determined by the delay spread  $T_M$  of (2.48) of the radio channel. Therefore, by such a reduction of  $T$  unfortunately the percentage  $T_s/(T + T_s)$  of the transmit time lost for the cyclic prefix would grow.

We set out from the model of the radio channel introduced in Section 2.3. In the following Section 7.2 we will briefly revisit pilot based channel estimation. Section 7.3 will describe the concept of data detection based on noise corrupted channel estimates, and in Section 7.4 we will present an approximate closed form approach to determining the symbol error probabilities. The topic of Section 7.5 is our approach to optimum energy partitioning, which is verified in Section 7.6 by simulations. Finally, Section 7.7 presents exemplary results for the symbol error probabilities.

With the total transmit energy  $E$ , with  $\sigma_h^2$  of (2.55) and with  $\sigma^2$  of (2.57) the average SNR per OFDM subcarrier at the receiver input becomes

$$\gamma = \frac{2\sigma_h^2 E/N_F}{\sigma_n^2} = \frac{2E\sigma_h^2}{N_F\sigma_n^2}. \quad (7.4)$$

## 7.2 Pilot based channel estimation

Skipping the zero padding in the CIR vector  $\underline{\mathbf{h}}$  of (2.38) yields the reduced CIR vector

$$\underline{\mathbf{h}}_{\text{red}} = \left( \underline{h}_1 \cdots \underline{h}_w \cdots \underline{h}_W \right)^T \in \mathbb{C}^{W \times 1}. \quad (7.5)$$

By decimation of the CTF vector  $\underline{\mathbf{h}}$  of (2.49) we obtain the decimated CTF vector

$$\underline{\mathbf{h}}_{\text{dec}} = \left( \underline{h}_1, \underline{h}_{1+\frac{N_F}{W}}, \underline{h}_{1+2\frac{N_F}{W}}, \cdots, \underline{h}_{1+\frac{N_F}{W}(W-1)} \right)^T \in \mathbb{C}^{W \times 1}. \quad (7.6)$$

With the  $W \times W$  Fourier matrix  $\underline{\mathbf{F}}^{W \times W}$ ,  $\underline{\mathbf{h}}_{\text{red}}$  of (7.5) and  $\underline{\mathbf{h}}_{\text{dec}}$  of (7.6) are related by

$$\underline{\mathbf{h}}_{\text{red}} = \sqrt{\frac{N_F}{W}} (\underline{\mathbf{F}}^{W \times W})^{-1} \underline{\mathbf{h}}_{\text{dec}}. \quad (7.7)$$

Setting out from (7.7),  $\underline{\mathbf{h}}$  of (2.38) can be expressed by  $\underline{\mathbf{h}}_{\text{dec}}$  as follows:

$$\underline{\mathbf{h}} = \left( \underline{\mathbf{h}}_{\text{red}}^{\text{T}}, \overbrace{0 \cdots 0}^{N_{\text{F}}-W} \right)^{\text{T}} = \left( \left( \sqrt{\frac{N_{\text{F}}}{W}} (\underline{\mathbf{F}}^{W \times W})^{-1} \underline{\mathbf{h}}_{\text{dec}} \right)^{\text{T}}, \overbrace{0 \cdots 0}^{N_{\text{F}}-W} \right)^{\text{T}}. \quad (7.8)$$

With  $\underline{\mathbf{h}}$  of (7.8), (2.49) can be written as

$$\underline{\mathbf{h}} = \underline{\mathbf{F}}^{N_{\text{F}} \times N_{\text{F}}} \underline{\mathbf{h}} = \underline{\mathbf{F}}^{N_{\text{F}} \times N_{\text{F}}} \left( \left( \sqrt{\frac{N_{\text{F}}}{W}} (\underline{\mathbf{F}}^{W \times W})^{-1} \underline{\mathbf{h}}_{\text{dec}} \right)^{\text{T}}, \overbrace{0 \cdots 0}^{N_{\text{F}}-W} \right)^{\text{T}}. \quad (7.9)$$

(7.9) is the key to pilot based channel estimation. If pilots are radiated on the  $W$  equidistant OFDM subcarrier frequencies corresponding to the components of  $\underline{\mathbf{h}}_{\text{dec}}$  of (7.6), then in the receiver an estimate  $\hat{\underline{\mathbf{h}}}_{\text{dec}}$  of  $\underline{\mathbf{h}}_{\text{dec}}$  can be obtained. This estimate can then be substituted in (7.9) in order to give an estimate  $\hat{\underline{\mathbf{h}}}$  of  $\underline{\mathbf{h}}$  of (2.49).

Without restricting generality we give each of the  $W$  pilots the real valued amplitude  $a_{\text{p}}$ . With  $\underline{\mathbf{h}}_{\text{dec}}$  of (7.6) and the noise vector

$$\underline{\mathbf{n}}_{\text{dec}} = \left( \underline{n}_{\text{Rx},1}, \underline{n}_{\text{Rx},1+\frac{N_{\text{F}}}{W}}, \underline{n}_{\text{Rx},1+2\frac{N_{\text{F}}}{W}}, \cdots, \underline{n}_{\text{Rx},1+\frac{N_{\text{F}}}{W}(W-1)} \right)^{\text{T}} \in \mathbb{C}^{W \times 1} \quad (7.10)$$

resulting from  $\underline{\mathbf{n}}_{\text{Rx}}$  of (2.57) by decimation, the vector of the  $W$  complex amplitudes observed in the receiver on the  $W$  pilot subcarrier frequencies becomes

$$\underline{\mathbf{r}}_{\text{dec}} = a_{\text{p}} \underline{\mathbf{h}}_{\text{dec}} + \underline{\mathbf{n}}_{\text{dec}}. \quad (7.11)$$

From (7.11) follows the Maximum-Likelihood (ML) [Wha71] estimate

$$\hat{\underline{\mathbf{h}}}_{\text{dec}} = \frac{1}{a_{\text{p}}} \underline{\mathbf{r}}_{\text{dec}} = \underline{\mathbf{h}}_{\text{dec}} + \frac{1}{a_{\text{p}}} \underline{\mathbf{n}}_{\text{dec}} \quad (7.12)$$

of  $\underline{\mathbf{h}}_{\text{dec}}$  of (7.6). Substitution of  $\hat{\underline{\mathbf{h}}}_{\text{dec}}$  of (7.12) in (7.9) yields the estimate

$$\begin{aligned} \hat{\underline{\mathbf{h}}} &= \underline{\mathbf{h}} + \underline{\mathbf{n}}_{\text{h}} = \\ & \underline{\mathbf{F}}^{N_{\text{F}} \times N_{\text{F}}} \left( \left( \sqrt{\frac{N_{\text{F}}}{W}} (\underline{\mathbf{F}}^{W \times W})^{-1} \hat{\underline{\mathbf{h}}}_{\text{dec}} \right)^{\text{T}}, \overbrace{0 \cdots 0}^{N_{\text{F}}-W} \right)^{\text{T}} = \\ & \underline{\mathbf{F}}^{N_{\text{F}} \times N_{\text{F}}} \left( \left( \sqrt{\frac{N_{\text{F}}}{W}} (\underline{\mathbf{F}}^{W \times W})^{-1} \left( \underline{\mathbf{h}}_{\text{dec}} + \frac{1}{a_{\text{p}}} \underline{\mathbf{n}}_{\text{dec}} \right) \right)^{\text{T}}, \overbrace{0 \cdots 0}^{N_{\text{F}}-W} \right)^{\text{T}} = \\ & \underbrace{\underline{\mathbf{h}} + \sqrt{\frac{N_{\text{F}}}{W}} \underline{\mathbf{F}}^{N_{\text{F}} \times N_{\text{F}}} (\underline{\mathbf{F}}^{W \times W})^{-1} \frac{1}{a_{\text{p}}} \underline{\mathbf{n}}_{\text{dec}}}_{\underline{\mathbf{n}}_{\text{h}}} \end{aligned} \quad (7.13)$$

of  $\underline{\mathbf{h}}$  of (2.49). This estimate is corrupted by the noise vector

$$\underline{\mathbf{n}}_{\mathbf{h}} = (\underline{n}_{h,1} \cdots \underline{n}_{h,n_F} \cdots \underline{n}_{h,N_F})^T = \sqrt{\frac{N_F}{W}} \underline{\mathbf{F}}^{N_F \times N_F} (\underline{\mathbf{F}}^{W \times W})^{-1} \frac{1}{a_p} \underline{\mathbf{n}}_{\text{dec}} \quad (7.14)$$

which can be considered the channel estimation error. With  $\sigma^2$  of (2.57) and with the pilot energy

$$E_p = \frac{W a_p^2}{2} \quad (7.15)$$

follows from (7.14) the variance

$$\sigma_{\mathbf{n}_{\mathbf{h}}}^2 = \frac{W}{E_p} \sigma^2 \quad (7.16)$$

of each of the  $N_F$  components of  $\underline{\mathbf{n}}_{\mathbf{h}}$ .

### 7.3 Data detection

All data subcarriers are equally affected by the channel estimation error  $\underline{\mathbf{n}}_{\mathbf{h}}$  of (7.14). Therefore, concerning the investigation of data transmission, we can adopt a subcarrier-wise approach and, for brevity, drop the component indices  $n_F$  of the CTF vector  $\underline{\mathbf{h}}$  of (2.49), of the noise vector  $\underline{\mathbf{n}}_{\text{Rx}}$  of (2.57), and of the channel estimation error  $\underline{\mathbf{n}}_{\mathbf{h}}$  of (7.14).

With  $\mathbb{V}$  of (2.9), the data elements at the output of the modulator can take the  $\tilde{M}$  values

$$\begin{aligned} \underline{t}_{\tilde{m}} &= \text{Re}(\underline{t}_{\tilde{m}}) + j\text{Im}(\underline{t}_{\tilde{m}}), \quad \tilde{m} = 1 \cdots \tilde{M}, \\ \text{Re}(\underline{t}_{\tilde{m}}), \text{Im}(\underline{t}_{\tilde{m}}) &\in \mathbb{V}, \\ \tilde{M} &= M^2. \end{aligned} \quad (7.17)$$

With the normalized delay spread  $W$ , which equals the number of required pilot subcarriers, the number of data subcarriers becomes  $N_F - W$ . In order to give the data energy the desired value  $E_t$ , with  $\sigma_t$  of (2.10) each data element is multiplied by a factor

$$a = \frac{1}{\sigma_t} \sqrt{\frac{E_t}{N_F - W}} \quad (7.18)$$

before being used as the complex amplitude of a data subcarrier.

With the vector components  $\underline{h}$  of  $\underline{\mathbf{h}}$  and  $\underline{n}_{\text{Rx}}$  of  $\underline{\mathbf{n}}_{\text{Rx}}$  and with  $a$  of (7.18), the received complex amplitude obtained for a transmitted data symbol  $\underline{t}_{\tilde{m}}$  becomes

$$\underline{r} = \underline{h} a \underline{t}_{\tilde{m}} + \underline{n}_{\text{Rx}}. \quad (7.19)$$

If  $\underline{h}$  would be known in the receiver, then channel equalization could be achieved simply

by dividing  $\underline{r}$  of (7.19) by  $\underline{h}a$ . However, in our case instead of  $\underline{h}$  only its estimate  $\hat{\underline{h}}$  of (7.13) is available in the receiver for such a division, which yields the data estimate

$$\hat{\underline{t}} = \frac{\underline{h}a\underline{t}_{\tilde{m}} + \underline{n}_{\text{Rx}}}{\hat{\underline{h}}a} = \frac{\underline{t}_{\tilde{m}} + \frac{1}{\underline{h}}\frac{\underline{n}_{\text{Rx}}}{a}}{1 + \frac{1}{\underline{h}}\frac{\underline{n}'}{a}}. \quad (7.20)$$

Substituting in (7.20) the bivariate Gaussian quantity  $\underline{h}$  by its Rayleigh distributed magnitude  $h$  leaves the statistics of  $\hat{\underline{t}}$  unaltered, and, therefore, we can write instead of (7.20)

$$\hat{\underline{t}} = \frac{\underline{t}_{\tilde{m}} + \frac{1}{h}\frac{\underline{n}_{\text{Rx}}}{a}}{1 + \frac{1}{h}\frac{\underline{n}'}{a}}. \quad (7.21)$$

For each channel snapshot characterized by its value  $h$ , the disturbing terms in the numerator and denominator on the right hand side of (7.21) are independent bivariate Gaussian noise quantities, for which we briefly write

$$\tilde{\underline{n}}' = \frac{1}{h}\frac{\underline{n}_{\text{Rx}}}{a} \quad (7.22)$$

and

$$\tilde{\underline{n}}'' = \frac{1}{h}\frac{\underline{n}'}{a}, \quad (7.23)$$

respectively. Then, (7.21) can be rewritten as

$$\hat{\underline{t}} = \frac{\underline{t}_{\tilde{m}} + \tilde{\underline{n}}'}{1 + \tilde{\underline{n}}''}. \quad (7.24)$$

By resorting to (2.55), we can substitute  $h$  in (7.22) and (7.23) by  $\sigma_{\tilde{h}}\tilde{h}$ , where  $\tilde{h}$  is a Rayleigh distributed quantity with the probability density function

$$p_{\tilde{h}}(\tilde{h}) = \tilde{h} \exp\left(-\frac{\tilde{h}^2}{2}\right). \quad (7.25)$$

Then, (7.22) and (7.23) yield the expressions

$$\sigma_{\tilde{\underline{n}}'}^2 = \frac{1}{2}\text{E}\left(|\tilde{\underline{n}}'|^2\right) = \frac{1}{\tilde{h}^2}\frac{1}{\gamma}\sigma_{\underline{t}}^2\frac{1}{v_{\text{E}}}\left(1 - \frac{W}{N_{\text{F}}}\right) \quad (7.26)$$

and

$$\sigma_{\tilde{\underline{n}}''}^2 = \frac{1}{2}\text{E}\left(|\tilde{\underline{n}}''|^2\right) = 2\frac{1}{\tilde{h}^2}\frac{1}{\gamma}\frac{1}{1 - v_{\text{E}}}\frac{W}{N_{\text{F}}}. \quad (7.27)$$

for the variances of  $\tilde{\underline{n}}'$  and  $\tilde{\underline{n}}''$ , respectively.

A transmitted data symbol  $\underline{t}_{\tilde{m}}$  is correctly detected, if the estimate  $\hat{\underline{t}}$  of (7.24) fulfills the condition

$$|\hat{\underline{t}} - \underline{t}_{\tilde{m}}| \leq |\hat{\underline{t}} - \underline{t}_{\tilde{m}'}| \text{ for } \tilde{m}' = 1 \cdots \tilde{M}. \quad (7.28)$$

For each triple  $\tilde{h}$ ,  $\tilde{\underline{n}}'$ ,  $\tilde{\underline{n}}''$ , (7.28) is either fulfilled or not, and if said three quantities vary over the ranges given by their probability density functions, then the error probability

$$P_{\tilde{m}} = 1 - \text{Prob} \left\{ |\hat{\underline{t}} - \underline{t}_{\tilde{m}}| \leq |\hat{\underline{t}} - \underline{t}_{\tilde{m}'}| \text{ for } \tilde{m}' = 1 \cdots \tilde{M} \mid \underline{t}_{\tilde{m}} \text{ transmitted} \right\} \quad (7.29)$$

of symbol  $\underline{t}_{\tilde{m}}$  is observed.  $P_{\tilde{m}}$  decreases with decreasing variances  $\sigma_{\tilde{n}}^2$  of (7.26) and  $\sigma_{\tilde{n}'}^2$  of (7.27). Concerning the dependence of these variances on  $\tilde{h}$  and  $\gamma$ , (7.26) and (7.27) reveal as expected that the variances decrease with  $\tilde{h}$  and  $\gamma$  increasing. However, the dependence of the variances on  $v_E$  is ambivalent in the sense that  $\sigma_{\tilde{n}}^2$  decreases with increasing  $v_E$ , whereas the opposite is true for  $\sigma_{\tilde{n}'}^2$ . This ambivalence is the key to performance optimization by a suitable energy partitioning, that is by giving the energy partitioning coefficient  $v_E$  an optimum value  $v_{E,\text{opt}}$ . According to (7.26) and (7.27), we have to expect that  $v_{E,\text{opt}}$  depends on the ratio  $W/N_F$ .

## 7.4 Approximate closed form expressions for the symbol error probabilities

### 7.4.1 Approximation rationale

In order to achieve a satisfying system performance, the SNR  $\gamma$  of (7.4) should be so large that in (7.24)

$$|\tilde{\underline{n}}'| \ll |\underline{t}_{\tilde{m}}|, \quad |\tilde{\underline{n}}''| \ll 1 \quad (7.30)$$

hold. Under these conditions we can approximate (7.24) as

$$\hat{\underline{t}} \approx (\underline{t}_{\tilde{m}} + \tilde{\underline{n}}') (1 - \tilde{\underline{n}}'') \approx \underline{t}_{\tilde{m}} + \tilde{\underline{n}}' - \underline{t}_{\tilde{m}} \tilde{\underline{n}}''. \quad (7.31)$$

The data estimate  $\hat{\underline{t}}$  of (7.31) is corrupted by the bivariate Gaussian noise term

$$\tilde{\underline{n}} = x + jy = \tilde{\underline{n}}' - \underline{t}_{\tilde{m}} \tilde{\underline{n}}'' \quad (7.32)$$

with the real part  $x$  and the imaginary part  $y$ . With  $\sigma_{\tilde{n}'}^2$  of (7.26) and  $\sigma_{\tilde{n}''}^2$  of (7.27), the variance of  $\tilde{n}$  becomes

$$\sigma^2(\tilde{h}, \tilde{m}) = \frac{1}{2} \mathbb{E}(|\tilde{n}|^2) = \sigma_{\tilde{n}'}^2 + |\underline{t}_{\tilde{m}}|^2 \sigma_{\tilde{n}''}^2 = \frac{1}{\tilde{h}^2} \frac{1}{\gamma} \underbrace{\left( 2\sigma_t^2 \frac{1}{v_E} \left(1 - \frac{W}{N_F}\right) + |\underline{t}_{\tilde{m}}|^2 \frac{2}{1 - v_E} \frac{W}{N_F} \right)}_{k_{\tilde{m}}} = \frac{k_{\tilde{m}}}{\tilde{h}^2}. \quad (7.33)$$

On the left most side of (7.33) we indicate by  $(\tilde{h}, \tilde{m})$  that this variance depends on  $\tilde{h}$  and  $\tilde{m}$ .

If the data symbol  $\underline{t}_{\tilde{m}}$  is transmitted, no detection error occurs as long as  $\tilde{n}$  of (7.32) stays within a complex region  $\mathbb{D}_{\tilde{m}}$  resulting from the Voronoi region [FJ89] of  $\underline{t}_{\tilde{m}}$  of (7.17). With  $\mathbb{D}_{\tilde{m}}$ , with  $\sigma^2(\tilde{h}, \tilde{m})$  of (7.33) and  $p_{\tilde{h}}(\tilde{h})$  of (7.25), the symbol error probabilities can be expressed as

$$\begin{aligned} P_{\tilde{m}} &= 1 - \text{Prob}(\tilde{n} \in \mathbb{D}_{\tilde{m}} \mid \underline{t}_{\tilde{m}} \text{ transmitted}) = \\ &= 1 - \frac{1}{2\pi} \int_{\tilde{h}=0}^{\infty} \frac{1}{\sigma^2(\tilde{h}, \tilde{m})} \times \\ &\quad \left( \int \int_{\mathbb{D}_{\tilde{m}}(x,y)} \exp\left(-\frac{x^2 + y^2}{2\sigma^2(\tilde{h}, \tilde{m})}\right) dx dy \right) p_{\tilde{h}}(\tilde{h}) d\tilde{h} = \\ &= 1 - \frac{1}{2\pi k_{\tilde{m}}} \int_{\tilde{h}=0}^{\infty} \tilde{h}^2 \times \\ &\quad \left( \int \int_{\mathbb{D}_{\tilde{m}}(x,y)} \exp\left(-\frac{(x^2 + y^2) \tilde{h}^2}{2\pi k_{\tilde{m}}}\right) dx dy \right) \tilde{h} \exp\left(-\frac{\tilde{h}^2}{2}\right) d\tilde{h}. \end{aligned} \quad (7.34)$$

If the information bits are assigned to the data symbols  $\underline{t}_{\tilde{m}}$  by Gray coding [Pro00] and if the SNR  $\gamma$  of (7.4) is sufficiently large, then the bit error probability  $P_b$  would result from the symbol error probabilities  $P_{\tilde{m}}$  of (7.34) in a straightforward manner.

## 7.4.2 QPSK

In the case of QPSK,  $\sigma^2(\tilde{h}, \tilde{m})$  and  $k_{\tilde{m}}$  of (7.33) are independent of  $\tilde{m}$ . Therefore, we drop the indicator  $\tilde{m}$  and obtain from (7.33) with  $\sigma_t$  of (2.21)

$$\sigma^2(\tilde{h}) = \frac{1}{\tilde{h}^2} \frac{1}{\gamma} \underbrace{\left( \frac{1}{2v_E} \left(1 - \frac{W}{N_F}\right) + \frac{1}{1 - v_E} \frac{W}{N_F} \right)}_k = \frac{k}{\tilde{h}^2}. \quad (7.35)$$

All four symbol error probabilities  $P_{\tilde{m}}$  attain the same value  $P$ , and in order to determine this value we consider the data symbol  $\underline{t}_1$  as a representative, for which

$$\mathbb{D}_1(x, y) : -0.5 \leq x < \infty, -0.5 \leq y < \infty, \quad (7.36)$$

holds. Substitution of  $\sigma^2(\tilde{h})$  of (7.35) and  $\mathbb{D}_1(x, y)$  of (7.36) in (7.34) and resorting to the definite integrals  $I_{\square}(k)$  and  $I_{\sqcup}(k)$  derived in Section 7.8 yields

$$\begin{aligned} P &= 1 - \frac{1}{2\pi k} \int_{\tilde{h}=0}^{\infty} \tilde{h}^2 \times \\ &\left( \int_{x=-0.5}^{\infty} \int_{y=-0.5}^{\infty} \exp\left(-\frac{(x^2 + y^2) \tilde{h}^2}{2k}\right) dx dy \right) \times \\ &\tilde{h} \exp\left(-\frac{\tilde{h}^2}{2}\right) d\tilde{h} = \\ &1 - \left(\frac{1}{4} + \frac{I_{\square}(k)}{4} + I_{\sqcup}(k)\right) = 1 - \frac{1}{\sqrt{1 + 4k}}. \end{aligned} \quad (7.37)$$

### 7.4.3 16QAM

In the case of 16QAM, (7.33) yields with  $\sigma_t$  of (2.26)

$$\frac{1}{\tilde{h}^2} \frac{1}{\gamma} \underbrace{\left( \frac{5}{2v_E} \left(1 - \frac{W}{N_F}\right) + |\underline{t}_{\tilde{m}}|^2 \frac{2}{1 - v_E} \frac{W}{N_F} \right)}_{k_{\tilde{m}}} = \frac{k_{\tilde{m}}}{\tilde{h}^2}. \quad (7.38)$$

The 16 symbol error probabilities  $P_{\tilde{m}}$  of 16QAM stem from a set of only three different values. In order to determine these values, we consider the three representative data symbols

$$\underline{t}_1 = 0.5 + j0.5, \underline{t}_2 = 0.5 + j1.5, \underline{t}_3 = 1.5 + j1.5. \quad (7.39)$$

Substituting these in  $k_{\tilde{m}}$  of (7.38) gives

$$k_{\tilde{m}} = \frac{1}{\gamma} \left( \frac{5}{2v_E} \left(1 - \frac{W}{N_F}\right) + \frac{1 + 4(\tilde{m} - 1)W}{1 - v_E} \frac{W}{N_F} \right), \quad (7.40)$$

$\tilde{m} = 1, 2, 3.$

The regions  $\mathbb{D}_{\tilde{m}}$  of the three data symbols of (7.39) are

$$\begin{aligned} \mathbb{D}_1(x, y) &: -0.5 \leq x \leq 0.5, -0.5 \leq y \leq 0.5, \\ \mathbb{D}_2(x, y) &: -0.5 \leq x \leq 0.5, -0.5 \leq y \leq \infty, \\ \mathbb{D}_3(x, y) &: -0.5 \leq x \leq \infty, -0.5 \leq y \leq \infty. \end{aligned} \quad (7.41)$$



Substitution of (7.41) in (7.34) yields with

$$x_1 = y_1 = 0.5, x_2 = 0.5, y_2 \rightarrow \infty, x_3 \rightarrow \infty, y_3 \rightarrow \infty \quad (7.42)$$

the three symbol error probabilities

$$P_{\tilde{m}} = 1 - \frac{1}{2\pi k_{\tilde{m}}} \int_{\tilde{h}=0}^{\infty} \tilde{h}^2 \times \left( \int_{x=-0.5}^{x_{\tilde{m}}} \int_{y=-0.5}^{y_{\tilde{m}}} \exp\left(-\frac{(x^2 + y^2) \tilde{h}^2}{2k_{\tilde{m}}}\right) dx dy \right) \times \tilde{h} \exp\left(-\frac{\tilde{h}^2}{2}\right) d\tilde{h}, \quad \tilde{m} = 1, 2, 3. \quad (7.43)$$

From (7.43) follow with the definite integrals  $I_{\square}(k_{\tilde{m}})$  and  $I_{\sqcup}(k_{\tilde{m}})$  derived in Section 7.8

$$P_1 = 1 - I_{\square}(k_1) = 2 \left( 1 - \frac{1}{\sqrt{1 + 4k_1}} \right), \quad (7.44)$$

$$P_2 = 1 - \left( \frac{I_{\square}(k_2)}{2} + I_{\sqcup}(k_2) \right) = \frac{3}{2} \left( 1 - \frac{1}{\sqrt{1 + 4k_2}} \right), \quad (7.45)$$

and

$$P_3 = 1 - \left( \frac{1}{4} + \frac{I_{\square}(k_3)}{4} + I_{\sqcup}(k_3) \right) = 1 - \frac{1}{\sqrt{1 + 4k_3}}. \quad (7.46)$$

Finally, (7.44) to (7.46) give the mean symbol error probability

$$P = \frac{1}{4}P_1 + \frac{1}{2}P_2 + \frac{1}{4}P_3. \quad (7.47)$$

## 7.5 Optimum power partitioning

### 7.5.1 QPSK

The symbol error probability  $P$  of (7.37) attains its minimum, if  $k$  is minimized by suitably choosing  $v_E$ . With respect to  $v_E$ ,  $k$  of (7.35) has the partial derivative

$$\frac{\partial k}{\partial v_E} = \frac{1}{\gamma} \left( \frac{1}{2v_E^2} \left( \frac{W}{N_F} - 1 \right) + \frac{1}{(1 - v_E)^2} \frac{W}{N_F} \right). \quad (7.48)$$

By setting  $\frac{\partial k}{\partial v_E}$  zero, we obtain

$$v_{E,\text{opt}} = \frac{\frac{W}{N_F} - 1 + \sqrt{-2 \left(\frac{W}{N_F}\right)^2 + 2\frac{W}{N_F}}}{3\frac{W}{N_F} - 1}. \quad (7.49)$$

Substitution of  $v_{E,\text{opt}}$  in (7.35) yields

$$k_{\min} = \frac{3}{\gamma} \left( \frac{\frac{W}{N_F} - 1}{-1 + \sqrt{\frac{2\frac{W}{N_F}}{1 - \frac{W}{N_F}}}} + \frac{\frac{W}{N_F} - 1}{1 - \sqrt{-\frac{1}{2} + \frac{1}{2\frac{W}{N_F}}}} \right), \quad (7.50)$$

which is then used to determine  $P_{\min}$  from (7.37).

### 7.5.2 16QAM

In order to determine  $v_{E,\text{opt}}$  for 16QAM, we first express, based on (7.40),  $k_1$ ,  $k_2$  and  $k_3$  in (7.44) to (7.46) as functions of  $v_E$ . By substituting these expressions in (7.44) to (7.46) we can also write the symbol error probability  $P$  of (7.47) as a function of  $v_E$ . After some algebra we obtain the partial derivative

$$\frac{\partial P}{\partial v_E} = \frac{1}{\gamma} \left( \frac{15}{v_E^2} \left( \frac{W}{N_F} - 1 \right) + \frac{26}{(1 - v_E)^2} \frac{W}{N_F} \right) \quad (7.51)$$

of this function with respect to  $v_E$ . Setting this derivative to zero yields

$$v_{E,\text{opt}} = \frac{\frac{W}{N_F} - 1 + \sqrt{-1.73 \left(\frac{W}{N_F}\right)^2 + 1.73\frac{W}{N_F}}}{2.73\frac{W}{N_F} - 1}. \quad (7.52)$$

This expression can be employed to determine the values  $k_1$ ,  $k_2$  and  $k_3$ , which then can be substituted in (7.44) to (7.47) to give  $P_{\min}$ . Astonishingly, the difference of the expressions (7.49) and (7.52) for  $v_{E,\text{opt}}$  in the cases QPSK and 16QAM, respectively, is only marginal. This result elucidates that the chosen modulation scheme has only a minor influence on how the transmit energy  $E$  should be partitioned.

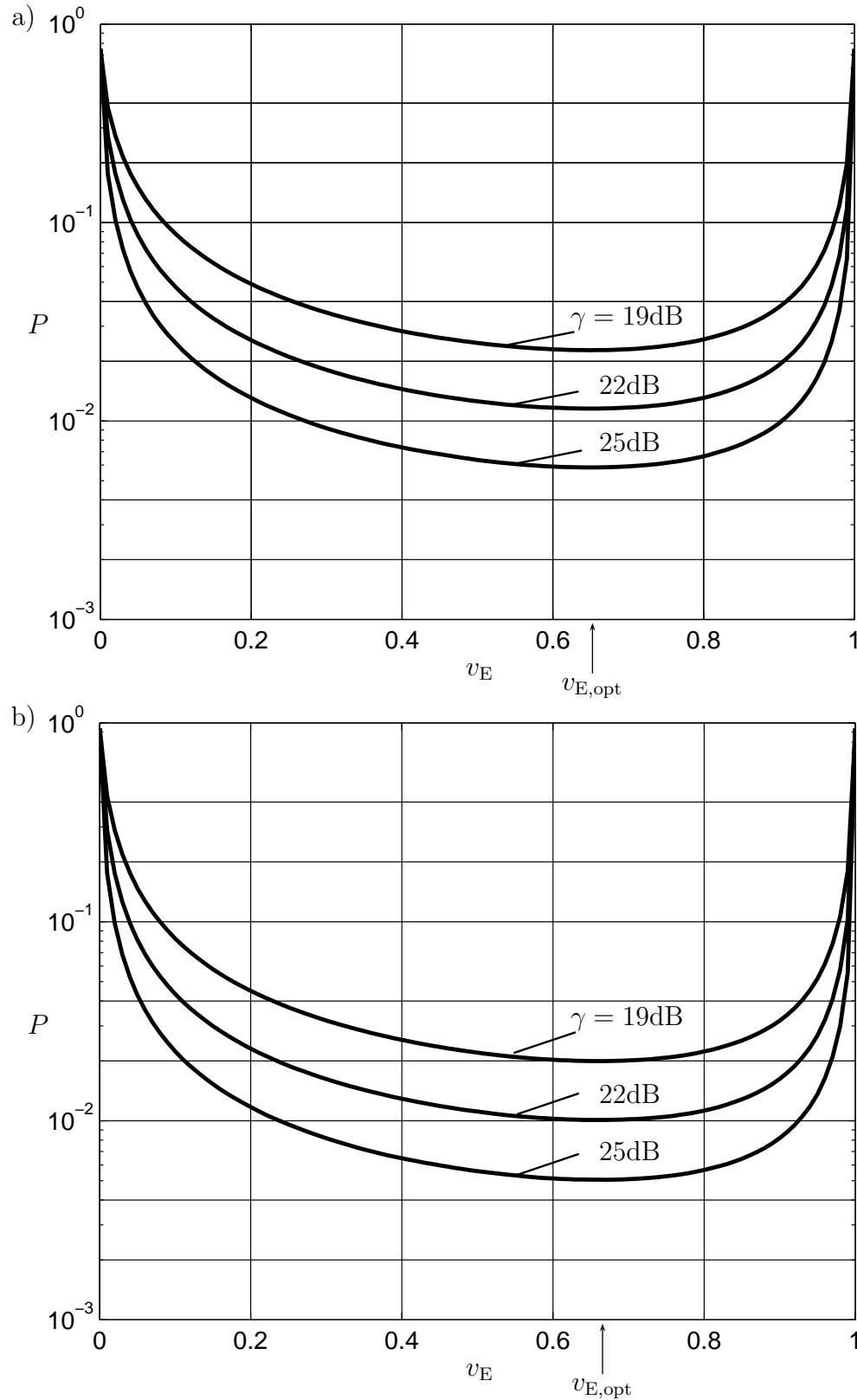


Fig. 7.1. Symbol error probability  $P$  versus the power partitioning coefficient  $v_E$  for the ratio  $W/N_F$  equal  $1/8$  and the SNR  $\gamma$  as the curve parameter

- a) QPSK
- b) 16QAM

## 7.6 Verification by simulations

In Fig. 7.1 we depict exemplary simulation results of the symbol error probability  $P$  versus  $v_E$  for the ratio  $W/N_F$  equal  $1/8$  with the SNR  $\gamma$  of (7.4) as the curve parameter. Figs. 7.1a and b hold for QPSK and for 16QAM, respectively.  $v_{E,\text{opt}}$  equals 0.65 in Fig. 7.1a and 0.66 in Fig. 7.1b. The figures show a significant increase of  $P$  if  $v_E$  deviates from  $v_{E,\text{opt}}$ . In order to verify the validity of our approximate approach to determining  $v_{E,\text{opt}}$ , we show in Table 7.1 the values  $v_{E,\text{opt}}$  obtained by our closed form approximation and, in parentheses, by simulations. The table shows results for the two considered modulation schemes QPSK and 16QAM and for different values of the ratio  $W/N_F$ . Obviously, the values obtained by simulations on the one side and by our approximation on the other side virtually coincide. According to the approximations (7.49) and (7.52),  $v_{E,\text{opt}}$  does not depend on  $\gamma$ . This independence is also confirmed by the curves in Fig. 7.1.

$W/N_F$	QPSK	16QAM
1/128	0.89 (0.89)	0.90 (0.89)
1/64	0.85 (0.85)	0.86 (0.85)
1/32	0.80 (0.80)	0.81 (0.81)
1/16	0.73 (0.73)	0.75 (0.74)
1/8	0.65 (0.65)	0.67 (0.66)
1/4	0.55 (0.55)	0.57 (0.57)
1/2	0.41 (0.41)	0.43 (0.43)

Table 7.1.  $v_{E,\text{opt}}$  of (7.49) and (7.52), respectively, for different ratios  $W/N_F$ ; in parentheses the values obtained by simulations

## 7.7 Results

In Figs. 7.2a and b we show the symbol error probability  $P_{\min}$  obtained for  $v_E = v_{E,\text{opt}}$  versus  $\gamma$  with the ratio  $W/N_F$  as the curve parameter for the modulation schemes QPSK and 16QAM, respectively. The results are obtained by our closed form approximation. A cross-check by simulations does not show deviations for the considered range of SNRs  $\gamma$ . A significant deviation of  $v_E$  from  $v_{E,\text{opt}}$  would entail a considerable growth of the symbol error probabilities.

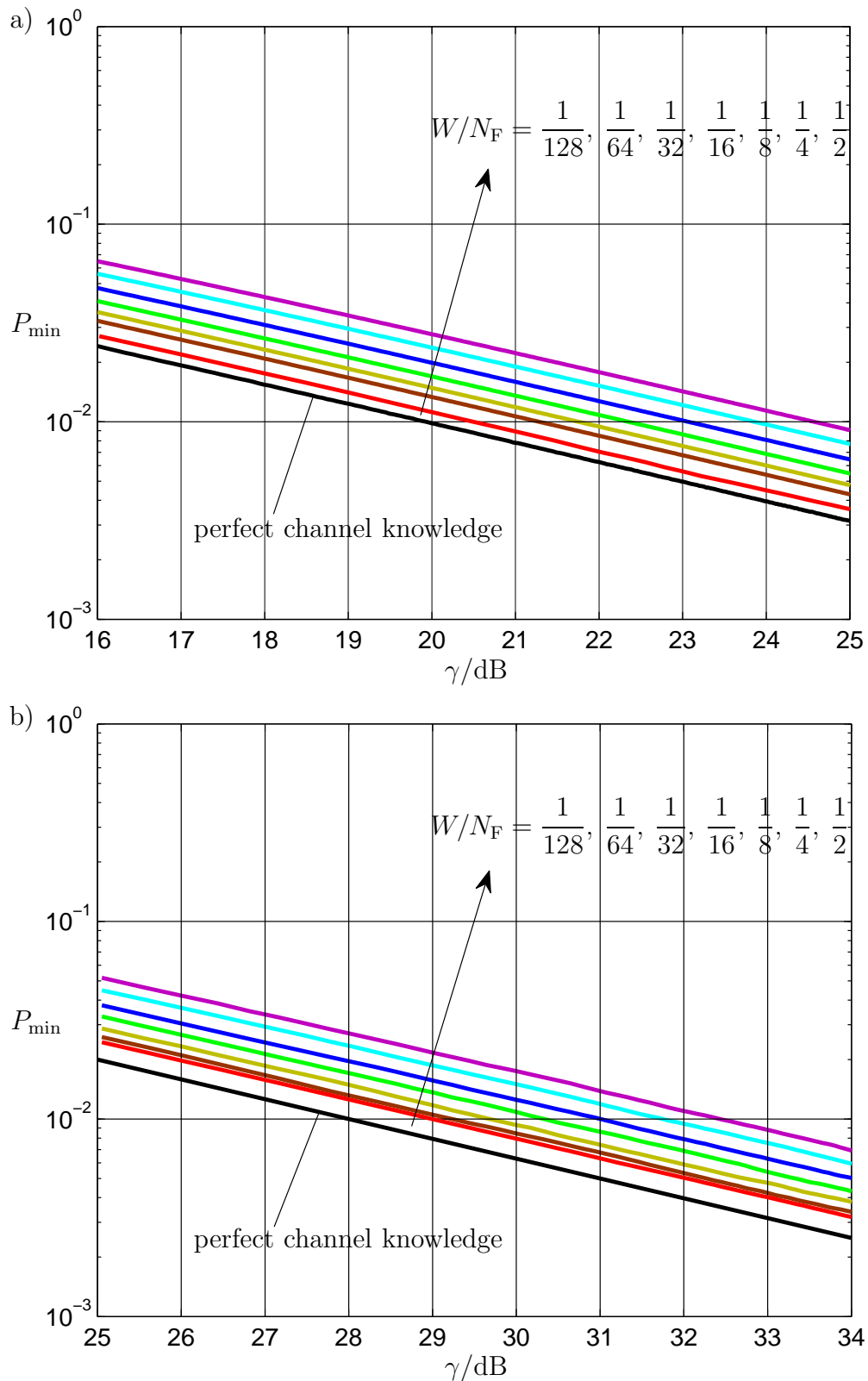


Fig. 7.2. Symbol error probability  $P_{\min}$  for  $v_E = v_{E,\text{opt}}$  versus  $\gamma$  with the ratio  $W/N_F$  as the curve parameter

a) QPSK

b) 16QAM

## 7.8 Derivation of integrals $I_{\square}(k_m)$ and $I_{\sqcup}(k_m)$

By resorting to the rationale of partial integration, the two definite integrals employed in Subsections 7.4.2 and 7.4.3 can be solved as follows:

$$\begin{aligned}
I_{\square}(k_m) &= \frac{1}{2\pi k_{\tilde{m}}} \int_{\tilde{h}=0}^{\infty} \tilde{h}^2 \times \\
&\left( \int_{x=-0.5}^{0.5} \int_{y=-0.5}^{0.5} \exp\left(-\frac{(x^2+y^2)\tilde{h}^2}{2k_{\tilde{m}}}\right) dx dy \right) \times \\
&\tilde{h} \exp\left(-\frac{\tilde{h}^2}{2}\right) d\tilde{h} = \\
\frac{4}{\pi} \int_{\tilde{h}=0}^{\infty} \left[ \int_{t=0}^{\infty} \exp(-t^2) dt - \int_{t=\tilde{h}/\sqrt{8k_m}}^{\infty} \exp(-t^2) dt \right]^2 \times \\
&\tilde{h} \exp\left(-\frac{\tilde{h}^2}{2}\right) d\tilde{h} \approx \\
1 - \frac{4}{\sqrt{\pi}} \int_{\tilde{h}=0}^{\infty} \left[ \int_{t=\tilde{h}/\sqrt{8k_m}}^{\infty} \exp(-t^2) dt \right] \times \\
&\tilde{h} \exp\left(-\frac{\tilde{h}^2}{2}\right) d\tilde{h} = \\
&-1 + \frac{2}{\sqrt{1+4k_m}}
\end{aligned} \tag{7.53}$$

and

$$\begin{aligned}
I_{\sqcup}(k_m) &= \frac{1}{2\pi k_{\tilde{m}}} \int_{\tilde{h}=0}^{\infty} \tilde{h}^2 \times \\
&\left( \int_{x=-0.5}^{0.5} \int_{y=0}^{\infty} \exp\left(-\frac{(x^2+y^2)\tilde{h}^2}{2k_{\tilde{m}}}\right) dx dy \right) \times \\
&\tilde{h} \exp\left(-\frac{\tilde{h}^2}{2}\right) d\tilde{h} = \\
\frac{1}{\sqrt{\pi}} \int_{\tilde{h}=0}^{\infty} \left( \int_{t=0}^{\tilde{h}/\sqrt{8k_m}} \exp(-t^2) dt \right) \times \\
&\tilde{h} \exp\left(-\frac{\tilde{h}^2}{2}\right) d\tilde{h} = \\
&\frac{1}{2\sqrt{1+4k_m}}.
\end{aligned} \tag{7.54}$$

The approximation  $\approx$  in (7.53) is valid, if the SNR  $\gamma$  is sufficiently large.

# Chapter 8

## Multipoint-to-point transmission

### 8.1 Introduction

The OFDM systems considered in the previous chapters of this thesis consist of a single transmitter and a single receiver. Such systems are also termed point-to-point transmission systems [FK04]. If we have a multitude of transmitters instead of only one, which communicate with a single receiver, we have a multipoint-to-point transmission system [FK04]. We have such a situation for instance in the uplink of mobile radio systems, because many users transmit to a single base station. In multipoint-to-point transmission systems the total transmission resources have to be shared by the individual users. The formation of partial transmission systems by PDS as described in Chapter 3 offers a viable approach to perform such a resource sharing. In the previous chapters the  $Z$  partial transmit systems were assigned to a single transmitter. In the present chapter we consider the case that each of these partial systems is assigned to a different transmitter. In this case FEC encoding across the  $Z$  partial systems is no longer possible, and, therefore, we consider here the case of uncoded transmission. Nevertheless, FEC encoding within each of the  $Z$  partial systems would be feasible.

For the case of uncoded transmission the results presented in Section 3.6 concerning the bit error probability  $P_b$  are valid now as before. However, the PAPR of the total transmit signal considered in Chapter 5 is no longer adequate. Rather, we have to attend to the PAPR of the  $Z$  partial transmit signals, because each of these signals is amplified by a separate PA.

### 8.2 PAPR

Each of the  $Z$  partial systems of OFDM employing PDS pertains to a certain uplink transmission system. Therefore, we use the superscripts ( $z$ ) of the partial systems now for designating the uplink transmission systems.

With the interleaved spread transmit vector  $\tilde{\mathbf{t}}_i$  of (3.19) the transmit vector of user  $z$  becomes

$$\mathbf{t}_{i,n_F}^{(z)} = \begin{cases} \tilde{\mathbf{t}}_i^{(z)} = (t_{i,1}^{(z)} \cdots t_{i,n_F}^{(z)} \cdots t_{i,N_F}^{(z)})^T & \\ \tilde{\mathbf{t}}_{i,n_F} & \text{for } n_F = z + Z(n-1), n = 1 \cdots N, \\ 0 & \text{else.} \end{cases} \quad (8.1)$$

$\tilde{\mathbf{t}}_i^{(z)}$  of (8.1) yields for user  $z$  the oversampled time domain transmit vector

$$\underline{\mathbf{s}}^{(z)} = \left( \underline{s}_1^{(z)} \cdots \underline{s}_{k_o N_F}^{(z)} \cdots \underline{s}_{k_o N_F}^{(z)} \right)^T = \left( \mathbf{F}^{(k_o N_F) \times (k_o N_F)} \right)^{-1} \left( \left( \tilde{\mathbf{t}}_i^{(z)} \right)^T, \underbrace{0 \cdots 0}_{(k_o - 1) N_F \text{ zeros}} \right)^T. \quad (8.2)$$

From  $\underline{\mathbf{s}}^{(z)}$  of (8.2) follows the PAPR

$$p^{(z)} = k_o N_F \frac{\max_{n_s \in \{1 \cdots k_o N_F\}} \left( \left| \underline{s}_{n_s}^{(z)} \right|^2 \right)}{\left( \underline{\mathbf{s}}^{(z)} \right)^H \underline{\mathbf{s}}^{(z)}}. \quad (8.3)$$

of the transmit signal of user  $z$ .

All  $Z$  users have the same CCDF of the PAPR. However, in the case of small spreading factors  $N$ , the CCDF is not well suited to show the PAPR performance. The reason is that in such a case there are only few different PAPR values. Therefore, we show in Table 8.1 the PAPR for Walsh-Hadamard PDS and Fourier PDS for  $N_F$  equal 128 for  $N = 1, 2, 4$ , whereas in Figs. 8.1 and 8.2 we depict the CCDF for  $N = 8, 16, 32, 64, 128$ . Fig. 8.1 holds for Walsh-Hadamard PDS and Fig. 8.2 for Fourier PDS. The larger the spreading factor  $N$ , the more Fourier PDS outperforms Walsh-Hadamard PDS. As explained in Section 3.9, this superiority of Fourier PDS has to be paid for by a higher computational complexity as compared to Walsh-Hadamard PDS. If a low computational complexity has a higher priority than achieving a PAPR as low as possible, the system designer should choose Walsh-Hadamard PDS, and in the opposite case Fourier PDS.

$N$	Walsh-Hadamard PDS	Fourier PDS
1	0	0
2	0, 3.0103	0, 3.0103
4	0, 2.3226, 2.6801, 3.0103 3.6800, 4.0835, 4.1565, 5.3329	0, 1.7609, 2.3226, 2.6801 3.0103, 4.0835, 4.6452

Table 8.1. PAPR/dB for the cases of Walsh-Hadamard PDS and Fourier PDS; QPSK,  $N_F = 128$ ,  $N = 1, 2, 4$



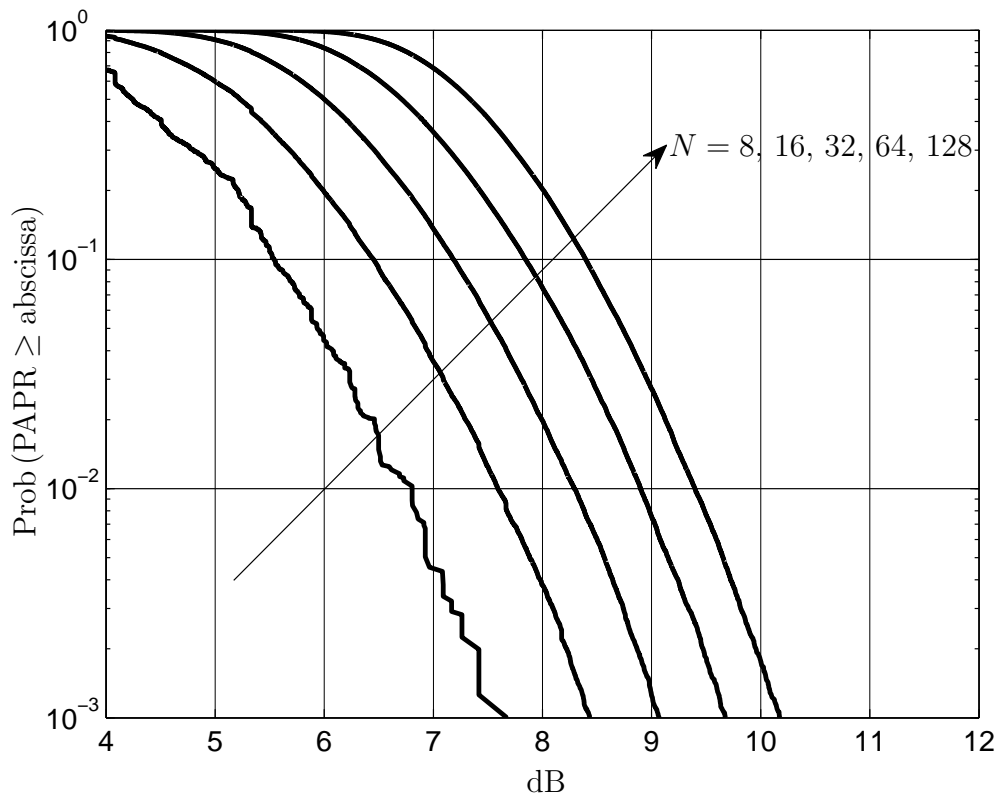


Fig. 8.1. CCDF of the PAPR for the case of Walsh-Hadamard PDS; QPSK,  $N_F = 128$ ,  $N = 8, 16, 32, 64, 128$

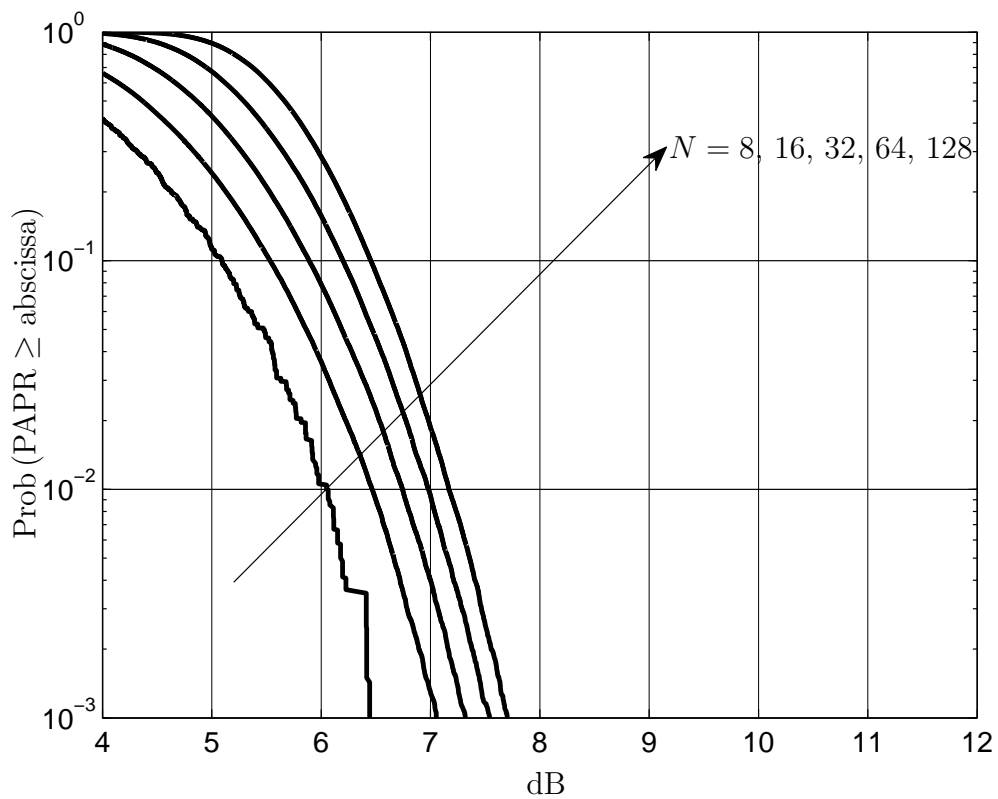


Fig. 8.2. CCDF of the PAPR for the case of Fourier PDS; QPSK,  $N_F = 128$ ,  $N = 8, 16, 32, 64, 128$

# Chapter 9

## Some open questions and proposals for further research

In this chapter we enumerate some open questions and present proposals for further research:

- The performance of our scheme PDS depends on the features of the radio channel model. In this thesis, we consider a radio channel model with a uniform PDP. Closer to real world radio channels would be an exponential PDP, and it would be interesting to learn how PDS would perform in the case of such channels.
- In Sections 3.8 and 3.9, we study and compare Walsh-Hadamard PDS and Fourier PDS. We found that Fourier PDS outperforms Walsh-Hadamard PDS for the case of ML detection at the cost of a higher computational complexity. A topic of future work could be the search for other spreading matrices which enable both a good performance and a low computational complexity.
- In Subsubsection 3.6.3.2 we empirically find how the reasonable spreading factor  $N$  depends on the channel parameter  $W$ . This empirical result would need a theoretical confirmation.
- In Chapter 4 we consider FEC encoded OFDM transmission incorporating PDS and ML detection, and we show how the system performance can be significantly enhanced by the utilization of reliability information in the receiver. In Chapter 4 the generation of this reliability information is inherently connected with ML detection. It would be worthwhile to study if such a reliability information can also be generated if we use, in order to reduce the computational complexity, MMSE detection instead of ML detection.
- In Chapter 5, the combination of PDS with SDM is used to reduce the PAPR. We consider both Walsh-Hadamard PDS and Fourier PDS. In the future, one could search for other PDS schemes featuring both a low PAPR and a low computational complexity. The phase factor sets play an important role in SDM. In addition to the phase factor sets considered in the thesis, alternative advantageous sets should be looked for.
- In our scheme PDS-SDM the receiver is informed by signaling from the transmitter about the used phase factor set. It may be possible that for small values  $N$  the ML

detector may be able to determine the used phase factor set in the sense of a blind estimation.

- A still open question would be the combination of PDS-SDM with FEC encoding.
- For the simulations of OC performed in Chapter 6 we resort to a specific Doherty PA. The performance of OC could be studied for other PAs, and it could be investigated how the performance of OC depends on the particular features of the PA.
- In Chapter 7, we consider the joint optimization of pilot based channel estimation and data detection for the modulation schemes of QPSK and 16QAM. In the future, this scheme could be extended to higher order modulation alphabets such as 64QAM and 256QAM. Additionally, we also could consider the case that the pilot subcarriers and the data subcarriers use different modulation schemes.
- The extension of OFDM transmission incorporating PDS to multipoint-to-point transmission systems briefly touched in Chapter 8 could be deepened.
- Finally, it would be interesting to extend the findings of the thesis to OFDM transmission systems with multi-antennas.

---

# Chapter 10

## Summary

### 10.1 English

This thesis has the goal to propose measures which allow an increase of the power efficiency of OFDM transmission systems.

As compared to OFDM transmission over AWGN channels, OFDM transmission over frequency selective radio channels requires a significantly larger transmit power in order to achieve a certain transmission quality. It is well known that this detrimental impact of frequency selectivity can be combated by frequency diversity. We revisit and further investigate an approach to frequency diversity based on the spreading of subsets of the data elements over corresponding subsets of the OFDM subcarriers and term this approach Partial Data Spreading (PDS). The size  $N$  of said subsets, which we designate as spreading factor, is a design parameter of PDS, and by properly choosing  $N$ , depending on the system designer's requirements, an adequate compromise between a good system performance and a low complexity can be found. We show how PDS can be combined with ML, MMSE and ZF data detection, and it is recognized that MMSE data detection offers a good compromise between performance and complexity. After having presented the utilization of PDS in OFDM transmission without FEC encoding, we also show that PDS readily lends itself for FEC encoded OFDM transmission. We display that in this case the system performance can be significantly enhanced by specific schemes of interleaving and utilization of reliability information developed in the thesis.

A severe problem of OFDM transmission is the large Peak-to-Average-Power Ratio (PAPR) of the OFDM symbols, which hampers the application of power efficient transmit amplifiers. Our investigations reveal that PDS inherently reduces the PAPR. Another approach to PAPR reduction is the well known scheme Selective Data Mapping (SDM). In the thesis it is shown that PDS can be beneficially combined with SDM to the scheme PDS-SDM with a view to jointly exploit the PAPR reduction potentials of both schemes. However, even when such a PAPR reduction is achieved, the amplitude maximum of the resulting OFDM symbols is not constant, but depends on the data content. This entails the disadvantage that the power amplifier cannot be designed, with a view to achieve a high power efficiency, for a fixed amplitude maximum, what would be desirable. In order to overcome this problem, we propose the scheme Optimum Clipping (OC), in which we obtain the desired fixed amplitude maximum by a specific combination of the measures clipping, filtering and rescaling.

In OFDM transmission a certain number of OFDM subcarriers have to be sacrificed

for pilot transmission in order to enable channel estimation in the receiver. For a given energy of the OFDM symbols, the question arises in which way this energy should be subdivided among the pilots and the data carrying OFDM subcarriers. If a large portion of the available transmit energy goes to the pilots, then the quality of channel estimation is good, however, the data detection performs poor. Data detection also performs poor if the energy provided for the pilots is too small, because then the channel estimate indispensable for data detection is not accurate enough. We present a scheme how to assign the energy to pilot and data OFDM subcarriers in an optimum way which minimizes the symbol error probability as the ultimate quality measure of the transmission.

The major part of the thesis is dedicated to point-to-point OFDM transmission systems. Towards the end of the thesis we show that the PDS can be also applied to multipoint-to-point OFDM transmission systems encountered for instance in the uplinks of mobile radio systems.

## 10.2 Deutsch

Die vorliegende Arbeit verfolgt das Ziel, Maßnahmen vorzuschlagen, durch die die Leistungseffizienz von OFDM-Übertragungssystemen erhöht werden kann.

Im Vergleich zur OFDM-Übertragung über AWGN-Kanäle erfordert die OFDM-Übertragung über frequenzselektive Funkkanäle eine wesentlich höhere Sendeleistung, um eine gewisse Übertragungsqualität zu erzielen. Es ist bekannt, daß dieser schädlichen Auswirkung der Frequenzselektivität durch Frequenzdiversität begegnet werden kann. Wir greifen ein im Prinzip bekanntes Verfahren der Frequenzdiversität auf und untersuchen dies in sehr detaillierter Weise, das darauf beruht, eine Untermenge der Datenelemente über eine entsprechende Untermenge der OFDM-Subträger zu spreizen, und wir bezeichnen dieses Verfahren als Partielle Datenspreizung (PDS). Die Größe  $N$  besagter Untermengen, die wir Spreizfaktor nennen, ist ein Entwurfparameter von PDS. Durch geeignete Wahl von  $N$  kann man abhängig von den Anforderungen des Systemdesigners angemessene Kompromisse von guter Systemperformanz und geringer Komplexität erreichen. Nachdem in der Arbeit die Anwendung von PDS bei der uncodierten OFDM-Übertragung dargelegt ist, wird gezeigt, daß PDS auch sehr geeignet ist für die OFDM-Übertragung mit Fehlerschutzcodierung. Wir führen aus, daß die Systemperformanz in diesem Fall durch spezielle Verfahren des Interleaving und der Ausnutzung von Zuverlässigkeitsinformation signifikant gesteigert werden kann.

Ein schwerwiegendes Problem der OFDM-Übertragung besteht in dem großen Peak-to-Average-Power Ratio (PAPR) der OFDM-Symbole. Dieses führt zu Einschränkungen beim Einsatz leistungseffizienter Sendeverstärker. Unsere Untersuchungen ergeben, daß PDS ein inhärentes Potential zur PAPR-Reduktion hat. Eine andere Möglichkeit der PAPR-Reduktion bietet das bekannte Verfahren des Selective Data Mapping (SDM). In der Arbeit wird gezeigt, daß PDS und SDM zu dem Verfahren PDS-SDM kombiniert werden können, das sich das Potential der PAPR-Reduktion beider Verfahren vorteilhaft zunutze macht. Allerdings ist auch nach erfolgter PAPR-Reduktion das Amplitudenmaximum der OFDM-Symbole nicht konstant, sondern es hängt vom Dateninhalt der OFDM-Symbole ab. Dies hat den Nachteil, daß der Leistungsverstärker nicht für ein festes Amplitudenmaximum entworfen werden kann, was im Hinblick auf eine hohe Leistungseffizienz wünschenswert wäre. Zum Überwinden dieses Problems schlagen wir das Verfahren Optimum Clipping (OC) vor; bei diesem wird das erwünschte feste Amplitudenmaximum durch eine spezielle Kombination der Maßnahmen Clipping, Filterung und Reskalierung erzielt.

Um im Empfänger den Funkkanal schätzen zu können, muß bei der OFDM-Übertragung eine gewisse Anzahl der OFDM-Unterträger als Piloten vorgesehen werden. Bei vorgegebener verfügbarer Energie der OFDM-Symbole stellt sich die Frage,

wie diese Energie auf die Piloten und die datentragenden OFDM-Unterträger aufgeteilt werden sollte. Wenn ein Großteil dieser Energie den Piloten zugewiesen wird, dann ist die Qualität der Kanalschätzung gut, aber die Qualität der Datendetektion ist gering. Diese Qualität ist auch gering, wenn für die Piloten zu wenig Energie vorgesehen wird, weil dann die für die Datendetektion unverzichtbare Kanalschätzung nicht genau genug ist. Wir schlagen ein Verfahren zur optimalen Energieaufteilung zwischen Piloten und datentragenden OFDM-Unterträgern vor. Dieses Verfahren gestattet es, die Symbolfehlerwahrscheinlichkeit als das letztlich relevante Performanzkriterium zu minimieren.

Der weitaus größte Teil der Arbeit ist der Punkt-zu-Punkt-OFDM-Übertragung gewidmet. Gegen Ende der Arbeit zeigen wir, daß PDS auch in Multipunkt-zu-Punkt-Übertragungssystemen eingesetzt werden kann, wie man sie zum Beispiel in der Aufwärtsstrecke von Mobilfunksystemen vorfindet.

# Appendix A

## Acronyms and symbols

### A.1 Acronyms

AWGN	<u>A</u> dditive <u>W</u> hite <u>G</u> aussian <u>N</u> oise
CCDF	<u>C</u> omplementary <u>C</u> umulative <u>D</u> istribution <u>F</u> unction
CDMA	<u>C</u> ode <u>D</u> ivision <u>M</u> ultiple <u>A</u> ccess
CI	<u>C</u> ode <u>I</u> nterleaving
CIR	<u>C</u> hannel <u>I</u> mpulse <u>R</u> esponse
CTF	<u>C</u> hannel <u>T</u> ransfer <u>F</u> unction
CP	<u>C</u> yclic <u>P</u> refix
DGUS	<u>D</u> eterministic <u>G</u> aussian <u>U</u> ncorrelated <u>S</u> cattering
EER	<u>E</u> nvelope <u>E</u> limination and <u>R</u> estoration
ET	<u>E</u> nvelope <u>T</u> racking
EVD	<u>E</u> igen <u>V</u> alue <u>D</u> ecomposition
FDS	<u>F</u> ull <u>D</u> ata <u>S</u> preading
FEC	<u>F</u> orward <u>E</u> rror <u>C</u> orrection
FFT	<u>F</u> ast <u>F</u> ourier <u>T</u> ransform
FHT	<u>F</u> ast <u>H</u> adamard <u>T</u> ransform
IFFT	<u>I</u> nverse <u>F</u> ast <u>F</u> ourier <u>T</u> ransform
LINC	<u>L</u> inear Amplification by <u>N</u> onlinear <u>C</u> omponents
MC	<u>M</u> ulti <u>C</u> arrier
MC-SS	<u>M</u> ulti <u>C</u> arrier <u>S</u> pread <u>S</u> pectrum
MF	<u>M</u> atched <u>F</u> ilter
ML	<u>M</u> aximum <u>L</u> ikelihood
MMSE	<u>M</u> inimum <u>M</u> ean <u>S</u> quare <u>E</u> rror
Nrc	<u>N</u> oisy <u>r</u> adio <u>c</u> hanel
OC	<u>O</u> ptimum <u>C</u> lipping
OFDM	<u>O</u> rthogonal <u>F</u> requency <u>D</u> ivision <u>M</u> ultiplexing
PA	<u>P</u> ower <u>A</u> mplifier
PAE	<u>P</u> ower <u>A</u> dded <u>E</u> fficiency
PAPR	<u>P</u> eak-to- <u>A</u> verage- <u>P</u> ower <u>R</u> atio
PDF	<u>P</u> robability <u>D</u> ensity <u>F</u> unction
PDP	<u>P</u> ower <u>D</u> elay <u>P</u> rofile
PDS	<u>P</u> artial <u>D</u> ata <u>S</u> preading
QAM	<u>Q</u> uadrature <u>A</u> mplitude <u>M</u> odulation



QPSK	<u>Q</u> uadrature <u>P</u> hase <u>S</u> hift <u>K</u> eying
RF	<u>R</u> adio <u>F</u> requency
Rx	<u>R</u> eceiver
SC	<u>S</u> ingle <u>C</u> arrier
SDM	<u>S</u> elective <u>D</u> ata <u>M</u> apping
SNIR	<u>S</u> ignal-to- <u>N</u> oise-plus- <u>I</u> nterference <u>R</u> atio
SNR	<u>S</u> ignal-to- <u>N</u> oise <u>R</u> atio
Tx	<u>T</u> ransmitter
URI	<u>U</u> talization of <u>R</u> eliability <u>I</u> nformation
VR	<u>V</u> oronoi <u>R</u> egion
WLAN	<u>W</u> ireless <u>L</u> ocal <u>A</u> rea <u>N</u> etwork
ZF	<u>Z</u> ero <u>F</u> orcing

## A.2 Symbols

$a_p$	amplitude of pilot
$\mathbf{a}_n^{(z)}$	the $n^{\text{th}}$ column of $\mathbf{A}^{(z)}$
$\mathbf{A}^{(z)}$	partial system matrix
$B$	system bandwidth
$B_{\text{coh}}$	coherence bandwidth
$\mathbf{c}$	code vector
$\mathbf{c}_i$	interleaved code vector
$\mathbf{c}_i^{(z)}$	partial interleaved code vector
$\hat{\mathbf{c}}_i$	estimate of $\mathbf{c}_i$
$\hat{\mathbf{c}}_i^{(z)}$	estimate of $\mathbf{c}_i^{(z)}$
$\hat{\mathbf{c}}_{i,\text{soft}}$	soft estimate of $\mathbf{c}_i$
$\hat{\mathbf{c}}_{\text{soft}}$	soft estimate of $\mathbf{c}$
$\mathbb{C}$	complex space
$\mathcal{C}(\cdot)$	coding operator
$\mathcal{CS}(\cdot)$	clipping & scaling operation
$\mathbb{D}$	complex region
$\text{diag}(\cdot)$	diagonal function
$\mathcal{D}(\cdot)$	detection operation
$\mathcal{D}^{(z)}(\cdot)$	partial detection operation
$\mathcal{D}_{\text{ds}}(\cdot)$	detection operation of $\mathbf{r}_{\text{eq}}$
$\mathcal{D}_{\text{eq}}(\cdot)$	detection operation of $\mathbf{r}_{\text{eq}}$

$\mathcal{D}_{\text{eq,ds}}(\cdot)$	detection operation of $\mathbf{r}_{\text{eq,ds}}$
$e$	number of bit errors in $\mathbf{u}^{(z)}$
$\mathbf{e}$	undisturbed receive vector
$E$	total transmit energy of an OFDM symbol
$E_t$	data energy of an OFDM symbol
$E_p$	pilot energy of an OFDM symbol
$\text{erfc}(\cdot)$	complementary error function
$E\{\cdot\}$	averaging function
$\eta$	power efficiency
$\eta_{\text{PAE}}$	power added efficiency
$f_n(s'_x, s_x)$	error coefficient of $x_n^{(z)\{s'_x\}}$
$\mathbf{F}$	Fourier matrix
$\text{floor}(\cdot)$	floor function
$\mathcal{F}^{-1}(\cdot)$	inverse Fourier transformation
$g_n(s'_y, s_y)$	error coefficient of $y_n^{(z)\{s'_y\}}$
$G$	power gain
$G_o$	power gain in linear range
$\underline{G}(f)$	transfer function
$\gamma$	average SNR per OFDM subcarrier
$\gamma_b$	gross average SNR per bit
$\gamma_{b,\text{MMSE,effct}}^{(z)}$	effective SNIR per bit of $\hat{\mathbf{t}}_{\text{MMSE,cont}}^{(z)}$
$\gamma_{b,\text{ZF,effct}}^{(z)}$	effective SNIR per bit of $\hat{\mathbf{t}}_{\text{ZF,cont}}^{(z)}$
$\gamma_{\text{MF}}^{(z)}$	SNR of $\hat{x}_{\text{MF,cont},n}^{(z)}$ or $\hat{y}_{\text{MF,cont},n}^{(z)}$
$\gamma_{\text{MMSE,effct}}^{(z)}$	effective SNIR of $\hat{\mathbf{t}}_{\text{MMSE,cont}}^{(z)}$
$\gamma_o$	gross average SNR
$\gamma_{\text{ZF,effct}}^{(z)}$	effective SNR of $\hat{\mathbf{t}}_{\text{ZF,cont}}^{(z)}$
$\mathbf{h}$	CTF magnitude vector
$\mathbf{h}'$	deinterleaved version of $\mathbf{h}$
$\mathbf{h}'^{(z)}$	partial deinterleaved version of $\mathbf{h}$
$\underline{\mathbf{h}}$	CTF vector
$\hat{\underline{\mathbf{h}}}$	estimate of $\underline{\mathbf{h}}$
$\underline{\mathbf{h}}_{\text{dec}}$	decimated CTF vector
$\hat{\underline{\mathbf{h}}}_{\text{dec}}$	estimate of $\underline{\mathbf{h}}_{\text{dec}}$
$\mathbf{H}$	CTF matrix
$\underline{\mathbf{h}}$	CIR vector
$\underline{\mathbf{h}}_{\text{red}}$	reduced CIR vector
$\mathbf{i}^{(z)}$	interference contained in $\hat{\mathbf{t}}_{\text{MMSE,cont}}^{(z)}$

$\mathbf{I}$	unit matrix
$\text{Im}(\cdot)$	imaginary part of a complex value
$\mathcal{I}^{(N,Z)}(\cdot)$	interleaving operator
$(\mathcal{I}^{(N,Z)}(\cdot))^{-1}$	deinterleaving operator
$\mathcal{I}_c^{(N_z,Z)}(\cdot)$	code interleaving operation
$k_o$	oversampling factor
$\underline{\kappa}$	Fourier transform of $\sigma_{\eta}^2$
$\lambda_{\text{cl}}$	clipping ratio
$\lambda_{\text{sc}}$	scaling factor
$M$	size of $\mathbb{V}$
$\max(\cdot)$	maximum function
$\mathcal{M}(\cdot)$	mapping operator
$\mathcal{M}^{-1}(\cdot)$	inverse of mapping operator $\mathcal{M}(\cdot)$
$\underline{\mathbf{n}}$	noise vector
$\underline{\mathbf{n}}'$	deinterleaved version of $\underline{\mathbf{n}}$
$\underline{\mathbf{n}}'^{(z)}$	partial deinterleaved version of $\underline{\mathbf{n}}$
$\underline{\mathbf{n}}_{\text{dec}}$	decimated noise vector
$\underline{\mathbf{n}}_{\text{ds}}$	despread noise vector
$\underline{\mathbf{n}}_{\text{eq}}$	channel equalized noise vector
$\underline{\mathbf{n}}_{\text{eq,ds}}$	channel equalized and despread noise vector
$\underline{\mathbf{n}}_e^{(z)}$	effective noise in $\hat{\underline{\mathbf{t}}}_{\text{MMSE,cont}}^{(z)}$
$\underline{\mathbf{n}}_h$	channel estimation error
$\underline{\mathbf{n}}_{\text{Rx}}$	received noise vector
$N$	spreading factor
$N_c$	dimension of $\mathbf{c}$
$N_F$	number of OFDM subcarriers
$N_u$	dimension of $\mathbf{u}$
$N_z$	dimension of $\mathbf{c}_i^{(z)}$
$p^{\{u\}}$	PAPR of $\underline{\mathbf{t}}^{\{u\}}$
$p^{(z)}$	PAPR of the transmit signal of user $z$
$p_o$	PAPR of an OFDM symbol
$p_{\text{I}}$	PAPR of PDS-SDM cases I
$p_{\text{II}}$	PAPR of PDS-SDM cases II
$p_{\text{III}}$	PAPR of PDS-SDM cases III
$p_{\text{PDS}}$	PAPR of PDS
$p_{\text{SDM}}$	PAPR of conventional SDM
$\underline{\mathbf{p}}^{\{u\}}$	phase factor set

$\underline{\mathbf{p}}^{\{\bar{u}\}}$	optimum phase factor set
$\underline{\mathbf{p}}^{\{\bar{u}\}^{-1}}$	inverse optimum phase factor set
$P$	symbol error probability
$P_b$	bit error probability
$P_b^{(z)}$	partial bit error probability
$P_{\text{DC}}$	DC input power
$\underline{P}_{\text{DC},k_o n_F}$	instantaneous DC power
$P_{\text{in}}$	RF input power
$\underline{P}_{\text{in},k_o n_F}$	instantaneous RF input power
$P_{\text{in,max}}$	maximum instantaneous RF input power
$P_{\text{min}}$	minimum symbol error probability
$P_{\tilde{m}}$	symbol error probability of $\underline{t}_{\tilde{m}}$
$P_{\text{out}}$	RF output power
$P_{\text{sup}}$	upper limit of RF input power
$\mathcal{P}(\cdot)$	PAPR determination operation
$\underline{\varphi}$	phase equalizer vector
$Q$	number of realizations of $\mathbf{x}$ and $\mathbf{y}$
$\tilde{Q}$	number of realizations of $\underline{\mathbf{t}}$
$Q_c$	number of realizations of $\mathbf{c}$
$Q_u$	number of realizations of $\mathbf{u}$
$\mathcal{Q}(\cdot)$	quantization operator
$\underline{\mathbf{r}}$	disturbed receive vector
$\underline{\mathbf{r}}'$	deinterleaved version of $\underline{\mathbf{r}}$
$\underline{\mathbf{r}}^{\{q_u\}}$	realization of $\underline{\mathbf{r}}$
$\underline{\mathbf{r}}'^{(z)}$	partial deinterleaved version of $\underline{\mathbf{r}}$
$\underline{\mathbf{r}}_{\text{dec}}$	decimated receive vector
$\underline{\mathbf{r}}_{\text{ds}}$	despread receive vector
$\underline{\mathbf{r}}_{\text{eq}}$	channel equalized receive vector
$\underline{\mathbf{r}}_{\text{eq,ds}}$	channel equalized and despread receive vector
$\mathbf{r}_{\text{I}}$	imaginary part vector of $\underline{\mathbf{r}}$
$\mathbf{r}'_{\text{I}}$	imaginary part vector of $\underline{\mathbf{r}}'$
$\mathbf{r}'_{\text{I}}^{(z)}$	imaginary part vector of $\underline{\mathbf{r}}'^{(z)}$
$\mathbf{r}_{\text{I}}^{\{q_u\}}$	realization of $\mathbf{r}_{\text{I}}$
$\mathbf{r}_{\text{R}}$	real part vector of $\underline{\mathbf{r}}$
$\underline{\mathbf{r}}_{\text{Rx}}$	input of the phase equalizer
$\mathbf{r}'_{\text{R}}$	real part vector of $\underline{\mathbf{r}}'$
$\mathbf{r}_{\text{R}}^{\{q_u\}}$	realization of $\mathbf{r}_{\text{R}}$

$\mathbf{r}'_{\text{R}}^{(z)}$	real part vector of $\underline{\mathbf{r}}'^{(z)}$
$R$	number of realizations of $\underline{\mathbf{t}}$
$R_{\text{c}}$	coding rate
$R_{\text{p}}$	number of realizations of phase factor sets
$\underline{\mathbf{R}}_{\text{h}}$	covariance matrix of CTF vector
$\underline{\mathbf{R}}_{\mathbf{n}_{\text{ds}}}$	covariance matrix of $\mathbf{n}_{\text{ds}}$
$\underline{\mathbf{R}}_{\mathbf{n}_{\text{eq}}}$	covariance matrix of $\mathbf{n}_{\text{eq}}$
$\underline{\mathbf{R}}_{\mathbf{n}_{\text{eq,ds}}}$	covariance matrix of $\mathbf{n}_{\text{eq,ds}}$
$\underline{\mathbf{R}}_{\mathbf{n}'}^{(z)}$	covariance matrix of vector $\underline{\mathbf{n}}'^{(z)}$
$\underline{\mathbf{R}}_{\mathbf{t}}^{(z)}$	covariance matrix of vector $\underline{\mathbf{t}}^{(z)}$
$\underline{\mathbf{R}}_{\text{h}}$	convariance matrix of CIR vector
$\text{rect}(\cdot)$	rectangular function
$\text{Re}(\cdot)$	real part of a complex value
$s_{\text{av}}$	root mean square of the component magnitudes of $\underline{\mathbf{s}}$
$s_{\text{max}}$	magnitude maximum
$\underline{\mathbf{s}}(t)$	complex envelope
$\underline{\mathbf{s}}$	discrete time low pass equivalent of $\underline{\mathbf{t}}$ in time domain
$\tilde{\underline{\mathbf{s}}}$	discrete time low pass equivalent of $\tilde{\underline{\mathbf{t}}}_i$ in time domain
$\underline{\mathbf{s}}^{\{u\}}$	discrete time low pass equivalent of $\underline{\mathbf{t}}^{\{u\}}$ in time domain
$\underline{\mathbf{s}}^{(z)}$	oversampled time domain transmit vector for user $z$
$\underline{\mathbf{s}}_{\text{cl}}$	clipped version of $\underline{\mathbf{s}}$
$\underline{\mathbf{s}}'_{\text{cl}}$	time domain representation of $\underline{\mathbf{t}}'_{\text{cl}}$
$S$	number of realizations of $\mathbf{x}$ and $\mathbf{y}$
$\mathbf{S}$	real valued spreading matrix
$\underline{\mathbf{S}}$	complex valued spreading matrix
$\text{sign}(\cdot)$	sign function
$\sigma^2$	variance of the real and imaginary parts of $\tilde{\underline{\mathbf{n}}}$
$\sigma_{\text{h}}^2$	variance of the components of the channel matrix $\underline{\mathbf{H}}$
$\sigma_{\text{i}}^{(z)2}$	interference variance
$\sigma_{\text{MF}}^{(z)2}$	variance of noise term of MF estimate
$\sigma_{\text{n}_e}^{(z)2}$	noise variance
$\sigma_{\text{n}_h}^2$	variance of each components of $\underline{\mathbf{n}}_h$
$\sigma_{\text{t}}^2$	variance of $\underline{\mathbf{t}}$
$\sigma_{\text{h}}^2$	power delay profile of the radio channel
$\hat{\underline{\mathbf{t}}}$	data estimate of $\underline{\mathbf{t}}_{\tilde{m}}$
$\underline{\mathbf{t}}_{\tilde{m}}$	data element at the modulator output
$\underline{\mathbf{t}}$	transmit vector

$\underline{\mathbf{t}}^{\{u\}}$	alternative transmit vector
$\underline{\mathbf{t}}^{(z)}$	partial transmit vector
$\tilde{\underline{\mathbf{t}}}$	spread transmit vector
$\tilde{\underline{\mathbf{t}}}^{(z)}$	partial spread transmit vector
$\hat{\underline{\mathbf{t}}}$	estimate of $\underline{\mathbf{t}}$
$\hat{\underline{\mathbf{t}}}^{(z)}$	estimate of $\tilde{\underline{\mathbf{t}}}^{(z)}$
$\tilde{\underline{\mathbf{t}}}^{\{q_u\}}$	realization of $\tilde{\underline{\mathbf{t}}}$
$\underline{\mathbf{t}}_{c1}$	frequency domain representation of $\underline{\mathbf{s}}_{c1}$
$\underline{\mathbf{t}}'_{c1}$	vector consisting of the first $N_F$ components of $\underline{\mathbf{t}}_{c1}$
$\tilde{\underline{\mathbf{t}}}_i$	interleaved spread transmit vector
$\tilde{\underline{\mathbf{t}}}_i^{\{u\}}$	alternative interleaved spread transmit vector
$\underline{\mathbf{t}}_u^{(z)}$	useful content of $\hat{\underline{\mathbf{t}}}_{\text{MMSE,cont}}^{(z)}$
$\underline{\mathbf{t}}_{u,\text{unbiased}}^{(z)}$	unbiased continuous valued version of $\underline{\mathbf{t}}_u^{(z)}$
$\hat{\underline{\mathbf{t}}}_{\text{ML}}$	ML estimate of $\underline{\mathbf{t}}$
$\hat{\underline{\mathbf{t}}}_{\text{ML}}^{(z)}$	ML estimate of $\underline{\mathbf{t}}^{(z)}$
$\hat{\underline{\mathbf{t}}}_{\text{MMSE,cont}}^{(z)}$	MMSE estimate of $\underline{\mathbf{t}}^{(z)}$
$\hat{\underline{\mathbf{t}}}_{\text{ZF,cont}}^{(z)}$	ZF estimate of $\underline{\mathbf{t}}^{(z)}$
$T$	OFDM symbol duration
$T_c$	duration of $\underline{\mathbf{h}}(\tau)$
$T_{\text{coh}}$	coherence time
$T_M$	delay spread
$T_s$	duration of the cyclic prefix
$\tau$	delay instants
$\tilde{u}$	superscript of the optimum phase factor set
$\mathbf{u}$	information vector
$\mathbf{u}^{\{q_u\}}$	transmitted realization of $\mathbf{u}$
$\mathbf{u}^{(z)}$	partial information vector
$\hat{\mathbf{u}}$	estimate of $\mathbf{u}$
$\hat{\mathbf{u}}^{(z)}$	estimate of $\mathbf{u}^{(z)}$
$U$	number of phase factor sets
$v_E$	energy partitioning coefficient
$v_{E,\text{opt}}$	optimum energy partitioning coefficient
$\mathbb{V}$	modulation alphabet
$\text{vec}(\cdot)$	vector function
$\mathbf{w}$	reliability vector
$\mathbf{w}^{(z)}$	partial reliability vector
$W$	normalized delay spread

<b>W</b>	Walsh-Hadamard matrix
<b>x</b>	real part of $\underline{\mathbf{t}}$
$\mathbf{x}^{(z)}$	real part of $\underline{\mathbf{t}}^{(z)}$
$\hat{\mathbf{x}}$	real part of $\hat{\underline{\mathbf{t}}}$
$\hat{\mathbf{x}}_{\text{ML}}$	ML estimate of $\mathbf{x}$
$\hat{\mathbf{x}}_{\text{ML}}^{(z)}$	ML estimate of $\mathbf{x}^{(z)}$
<b>y</b>	imaginary part of $\underline{\mathbf{t}}$
$\mathbf{y}^{(z)}$	imaginary part of $\underline{\mathbf{t}}^{(z)}$
$\hat{\mathbf{y}}$	imaginary part of $\hat{\underline{\mathbf{t}}}$
$\hat{\mathbf{y}}_{\text{ML}}$	ML estimate of $\mathbf{y}$
$\hat{\mathbf{y}}_{\text{ML}}^{(z)}$	ML estimate of $\mathbf{y}^{(z)}$
<b>Z</b>	number of subsets

---

## References

- [ARDK07] Auer, G.; Raulefs, R.; Dammann, A.; Kaiser, S.: Apparatus and method for detecting a group of received symbols. *European Patent Specification EP1602192B1*, 2007.
- [BEL03] Bury, A.; Egle, J.; Lindner, J.: Diversity comparison of spreading transforms for multicarrier spread spectrum transmission. *IEEE Trans. Commun.*, vol. 51, 2003, pp. 774–781.
- [BFH96] Bäuml, R. W.; Fischer, R. F. H.; Huber, J. B.: Reducing the peak-to-average power ratio of multicarrier modulation by selected mapping. *Electronics Letters*, vol. 32, Oct. 1996, pp. 2056–2057.
- [BN10] Bai, Q.; Nossek, J. A.: On the effects of carrier frequency offset on cyclic prefix based OFDM and filter bank based multicarrier systems. *11th IEEE Workshop on Signal Processing Advances in Wireless Communications (SPAWC'10)*, 2010, pp. 1–5.
- [Bou08] Boumaiza, S.: Advanced techniques for enhancing wireless RF transmitters' power efficiency. *International Conference on Microelectronics (ICM)*, 2008, pp. 68–73.
- [Bri46] Brinkley, J. R.: A method of increasing the range of VHF communications systems by multi-carrier amplitude modulation. *IEE Journal - Part III: Radio and communication engineering*, vol. 93, 1946, pp. 159–166.
- [BWW99] Baier, P. W.; Weber, T.; Weckerle, M.: "Spreading Techniques, A Far-reaching Technology", in *CDMA Techniques for Third Generation Mobile Systems*, edited by F. Swarts et al. Boston: Kluwer Academic Publishers, pp. 1-22, 1999.
- [Chi35] Chireix, H.: High power outphasing modulation. *Proc. IRE*, vol. 23, 1935, pp. 1370–1392.
- [Cox74] Cox, D. C.: Linear amplification with non-linear components. *IEEE Trans. Commun.*, vol. 22, 1974, pp. 1942–1945.
- [Cri02] Cripps, S. C.: *Advanced Techniques in RF Power Amplifiers*. Boston: Artech House, 2002.



- [CT65] Cooley, J. W.; Tukey, J. W.: An algorithm for the machine calculation of complex Fourier series. *Mathematics of Computation*, vol. 19, 1965, pp. 297–301.
- [DPSB08] Dahlman, E.; Parkvall, S.; Skjöld, J.; Beming, P.: *3G Evolution: HSPA and LTE for Mobile Broadband (2nd Edition)*. Amsterdam: Academic Press, 2008.
- [FA76] Fino, B. J.; Algazi, V. R.: Unified matrix treatment of the fast Walsh-Hadamard transform. *IEEE Trans. Computers*, vol. 25, 1976, pp. 1142–1146.
- [FJ89] Forney Jr., G. D.: Multidimensional constellations—part II: Voronoi constellations. *IEEE Journal on Selected Areas in Commun.*, vol. 7, 1989, pp. 941–958.
- [FK03] Fazel, F.; Kaiser, S.: *Multi-Carrier and Spread Spectrum Systems*. Chichester: Wiley, 2003.
- [FK04] Fazel, K.; Kaiser, S.: *Multi-Carrier Spread-Spectrum: for Future Generation Wireless Systems*. Boston: Kluwer Academic Publishers, 2004.
- [Fri95] Friedrichs, B.: *Kanalcodierung: Grundlagen und Anwendungen in modernen Kommunikationssystemen*. Berlin: Springer, 1995.
- [Fun79] Funk, H.: Über die grenzen idealer tiefpässe in mathematischen modellen für schaltungen zur korrelation binärer zufallssignale. *Archive für Elektronik und Übertragungstechnik*, vol. 33, 1979, pp. 325–327.
- [GB09a] Guo, S.; Baier, P. W.: Optimum power assignment to data and pilots in OFDM transmission over very fast fading radio channels. *Proc. 14th International OFDM-Workshop (InOWo'09)*, 2009, pp. 78–82.
- [GB09b] Guo, S.; Baier, P. W.: Optimized power amplification in OFDM transmission by selective data mapping and envelope scaling. *Proc. 12th International Symposium on Wireless Personal Multimedia Communications (WPMC'09)*, paper ID:1569203883, 2009.
- [GB10] Guo, S.; Baier, P. W.: Partial data spreading, an efficient and inexpensive approach to combating frequency selectivity in coded OFDM transmission. *Proc. 11th International Symposium on Spread Spectrum Techniques and Applications (ISSSTA '10)*, 2010, pp. 87–92.
- [HCC<sup>+</sup>01] Hwang, H. k.; Charroux, J. M.; Cooper, L.; Nguyen, T. M.; Goo, G. W.: Performance of the 16QAM modem in the satellite communications environment.

- IEEE Military Communications Conference (MILICOM'2001)*, vol. 1, 2001, pp. 647–651.
- [HF05] Herhold, P., Z. E.; Fettweis, G.: Cooperative multi-hop transmission in wireless networks. *Computer Networks*, vol. 49, 2005, pp. 299–324.
- [HH89] Hagenauer, J.; Hoehner, P.: A viterbi algorithm with soft-decision outputs and its applications. *Proc. IEEE Global Telecommunications Conference*, vol. 3, 1989, pp. 1680–1686.
- [HJ85] Horn, R. A.; Johnson, C. A.: *Matrix Analysis*. Cambridge: Cambridge University Press, 1985.
- [HL05] HAN, S. H.; Lee, J. H.: An overview of Peak-to-Average Power Ratio reduction techniques for multicarrier transmission. *IEEE Wireless Communications*, vol. 12, 2005, pp. 56–65.
- [HT01] Heiskala, J.; Terry, J.: *OFDM Wireless LANs: A Theoretical and Practical Guide*. Indianapolis: Sams, 2001.
- [HYW<sup>+</sup>09] Hwang, T.; Yang, C.; Wu, G.; Li, S.; Li, G.: OFDM and its wireless applications: a survey. *IEEE Vehic. Techn.*, vol. 58, 2009, pp. 1673–1684.
- [JW07] Jiang, Y.; Wang, C.: Technical challenges for the OFDM mobile communication system. *Huawei Publications Issue 35*. Available at <http://www.huawei.com/>, 2007, pp. 63–65.
- [KJS03] Kim, J.; Jeung, C.; Shin, P.: Advanced power amplifier design using doherty configurations. *Ansoft Corporation Global Seminars: Delivering Performance*. Available at [www.ansoft.com/deliveringperformance/poweramp.pdf](http://www.ansoft.com/deliveringperformance/poweramp.pdf), 2003.
- [Kle96] Klein, A.: *Multi-user Detection of CDMA Signals - Algorithms and their Application to Cellular Mobile Radio*. Duesseldorf: VDI Verlag, 1996.
- [LCCP10] Lavrador, P. M.; Cunha, T. R.; Cabral, P. M.; Pedro, J. C.: The linearity-efficiency compromise. *IEEE Microwave Magazine*, vol. 11, 2010, pp. 44–58.
- [Lin08] Lin, J.-C.: Least-square channel estimation for mobile OFDM communication on time-varying frequency-selective fading channels. *IEEE Trans. Vehicular Technology*, vol. 57, 2008, pp. 3538–3550.
- [LvdTV01] Leenaerts, D.; van der Tang, J.; Vaucher, C.: *Circuit Design for RF Transceivers*. Boston: Kluwer Academic Publishers, 2001.

- [Mar87] Marple, S. L. J.: *Digital Spectral Analysis with Applications in C and Matlab*. New Jersey: Prentice Hall, 1987.
- [MS96] Mestdagh, D. J. G.; Spruyt, P. M. P.: A method to reduce the probability of clipping in DMT-based transceivers. *IEEE Trans. Commun.*, vol. 44, 1996, pp. 1234–1238.
- [Myu07] Myung, H. G.: Introduction to single carrier FDMA. *Proc. 15th European Signal Processing Conference (EUSIPCO'2007)*, 2007, pp. 2144–2148.
- [OA07] Ozdemir, M.; Arslan, H.: Channel estimation for wireless OFDM systems. *IEEE Communication Surveys and Tutorials*, vol. 9, 2007, pp. 18–48.
- [OHA07] Omiyi, P.; Haas, H.; Auer, G.: Analysis of TDD cellular interference mitigation using busy-bursts. *IEEE Trans. Wireless Commun.*, vol. 6, 2007, pp. 2721–2731.
- [OO03] Ohkubo, N.; Ohtsuki, T.: Design criteria for phase sequences in selected mapping. *IEICE Trans. Commun*, vol. E86-B, 2003, pp. 2628–2636.
- [Pro00] Proakis, J. G.: *Digital Communication (4th edition)*. New York: McGraw-Hill, 2000.
- [Pät02] Pätzold, M.: *Mobile Fading Channels*. Chichester: Wiley, 2002.
- [RAC02] Raab, F.; Asbeck, P.; Cripps, S.: Power amplifiers and transmitters for RF and microwave. *IEEE Trans. on Microwave Theory and Techniques*, vol. 50, 2002, pp. 814–826.
- [SBNS04] Simeone, O.; Bar-Ness, Y.; Spagnolini, U.: Pilot-based channel estimation for OFDM systems by tracking the delay subspace. *IEEE Trans. Wireless Commun.*, vol. 3, 2004, pp. 315–325.
- [SJ67] Stein, S.; Jones, J. J.: *Modern Communication Principles*. New York: McGraw-Hill, 1967.
- [SK93] Steiner, B.; Klein, A.: Kanal- und Datenschätzung in Synchronen CDMA-Mobilfunksystemen mit Interferenzeliminierung. *Kleinheubacher Berichte*, vol. 36, 1993, pp. 253–268.
- [Sta08] Statistisches Bundesamt Wiesbaden: Tabellen zu den umweltökonomischen Gesamtrechnungen 2008. Teil 5: Energie. 2008.

- 
- [VB00] Visoz, R.; Bejjani, E.: Matched filter bound for multichannel diversity over frequency-selective Rayleigh-fading mobile channels. *IEEE Trans. Vehicular Technology*, vol. 49, 2000, pp. 1832–1845.
- [vNP00] van Nee, R.; Prasad, R.: *OFDM Wireless Multimedia Communications*. Boston, London: Artech House Publishers, 2000.
- [VO79] Viterbi, A. J.; Omura, J. K.: *Principles of Digital Communication and Coding*. McGraw-Hill, 1979.
- [Wha71] Whalen, A. D.: *Detection of Signals in Noise*. New York: Academic Press, 1971.
- [WJ08] Wang, L.; Jezek, B.: OFDM modulation schemes for military satellite communications. *IEEE Military Communications Conference (MILICOM'2008)*, vol. 27, 2008, pp. 3126–3132.
- [WZZ10] Wang, S.; Zhu, S.; Zhang, G.: A Walsh-Hadamard of coded spectral efficient full frequency diversity OFDM system. *IEEE Trans. Commun.*, vol. 58, 2010, pp. 28–34.
- [ZL10] Zhou, W.; Lam, W.: Channel estimation and data detection for OFDM systems over fast-fading and dispersive channels. *IEEE Trans. Vehicular Technology*, vol. 59, 2010, pp. 1381–1392.



---

## Tabellarischer Lebenslauf



Name: Shengqiang Guo

Adresse: Kurt-Schumacher-Str. 32  
D-67663 Kaiserslautern

Geburtsdatum: 29.12.1983

Staatsangehörigkeit: VR China

Familienstand: ledig

Studium: 2002-2008  
Huazhong University of Science and Technology  
in Wuhan, VR China.  
Vertiefungsrichtung Kommunikationssysteme

2006 Abschluß: Bachelor of Engineering (B. Eng.)

2008 Abschluß: Master of Engineering (M. Eng.)

Berufstätigkeit: seit August 2008  
Promotionsstipendiat Prof. Baiers am Lehrstuhl  
für Funkkommunikation und Navigation im Fachbereich EIT  
der Technischen Universität Kaiserslautern